

Changes in minerals and organic-mineral associations during paddy soil development

Dissertation

zur Erlangung des

Doktorgrades der Naturwissenschaften (Dr. rer. nat.)

der

Naturwissenschaftlichen Fakultät III

Agrar- und Ernährungswissenschaften,

Geowissenschaften und Informatik

der

Martin-Luther-Universität Halle-Wittenberg

vorgelegt von

Frau Dipl.-Geoökologin Pauline Winkler

Geb. am 23.11.1984 in Finsterwalde

Gutachter: Prof. Reinhold Jahn, Prof. Karsten Kalbitz, Prof. Georg Guggenberger

Tag der Verteidigung: 16. November 2020

Table of Contents

Table of Contents	1
List of Figures	6
List of Tables	8
List of Appendices.....	9
1 General Introduction.....	11
1.1 Biogeochemistry of paddy soils.....	11
1.2 Soil types under paddy management and their mineral properties	14
1.2.1 Andosols.....	15
1.2.2 Alisols.....	16
1.2.3 Vertisols	16
1.3 Mineral-organic-carbon associations.....	17
1.4 Objectives.....	19
2 Response of Vertisols, Andosols, and Alisols to paddy management.....	20
2.1 Abstract.....	21
2.2 Introduction	22
2.3 Materials & Methods	24
2.3.1 Investigation area & soil sampling.....	24
2.3.2 Laboratory analyses of the bulk soil	24
2.4 Results & Discussion	26
2.4.1 Vertisols	26
2.4.2 Andosols.....	27
2.4.3 Clayey Alisols (on Java).....	37
2.4.4 Sandy Alisols (in China).....	38
2.5 Implications	39
2.5.1 The fate of Fe oxides under paddy management depends on initial soil properties 39	
2.5.2 Accumulation of OC in paddy soils mainly depends on OM input.....	41
2.5.3 Desilication slowed down in Andosol-derived paddy soils.....	41
2.5.4 No evidence of ferrollysis.....	41
2.6 Conclusions	42
2.7 Acknowledgements.....	42
3 Contrasting evolution of iron phase composition in soils exposed to redox fluctuations	43

3.1	Abstract.....	44
3.2	Introduction.....	45
3.3	Materials & Methods	47
3.3.1	Field soil sampling.....	47
3.3.2	Incubation experiment	49
3.3.3	Analytical methods.....	50
3.3.4	⁵⁷ Fe Mössbauer spectroscopy	51
3.4	Results.....	53
3.4.1	Chemical extraction of pedogenic Fe	53
3.4.2	Fe phases identified by ⁵⁷ Fe Mössbauer spectroscopy.....	53
3.4.3	Fe (oxy-)hydroxide changes in soils under paddy management	56
3.4.4	Soil solution composition during incubation of non-paddy topsoils.....	57
3.4.5	Fe (oxy-)hydroxide changes in laboratory-incubated soils.....	58
3.5	Discussion.....	59
3.5.1	Contrasting shifts in Fe crystallinity during redox fluctuations.....	59
3.5.2	Chemical extraction vs. ⁵⁷ Fe Mössbauer spectroscopy.....	61
3.5.3	Associations of Fe and OM in the Andosol.....	62
3.5.4	Fe-substituted halloysite formation probable in the Andosol-derived paddy soil.....	62
3.6	Conclusions	63
3.7	Acknowledgements.....	64
4	Tracing organic carbon and microbial community structure in mineralogically different soils exposed to redox fluctuations	65
4.1	Abstract.....	66
4.2	Introduction	66
4.3	Materials & Methods	69
4.3.1	Soil selection and sampling.....	69
4.3.2	Specific surface area and surface element composition of initial soils.....	70
4.3.3	Laboratory incubation experiment	71
4.3.4	Headspace analyses.....	72
4.3.5	Soil solution analyses	73
4.3.6	Density fractionation of soil OM	73
4.3.7	Calculation of OC budget.....	74
4.3.8	Lignin-derived phenols.....	74
4.3.9	Non-cellulosic carbohydrates	74
4.3.10	Microbial DNA extraction and sequencing data analysis	75
4.3.11	Microbial cell membrane lipids.....	76

4.3.12	Statistics.....	76
4.4	Results.....	77
4.4.1	Surface characteristics of initial soils.....	77
4.4.2	Soil respiration.....	77
4.4.3	Soil solution chemistry during incubation.....	78
4.4.4	Organic matter fractions.....	79
4.4.5	Fate of straw OC.....	80
4.4.6	Lignin-derived phenols in mineral-associated OM.....	81
4.4.7	Non-cellulosic carbohydrates in mineral-associated OM.....	82
4.4.8	Microbial community composition.....	83
4.5	Discussion.....	86
4.5.1	Respiration and OC storage in bulk samples under different redox regimes.....	86
4.5.2	SOC formation depends on soil type.....	87
4.5.3	Role of Fe oxides for SOC stabilization.....	88
4.5.4	Impact of soil water on SOC formation.....	88
4.5.5	Lignin-derived phenols in mineral-associated OM.....	89
4.5.6	Non-cellulosic carbohydrates in mineral-associated OM.....	90
4.5.7	Soil type has an impact on bacterial community composition.....	90
4.5.8	Activity of methanogens depends on soil type.....	91
4.6	Summary & Conclusions.....	92
4.7	Acknowledgements.....	93
5	Synthesis.....	94
5.1	Discussion.....	94
5.1.1	Do several decades of paddy management have an effect on minerals and OC stocks of Vertisol, Alisol, and Andosol?.....	94
5.1.2	Do several decades of redox fluctuation in Alisol- and Andosol-derived paddy soils result in increasing or decreasing Fe oxide crystallinity?.....	96
5.1.3	What is the effect of Alisol and Andosol incubation with eight redox cycles on OM turnover and microbial communities? Do we find similar effects in the field paddy soils? ..	97
5.1.4	Do Fe oxide dynamics in paddy soils promote OC stabilization?.....	100
5.1.5	Do paddy management-induced processes described above depend on the initial soil type?.....	104
5.2	Summary & Conclusions.....	104
	Summary.....	104
	Zusammenfassung.....	109
	References.....	112
	List of Abbreviations.....	129

Table of Contents

Danksagung	131
Appendix	133
Publikationsliste (List of publications)	157
Lebenslauf (Curriculum Vitae)	159

List of Figures

Fig. 1.1	Valley used for lowland rice cultivation in Vietnam.	11
Fig. 1.2	Scheme of a rice paddy field with bunds and puddled topsoil.....	12
Fig. 1.3	Vertisol, Andosol, and Alisol under sugarcane (Vertisol) and vegetables (Andosol and Alisol) representing non-paddy study sites and neighboring paddy soils deriving from Vertisol, Andosol and Alisol.	15
Fig. 1.4	Example for ligand exchange resulting in an inner-sphere complex.	18
Fig. 2.1	Maps of the sampling sites in China and on Java (Indonesia).....	24
Fig. 2.2	XRD patterns of clay fractions.	30
Fig. 2.3	Organic carbon (OC) concentrations of the non-paddy and their subsequent paddy profiles (main and subsites).	31
Fig. 2.4	Fe _{DCB} depth profiles of the non-paddy and subsequent paddy profiles (main and subsites).	32
Fig. 2.5	Fe _{AAO} depth profiles of the non-paddy and subsequent paddy profiles (main and subsites).	33
Fig. 2.6	Topsoil stocks of crystalline (Fe _c) and short range-ordered Fe (Fe _{AAO}).	34
Fig. 2.7	Subsoil stocks of crystalline (Fe _c) and short-range-ordered Fe (Fe _{AAO}).	34
Fig. 2.8	Si/Zr ratios (means) of paddy soils plotted against respective non-paddy soils.	35
Fig. 3.1	Depth profile of dithionite-bicarbonate-citrate-extractable Fe (Fe _{DCB}) and acidic ammonium-oxalate-extractable Fe (Fe _{AAO}) of non-paddy (NP) and respective paddy (P) soils.	49
Fig. 3.2	Fitted Mössbauer spectra of Alisol topsoils at 295, 77 and 4.2 K.	54
Fig. 3.3	Fitted Mössbauer spectra of Andosol topsoils at 295, 77 and 4.2 K.	55
Fig. 3.4	Iron phase composition of Alisols and Andosols under different land use and of laboratory incubated non-paddy soils as calculated from Mössbauer spectra.	57
Fig. 3.5	Changes in redox potential, pH and dissolved Fe ²⁺ concentrations with time in soil solutions (filtered with 0.45 μm) of Alisol and Andosol non-paddy topsoils incubated with (+straw) and without straw (-straw) addition.	58
Fig. 4.1	Overview of Materials & Methods.	70

Fig. 4.2 Cumulative sum of CO ₂ -C and CH ₄ -C respired from the Alisol (left) and Andosol (right) incubated with alternating redox (a-o) and permanently oxic (o) conditions as well as with (+) and without (-) straw addition.	78
Fig. 4.3 Evolution of redox potential (a and b), pH (a and b), dissolved Fe ²⁺ (c and d), and DOC (e and f) concentrations in soil solutions of the Alisol (left) and Andosol (right) incubated with redox fluctuation and straw addition (+straw) or without straw addition (-straw).....	79
Fig. 4.4 Amount of OC in different density fractions in g per kg of soil (FPOM = free particulate organic matter, OPOM = occluded particulate organic matter, MOM = mineral associated organic matter) before (initial) and after the incubation experiment.	80
Fig. 4.5 Fate of straw OC as calculated by δ ¹³ C of CO ₂ in headspace samples, of DOC in soil solutions ¹⁾ and of different density fractions (FPOM = free particulate organic matter, OPOM = occluded particulate organic matter, MOM = mineral-associated organic matter) in soils.	81
Fig. 4.6 Lignin-derived mineral-associated OM (VSC; sum of Vanillyl (V), Syringyl (S) and Cinnamyl (C) units resulting from CuO oxidation). Acid-to-Aldehyde ratio of Vanillyl ((Ac/Al) _v) and Syringyl ((Ac/Al) _s) units as indicator for oxidation state of lignin compounds.	82
Fig. 4.7 Sum of concentrations of non-cellulosic carbohydrates in mineral-associated OM. GM/AX = (Galactose + Mannose)/(Arabinose + Xylose) with plant sugars showing GM/AX < 0.5 and microbial sugars showing GM/AX > 2.	83
Fig. 4.8 Principal Coordinate Analysis (PCoA) plot based on DNA sequencing and the resulting unweighted (a) and weighted (b) UniFrac distance matrix of initial non-paddy soils and soils incubated with straw addition.	84
Fig. 4.9 Heatmap of the relative abundance of bacterial families based on 16S rRNA gene sequences.....	85
Fig. 4.10 Ratio of GDGT-0 and Crenarchaeol lipids in bulk samples, whereby large ratio indicates presence of methanogenic archaea.	86
Fig. 5.1 Example of how the initial portion of short-range-ordered (SRO) Fe oxides may influence Fe oxide crystallinity changes in paddy soils with redox fluctuation.....	97
Fig. 5.2 Concentration of organic carbon (OC) plotted against acid ammonium oxalate-extractable Fe (= FeAAO representing SRO Fe oxides) of non-paddy (NP) and paddy (P) topsoils with Ando = Andosol, cAli = clayey Alisol, Verti = Vertisol and sAli = sandy Alisol.	101
Fig. 5.3 Stabilizing and destabilizing effects of (short-range-ordered = SRO) Fe oxides on organic carbon (OC) in soils with redox fluctuation.....	103

List of Tables

Table 2.1 Site description, horizons, texture, bulk density (BD), pH, potential cation exchange capacity (CEC_{pot}), base saturation (BS), phosphorus (P) retention, total Fe contents (Fe_{total}), proportion of pedogenic Fe oxides (Fe_{DCB}/Fe_{total}), and proportion of short range-ordered Fe oxides (Fe_{AAO}/Fe_{DCB}) of the non-paddy sites. Where data were obtained for main and subsite samples, the means \pm standard errors (n=3) are given.....	28
Table 2.2 Site description, horizons, texture, bulk density (BD), pH, potential cation exchange capacity (CEC_{pot}), base saturation (BS), phosphorus (P) retention, total Fe contents (Fe_{total}), proportion of pedogenic Fe oxides (Fe_{DCB}/Fe_{total}), and proportion of short range-ordered Fe oxides (Fe_{AAO}/Fe_{DCB}) of the respective paddy sites. Where data were obtained for main and subsite samples, the means \pm standard errors (n=3) are given.....	29
Table 3.1 Profile description of non-paddy and respective paddy soils (BD = bulk density, OC = organic carbon). Where data were obtained for main and subsites, the means \pm standard errors (n=3) are given. Data taken from Winkler et al. (2016). Non-paddy soils used for Mössbauer measurements and incubation experiment are framed. Respective paddy soils used for Mössbauer analyses are framed with dashed lines.....	48
Table 3.2 Identification of Mössbauer spectral components (for references see Appendix 2.1)	52
Table 3.3 Abundance of Fe in different Fe phases as calculated from respective Mössbauer spectra. Standard deviations in brackets are fitting errors as calculated by Recoil™ software.....	56
Table 4.1 Ratio of surface element composition as determined by X-ray photoelectron spectroscopy (XPS) and total element concentration as determined by X-ray fluorescence (XRF) spectroscopy (Si, Al, Fe) and elemental analyzer (C). Concentrations of OC refer to the mineral associated OC since respective data were determined after the removal of particulate OC via density fractionation. A ratio <1 indicates surface depletion and a ratio >1 surface accumulation of the respective element. Specific surface area (SSA) is given for soils after OM removal.....	77
Table 5.1 C species at mineral surfaces of field soils according to fitted C 1s spectra of X-ray photoelectron spectroscopy (XPS) as well as Acid-to-Aldehyde ratio of Vanillyl ((Ac/Al) _v) and Syringyl ((Ac/Al) _s) units as indicator for oxidation state of lignin compounds and GM/AX = (Galactose + Mannose)/(Arabinose + Xylose) with plant sugars showing GM/AX < 0.5 and microbial sugars showing GM/AX > 2. Numbers in brackets represent standard deviations with n = 3.....	99

List of Appendices

Appendix 1: Fe extraction techniques	133
Appendix 1.1: Extraction of total pedogenic Fe with dithionite–citrate–bicarbonate solution (Fe _{DCB})	133
Appendix 1.2: Extraction of pedogenic short-range-ordered Fe with acidic ammonium oxalate at pH 3 (Fe _{AAO})	134
Appendix 2: Supplemental Mössbauer information	134
Appendix 2.1: Identification of different ⁵⁷ Fe Mössbauer components	134
Appendix 2.2: Additional Mössbauer data	136
Fig. A-1: Fitted Mössbauer spectra of Alisol topsoils at 140 and 40 K	136
Fig. A-2: Fitted Mössbauer spectra of Andosol topsoils at 140, 40 and 13 K	137
Table A-1: Fitting parameters and calculated Mössbauer parameters	138
Appendix 3: Detailed methods description	145
Appendix 3.1: Specific surface area (SSA)	145
Appendix 3.2: Elemental composition and C speciation of particle surfaces	145
Appendix 3.3: Headspace analyses and calculation of proportion of straw-derived CO ₂ and CH ₄	145
Appendix 3.4: Measurement of DO ¹³ C and calculation of proportion of straw-derived DOC	147
Appendix 3.5: Density fractionation of soil OM and calculation of proportion of straw-derived OC	148
Appendix 3.6: Lignin-derived phenols	149
Appendix 3.7: Non-cellulosic carbohydrates	150
Appendix 3.8: Microbial analyses	150
Appendix 3.8.1: DNA extraction and sequencing library preparation	150
Appendix 3.8.2: Sequencing data analysis and statistics	151
Appendix 3.8.3: Microbial cell membrane lipids	152
Appendix 4: Additional Tables & Figures	153
Table A-4.1: Total organic carbon (OC) budget of the incubation experiment showing soil OC	

amounts of initial soils, amount of added straw OC, mineralized OC, retrieved DOC and final SOC amounts	153
Table A-4.2: Proportion of straw OC in individual non-cellulosic carbohydrates [%] based on respective $\delta^{13}\text{C}$ measurements	153
Table A-4.3: Summary of the sequencing run and sequence processing with QIIME	154
Fig. A-4.1: Exemplary C 1s spectra of mineral-organic associations isolated from each soil, with peaks fitted with subcomponents reflecting different carbon oxidation states	154
Fig. A-4.2: Cumulative $\text{CH}_4\text{-C}$ emitted from the Alisol (left) and Andosol (right) incubated with alternating redox (a-o) and permanently oxic (o) conditions as well as with (+) and without (-) straw addition	155
Fig. A-4.3 Rarefaction curve of 16S rRNA sequences of all samples rarefied to a sequence level of 19,508 reads per sample	155
Fig. A-4.4: Concentrations of dissolved organic carbon (DOC) plotted over Fe^{2+} concentrations of Alisol and Andosol samples incubated with straw addition and redox fluctuation	156

1 General Introduction

Archaeological findings suggest that rice farming developed about 8,000 years ago. When farmers in China started to prepare rice paddy fields for optimized plant growth, rice was entirely domesticated (Greenland, 1997). Today, rice is the staple food for almost half of the world's population and is grown on about 160 million hectares of land (GRiSP, 2013). The unique hydrological conditions of paddy soils (alternation of submergence and drainage) entail complex biogeochemical processes that are not yet fully understood. Moreover, climate change will likely increase the occurrence of extreme weather events such as heavy rains and heatwaves (Coumou and Rahmstorf, 2012), so that also soils not managed for paddy cultivation might more frequently be subject to alternation of water-logging and desiccation in the future. Studying the biogeochemistry of paddy soils is therefore also relevant for other soils under various land use.

1.1 Biogeochemistry of paddy soils

Rice (*Oryza*) is a semiaquatic annual grass requiring large amounts of water. Hence, most of the rice is grown on rainfed or irrigated lowlands (Fig. 1.1).



Fig. 1.1 Valley used for lowland rice cultivation in Vietnam.

Rice paddy fields are surrounded by bunds and soils are puddled (Fig. 1.2) in order to minimize lateral and vertical water losses (GRiSP, 2013). Puddling is the repeated ploughing of water-saturated soil destroying soil structure and resulting in dispersively homogenized topsoil with a dense and platy plough pan underneath (Sharma and De Datta, 1985). Due to the aquic soil conditions redoximorphic features arise. Soils with such topsoil characteristics forming in

response to long-term wet cultivation practices are classified as Hydragric Anthrosols (IUSS Working Group, 2006).

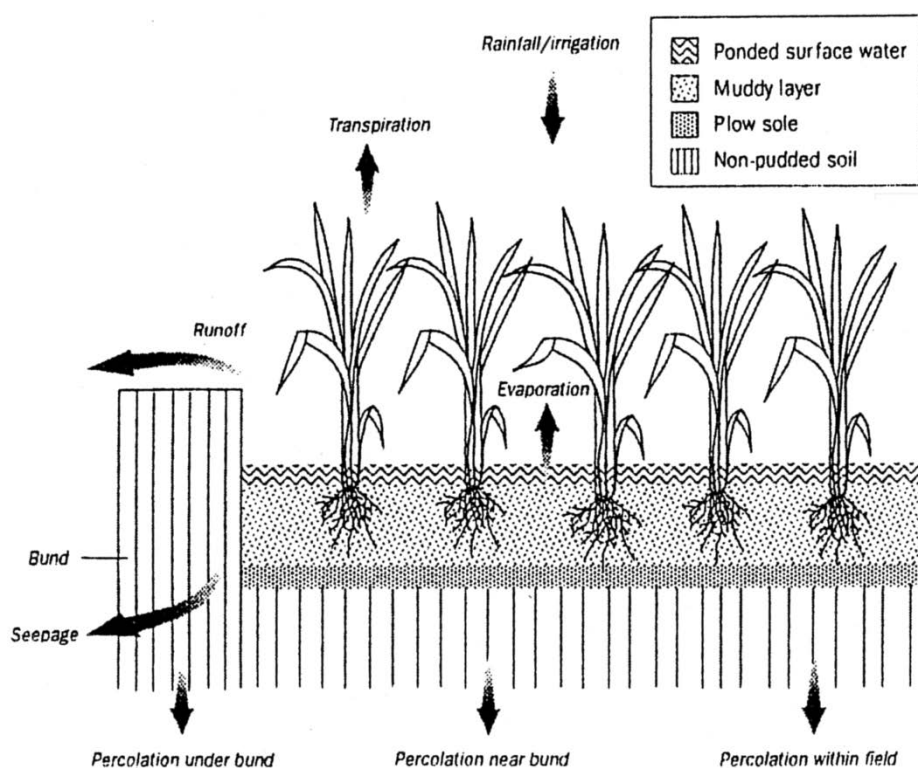


Fig. 1.2 Scheme of a rice paddy field with bunds and puddled topsoil (after Wopereis et al., 1994).

Puddling reduces soil permeability allowing the topsoil to remain submerged during rice growth. Before harvest the soil is drained by partially opening the bunds (Ponnamperuma, 1972; Sharma and De Datta, 1986). The repeated submergence and drainage of paddy soils causes redox fluctuation, i.e. periodic alternation of anoxic and oxic conditions. Anoxic conditions evolve when the consumption of oxygen (O_2) that accompanies organic matter (OM) decomposition is faster than the diffusive replenishment of O_2 from the atmosphere (Reddy and Patrick, 1983). This is the case in submerged soils where O_2 diffusion is restricted to water-filled pores, which is distinctly slower than diffusion through air-filled pores (Grable and Siemer, 1968). Consequently, submerged soils become depleted in O_2 so that it is no longer available as electron acceptor during microbial OM decomposition. Microorganisms able to use alternative electron acceptors such as nitrate, manganese, iron (Fe), and sulfate take advantage and become dominant. The redox potential decreases accordingly. When alternative electron acceptors are used up as well, methanogenic bacteria are stimulated, which decompose organic carbon (OC) to carbon dioxide (CO_2) and methane (CH_4) (Takai and Kamura, 1966; Connell and Patrick, 1969; Patrick and Jugsujinda, 1992; Peters and Conrad, 1996). Drainage of submerged soils leads to the reintroduction of O_2 and a rise in redox potential. Hence, the repeated submergence and

drainage of paddy soils results in redox fluctuations. These go along with pH oscillation induced by the consumption and release of H^+ accompanying the reduction and oxidation of Fe, which represents the most abundant alternative electron acceptor in tropical soils (Kirk, 2004; Sahrawat, 2004; Pan et al., 2014).

Fluctuation of redox potential and pH leads to characteristic biogeochemical processes in paddy soils. The most pronounced effect is the reductive dissolution of Fe oxides and mobilization of the released Fe. As a result, paddy topsoils are depleted in Fe (Ratering and Schnell, 2000; Zhang and Gong, 2003; Kirk, 2004); Fig. 1.3). Changes in crystallinity of the remaining Fe oxides are described contrarily. Several authors (Moormann and van Breemen, 1978; Willett and Higgins, 1978; Wang et al., 1993; Kirk, 2004) report that the proportion of SRO Fe oxides tends to increase since both fractions (short and long range-ordered) undergo reductive dissolution but only the SRO fraction (partly) recovers when oxic conditions recur. Tian-ren (1985), however, assumes crystallinity increase in paddy soils due to the mobilization of Fe preferentially from SRO Fe oxides and hence the relative enrichment of crystalline Fe oxides. Furthermore, changes in clay minerals have been reported for soils under prolonged paddy management. Soils rich in illite undergo accelerated depotassification when used for paddy cultivation unless K losses are compensated by fertilizers (Tian-ren, 1985; Li et al., 2003; Han et al., 2015). Exchange of alkali and earth alkali cations by dissolved Fe^{2+} under anoxic conditions may lead to their removal by vertical or lateral leaching. Re-oxidation of the sorbed Fe^{2+} upon drainage produces H^+ ions, which may attack the clay minerals (ferrolysis). Their partial destruction results in the release of aluminum (Al) that together with Fe can form interlayers. Hence paddy management may lead to partial clay mineral destruction and chloritization (Brinkman, 1970; Wakatsuki et al., 1984; Tian-ren, 1985; Li et al., 2003). Ferrolysis, however, is still controversially debated (Eaqub and Blume, 1982; Van Ranst and De Coninck, 2002). For soils rich in allophane and imogolite, advanced disintegration of these mineral phases and subsequent formation of halloysite and gibbsite were observed under paddy management (Tan, 1968; Mizota et al., 1982). Furthermore, paddy management is associated with phytolith formation. Phytoliths are SRO silicon (Si) oxides formed in rice plants. They may counteract desilication of paddy soils if rice straw is returned to the soil (Kögel-Knabner et al., 2010; Seyfferth et al., 2013).

Finally, redox fluctuation during paddy cultivation also has an effect on soil organic matter (SOM) formation. Submerged paddy soils are generally proposed to store more OC than the respective non-paddy soils due to less efficient decomposition under anoxic conditions (Ponnamperuma, 1972; Pan et al., 2003; Sahrawat, 2004; Zhang and He, 2004; Cheng et al., 2009; Wissing et al., 2011; Kalbitz et al., 2013; Yan et al., 2013). Paddy soils with particularly large organic matter (OM) contents, however, are rare (Greenland, 1997). Iron oxides are generally important for OM stabilization in soils (Kaiser and Guggenberger, 2000; Kleber et al., 2005). Their reductive dissolution in paddy soils, however, destabilizes the associated OM and

enables anoxic OM decomposition (Lovley and Phillips, 1988; Zhao et al., 2017). The net result of stabilizing and destabilizing effects of Fe oxides in paddy soils is not yet known.

This literature review shows that paddy soil development is not straight-forward. Characteristic biogeochemical processes seem to proceed at varying intensity. The underlying soil type used for paddy cultivation might play a role (Kögel-Knabner et al., 2010; Huang et al., 2015). Hence, this thesis addresses paddy soils deriving from different soil types.

1.2 Soil types under paddy management and their mineral properties

Managing soils for submerged paddy cultivation improves soil properties important for optimal rice growth. The soil's permeability is reduced, while pH and nutrient availability are increased (Greenland, 1997; Neue et al., 1997). Hence, a variety of soil types can be used for submerged paddy cultivation (Keersebilck and Soeprapto, 1985). These include Gleysols, Fluvisols, Vertisols, Cambisols, Alisols, Acrisols, Ferralsols, Lixisols, Luvisols, Ultisols, and Andosols (Moormann and van Breemen, 1978; Kögel-Knabner et al., 2010). This thesis focused on paddy soils (Hydragric Anthrosols) that derived from Alisols, Andosols, and Vertisols (Fig. 1.3).

Soils are open systems with water and acid input. The main source of acids are atmospheric CO₂ and CO₂ produced by plant roots and soil organisms forming carbonic acid (H₂CO₃) when dissolved in water. Roots and microorganisms further excrete organic acids. These acids are buffered by mineral weathering. Resulting solutes can be laterally or vertically removed with soil water or re-precipitate to form secondary minerals (Vitousek et al., 1997; Chadwick and Chorover, 2001). While Andosols are young soils rich in easily weatherable mineral phases, Alisols are at an advanced stage of weathering already containing rather stable secondary minerals (kaolinite and gibbsite) (Dahlgren et al., 1993; Jahn and Asio, 1998). Vertisols dominated by smectites are roughly in between since weathering of metastable smectites is limited due to restricted leaching of these naturally poorly drained soils (Ahmad, 1996). Hence, under natural conditions, Andosols, Alisols and, Vertisols weather quite differently.

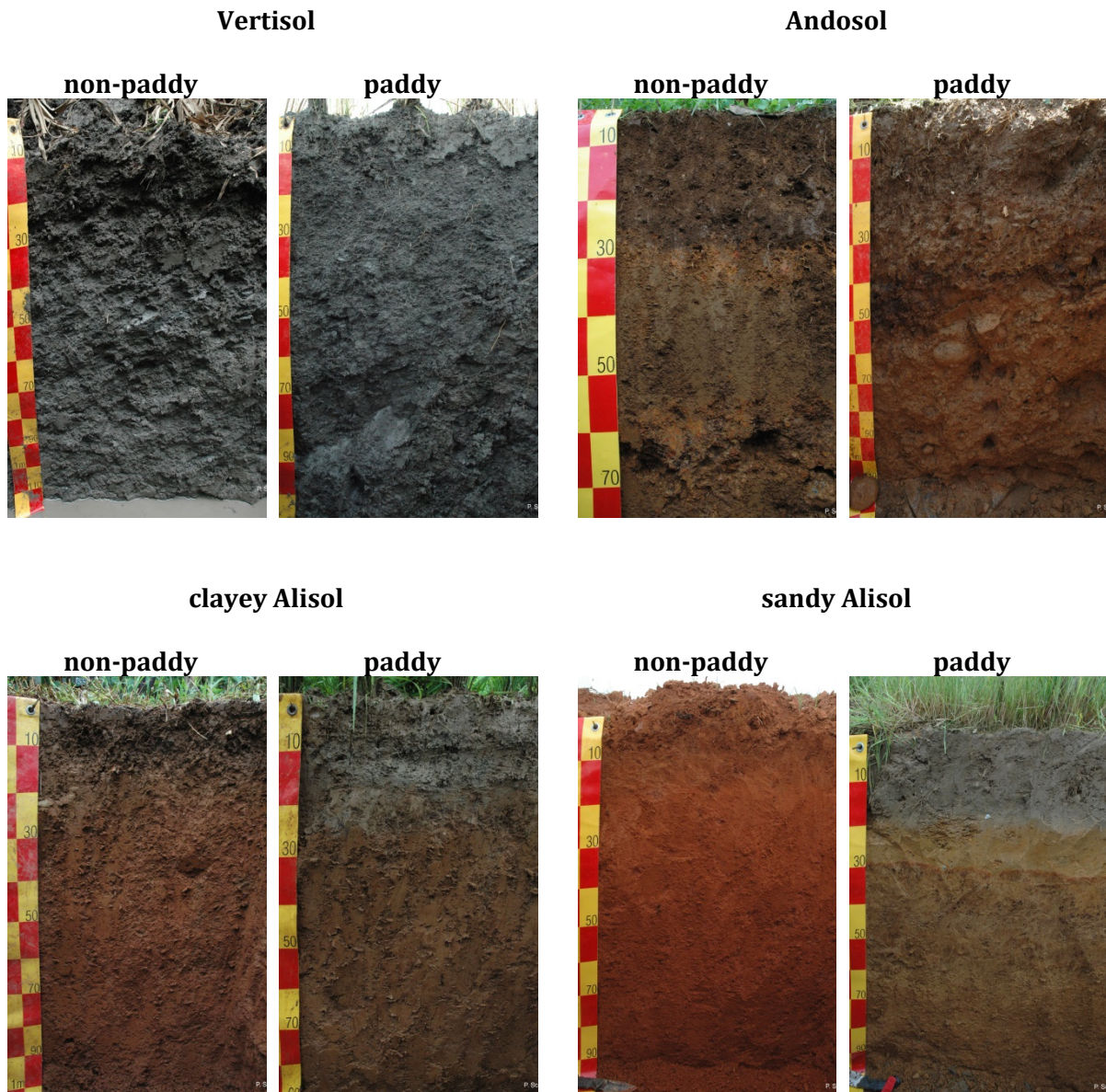


Fig. 1.3 Vertisol, Andosol, and Alisol under sugarcane (Vertisol) and vegetables (Andosol and Alisol) representing non-paddy study sites and neighboring paddy soils deriving from Vertisol, Andosol and Alisol; credit: Peter Schad, Chair of Soil Science, Technical University of Munich.

1.2.1 Andosols

In most cases, Andosols are derived from highly weatherable volcanic tephra. Weathering of tephra is faster than the crystallization of stable secondary minerals. Therefore, the formation of SRO, metastable phases (allophane, imogolite, ferrihydrite) is kinetically favored (Dahlgren et al., 1993; Chadwick and Chorover, 2001). The type of phase precipitating from the soil solution mainly depends on its pH, Si and OC content. Soil pH > 5 favors the formation of SRO Al-Si phases (Shoji et al., 1982; Parfitt and Saigusa, 1985). Precipitation of less than 1500 mm, a seasonal dry period or poor drainage of the soil support Si enrichment and the subsequent formation of Si-rich allophane (Al:Si = 1:1) and halloysite. In contrast, Si-poor soil solutions preferably result in

Al-rich allophane (Al:Si = 2:1) and imogolite (Parfitt et al., 1983; Shoji and Fujiwara, 1984; Parfitt et al., 1984; Dahlgren et al., 1993). At pH below 5 in combination with large amounts of OC the formation of Al-humus complexes instead of SRO Al-Si phases is facilitated (Shoji et al., 1982; Parfitt and Saigusa, 1985). These Al-humus complexes are responsible for the remarkable storage of OC in Andosols (Driessen and Dudal, 1991). Besides metastable Al-Si phases and Al-humus complexes, poorly crystalline Fe oxides (mainly ferrihydrite) precipitate due to the fast release of Fe²⁺ from the parent material and its immediate oxidation (Dahlgren et al., 1993). In more advanced stages of weathering the metastable phases transform to more crystalline and stable minerals (Dahlgren et al., 1993; Vitousek et al., 1997; Chadwick and Chorover, 2001). Dehydration and desilication of halloysite, allophane, and imogolite result in kaolinite and gibbsite (Violante and Wilson, 1983; Ndayiragije and Delvaux, 2003). Aging of ferrihydrite leads to goethite and/or haematite (Dahlgren et al., 1993; Malucelli et al., 1999; Cornell and Schwertmann, 2003). The presence of these stable minerals is indicative of the final stage of Andosol weathering and may eventually result in other soil types such as Acrisols and Ferralsols (Dahlgren et al., 1993; Jongmans et al., 1995; Joussein et al., 2005).

1.2.2 Alisols

Alisols, in contrast, are already at a more advanced stage of weathering. They mostly derive from mafic parent rocks and are dominated by a mineral assemblage comprising kaolinite, crystalline Fe oxides (Jahn and Asio, 1998; Funakawa et al., 2008) and variable amounts of high-activity clays, such as vermiculite or smectite with considerable cation exchange capacity (CEC) (FAO, 2006). Progressing weathering leads to a transition from high-activity clays to kaolinite and a subsequent decrease in CEC, resulting in Ferralsols (Driessen and Dudal, 1991; Bridges, 1997).

1.2.3 Vertisols

Most Vertisols are composed of weathering products from upland soils that are deposited in lowlands and are thus rich in clay. They are usually found in areas with distinct wet and dry season. During wet seasons, lowlands are susceptible to waterlogging so that primary minerals are weathered but leaching of weathering products is limited. This favors the crystallization of smectite during dry periods (Dudal, 1963; Ahmad, 1996). Hence, Vertisols contain large amounts of expanding smectites and are characterized by swelling during wet seasons and shrinking during dry seasons accompanied by slickenside and crack formation, respectively. Fine cracks near the surface lead to a granular soil structure (=self-mulching). Also, deep cracks form down to the subsoil, which become partially filled with surface granules. Upon re-wetting and swelling,

pressures are generated resulting in shearing and a mixing of surface and subsoil (= pedoturbation) (IUSS Working Group, 2006). Depending on drainage, pH and subsequent leaching rates, smectites might become instable. Silicon and alkali and earth alkali cations (mainly Ca^{2+} and Mg^{2+}) are washed out, while Al and Fe remain as kaolinite/Al oxides and Fe oxides, respectively (Ahmad and Jones, 1969; Ahmad, 1996).

1.3 Mineral-organic-carbon associations

The mineral assemblage of soils and potential mineral changes in soils under paddy management determine the stabilization of OM via mineral-organic carbon associations. Organic matter formed by plants via photosynthesis is the primary source of SOM (Kögel-Knabner, 2002). During photosynthesis, inorganic carbon is converted into OC by using solar energy to combine atmospheric CO_2 with water molecules. The resulting organic molecules provide fuel and biomass for the plants to grow. When the plants are consumed by animals, shed their leaves or die, their residues are finally added to the soil where microbes partly oxidize, and thus, mineralize them and release CO_2 back to the atmosphere. Hence, SOM comprises dead residues of plants, animals and microorganisms at different degradation stages as well as secondary products of decomposition (Lehmann and Kleber, 2015). The rate of decomposition depends on the environmental factors that influence microbial activity (soil temperature, moisture, pH, and aeration) as well as on the physical availability and chemical lability of the organic residues in the soil. In moist and warm climates SOM is decomposed more rapidly than in wet and cool climates. Organic residues that have been ground by the soil fauna provide an increased surface for microbial attack and labile substances such as sugars and proteins are more readily degraded than more recalcitrant substances such as cellulose and lignin (Van Breemen and Buurman, 2002; Charman and Murphy, 2007). The rate of decomposition in conjunction with the input of organic residues determines the storage of OC in the soil. Besides promoting soil fertility, SOM plays an important role in climate change. Carbon that is stored in soils does not contribute to the greenhouse effect in the atmosphere. Hence, soils serve as sink for CO_2 and other greenhouse gases (Vitousek et al., 1997).

From the biochemical point of view, all naturally formed molecules are completely microbially degradable given the respective microorganisms are present and environmental conditions are favorable (Marschner et al., 2008; Lehmann and Kleber, 2015). However, SOM that is hundreds to thousands of years old exists in soils because it is protected against microbial decomposition through interaction with minerals (Baldock and Skjemstad, 2000; Lützow et al., 2006; Han et al., 2016). In the early stage of decomposition, fresh plant debris present as free particulate OM is usually quickly decomposed, with preferential mineralization of the more easily degradable

biomolecules. The partly decomposed OM is thus enriched in the relatively recalcitrant biomolecules. The microbes colonizing the particulate OM excrete metabolites which glue minerals to the particulate OM. The resulting occluded particulate OM is degraded more slowly due to the surrounding minerals, which physically prevent access of microorganisms and their exoenzymes. The metabolites of active microorganisms (polysaccharides and proteins) as well as biopolymers released by autolyzing dead microorganisms are rich in functional groups enabling the interaction of the microbial-derived OM with minerals of the clay fraction (mainly Fe/Al oxides and clay minerals) (Oades, 1993; Baldock and Skjemstad, 2000; Six et al., 2000). The resulting mineral-associated OM is chemically protected against decomposition, and thus, least degradable. The interaction of OM and mineral surfaces is based on several binding mechanisms. In acidic soils, ligand exchange between singly coordinated, protonated hydroxyl groups of minerals (especially Fe and Al oxides, allophane and imogolite with large specific surface area (SSA) and deprotonated carboxyl groups of OM leads to strong inner-sphere complexes (Fig. 1.4) (Gu et al., 1994; Kleber et al., 2005; Kaiser and Guggenberger, 2007; Mikutta et al., 2007).

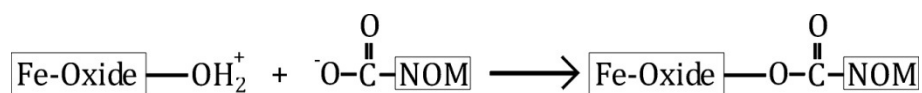


Fig. 1.4 Example for ligand exchange resulting in an inner-sphere complex (from Gu et al., 1994).

Besides the usually deprotonated and hence negatively charged carboxyl groups of OM, there are also amino groups, which have an alkaline point of zero charge and are thus protonated and positively charged in acidic soils. The portion of amino groups on SOM is small compared to carboxyl groups. However, those that are present can form ionic bonds with negatively charged surfaces of clay minerals. This binding mechanism is equivalent to cation exchange (Sørensen, 1972; Lützwow et al., 2006). If multivalent cations are present (Ca^{2+} and Mg^{2+} in alkaline soils or Al^{3+} and Fe^{3+} in strongly acidic soils), negatively charged carboxyl groups may also bind to negatively charged clay mineral surfaces via cation bridges (Oades, 1988; Kayler et al., 2011). The resulting outer-sphere complexes are weaker than the inner-sphere complexes formed through ligand exchange (Kleber et al., 2015). Uncharged OM may also interact with soil minerals by van-der-Waals forces as well as hydrogen bonds and hydrophobic interactions (Schulten and Leinweber, 2000). Van-der-Waals forces allow the interaction of organic molecules with uncharged mineral surfaces of, e.g., kaolinite and quartz. Here, two apolar molecules approaching each other mutually distort their electron clouds thereby inducing temporary dipoles that attract each other (Maréchal, 2007; Mikutta et al., 2007; Singh et al., 2018). If a large organic molecule interacts this way with a mineral surface, the van-der-Waals

forces are additive and may result in strong binding (Kleber et al., 2015). Hydrogen bonds form between OM and cations adsorbed to mineral surfaces as well as between OM already associated with minerals and OM not yet associated with minerals (Piccolo, 2001; Lützow et al., 2006). If a hydrogen atom is covalently bound to an electronegative atom, the hydrogen atom exhibits a positive partial charge. That positive partial charge is attracted by the negative partial charge of the electronegative atom of another molecule (Maréchal, 2007). The resulting hydrogen bonds are also referred to as dipole-dipole interactions. Finally, hydrophobic interactions bind organic molecules to other organic molecules that are already associated with minerals. Here, apolar, and thus, hydrophobic parts of OM group together and in doing so exclude water (Piccolo et al., 1996; Lützow et al., 2006; Kleber et al., 2015).

Besides the interaction of OM with mineral surfaces (adsorption), OM may also be occluded in mineral phases through co-precipitation (Henneberry et al., 2012; Lalonde et al., 2012; Mikutta et al., 2014; Herndon et al., 2017). Especially in soils with redox fluctuation and respective Fe dynamics, the formation of Fe-OM co-precipitates contributes to the stabilization of OM (Chen et al., 2014).

1.4 Objectives

The main objective of the thesis was to assess redox-mediated changes in mineral composition and mineral-associated organic matter (OM) during paddy soil formation from different parent soil types. Since redox-sensitive, Fe oxides were of special interest with the cycling of Fe being coupled to the cycling of OC via microorganisms. The following research questions were addressed:

1. Do several decades of paddy management have an effect on minerals and OC stocks of Vertisol, Alisol, and Andosol?
2. Do several decades of redox fluctuation in Alisol- and Andosol-derived paddy soils result in increasing or decreasing Fe oxide crystallinity?
3. What is the effect of Alisol and Andosol incubation with eight redox cycles on OM turnover and microbial communities? Do we find similar effects in the field paddy soils?
4. Do Fe oxide dynamics in paddy soils promote OC stabilization?
5. Do paddy management induced processes described above depend on the initial soil type?

2 Response of Vertisols, Andosols, and Alisols to paddy management

P. Winkler, K. Kaiser, A. Kölbl, T. Kühn, P. Schad, L. Urbanski, S. Fiedler, E. Lehndorff, K. Kalbitz, S.R. Utami, Z. Cao, G. Zhang, R. Jahn, I. Kögel-Knabner

P.W. wrote the manuscript; S.R.U., Z.C. and G.Z. coordinated soil sampling; P.W., K. Kaiser, P.S. and E.L. conducted soil sampling; P.W., A.K., T.K., L.U., S.F. and E.L. measured samples and analyzed data; I.K.-K., A.K., K. Kaiser, K. Kalbitz, S.F., R.J. designed the study; all authors commented on the manuscript

Published in Geoderma (2016) 261: 23-35.

2.1 Abstract

Interchanging submergence and drainage in paddy soils induce alternating redox conditions. It is known that this causes changes in organic carbon stocks, in amounts and crystallinity of Fe oxides as well as transformation of clay minerals and subsequent changes in cation exchange capacity (CEC). However, the influence of the initial soil type on the extent of these changes is not yet well understood. Therefore, we studied paddy soils that derived from three different soil types (Vertisols, Andosols, Alisols) on volcanic parent material on Java (Indonesia). To account for the variability in parent materials, we additionally sampled sandstone-derived Alisols in China. Adjacent non-paddy soils were sampled as references. Samples were analyzed for texture, bulk density, clay mineral composition, total element content, pH, CEC, phosphorus retention, organic carbon (OC), and acid oxalate- (Fe_{AAO}) and dithionite–citrate–bicarbonate-extractable Fe (Fe_{DCB}).

Only the Alisol-derived paddy soil in China showed textural changes, compared to the non-paddy soil. Evidence for paddy management induced ferrolysis was not found. The smaller topsoil clay content in the paddy soil is most probable caused by clay migration. Only minor differences in clay minerals were found; topsoils of Andosol-derived paddy soils, however, tend to be less desilicated, indicating phytolith accumulation. Except for Vertisols, paddy management caused significant depletion in Fe oxides in the topsoils (puddled layer and plough pan) due to redox processes. The extent to which the reduced Fe was leached or re-oxidized as SRO Fe oxides depended on the soil texture. Andosols and sandy Alisols facilitated leaching, clayey Alisols re-oxidation. In either case, the stocks of crystalline Fe oxides diminished, causing increased proportions of SRO Fe oxides. Retention of phosphorus was directly related to changes in the absolute amounts of SRO Fe oxides. An accumulation of Fe oxides in paddy subsoils was not found. Lateral transport with drainage water might be a reason. In highly permeable soils with large vertical water fluxes (e.g., Andosols under paddy management), colloidal transport might also play a role. Despite losses in potential OC storage capacity (i.e., Fe oxides, clay minerals, allophane), paddy soils derived from Andosols and sandy Alisols in China had larger OC concentrations in the puddled topsoil, whereby the other soils showed no increase in OC under paddy management. Therefore, paddy management does not necessarily enhance carbon sequestration. Rather, differences in organic matter input between non-paddy and paddy soils seem to determine whether OC is accumulated under paddy management or not. Effects of paddy management on CEC were little and mainly due to OC accumulation and Fe oxide coating removal from clay minerals.

Overall, paddy management-induced changes were partly influenced by the original soil and the parent material. In turn, the main characteristics of the initial soil type were preserved and not overridden by paddy management.

2.2 Introduction

Rice paddy cultivation includes ploughing of waterlogged soils, causing dispersive homogenisation of topsoils (= puddling). Beneath, a dense plough pan is generated that allows for submerging the topsoil throughout the growing season. Submergence impairs O₂ supply, and so, continuing microbial activity induces anoxic conditions. Before harvest, the soil is drained and O₂ is available again. Hence, paddy management causes sharply alternating redox conditions in topsoils, including the plough pan (Ponnamperuma, 1972; Kirk, 2004; Kögel-Knabner et al., 2010).

When O₂ becomes deficient in soil, alternative electron acceptors are used in the metabolic decomposition of organic matter (OM). Due to their abundance, the redox-sensitive Fe oxides are major alternative electron acceptors and therefore play a crucial role in paddy soil evolution (Ponnamperuma, 1972; Patrick Jr., 1981; Kirk, 2004). Anoxic conditions in paddy soils cause reductive Fe oxide dissolution. Dissolved Fe²⁺ can be leached into the more oxic subsoil, where it re-oxidizes to Fe³⁺ and subsequently re-precipitates (Yu, 1985; Kyuma, 2004). Dissolved Fe²⁺ remaining in the topsoil after drainage is also re-oxidized and re-precipitated there, mainly forming SRO oxides (Kirk, 2004). Overall, paddy cultivation decreases the total amounts of Fe oxides in the topsoil due to reductive Fe dissolution and leaching (Yu, 1985; Kyuma, 2004), whereby the remaining part shows an increased proportion of SRO Fe oxides (Moormann and van Breemen, 1978; Wang et al., 1993). Paddy subsoils are characterized by Fe oxide accumulation (Tan, 1968; Okazaki et al., 1981; Kölbl et al., 2014). However, according to Kyuma and Kawaguchi (1966) subsoil accumulation is missing in ground water-affected paddy soils.

Since Fe oxides act as major anion adsorbers in soils, paddy management induced changes in Fe oxides can affect the availability of phosphorus (Cornell and Schwertmann, 2003). Dissolution of Fe oxides and subsequent pH increases under anoxic conditions initially releases phosphorus (Kirk et al., 1990; Chacon et al., 2006). In the long term, however, increasing proportions of SRO Fe oxides due to interchanging redox conditions may increase phosphorus retention in paddy soils (Willett and Higgins, 1978).

Reductive dissolution of Fe oxides also affects other soil properties such as pH, CEC, clay mineralogy and texture. As described by Brinkman (1970), Fe²⁺ ions released under anoxic conditions may displace other cations from their exchange sites. The displaced cations are leached from the soil while upon recurring oxic conditions Fe²⁺ is oxidized. Subsequent hydrolysis of the formed Fe³⁺ results in precipitation of Fe^{III} oxides and releases H⁺. Consequently, the soil pH decreases over time. Progressing acidification may cause Al hydroxyl interlayering of 2:1 clay minerals as well as complete dissolution of clay minerals, resulting in a decrease in the soil's CEC and clay content. That process, proposed by Brinkman (1970), is called ferrollysis and considered being characteristic for paddy soils but is still controversially debated

(Eaqub and Blume, 1982; Van Ranst and De Coninck, 2002). Some authors, in contrast, found increases in pH and CEC in paddy soils (Roth et al., 1969; Favre et al., 2002).

Storage of OC is thought to be affected by paddy management as well. Anoxic decomposition of OM is assumed to be less efficient than oxic decomposition. Thus, frequent inundation leads to reduced rates of OM decomposition (Sahrawat, 2004; Sahrawat, 2005), which may result in increases in OM storage (Cheng et al., 2009; Kögel-Knabner et al., 2010). Most OM storage under paddy management is restricted to the puddled layer (Roth et al., 2011; Chen et al., 2011; Wissing et al., 2011; Kalbitz et al., 2013; Bräuer et al., 2013). The paddy-specific dense plough pan prevents OM from entering deeper soil layers, likely due to less deep rooting and diminished vertical water fluxes (Janssen et al., 2006; Janssen and Lennartz, 2006; Janssen and Lennartz, 2007; Kalbitz et al., 2013). Thus, the dense plough pan decouples topsoil from subsoil OM cycling (Wissing et al., 2011; Kalbitz et al., 2013). In addition to the numerous publications that show OM accumulation in paddy soils, Kirk (2004) and Kögel-Knabner et al. (2010) reviewed studies that are not in line with that generally accepted theory. These contrasting results indicate that paddy cultivation may not necessarily lead to OM accumulation but that factors such as OM input (residue management), decomposition rates depending on the availability of alternative electron acceptors (mainly Fe), and OM stabilization by clay minerals and Fe oxides play an essential role. When considering the wide range of different soil types transformed into paddy soils, the question raising is to what extent the initial soils, differing strongly in mineral assemblage and OM, direct paddy development. One scenario could be that paddy conditions overrule in little time all original differences. The other possibility is that paddy soils, at least partly, retain certain properties of the initial soil (e.g. Huang et al., 2015). Therefore, the present study aims at investigating the response of soil type-specific soil parameters to paddy management by direct comparison of paddy and non-paddy agricultural soils. The study focused on major soil types used for rice cultivation in Asia: Andosols, Vertisols, and Alisols. The sensitivity of the different soil types to paddy management-induced changes might be of practical importance.

We addressed the topic by studying paddy soils that derived from soils with volcanic parent material on Java (Indonesia). Soil types with contrasting mineralogy were selected: Vertisols, characterized by large amounts of smectites and little Fe oxides; Andosols, dominated by highly reactive minerals (e.g., allophane and ferrihydrite), and Alisols with kaolinite, gibbsite, and crystalline Fe oxides. To account for the variability of parent materials, we additionally sampled sandstone-derived Alisols in China. Results for each soil type are discussed in detail in section 2.4, while the direct comparison between soil types is presented in section 2.5.

2.3 Materials & Methods

2.3.1 Investigation area & soil sampling

We sampled sites where Vertisols, Andosols, and Alisols developed from similar geological substrates and under similar climatic conditions on Java (Indonesia) (Fig. 2.1). The geology of Java is dominated by volcanic rocks, varying from dacites and andesites to basalts (Tan, 2008). The island has tropical monsoon climate, with more intense droughts towards the east (Tan, 2008).

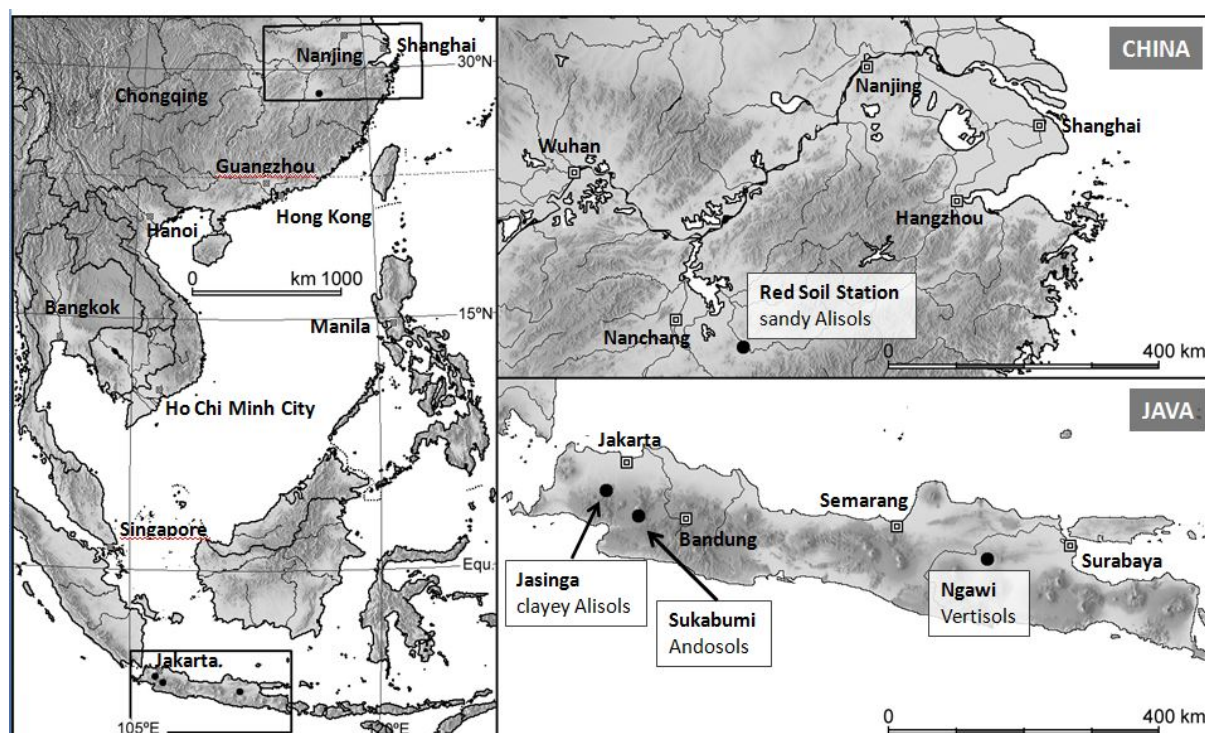


Fig. 2.1 Maps of the sampling sites in China and on Java (Indonesia); credit: Reinhold Jahn, Chair of Soil Science and Soil Protection, Martin Luther University Halle-Wittenberg.

2.3.2 Laboratory analyses of the bulk soil

Particle-size distribution of the <2 mm fraction was determined for the main sites of Alisols (China and Java) and Vertisols, after removal of OM with H_2O_2 . Dispersion was achieved with $Na_4P_2O_7$ (Vertisol) or by adjusting the solution pH to 8 with NaOH (Alisols). The sand content was obtained via wet-sieving with a 63- μ m screen, and silt and clay were determined by sedimentation and X-ray absorption (Sedigraph 5100, Micromeritics Corp, Norcross, GA, USA). Soil texture classes of Andosol sites were estimated by field tests according to FAO (2006). Soil pH was determined potentiometrically in 0.02 M $CaCl_2$ at a soil-solution ratio of 1:2.5. Suspensions were shaken for 5 min, and then allowed to settle for 1 h.

Determination of the potential CEC (CEC_{pot}) and exchangeable cations were carried out using ammonium acetate at pH 7 and KCl (Hendershot et al., 2008). Concentrations of extracted Ca, Mg, K, and Na were determined by inductively coupled plasma–optical emission spectroscopy (ICP-OES, Ultima 2, Horiba Jobin-Yvon S.A.S., Longjumeau, France); ammonium in KCl extracts was determined using an automated photometer (SANplus, Skalar Analytical B.V., Breda, The Netherlands).

Phosphorus retention was analysed according to the New Zealand method (Blakemore et al., 1981) by equilibrating the soil with a KH_2PO_4 solution and determining the remaining phosphorus in solution with a photometer (SPECORD 205, Analytik Jena AG, Jena, Germany).

Total carbon concentrations (TC) were determined by dry combustion at 950°C using a Vario MAX elemental analyser (Elementar Analysensysteme GmbH, Hanau, Germany). Since all samples of the Alisol and Andosol sites were free of carbonate, the TC concentration equals the OC concentration. Inorganic carbon (IC) contents of Vertisol samples were determined by dissolution of carbonates with 42% phosphoric acid and subsequent infrared detection of the evolving CO_2 (C-MAT 550, Ströhlein GmbH, Viersen, Germany). For Vertisol samples, OC was calculated by subtracting the concentration of IC from TC.

Total pedogenic Fe oxides were determined by dithionite–citrate–bicarbonate extraction (Fe_{DCB}) as outlined by Mehra and Jackson (1960). Extraction of SRO Fe oxide fraction (Fe_{AAO}) and allophane and imogolite-type phases (Si_{AAO} and Al_{AAO}) was carried out with acid ammonium oxalate at pH 3.0 and 2 h shaking in the dark according to Schwertmann (1964). The concentrations of extracted Fe, Al, and Si were determined by ICP-OES (Ultima 2). All analyses were done in duplicate or triplicate. The ratio of Fe_{AAO} to Fe_{DCB} is indicative of the contribution of SRO Fe oxide phases to total Fe oxides, and the difference between Fe_{DCB} and Fe_{AAO} allows for estimating the content of more crystalline Fe oxides (Fe_c). Contents of allophane and imogolite-type phases were estimated using a slightly modified version of the formula by Parfitt and Wilson (1985):

$$\text{Allophane \& imogolite – type phases [\%]} = 100 * \frac{Si_{ox}}{23.4 - 5.1 * \left(\frac{Al_{ox}}{Si_{ox}}\right)} \quad (2.1)$$

We did not extract Al with pyrophosphate to correct Al_{AAO} for organically bound Al since several studies showed that pyrophosphate is not selective for organically bound Al but may additionally extract considerable amounts of SRO Al phases (summarized by Bertsch and Bloom, 1996). In addition, OC contents of the examined Andosols were relatively small and $pH > 4.5$, which inhibits the release of Al ions from Al hydroxo phases. Therefore, we suppose estimation of allophane and imogolite-type phases is more accurate this way.

Bulk density was calculated according to Blake and Hartge (1986) by dividing the mass of oven dry soil (105°C) by the sampled core volume. Stocks of Fe oxides as well as of OC were calculated for each horizon by multiplying the respective concentrations, thickness, and bulk density. Stocks of Andosols were additionally corrected for rock contents. Total stocks for each profile were derived by summing up stocks of individual horizons down to 100 cm.

Total element concentrations of all samples were measured by X-ray fluorescence spectroscopy (XRF) (SRS 3000, Siemens AG, Germany, wavelength dispersive with Rh tube) of pressed pellets. Uniformity of parent material at non-paddy and paddy sites was tested by using a common indicator, the ratio of the largely immobile elements Ti and Zr (Finlow-Bates and Stumpfl, 1981; Buurman et al., 2004). Nevertheless, it should be noted that several studies pointed out that under certain circumstances Ti and Zr might be mobilized; thus, their ratio is not always suitable to test for parent material uniformity (Hodson, 2002; Anda et al., 2009). In addition, the Si/Zr ratio was calculated as indicator for desilication.

All quantitative data were corrected to an oven-dry (105°C) basis. The qualitative mineral composition of the fine earth (<2 mm) and clay fractions of topsoils was determined on powder (bulk soil) and orientated (clay fraction) specimens, using X-ray diffraction (XRD) (D5005, Siemens AG, Karlsruhe, Germany) with Cu K α -radiation ($\lambda = 1.541$ nm). Clay minerals were identified according to Moore and Reynolds (1997) after saturation with 1 M MgCl₂ or 1 M KCl.

2.4 Results & Discussion

The non-paddy Alisols and Vertisols had similar Ti/Zr ratios as their paddy-managed counterparts (sandy Alisols ≈ 15 , clayey Alisols and Vertisol ≈ 30). Hence, we assume parent material uniformity. Slightly higher Ti/Zr ratios throughout the Andosol profiles under paddy management (45 vs. 35) indicate a small difference in parent material for the non-paddy and paddy sites. This is linked to the fact that the Andosols formed on a lahar, which consists of a heterogeneous mixture of different volcanic materials.

2.4.1 Vertisols

Vertisols had a clayey texture not affected by paddy management (Tables 2.1 and 2.2), which constrains water movement. The site is characterized by high groundwater level, usually <2 m beneath the soil surface. Therefore, drainage might be impeded and the amplitude of redox alternation diminished. In addition, vertical leaching of solutes and colloids is at a minimum. Hence, paddy management-induced processes, e.g., dissolution and removal of Fe oxides,

conversion and destruction of clay minerals, are minimal. At the same time, fresh clay minerals and nutrients are supplied regularly since the soil is situated in a floodplain and irrigated with groundwater. For those reasons and due to the Vertisol-inherent self-mulching, we found hardly any changes in the Vertisols under paddy management. Smectites dominating Vertisols (Fig. 2.2) are capable to stabilize some OC but are much less effective than Fe oxides (Mikutta et al., 2007). Consequently, OC concentrations and stocks remained similar (Fig. 2.3); the OC stocks were among the smallest of the soils under study (6-8 kg m⁻²). Vertisols and Vertisol-derived paddy soils had only very small amounts of Fe oxides (Fig. 2.4-2.7) due to the sedimentary nature of the parent material; nevertheless, the portions of SRO Fe oxides in the topsoils increased upon paddy management (Tables 2.1 and 2.2). While the non-paddy topsoils still contained a reddish component (color = 10 YR), the respective paddy soils partly missed that component (color = 2.5Y – 10YR).

2.4.2 Andosols

Andosols had a silty loam texture that was not affected by paddy management. Its low-density structure is prone to compaction under paddy management, as indicated by the formation of a rather dense plough pan and relatively dense subsoils (Tables 2.1 and 2.2).

Besides the minerals identified by XRD (Fig. 2.2), Andosols contained allophane and imogolite-type phases. Contents ranged from 17 to 46% (mean = 29% ± 2.4) in non-paddy and from 10 to 17% (mean = 12% ± 0.4) in respective paddy soils. Molar Si_{AAO}/Al_{AAO} ratios were 1:2 throughout non-paddy and paddy profiles. This ratio is characteristic for proto-imogolite allophanes (Levard et al., 2012). The constant ratio with soil depth points at little to no effect of organically complexed Al and supports the use of the modified formula for estimating contents of allophane and imogolite-type phases. Considering similar initial parent material, the smaller content of allophane and imogolite-type phases in Andosol-derived paddy soils indicates its accelerated weathering under paddy management. As a result, halloysite is formed, as suggested by the more pronounced halloysite reflection in paddy samples (Fig. 2.2).

Table 2.1 Site description, horizons, texture, bulk density (BD), pH, potential cation exchange capacity (CEC_{pot}), base saturation (BS), phosphorus (P) retention, total Fe contents (Fe_{total}), proportion of pedogenic Fe oxides (Fe_{DCB}/Fe_{total}), and proportion of short range-ordered Fe oxides (Fe_{AAO}/Fe_{DCB}) of the non-paddy sites. Where data were obtained for main and subsite samples, the means ± standard errors (n=3) are given.

Location & climate	Parent material	Soil type	Horizons		Sand [%]	Silt [%]	Clay [%]	BD [g cm ⁻³]	pH CaCl ₂	CEC _{pot} [cmol _c kg ⁻¹]	BS [%]	P-retent. [%]	Fe _{total} [g kg ⁻¹]	Fe _{DCB} /Fe _{total}	Fe _{AAO} /Fe _{DCB}
			Depth [cm]	Identifier											
Indonesia East-Java Ngawi 22-31°C 2500-6700 mm	alluvial-volcanic material	Pellic Vertisol (Protocalcic, Grumic, Hypereutric, Humic, Mollic)	0-10	Ah1	15	17	68	0.82 ±0.06	5.5 ±0.2	79 ±3	75 ±2	34	68.5 ±1.3	0.09	0.58
			10-21	Ah2	27	14	59	0.94 ±0.08	5.8 ±0.0	83 ±1	75 ±1	34	69.7 ±1.1	0.09	0.57
			21-29	Bw	22	11	66	0.96 ±0.03	6.3 ±0.1	84 ±0	78 ±3	30	68.6 ±0.9	0.09	0.56
			29-50	Bwi1	12	15	73	0.97 ±0.03	6.7 ±0.1	83 ±1	80 ±1	26	70.9 ±1.0	0.08	0.53
			50-90	Bwi2	15	14	71	1.02 ±0.02	7.2 ±0.2	84 ±1	83 ±4	22	71.9 ±0.3	0.07	0.32
90-113+	Bwi3	14	14	72	0.99 ±0.03	7.4 ±0.1	83 ±1	87 ±6	20	73.3 ±0.4	0.07	0.26			
Indonesia West-Java Sukabumi 21°C 2300-6700 mm	andesitic pyroclastics (lahar of Gede volcano)	Dystric Silandic Andosol (Loamic, Thixotropic)	0-10	Ah1	silt loam			0.67 ±0.03	4.6 ±0.1	70 ±1	6 ±2	97	96.4 ±1.4	0.44	0.38
			10-22	Ah2	silt loam			0.65 ±0.02	4.6 ±0.1	70 ±2	5 ±2	98	93.0 ±1.2	0.46	0.39
			22-35	BwAh	silt loam			0.51 ±0.03	5.2 ±0.3	82 ±3	5 ±2	99	107.0 ±6.2	0.46	0.49
			35-59	Bw1	silt clay loam			0.53 ±0.03	5.2 ±0.1	80 ±4	9 ±3	99	107.2 ±0.5	0.52	0.37
			59-78	Bw2	silt clay loam			0.63 ±0.06	5.6 ±0.1	81 ±6	13 ±2	99	131.6 ±20.6	0.47	0.43
78-103+	Bw3	silty clay			0.63 ±0.10	5.5 ±0.3	83 ±6	13 ±5	99	104.5 ±2.1	0.54	0.42			
Indonesia West-Java Jasinga 26°C 1900-4700 mm	andesitic tuffs	Chromic Abruptic Alisol (Pantoclayic, Humic, Hyperallic)	0-9	Ah1	16	44	40	0.83 ±0.10	4.4 ±0.4	39 ±1	16 ±10	47	85.8 ±2.1	0.67	0.06
			9-18	Ah2	13	46	41	0.88 ±0.08	4.4 ±0.5	39 ±1	15 ±10	49	90.0 ±2.3	0.65	0.07
			18-34	B(t)o1	9	44	48	0.94 ±0.09	4.5 ±0.5	38 ±2	13 ±10	51	90.7 ±3.6	0.65	0.06
			34-63	B(t)o2	4	17	79	0.90 ±0.04	4.3 ±0.1	46 ±2	7 ±2	58	94.6 ±2.2	0.67	0.03
			63-87	B(t)o3	3	22	75	0.91 ±0.01	4.2 ±0.0	47 ±2	4 ±1	63	96.3 ±1.2	0.66	0.04
87-101+	B(t)o4	26	37	38	0.93 ±0.09	4.2 ±0.0	41 ±4	3 ±1	66	124.7 ±28.6	0.66	0.03			
China Jiangxi province Yingtian 18°C 1625 mm	red Cretaceous sandstones with some basalt	Chromic Alisol (Aric, Cutanic, Hyperallic, Pantoloamic)	0-10	Ap1	64	16	20	1.16 ±0.03	4.6 ±0.3	18 ±1	19 ±4	25	40.8 ±1.8	0.61	0.05
			10-19	Ap2	56	17	27	1.35 ±0.03	4.3 ±0.1	18 ±1	15 ±4	29	43.1 ±2.0	0.61	0.04
			19-30	Bt1	57	17	27	1.28 ±0.06	4.1 ±0.0	13 ±0	9 ±1	37	46.4 ±1.9	0.58	0.04
			30-51	Bt2	48	19	33	1.22 ±0.03	4.0 ±0.1	15 ±0	7 ±0	40	49.0 ±1.0	0.62	0.03
			51-80	Bt3	42	21	37	1.24 ±0.07	4.1 ±0.1	14 ±1	9 ±0	39	51.2 ±1.1	0.61	0.03
80-102+	Bt4	49	18	32	1.28 ±0.07	4.1 ±0.0	14 ±0	5 ±0	38	50.5 ±0.3	0.61	0.03			

Table 2.2 Site description, horizons, texture, bulk density (BD), pH, potential cation exchange capacity (CEC_{pot}), base saturation (BS), phosphorus (P) retention, total Fe contents (Fe_{total}), proportion of pedogenic Fe oxides (Fe_{DCB}/Fe_{total}), and proportion of short range-ordered Fe oxides (Fe_{AAO}/Fe_{DCB}) of the respective paddy sites. Where data were obtained for main and subsite samples, the means ± standard errors (n=3) are given.

Location	Initial soil type	Soil type	Horizons		Sand [%]	Silt [%]	Clay [%]	BD [g cm ⁻³]	pH CaCl ₂	CEC _{pot} [cmol _c kg ⁻¹]	BS [%]	P-retent. [%]	Fe _{total} [g kg ⁻¹]	Fe _{DCB} /Fe _{total}	Fe _{AAO} /Fe _{DCB}
			Depth [cm]	Identifier											
Indonesia East-Java Ngawi	Vertisol	Hydragric Anthrosol (Protocalcic, Pantoclayic, Hypereutric, Vertic)	0-8	Alp1	26	21	54	0.92 ± 0.01	6.7 ± 0.1	80 ± 1	80 ± 2	37	69.4 ± 2.6	0.09	0.74
			8-18	Alp2	8	20	72	1.04 ± 0.04	7.0 ± 0.0	80 ± 0	78 ± 1	37	69.8 ± 2.1	0.09	0.69
			18-25	Aidp	8	16	76	1.03 ± 0.02	7.2 ± 0.1	81 ± 1	78 ± 0	30	73.9 ± 3.5	0.07	0.61
			25-45	Bwi	12	14	74	1.00 ± 0.03	7.2 ± 0.1	82 ± 1	81 ± 3	25	75.3 ± 1.5	0.06	0.41
			45-80	Bigc	5	17	78	1.01 ± 0.02	7.3 ± 0.1	82 ± 0	81 ± 3	23	75.0 ± 1.4	0.06	0.29
			80-105+	Bikgc	19	17	64	0.99 ± 0.03	7.5 ± 0.2	82 ± 1	83 ± 2	24	71.7 ± 3.8	0.07	0.25
Indonesia West-Java Sukabumi	Andosol	Hydragric Anthrosol (Andic, Dystric, Escalic, Loamic)	0-9	Alp1	silt loam			0.67 ± 0.04	5.0 ± 0.0	76 ± 0	20 ± 0	78	59.3 ± 7.5	0.40	0.40
			9-22	Alp2	silt loam			0.76 ± 0.03	5.0 ± 0.0	76 ± 0	21 ± 1	79	62.4 ± 5.4	0.39	0.43
			22-31	Aldp	silt loam			0.84 ± 0.06	5.3 ± 0.1	72 ± 2	24 ± 1	78	63.9 ± 2.2	0.35	0.37
			31-54	Bgc1	clay loam			0.86 ± 0.01	6.0 ± 0.1	70 ± 1	24 ± 1	82	123.5 ± 8.0	0.47	0.19
			54-78	Bgc2	clay loam			0.78 ± 0.03	6.2 ± 0.1	73 ± 1	24 ± 1	91	92.3 ± 2.2	0.41	0.30
			78-107+	Bw	clay loam			0.72 ± 0.02	6.2 ± 0.1	72 ± 1	26 ± 1	88	93.1 ± 1.5	0.40	0.34
Indonesia West-Java Jasinga	clayey Alisol	Hydragric Anthrosol (Alic, Clayic, Dystric, Escalic)	0-7	Alp1	13	50	37	0.88 ± 0.03	4.2 ± 0.0	41 ± 0	23 ± 1	57	74.3 ± 1.6	0.57	0.25
			7-16	Alp2	6	53	41	0.97 ± 0.02	4.3 ± 0.0	43 ± 1	22 ± 1	60	74.4 ± 2.6	0.56	0.24
			16-22	Alcdp	7	50	43	1.13 ± 0.04	4.6 ± 0.1	42 ± 1	27 ± 4	49	86.5 ± 4.2	0.57	0.10
			22-50	B(t)gc1	5	29	66	0.97 ± 0.01	4.4 ± 0.0	43 ± 1	12 ± 2	57	106.5 ± 1.1	0.60	0.03
			50-75	B(t)gc2	7	35	58	0.93 ± 0.00	4.3 ± 0.0	46 ± 2	9 ± 2	58	100.9 ± 3.7	0.62	0.02
			75-95+	B(t)gc3	3	41	57	0.88 ± 0.02	4.2 ± 0.0	48 ± 3	7 ± 1	57	104.5 ± 4.7	0.60	0.02
China Jiangxi province Yingtang	sandy Alisol	Hydragric Anthrosol (Alic, Endoclayic, Dystric, Escalic, Amphiloamic)	0-9	Alp1	58	29	13	0.89 ± 0.04	4.3 ± 0.1	14 ± 1	14 ± 1	27	21.2 ± 1.8	0.43	0.15
			9-16	Alp2	58	27	15	0.93 ± 0.05	4.3 ± 0.0	14 ± 0	13 ± 1	28	20.4 ± 1.2	0.43	0.16
			16-20	Ardp	71	19	10	1.58 ± 0.01	4.3 ± 0.0	11 ± 0	12 ± 0	26	20.4 ± 0.2	0.43	0.15
			20-30	Bl	55	28	17	1.45 ± 0.03	4.4 ± 0.1	14 ± 1	12 ± 2	32	59.6 ± 1.6	0.62	0.05
			30-43	Bg1	50	26	24	1.43 ± 0.03	4.8 ± 0.2	17 ± 1	17 ± 2	34	52.6 ± 3.1	0.60	0.08
			43-57	Bg2	36	36	28	1.37 ± 0.03	5.1 ± 0.0	20 ± 1	21 ± 0	38	47.2 ± 2.4	0.60	0.09
			57-100+	Bg3	19	38	43	1.27 ± 0.05	5.4 ± 0.1	21 ± 1	27 ± 2	50	44.9 ± 5.2	0.56	0.06

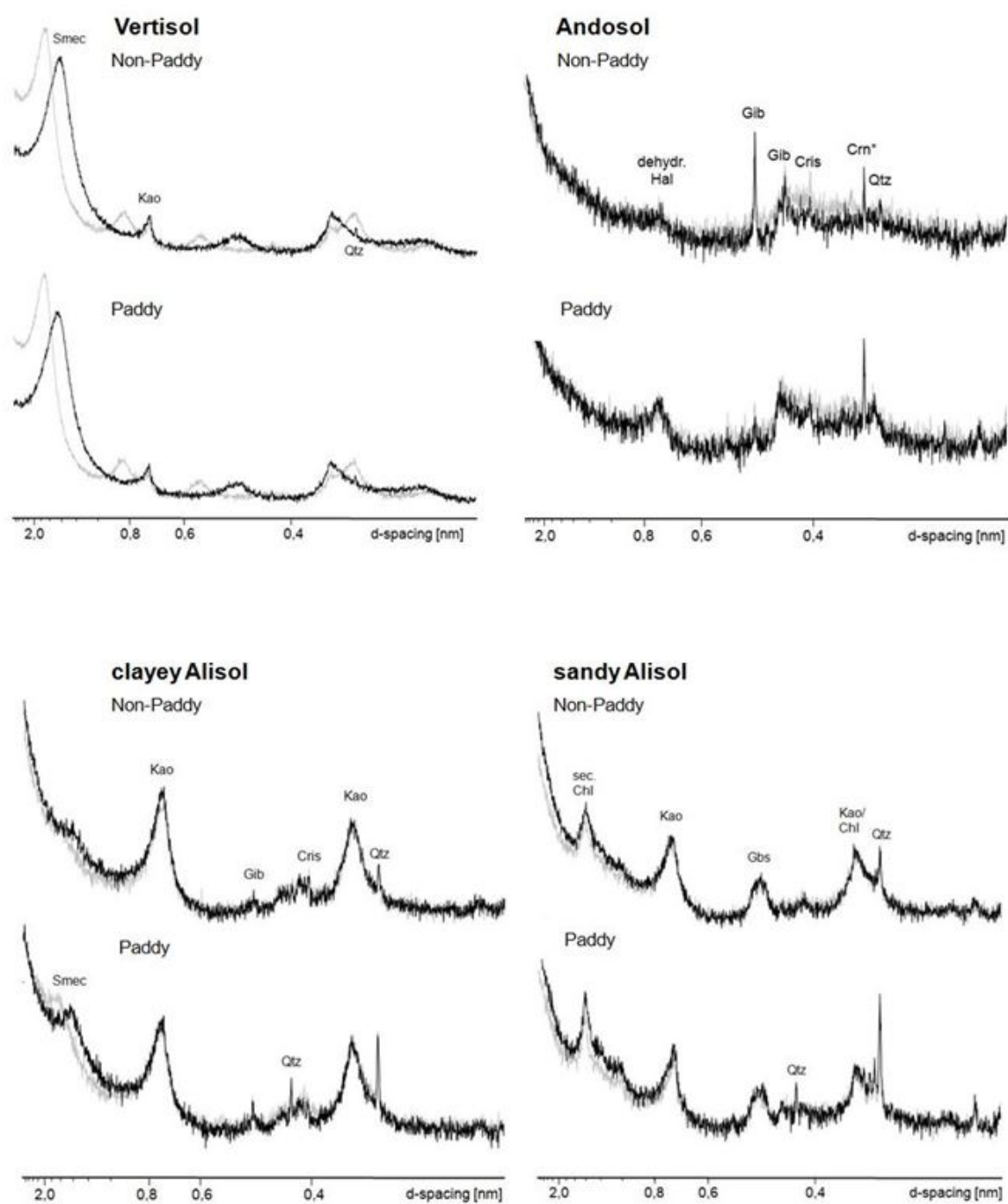


Fig. 2.2 XRD patterns of clay fractions (Smec = smectite, Kao = kaolinite, Qtz = quartz, Hal = halloysite, Gib = gibbsite, Cris = cristobalite, Crn* = corundum, Chl = chlorite; grey line = Mg saturated samples, black line = Mg-glycerin saturated samples; three topsoil samples were analysed per soil type and land use, one representative example is shown [Vertisol: NP 0-10cm, P 8-20cm; Andosol: NP 0-7cm, P 8-22cm; clayey Alisol: NP 7-14cm, P 7-17cm; sandy Alisol: NP 0-12cm, P 0-8cm]; *internal standard).

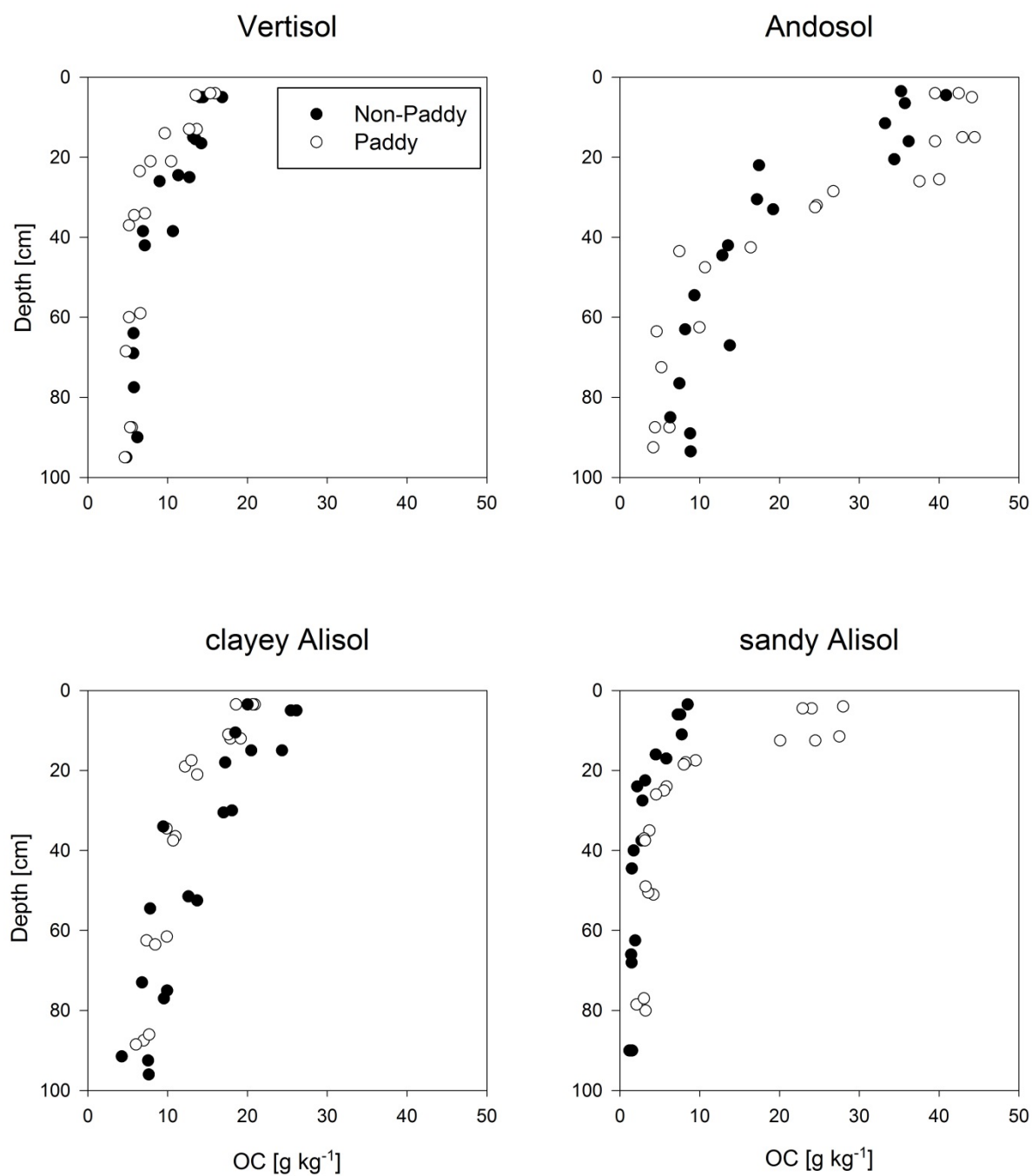


Fig. 2.3 Organic carbon (OC) concentrations of the non-paddy and their subsequent paddy profiles (main and subsites).

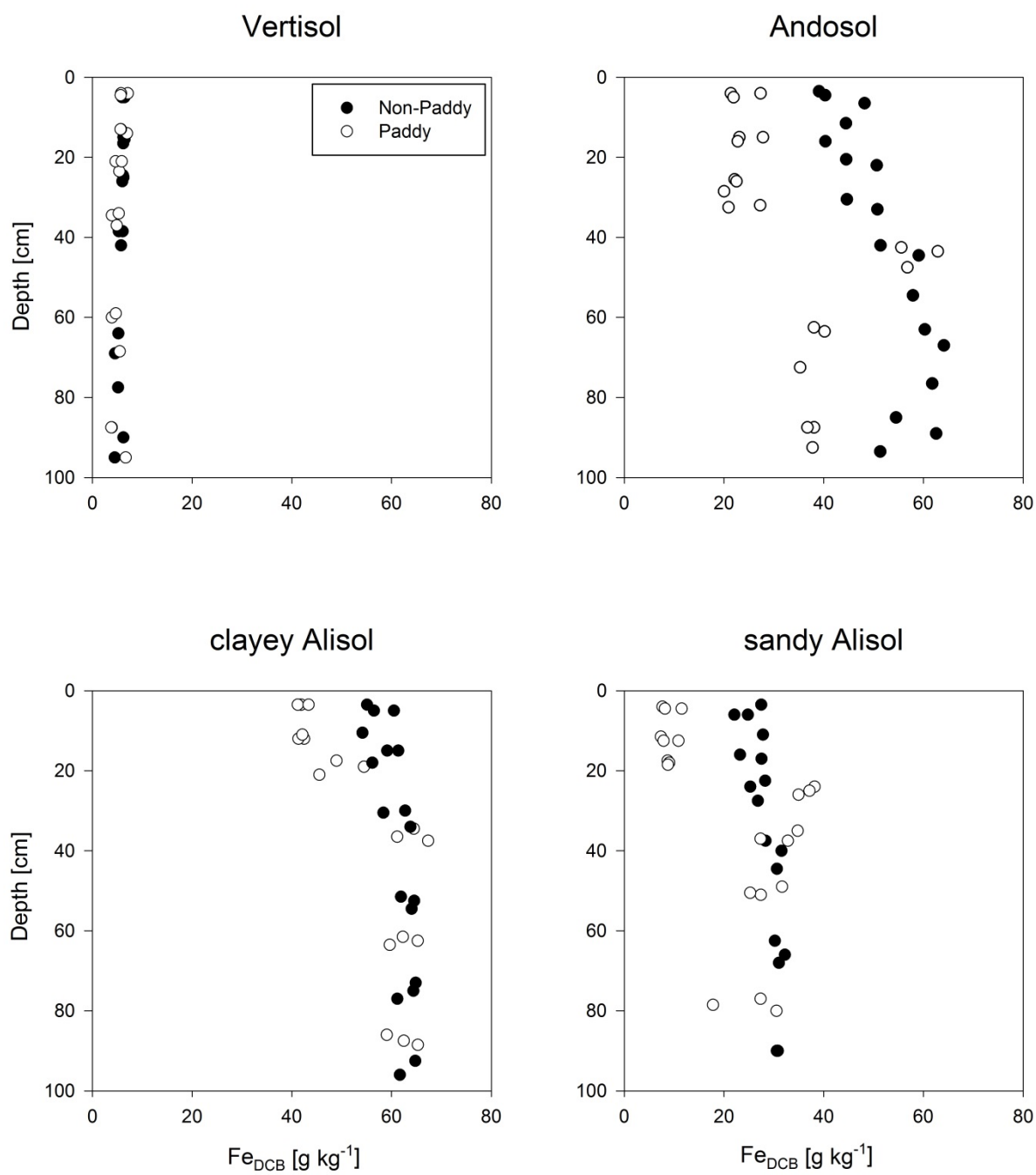


Fig. 2.4 Fe_{DCB} depth profiles of the non-paddy and subsequent paddy profiles (main and subsites).

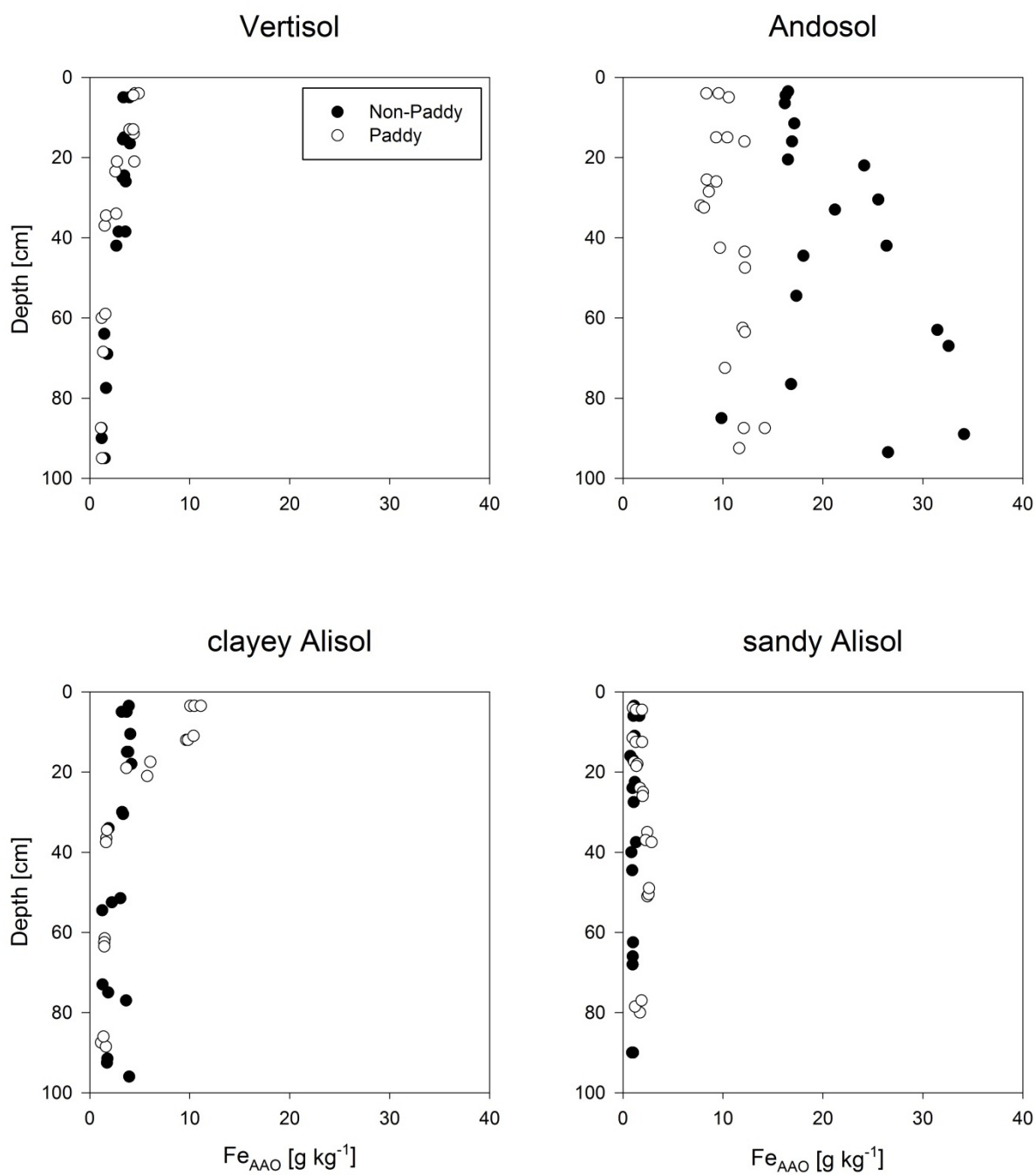


Fig. 2.5 Fe_{AAO} depth profiles of the non-paddy and subsequent paddy profiles (main and subsites).

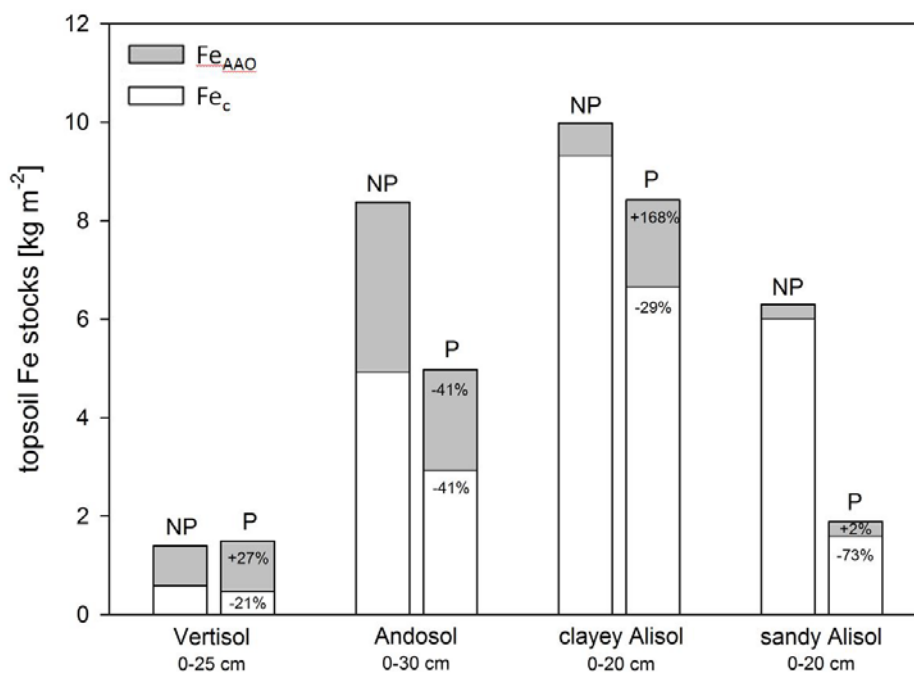


Fig. 2.6 Topsoil stocks of crystalline (Fe_c) and short range-ordered Fe (Fe_{AAO}). The percentages indicate the differences from non-paddy (NP) to paddy (P) soil.

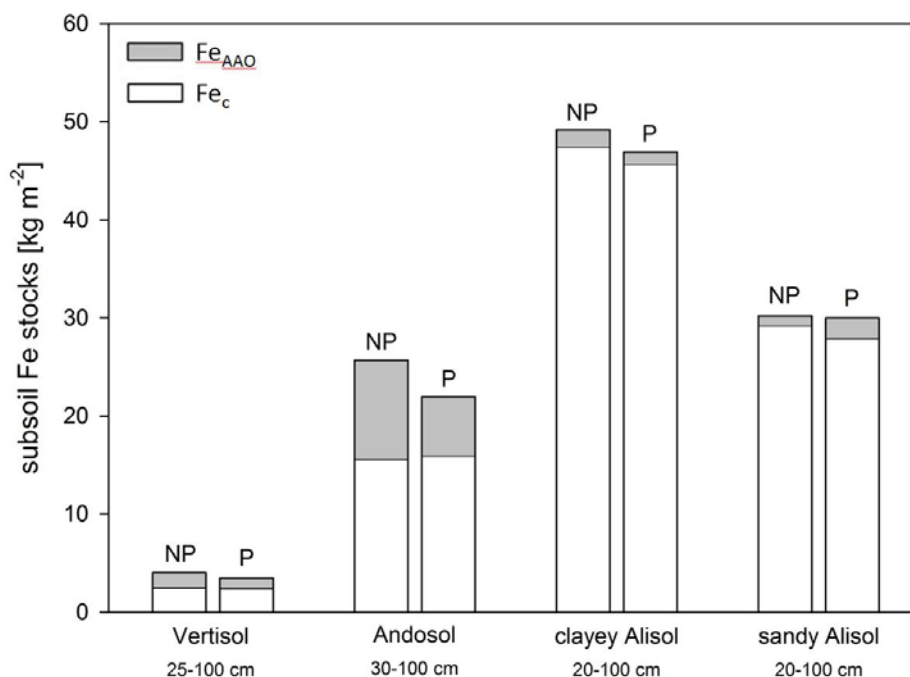


Fig. 2.7 Subsoil stocks of crystalline (Fe_c) and short-range-ordered Fe (Fe_{AAO}) (NP = non-paddy, P = paddy). Please note the different scaling of the y-axis compared to topsoil stocks.

The formation of halloysite requires additional Si. Usually Si is more mobile than Al and therefore preferentially leached. That means in the Andosol-derived paddy soils, which are quite porous, Si should be leached and allophane preserved over halloysite (Parfitt et al., 1983). However, this is not the case and could be explained by the retention of Si in topsoils via phytoliths. These rather soluble amorphous Si phases form in rice plants and are known to accumulate in paddy topsoils (Seyfferth et al., 2013). Phytoliths might be relevant in Andosols due to the relatively young parent material with considerable amounts of easily soluble Si. The mean Si/Zr ratios of the non-paddy and paddy soils (Fig. 2.8) revealed less desilication in Andosol topsoils under paddy management, which supports the phytolith idea. Differing parent material should not play a role since there is a distinct Si/Zr difference between top- and subsoils whereas the small difference in Ti/Zr between non-paddy and paddy managed Andosols holds for the entire profiles. Paddy soils seemingly had less gibbsite than halloysite (Fig. 2.2), which is in line with less advanced desilication.

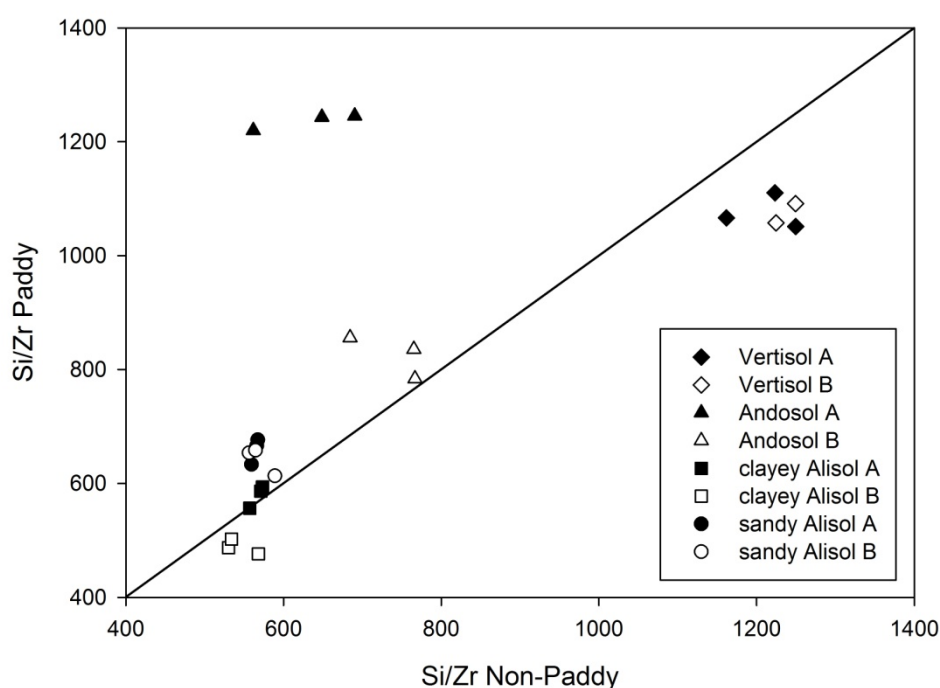


Fig. 2.8 Si/Zr ratios (means) of paddy soils plotted against respective non-paddy soils (topsoils in black and subsoils in white).

Redox processes in Andosols under paddy management caused equal topsoil losses of crystalline and SRO Fe oxides (Fig. 2.4-2.6); therefore, the proportions of Fe_{AAO} did not change (Tables 2.1 and 2.2). The Andosols were characterized by large initial proportions of SRO Fe oxides. Short range-ordered Fe oxides are less stable and have larger surface areas, thus, are more easily reducible than the crystalline ones (Ottow, 1981; Roden, 2003; Cornell and Schwertmann,

2003). Much of them, as well as part of the crystalline Fe oxides, seem to be dissolved during anoxic conditions. In contrast to oxidized Fe, reduced Fe is mobile at $\text{pH} > 4$ (Cornell and Schwertmann, 2003; Weber et al., 2006) and can, therefore, be removed by vertical leaching or with laterally moving drainage water. Even though SRO Fe oxides are partly recovered during re-oxidation of the soil, their amount can decrease from the initial value when leaching under anoxic conditions is large enough. The strong losses in the Andosol-derived paddy soils are likely supported by their low bulk density, which favours water percolation, thus leaching. The horizon below the plough pan was enriched in Fe oxides relative to the overlying puddled topsoil (Fig. 2.4). Also, the horizon was partly cemented by Fe oxides, as observed in the field. Thus, O_2 seems to be present there, resulting in oxidative precipitation of the dissolved Fe leached from the topsoil. The proportion of crystalline Fe oxides in that horizon is larger than in the respective non-paddy soil, underlining the prevalence of oxic conditions. However, despite these indications of accumulating Fe oxides, the total Fe oxide content was just at the level of the respective non-paddy horizons. The deeper subsoil showed losses of Fe oxides (Fig. 2.4 and 2.7). Probably, water percolating through the subsoil, favoured by the Andosols' loose structure, caused dispersion and subsequent leaching of colloidal Fe oxides. Slight differences in parent material might also contribute to the different contents of Fe oxides in Andosols and their respective paddy soils.

Andosols accumulate OC (Fig. 2.3), resulting in cumulative OC stocks increasing from 8-10 kg m^{-2} in non-paddy to 10-14 kg m^{-2} in the respective paddy soils. Accumulation of OC is likely supported by the large content of SRO Fe oxides and allophane and imogolite-type phases. Pedogenic Fe oxides are of utmost importance for the stabilization of OM (Wagai and Mayer, 2007; Kögel-Knabner et al., 2008). Mineral-associated OM of soils rich in Fe oxides is considered as strongly stabilized because of strong bonds with oxide surfaces (Mikutta et al., 2007). Short range-ordered minerals, such as allophanes, play also a decisive role for OM stabilization (Torn et al., 1997). They are particularly dominant in Andosols, explaining their large OC stocks (Dahlgren et al., 2004). Contents of Fe oxides and allophane and imogolite-type phases decreased in Andosols under paddy management. However, OC still accumulated, which shows that the OC storage capacity was not the limiting factor.

The slight increase in pH and base saturation throughout the profile (Tables 2.1 and 2.2) might be attributed to the consumption of H^+ upon Fe reduction. Part of the reductively dissolved Fe^{2+} is leached from the topsoil, thus, less H^+ is released upon re-oxidation of the remaining Fe^{2+} than consumed during reduction. As a result, the pH increasing effect is preserved.

Phosphorus retention was smaller throughout the paddy as compared to the non-paddy profiles (Tables 2.1 and 2.2). That is in line with the loss of poorly crystalline Fe oxides. Also, the CEC of topsoils slightly increased upon paddy management (Tables 2.1 and 2.2). Iron oxides have points of zero charge > 8 and therefore feature positive charge in all soils under study (Cornell

and Schwertmann, 2003). Thus, Fe oxide coatings can block part of the clay minerals' cation exchange sites. In turn, removal of Fe oxide coatings increases soils' CEC (Roth et al., 1969). Reduction of structural Fe^{III} in clay minerals raises the CEC as well, by increasing their negative charge (Favre et al., 2002). In addition, rising OC contents increase the amount of cation adsorbing functional groups and therefore enhance CEC (Kirk, 2004). In the subsoils, however, the CEC decreased despite the loss of Fe oxides. This could be due to slightly smaller OC contents.

2.4.3 Clayey Alisols (on Java)

Soil texture of Alisols on Java was silty clay, with increasing clay contents with depth. Paddy management had no effect on soil texture. Bulk density partly increased in paddy soils as result of the formation of a plough pan at about 15 cm depth (Tables 2.1 and 2.2). The kaolinite-dominated clay mineral assemblage of the non-paddy soil hardly changed under paddy management. There is merely a more pronounced smectite peak in the paddy soils (Fig. 2.2). This is probably not due to different weathering intensities but might refer to transport of smectite to paddy soils with irrigation water.

Paddy topsoils that derived from clayey Alisols are characterized by proportions of Fe_{AAO} that increased from 5 to 25% (Tables 2.1 and 2.2). This change was due to the decrease in crystalline Fe oxides along with increasing contents of SRO Fe oxides (Fig. 2.4–2.6). That means part of the dissolved Fe²⁺ released from crystalline Fe oxides is not leached or transported laterally but remains in the topsoil and precipitates as SRO Fe oxides upon aeration of the soils (Kirk, 2004). The loss of dissolved Fe²⁺ might be constrained by the clayey texture of the Java Alisols. However, the total contents of Fe oxides decreased due to paddy cultivation. That means, a larger part of the dissolved formerly crystalline Fe was removed rather than transformed into SRO Fe oxides over the years of paddy management. Several authors (Moormann and van Breemen, 1978; Willett and Higgins, 1978; Eaquib and Blume, 1982; Wang et al., 1993; Kirk, 2004) report that the proportion of SRO Fe oxides tends to increase since both fractions (short and long range-ordered) undergo reductive dissolution but only the SRO fraction (partly) recovers when oxic conditions recur. Crystalline Fe oxides form when poorly crystalline precursors age with time (Schwertmann, 1964). We suggest the short duration of oxic conditions prevents the re-formation of crystalline forms. Therefore, as our results show, crystalline Fe oxides were gradually lost during paddy soil evolution. Thompson et al. (2006), however, found evidence for the opposite. They used an Inceptisol topsoil rich in OC and SRO Fe oxides for an eight week incubation experiment with alternating redox conditions and observed

a shift towards more crystalline Fe oxides by Mössbauer spectroscopy. In subsoils, we did not observe clear changes in Fe oxide contents and stocks (Fig. 2.4, 2.5, and 2.7).

Accumulation of OC under paddy management was expected because of the large initial amounts of Fe oxides and the increasing contents of Fe_{AAO} under paddy management. Wissing et al. (2013) found that high proportions of SRO Fe oxides in paddy topsoils go along with large OM accumulation. However, no OC accumulation upon paddy management was found for the clayey Alisols. Cumulative OC stocks ranged from 10 and 12 kg m⁻² in non-paddy and paddy soils. This might be due to the already large initial OC contents of the non-paddy soils. The larger initial organic loading of the mineral phase probably made the clayey Alisols more prone to topsoil losses of OC with decreasing contents of Fe oxides.

Phosphorus retention in topsoils increased under paddy management (Tables 2.1 and 2.2), which is explained by the topsoil increase in SRO Fe oxides. The CEC slightly increased in paddy soils while the clay content as well as the pH did not change significantly (Tables 2.1 and 2.2). Removal of Fe oxide coatings from clay minerals may explain the increase in CEC. The unchanged clay contents indicate that ferrollysis is likely not affecting the soils.

2.4.4 Sandy Alisols (in China)

The Alisols in China were sandy clay loam. Clay contents increased with depth in non-paddy and paddy soils, however, the increase was more pronounced in the paddy soils (Tables 2.1 and 2.2). The larger loss of clay within the top 50 cm of the paddy soil might be due to larger amounts of percolating water and higher pH values under anoxic conditions. Ferrollysis could have contributed; however, redox-induced Fe dynamics should be restricted to basically the top 20 cm of the paddy soil. Besides kaolinite and gibbsite, sandy Alisols contained secondary chlorite (Fig. 2.2). Chlorite is supposed to be characteristic for ferrollysis-affected soils. Since the paddy as well as the non-paddy soils had chlorite, ferrollysis under paddy management is not likely here.

Puddling of the topsoil resulted in a typical paddy profile, with plough pan bulk densities that exceed that of the puddled layer by 74% (Table 2.2).

Considerable amounts of crystalline Fe oxides were removed from the topsoils of the sandy Alisols during paddy soil evolution, while the amounts of SRO Fe oxides remained similar (Fig. 2.4-2.6). Hence, most dissolved Fe was removed from the topsoils before re-oxidation. The strong leaching of dissolved Fe²⁺ might be attributed to the sandy texture of the China Alisols. In turn, small amounts of predominantly crystalline Fe oxides accumulated right beneath the plough pan (Fig. 2.4 and 2.5). Here, more oxic conditions seem to prevail, allowing for aging of precipitated Fe oxides. However, the largely unchanged Fe oxide stocks in the non-paddy and

paddy subsoils (Fig. 2.7) indicate that the Fe lost from the topsoil does not accumulate in the subsoil. It may have been leached further with fluctuating ground water or transported laterally during drainage (Kawaguchi and Matsuo, 1957; Van Breemen, 1988).

The sandy Alisol-derived paddy soils are characterized by distinctly larger OC concentrations in the puddled topsoil (Fig. 2.3), leading to larger cumulative OC stocks in the paddy (7.8 kg m^{-2}) than in the respective non-paddy soils (3.4 kg m^{-2}). The accumulation of OC in the topsoils under paddy management might be result of larger inputs of fresh organic matter and retarded decomposition of OM under anoxic conditions (Kyuma, 2004). Density fractionation showed that the accumulation of OC actually relates to the mineral-associated OM fraction (Urbanski, unpublished data). A major factor in the accumulation of mineral-associated OM in soils is the content of Fe oxides (e.g. Kaiser and Guggenberger, 2000). However, paddy management decreased the amount of Fe oxides considerably. This shows that the OC concentration in the non-paddy soil is far below the potential OC storage capacity and that even under paddy management, when the storage capacity is reduced, it is still large enough to support OC accumulation.

Topsoil loss of Fe oxides and the accumulation of OC upon paddy management should have resulted in larger CEC. Nevertheless, the CEC rather slightly decreased (Tables 2.1 and 2.2). The loss of clay from the topsoil may have over compensated the positive effects of removal of Fe oxide coatings and organic matter accumulation.

Despite total losses of Fe oxides, amounts of SRO Fe oxides did not change. In consequence, also the closely related phosphorus retention did not change upon paddy management (Tables 2.1 and 2.2).

2.5 Implications

2.5.1 The fate of Fe oxides under paddy management depends on initial soil properties

Iron oxides are lost from paddy topsoil as long as not mixed with the subsoil or replenished with irrigation water as in the Vertisols. In all studied paddy soils, crystalline Fe oxides were depleted, which means that we cannot confirm Thompson et al. (2006) who reported increasing crystallinity due to alternating redox conditions. The observed losses can be explained by dissolution and re-precipitation cycles resulting from alternating redox conditions. Considering that crystalline as well as SRO Fe oxides are prone to reductive dissolution but only SRO Fe oxides are formed when the soil is re-oxidized, the following can be generalized for the SRO Fe oxide fraction (Fe_{AAO}) in the topsoils during paddy soil evolution:

- (1) leaching = dissolution from crystalline fraction → no change in Fe_{AAO}
- (2) leaching < dissolution from crystalline fraction → increasing Fe_{AAO}
- (3) leaching > dissolution from crystalline fraction → decreasing Fe_{AAO}

The leaching rate depends on the texture-related permeability of the soil. The Java Alisols have a clayey texture, resulting in a leaching rate smaller than the dissolution rate of crystalline Fe oxides. That explains increase in SRO Fe oxides in the topsoils of the clayey Alisol-derived paddy soils, contrary to the paddy soils derived from the sandy Alisols. With increasing time of paddy use, however, clay migration might proceed in the clayey Alisols and allow for more transport of Fe. This might again decrease the amounts of SRO Fe oxides to the initial level as in the sandy Alisols that have been under paddy use much longer. The Andosols were characterized by the largest initial amounts of SRO Fe oxides. They tend to dissolve more rapidly under reductive conditions than crystalline Fe oxides. Also, the Andosols' porous structure supports rapid water percolation, which likely increases leaching. For those reasons the topsoil amounts of SRO Fe oxides are lower in the Andosol-derived paddy than in the non-paddy soils.

Paddy management-induced topsoil losses of Fe oxides were largest in the Alisols from China. In addition to its sandy structure, the much longer paddy use history (>300 years) than of the soils from Java (at least 100 years) might have contributed to the large losses of Fe oxides. At the same time, mean annual precipitation is lower at the Chinese Alisol site but that should be compensated by concurrent lesser evapotranspiration. Even though the majority of the studied soils lost considerable amounts of crystalline Fe oxides and showed varying changes in the amount of SRO Fe oxides, the initial distribution of Andosols having large amounts of SRO Fe oxides and Alisols being characterized by mainly crystalline Fe oxides is preserved in respective paddy soils.

We did not find Fe oxide accumulation in the fine earth of any of the studied paddy subsoils. Considerable amounts of dissolved Fe^{2+} might be transported laterally. Takeda and Fukushima (2004) reported a net-outflow of 150-220 kg Fe (ha·a)⁻¹ from a paddy-dominated watershed with clay loam texture and precipitation of >1500 mm. In accordance with the observed losses in the deeper subsoil of the Andosol-derived paddy soils, we think colloidal leaching with large vertical fluxes of water due to the flooding may affect Fe oxides even in the layers far beneath the plough pan.

Iron oxides could not be detected with the given XRD instrument, even though considerable amounts could be extracted chemically. Paddy management induced changes in the different Fe oxide phases are probably more pronounced than for clay minerals, however, detection requires more sensitive analytical instruments (e.g., Mössbauer spectroscopy).

2.5.2 Accumulation of OC in paddy soils mainly depends on OM input

The Andosols with large amounts of reactive minerals (Fe oxides, allophane and imogolite-type phases) stored OC despite the partial loss of these minerals under paddy management. Paddy soils derived from sandy Alisols with the smallest clay contents and the strongest paddy management-induced loss of Fe oxides gained considerable amounts of OC as well. Hence, the capacity to store OC is not the limiting factor in the tested soils. Wissing et al. (2011) studied a chronosequence of paddy soils in China and showed that even after 2000 years of OC accumulation under paddy management the calculated OC storage capacity was not completely used. In case of the OC accumulating sandy Alisol-derived paddy soils, the initial amounts of OC were very small, while the clayey Alisols, which did not accumulate OC under paddy management, already had large initial OC contents. This shows that possible OC accumulation in paddy soils may strongly depend on differences in residue management (OM input) between the non-paddy and paddy sites.

2.5.3 Desilication slowed down in Andosol-derived paddy soils

It has been assumed that parent material rather than paddy specific alternation of submergence and drainage influence clay mineral composition (Hassannezhad et al., 2008). Overall, this is confirmed by our results. Andosols, however, indicate less desilication under paddy management, which might be attributed to phytolith accumulation and/or pH increases during anoxic conditions in paddy soils. Allophane and imogolite-type phases in Andosols under paddy management weathered faster and in combination with the larger Si contents resulted in the formation of halloysite.

2.5.4 No evidence of ferrollysis

Textural changes could only be seen in sandy Alisols, being longest under paddy management (>300 years). Its topsoil lost clay and CEC decreased slightly, despite the increase in OM. However, pH values were slightly higher in the paddy soils and mineralogical composition was similar. Therefore, clay loss is probably not caused by ferrollysis but mainly due to colloidal transport with drainage water (Eaqub and Blume, 1982; Van Ranst and De Coninck, 2002). Soils on Java that have been under paddy management for at least 100 years do not exhibit any textural effects.

2.6 Conclusions

At the four examined sites on Java and in China we observed that topsoil changes in proportions of crystalline and SRO Fe oxides upon paddy management depended on the hydrological regime of the different soils, which is determined by their texture. The Andosols, e.g., had large initial amounts of SRO Fe oxides but lost part of it during paddy management due to its porous structure. The clayey Alisols, in contrast, gained SRO Fe oxides, since leaching of the previously dissolved Fe^{II} seems to be more restricted. Despite the paddy management-induced changes, the characteristic distribution of SRO and crystalline Fe oxide in topsoils of the different soil types was mainly preserved. Against the general perception, we could not find Fe oxide accumulation in the subsoils. Even though Fe oxide concentrations suggest that at some points, it is not confirmed by Fe oxide stocks. Accumulation of OC in part of the studied paddy soils probably depends mainly on larger plant residue inputs than in the respective non-paddy soils. Despite OC increases upon paddy management, the sandy Alisols remained the soils with the lowest OC stocks. Plough pan formation occurred in Andosol- as well as in Alisol-derived paddy soils. However, Andosol-derived paddy soils retained the lowest and sandy Alisol-derived paddy soils the highest bulk densities. Effects of paddy management on texture, clay mineral composition, and CEC were little and initial differences between soil types were not overruled. Topsoil clay loss in the sandy Alisol, being longest under paddy management, is mainly attributed to colloidal transport with drainage water. Vertisols, due to their massive clay contents, the self-mulching, and the shallow groundwater table were hardly affected by paddy management. Overall, our study of different soil types at four sites on Java and in China showed that initial soil properties, most of all soil texture and contents and type of Fe oxides, influenced the evolution of paddy soils. Major characteristics of the studied soil types were largely preserved even in the soil that has been longest under paddy management.

2.7 Acknowledgements

The authors thank Robert Banks and Matthias Lebert for pre-investigations that allowed us to find appropriate sampling sites. We thank Christanti Agustina, Dewo Ringgih, Miriam Houtermans, Urs Dieterich, and Susanne Drechsler for support during sampling and Silvia Bonzio, Herbert Pöllmann, Gabriele Kummer, Christine Krenkewitz, Gudrun von Koch, and Alexandra Boritzki for analytical support. We are grateful to the Deutsche Forschungsgemeinschaft (DFG) for their generous funding of Research Unit FOR 995 „Biogeochemistry of paddy soil evolution“.

3 Contrasting evolution of iron phase composition in soils exposed to redox fluctuations

P. Winkler, K. Kaiser, A. Thompson, K. Kalbitz, S. Fiedler, R. Jahn

Author contributions:

P.W. wrote the manuscript; P.W. and K. Kaiser conducted soil sampling, incubation experiment and data analyses; A.T. performed Mössbauer analyses; K. Kaiser, K. Kalbitz, S.F., R.J. and P.W. designed the study; all authors commented on the manuscript

Published in Geochimica Cosmochimica Acta (2018) 235: 89-102.

3.1 Abstract

Ferric iron (Fe^{III}) solid phases serve many functions in soils and sediments, which include providing sorption sites for soil organic matter, nutrients, and pollutants. The reactivity of Fe solid phases depends on the mineral structure, including the overall crystallinity. In redox-active soils and sediments, repeated reductive dissolution with subsequent exposure to aqueous ferrous iron (Fe^{2+}) and oxidative re-precipitation can alter Fe phase crystallinity and reactivity. However, the trajectory of Fe mineral transformation under redox fluctuations is unclear and has been reported to result in both increases and decreases in Fe phase crystallinity. Several factors such as water budget, organic matter input, redox dynamics as well as the initial Fe phase composition might play a role. The objective of our study was to examine if Fe minerals in soils that differ in porosity-dependent water leaching rate and initial Fe phase crystallinity, demonstrate distinct mineral transformations when subjected to redox fluctuations. We sampled paired plots of two soil types under similar management but with different water leaching rates and contrasting Fe oxide crystallinity — an Alisol rich in crystalline Fe phases and an Andosol rich in short-range-ordered (SRO) Fe phases. The two soils were either exposed to several decades of redox fluctuations during rice paddy cultivation (paddy) or to predominantly oxic conditions in neighboring vegetable gardens (non-paddy). Paddy soils are uniquely suited for this type of study because they are regularly submerged and develop regular redox fluctuations. We also incubated the non-paddy soils in the laboratory for one year through eight anoxic/oxic cycles and monitored the aqueous soil geochemistry. Mössbauer spectroscopy was then used to evaluate Fe mineral speciation in field soils (paddy and non-paddy) and laboratory incubations. In the field soils, we found that redox fluctuation had contrasting effects on Fe oxide crystallinity, with crystallinity being lower in the Alisol paddy soil and higher in the Andosol paddy soil than in their corresponding non-paddy controls. In the laboratory incubation experiment, Eh, pH and dissolved Fe^{2+} responded as anticipated, with elevated Fe^{2+} concentrations during the anoxic periods as well as low Eh and high pH. Mössbauer measurements suggest the fluctuating redox incubation was beginning to alter Fe oxide crystallinity along the same trajectory as observed in the field, but the changes were within the range of fitting errors. We propose that reductive dissolution of crystalline Fe oxides prevails in the soil rich in crystalline Fe oxides (Alisol) and that re-precipitation as SRO Fe oxides is favored by constrained leaching, which leads to the observed decrease in Fe oxide crystallinity. In the soil rich in SRO Fe phases (Andosol), preferential reductive dissolution of SRO Fe oxides coupled with stronger leaching of dissolved Fe causes the observed relative increase in crystallinity of the remaining Fe oxides. The observed increase in Fe oxide crystallinity may further be a result of Fe(II)-catalyzed re-crystallization of SRO Fe oxides. These findings indicate that, besides other

factors, the Fe mineral composition of the initial soil or sediment as well as the leaching rate likely influence the trajectory of Fe oxide evolution under alternating redox-conditions.

3.2 Introduction

Iron oxides and (oxy-)hydroxides (hereafter referred to as Fe oxides) have numerous functions in soils and sediments. They offer sorption sites for nutrients (especially phosphorus), pollutants (e.g., arsenic, uranium, lead) and soil organic matter (McKenzie, 1980; McGeehan et al., 1998; Kaiser and Guggenberger, 2000; Miller et al., 2001; Stewart et al., 2009). Besides environmental factors like pH, the adsorption capacity of Fe oxides depends on their crystallinity. Since Fe oxides are redox sensitive, continuous alternation of redox conditions can alter Fe oxide crystallinity. Iron is biologically reduced from ferric (Fe^{III}) to ferrous (Fe^{II}) in the anoxic conditions that accompany organic matter (OM) decomposition in saturated soils (Kirk, 2004). Here, SRO Fe^{III} oxides are preferentially reduced relative to more crystalline forms (Postma, 1993; Roden, 2003). In the common pH range of soils, the reduced species (Fe^{II}) is more soluble than the oxidized species (Fe^{III}) and can be either lost from the system as aqueous Fe^{2+} ions or complexes or become adsorbed to solid surfaces. Once O_2 re-enters the soil, much of this Fe^{II} is re-oxidized and subsequently precipitated as Fe^{III} oxides, often of low crystallinity. Hence, continuous alternation of redox conditions leads to repeated reductive dissolution and oxidative re-precipitation of Fe oxides, which can alter Fe oxide composition of soils and sediments.

In their review on paddy soils, representing one group of soils under redox oscillation, Moormann and Breemen (1978) postulated that redox fluctuation leads to an increase in SRO Fe oxides at the expense of crystalline Fe oxides such as goethite and haematite. This was also found in a study of Vogelsang et al. (2016b) and is explained by the reductive dissolution of both Fe phases (SRO Fe oxides dissolving fast and crystalline Fe oxides dissolving slowly) coupled with the rapid oxidative precipitation of mainly SRO Fe oxides that were slow to ripen to crystalline phases. In his review on submerged soils, Kirk (2004) repeats that theory, but adds that removal of dissolved Fe^{2+} with soil drainage, i.e., leaching, may also lead to a loss of the more rapidly dissolving SRO Fe oxides. Kirk (2004) hereby highlights the effect of the soil's hydrological regime on the retention of SRO vs. crystalline Fe oxides. This effect is supported by studies of Thompson et al. (2006; 2011). In a field study along a precipitation gradient, Thompson et al. (2011) showed the wettest sites had lower Fe oxide content, but a larger fraction of SRO Fe oxides suggesting a decrease in Fe oxide crystallinity in a redox fluctuating and leaching environment. However, when soils from a mid-point along that gradient were incubated in a closed system (no leaching) over four redox cycles, Fe oxide crystallinity increased (Thompson et al., 2006). Coby et al. (2011) performed a similar incubation experiment

with synthetic Fe oxides. In contrast to Thompson et al. (2006), they found redox fluctuations resulted in a decrease in Fe oxide crystallinity. The synthetic Fe oxides that Coby et al. (2011) used as starting material were of higher crystallinity than those in the natural soils incubated by Thompson et al. (2006), suggesting the initial Fe oxide composition might play a role here. The oxidation of Fe(II) and subsequent precipitation of Fe oxides was induced by very slow addition of O₂ in the presence of high amounts of natural dissolved organic matter (DOM) at a pH of ~5 in Thompson et al. (2006) and likely involved significant abiotic oxidation, whereas Fe(II) was oxidized biotically by nitrate-reducing microbes at near neutral pH in a system with only acetate as DOM in Coby et al. (2011). These conditions might have affected the crystallinity of the resulting Fe oxides and underlines the importance of a study that considers two soils with contrasting initial Fe oxide crystallinity undergoing comparable redox cycles.

We propose that differences in the leaching rate and the initial Fe oxide crystallinity are likely to impact the trajectory of Fe mineral evolution in soils with redox fluctuations. To test this, we examined the Fe mineral composition in redox-active soils with similar management but differing leaching rate and contrasting Fe oxide crystallinity (Alisol and Andosol). We used established plots of Hydragric Anthrosols that developed from Alisol and Andosol (WRB classification; IUSS Working Group WRB, 2006) and that have been under paddy management for several decades prior to our sampling and analyses. The alternate submergence and drainage of paddy fields leads to sharply fluctuating redox conditions within the soil profile (Vogelsang et al., 2016a). Therefore, paddy soils can function as large-scale experimental sites that are excellent for studying the effect of redox alternation over longer time scales. For comparison, neighboring garden soils never used for paddy cultivation and therefore mainly under oxic conditions were sampled. In addition, to evaluate the timescale of Fe mineral transformations and to examine the evolution of the two soil's Fe mineral composition under controlled laboratory conditions, we incubated the non-paddy Alisol and Andosol samples for one year with alternating redox conditions and periodic rice straw addition.

Prior work at these sites (Winkler et al., 2016) has shown the total Fe oxide concentrations and stocks of the surface soils were lower in the rice paddy than in the non-paddy soils. This was likely due to loss of dissolved Fe²⁺ either through the plough pan or laterally along with the drainage water. At the same time, ratios of SRO Fe to total Fe oxides was larger in the Alisol and similar in the Andosol paddy soils compared to the respective non-paddy soils (Winkler et al., 2016). However, Winkler et al. (2016) relied on chemical extractions of Fe oxides, which have restricted precision as pointed out by several authors (Thompson et al., 2011; Mansfeldt et al., 2012; Filimonova et al., 2016; Vogelsang et al., 2016a). In the present study, we re-examined those field soils as well as the laboratory-incubated soils with variable-temperature ⁵⁷Fe Mössbauer spectroscopy, which allows for the detailed differentiation of different degrees of Fe mineral crystallinity.

3.3 Materials & Methods

3.3.1 Field soil sampling

The non-paddy Alisol and Andosol as well as the respective paddy soils were collected from Java (Indonesia). Prior to sampling, a farm and soil survey was conducted to make sure that comparable sites are sampled. Both sampling sites have a tropical monsoon climate and an andesitic parent material. The Alisol site is located near Jasinga (West Java, 6.54°S, 106.52°E, 250 m a.s.l.). Parent material is tertiary andesitic tuff. Alisols are already at an advanced stage of weathering, and thus, have a mineral assemblage comprising kaolinite, high-activity clays and more crystalline Fe oxides. Mean annual temperature is around 26 °C and annual rainfall ranges from 1900 to 4700 mm a⁻¹, with a drier season from June/July through September (Winkler et al., 2016). The Andosol site is near Sukabumi (West Java, 6.88°S, 106.94°E, 900 m a.s.l.) on the terraced slope of the still active volcano Mount Gede. Parent material is a Quaternary lahar, mainly composed of andesitic pyroclasts. Andosols are relatively young soils and therefore are comprised of SRO metastable phases like allophane, imogolite and ferrihydrite. Mean annual temperature is around 21 °C and annual rainfall ranges from 2300 to 6700 mm a⁻¹, with a relatively dry season between June/July to September/October (Winkler et al., 2016). Water tables were >5m beneath the soil surface at both sites. Rice is cultivated twice per year under flooded conditions, followed by an upland crop. Long-term flooding is enabled by puddling of soils for plough pan formation and by construction of bunds around the fields to minimize vertical and lateral water losses. Rainwater managed in canals is used for irrigation to induce the flooding. The period of submergence lasts until rice plants reach maturity (about 100 days). Then paddy bunds are opened to drain soils for harvest (about 20 days). According to the local farmers, rice straw was managed by burning it and spreading the ashes on the field. The sampled fields have been under paddy management for at least 100 years. Agricultural soils not used for paddy rice production (non-paddy soils) were sampled in adjacent settings. Non-paddy Alisol and Andosol have been managed under crops of cassava, cabbage and bananas. None of the sites were limed. As a result of the different water regimes, paddy and non-paddy soils developed along different lines from the beginning of submerged rice cultivation (about 100 years ago). Changes in mineral assemblage may occur also over time in the non-paddy soils but will be minimal compared to the drastic nature of the exposition to strong fluctuation in redox conditions.

At both sampling sites, three paddy and three non-paddy fields (one main site, two sub-sites) were sampled, with the distance between main and subsites <200 m. Profiles were dug to >1 m, described according to FAO (2006), classified according to IUSS Working Group WRB (2006), and sampled horizon by horizon. To ensure well-defined conditions and to simplify the procedure, paddy soils were sampled after they had been recently drained (i.e., following

completion of an anoxic-oxic cycle). Bulk samples of each horizon were directly air-dried in Indonesia and after their transport to Germany, the soils were sieved to <2 mm. Undisturbed soil cores (100 cm³, in triplicate) were taken under field-moist conditions to determine bulk density (BD). Detailed profile descriptions are given by Winkler et al. (2016). Some relevant data are re-drawn in Table 3.1 and Fig. 3.1.

Table 3.1 Profile description of non-paddy and respective paddy soils (BD = bulk density, OC = organic carbon). Where data were obtained for main and subsites, the means ± standard errors (n=3) are given. Data taken from Winkler et al. (2016). Non-paddy soils used for Mössbauer measurements and incubation experiment are framed. Respective paddy soils used for Mössbauer analyses are framed with dashed lines.

Soil type	Horizons		Sand [%]	Silt [%]	Clay [%]	BD [g cm ⁻³]	pH CaCl ₂	OC [g kg ⁻¹]
	Depth [cm]	Identifier						
Alisol	0-9	Ah1	16	44	40	0.83 ± 0.10	4.4 ± 0.4	23.9 ± 1.9
Non-Paddy	9-18	Ah2	13	46	41	0.88 ± 0.08	4.4 ± 0.5	21.1 ± 1.7
	18-34	B(t)o1	9	44	48	0.94 ± 0.09	4.5 ± 0.5	17.4 ± 0.3
	34-63	B(t)o2	4	17	79	0.90 ± 0.04	4.3 ± 0.1	10.9 ± 1.4
	63-87	B(t)o3	3	22	75	0.91 ± 0.01	4.2 ± 0.0	8.7 ± 1.0
	87-101+	B(t)o4	26	37	38	0.93 ± 0.09	4.2 ± 0.0	6.5 ± 1.1
Anthrosol from	0-7	Alp1	13	50	37	0.88 ± 0.03	4.2 ± 0.0	20.0 ± 0.7
Alisol	7-16	Alp2	6	53	41	0.97 ± 0.02	4.3 ± 0.0	18.2 ± 0.5
Paddy	16-22	Alcdp	7	50	43	1.13 ± 0.04	4.6 ± 0.1	12.9 ± 0.4
	22-50	B(t)gc1	5	29	66	0.97 ± 0.01	4.4 ± 0.0	10.5 ± 0.3
	50-75	B(t)gc2	7	35	58	0.93 ± 0.00	4.3 ± 0.0	8.6 ± 0.7
	75-95+	B(t)gc3	3	41	57	0.88 ± 0.02	4.2 ± 0.0	6.9 ± 0.5
Andosol	0-10	Ah1	silt loam			0.67 ± 0.03	4.6 ± 0.1	37.3 ± 1.8
Non-Paddy	10-22	Ah2	silt loam			0.65 ± 0.02	4.6 ± 0.1	34.6 ± 0.9
	22-35	BwAh	silt loam			0.51 ± 0.03	5.2 ± 0.3	17.9 ± 0.6
	35-59	Bw1	silt clay loam			0.53 ± 0.03	5.2 ± 0.1	11.9 ± 1.3
	59-78	Bw2	silt clay loam			0.63 ± 0.06	5.6 ± 0.1	9.8 ± 2.0
	78-103+	Bw3	silty clay			0.63 ± 0.10	5.5 ± 0.3	8.0 ± 0.8
Anthrosol from	0-9	Alp1	silt loam			0.67 ± 0.04	5.0 ± 0.0	42.0 ± 1.4
Andosol	9-22	Alp2	silt loam			0.76 ± 0.03	5.0 ± 0.0	42.3 ± 1.5
Paddy	22-31	Aldp	silt loam			0.84 ± 0.06	5.3 ± 0.1	30.7 ± 3.4
	31-54	Bgc1	clay loam			0.86 ± 0.01	6.0 ± 0.1	11.5 ± 2.6
	54-78	Bgc2	clay loam			0.78 ± 0.03	6.2 ± 0.1	6.6 ± 1.7
	78-107+	Bw	clay loam			0.72 ± 0.02	6.2 ± 0.1	4.9 ± 0.6

For this study, paddy soil samples from the second topsoil horizon of the main site profiles (Alisol = 7-16 cm; Andosol = 9-22 cm) were chosen for Mössbauer analyses. That horizon directly overlays the plough pan and therefore remained constantly reduced over the entire submergence period. From the non-paddy sites, the second topsoil horizon (Alisol = 9-18 cm;

Andosol = 10-22 cm) was chosen accordingly. The respective non-paddy samples were used for the one-year incubation.

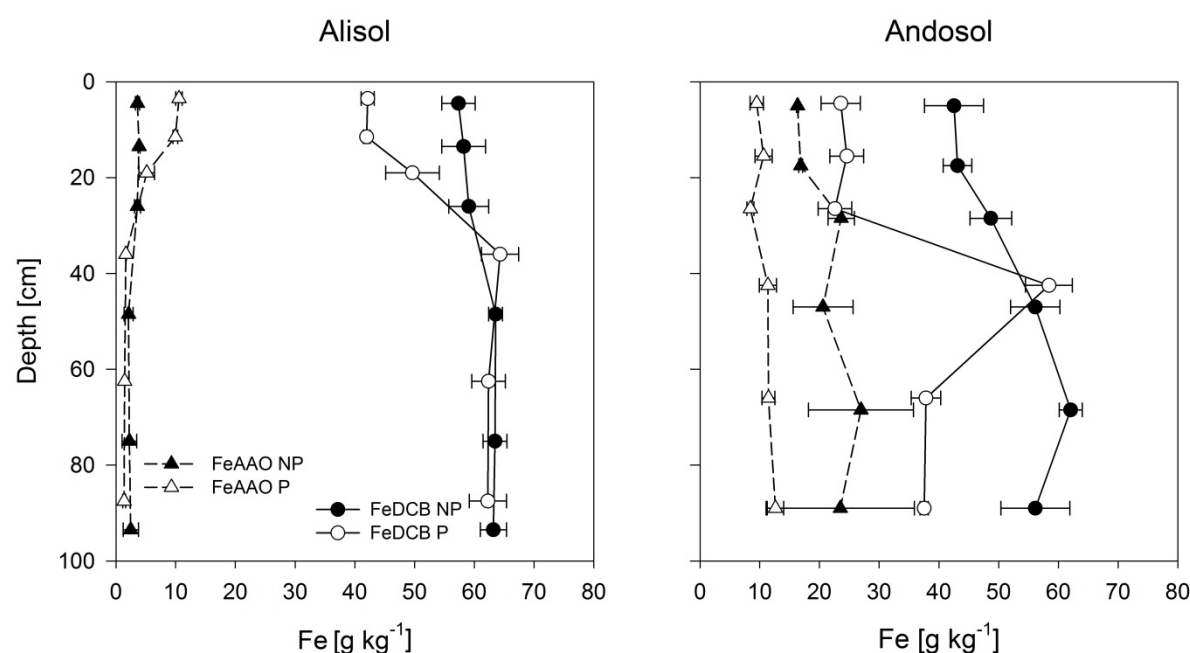


Fig. 3.1 Depth profile of dithionite-bicarbonate-citrate-extractable Fe (Fe_{DCB}) and acidic ammonium-oxalate-extractable Fe (Fe_{AAO}) of non-paddy (NP) and respective paddy (P) soils. Data are means of main and subsites, with the errors representing standard deviations ($n=3$). Re-drawn from Winkler et al. (2016). The second topsoil horizons of non-paddy main sites were used for incubation; the respective indicators of Fe oxide crystallinity were: $Fe_{DCB} = 54 \text{ g kg}^{-1}$, $Fe_{AAO} = 4 \text{ g kg}^{-1}$, $Fe_{AAO}/Fe_{DCB} = 0.07$ for the Alisol NP and $Fe_{DCB} = 45 \text{ g kg}^{-1}$, $Fe_{AAO} = 17 \text{ g kg}^{-1}$, $Fe_{AAO}/Fe_{DCB} = 0.38$ for the Andosol NP. The respective numbers for the field paddy soils were: $Fe_{DCB} = 42 \text{ g kg}^{-1}$, $Fe_{AAO} = 10 \text{ g kg}^{-1}$, $Fe_{AAO}/Fe_{DCB} = 0.24$ for the Alisol P and $Fe_{DCB} = 28 \text{ g kg}^{-1}$, $Fe_{AAO} = 10 \text{ g kg}^{-1}$, $Fe_{AAO}/Fe_{DCB} = 0.36$ for the Andosol P.

3.3.2 Incubation experiment

The incubation of the Alisol and Andosol non-paddy topsoils was performed in 1.2 L glass flasks closed by a gas-tight septum. Two hundred gram aliquots of air dried soils were pre-incubated at 50% field capacity for two weeks to re-constitute microbial activity. Then the soils were submerged in 500 ml of degassed $CaCl_2$ solution (5 mM). The degassed solution was prepared by connecting the respective bottle to a pump, which evacuated the headspace for several hours while the solution was continuously stirred by a magnetic stir bar. Rice straw (450 g OC kg^{-1} straw) was added to the incubation flasks at the beginning of each anoxic phase at the rate of 0.3 g of straw OC per 1 g of soil OC across eight addition time points. A second set of samples was incubated without straw addition. To initiate the anoxic phase, all samples were flushed with nitrogen (N_2). After five weeks, Eh (referenced to the standard H_2 electrode) and pH were directly measured in the supernatant (24 h after homogenization and sedimentation). A glass

pipette was then used to carefully withdraw 300 ml of the supernatant, which was replaced by fresh CaCl₂ solution. To induce oxic conditions, the soil slurry was strongly flushed with pure O₂ for one minute and before closing the flask, the headspace, making up ½ of the vessels' volume, was filled with pure O₂. After one week, Eh and pH were again measured and 300 ml of the soil solution was exchanged for fresh degassed CaCl₂ solution. N₂ and straw were added to the slurry to start the second redox cycle. The procedure was repeated until eight redox cycles were completed. Each cycle included a five week anoxic period and a one week oxic period ($\tau_{\text{oxic}}:\tau_{\text{anoxic}} = 1:5$), which roughly simulates field conditions. Throughout the anoxic phase the flask headspace was regularly exchanged by N₂, to remove accumulated CO₂ and CH₄. The collected soil solutions were filtered (0.45- μm polyether sulfone filter), either in a glove box with argon atmosphere (anoxic samples) or in the laboratory atmosphere (oxic samples). The incubations were carried out at a constant temperature of 25°C and with three replicates for both soil types and treatments. The soil was destructively sampled under oxic conditions at the end of the incubation.

3.3.3 Analytical methods

Soil samples (non-paddy and paddy soils from the field as well as laboratory-incubated topsoils at the end of 8 redox cycles) underwent chemical extraction of pedogenic Fe. Total pedogenic Fe was extracted by dithionite–citrate–bicarbonate solution (Fe_{DCB}) as outlined by Mehra and Jackson (1960). Extraction of the SRO Fe oxide fraction was carried out with acid ammonium oxalate (Fe_{AAO}) at pH 3.0 and 2 h shaking in the dark according to Schwertmann (1964). Further details on the extraction methods are given in Appendix 1. The concentrations of extracted Fe were determined by ICP-OES (Ultima 2). All analyses were done in duplicate or triplicate. The ratio of Fe_{AAO} to Fe_{DCB} is indicative of the contribution of SRO Fe oxide phases to total Fe oxides.

Bulk samples of the laboratory-incubated topsoils (+straw) as well as the corresponding initial non-paddy and the actual field paddy topsoils were analyzed by variable-temperature ⁵⁷Fe Mössbauer spectroscopy with one replicate per treatment (details given in section 3.3.4).

Soil solutions from the incubation experiment were analyzed for their dissolved Fe²⁺ content immediately after sampling by reaction of Fe²⁺ with ferrozine in the glovebox and subsequent photometric detection at 562 nm (modified after Stookey, 1970).

3.3.4 ^{57}Fe Mössbauer spectroscopy

The Fe mineral composition of the bulk soils (non-paddy, paddy and laboratory-incubated non-paddy topsoils) was assessed using ^{57}Fe Mössbauer spectroscopy collected at 295, 140, 77, 40 and 4.2 K with additional measurements at 13 K for the Andosol to confirm certain Fe species. The specific temperature cut-offs are arbitrary and based on common temperatures used previously. For instance, there is ample data at 4.2 K and 77 K based on use of He (4.2 K) and N_2 (77 K) as a coolant. Mössbauer spectral fitting was performed using the Voigt-based fitting method of Rancourt and Ping (1991), as implemented in the Recoil™ software. All fitting parameters are given in Appendix 2.2 (Table A-1). Given errors are standard deviations of the fitting procedure as calculated by Recoil™. The relative abundance of each Fe site population (e.g., mineral phase) was extracted from the spectral fitting as a fraction of the total Fe spectral area. Quantifying Fe phase abundance in this manner assumes equal Mössbauer recoilless fractions of all detected phases; this assumption is expected to be valid at cryogenic temperatures, and also to be a good approximation at least up to 295 K with dry samples (Lalonde et al., 1998; Rancourt, 1998).

Fe^{III} oxides and (oxy-)hydroxides (e.g., haematite, goethite, ferrihydrite) order magnetically, and thereby transform from a doublet into a sextet in the Mössbauer spectrum at a characteristic measurement temperature, based on their relative crystallinity. Well-crystallized haematite and goethite can easily be identified as they form sextets at 295 K that can be distinguished by their width (Murad and Cashion, 2004; Thompson et al., 2011). Differentiation of nano-goethite and ferrihydrite, which both form similar-width sextets at temperatures <77 K, can be made on the basis of quadrupole splitting of the sextets (Thompson et al., 2011). However, in many natural systems nano-goethite and ferrihydrite are strongly substituted with foreign ions and co-precipitated with organic matter, yielding a continuum of quadrupole splitting parameters within the range of the pure phases. Extracting precise proportions of nano-goethite and ferrihydrite thus becomes difficult. Distinguishing these phases is also likely of little environmental value given that they likely both behave similarly in terms of sorption/desorption or dissolution reaction kinetics. In this work, we thus refrain from differentiating nano-goethite and ferrihydrite (except when two distinct sites improve the spectral fit), but instead use a subdivision of the respective Fe^{III} (oxy-)hydroxide phases (nano-goethite + ferrihydrite = Fe^{III} OxHy) based on ordering temperature, and hence, crystallinity (Fe^{III} OxHy SRO-1 to SRO-5). At the lowest measurement temperature (4.2 K in our case), there are sometimes highly disordered phases that remain as a collapsed sextet; these portions of the population represent the least ordered Fe^{III} (oxy-)hydroxide phases (Fe^{III} OxHy SRO-5), sometimes termed “nano-Fe” (Murad and Cashion, 2004; Thompson et al., 2011). When all Fe^{III} oxides have ordered into a (collapsed) sextet at 4.2 K, the remaining Fe^{III} doublet represents Fe^{III}

in phyllosilicates and/or in Fe–OM complexes. The ferrous doublet represents Fe^{II} in primary minerals, in phyllosilicates and/or adsorbed to organic or mineral surfaces (Thompson et al., 2011). At low temperatures (4.2 K in our case), some ferrous populations can order into a collapsed octet characterized by strong asymmetry, which likely represents Fe^{II} sorbed onto a magnetically ordered Fe^{III} phase. A summary of the spectral components defined in this paragraph is given in Table 3.2. More details on the identification of different ⁵⁷Fe Mössbauer components are given in Appendix 2.1.

Table 3.2 Identification of Mössbauer spectral components (for references see Appendix 2.1)

Spectral component	Identification
Fe ^{III} doublet at 4.2 K (Q-Fe ^{III})	Fe in phyllosilicates and in Fe–OM complexes
Fe ^{II} doublet at all temperatures (Q-Fe ^{II})	Fe ^{II} in primary minerals, in phyllosilicates and/or adsorbed to organic or mineral surfaces
Fe ^{II} collapsed octet at 4.2 K (HFD-Fe ^{II})	Fe ^{II} sorbed onto a magnetically ordered Fe ^{III} phase
wide Fe ^{III} sextet with constant area at all measurement temperatures (HFD-Hae)	haematite
Fe ^{III} sextet with increasing area as measurement temperature decreases (HFD-OxHy)	goethite and short-range-ordered (SRO) Fe ^{III} (oxy-) hydroxide (OxHy) phases (including ferrihydrite and nano-goethite)
>295 K	goethite
295-140 K ¹⁾	Fe ^{III} OxHy SRO-1
140-77 K ¹⁾	Fe ^{III} OxHy SRO-2
77-40 K ¹⁾	Fe ^{III} OxHy SRO-3
40-4.2 K ¹⁾	Fe ^{III} OxHy SRO-4
<4.2 K ²⁾	Fe ^{III} OxHy SRO-5

decreasing crystallinity
(due to decreasing particle size, i.a. induced by substitution and/or co-precipitation with organic matter)

¹⁾ corresponds to area calculated by subtracting sextet area at higher temperature from sextet area at lower temperature

²⁾ area of collapsed sextet at 4.2K

3.4 Results

3.4.1 Chemical extraction of pedogenic Fe

Based on our previous study using chemical extractions (Winkler et al., 2016), 62% of the total Fe in the non-paddy Alisol topsoil is DCB-extractable, with 7% of the Fe_{DCB} present as SRO phases (AAO-extractable) (Fig. 3.1). When subjected to redox fluctuations as part of rice paddy cultivation, Fe_{DCB} is smaller (42 g kg⁻¹ soil) than in the respective non-paddy Alisol topsoils (54 g kg⁻¹ soil), whereby the fraction of AAO-extractable Fe is distinctly larger (24 vs. 7%) (Winkler et al., 2016). For the Andosol non-paddy topsoil, chemical extractions suggest Fe_{DCB} is 47% of the total Fe, with AAO-extractable Fe accounting for 38% of Fe_{DCB} . Andosol topsoils under paddy management show distinctly smaller concentrations of Fe_{DCB} (28 g kg⁻¹ soil) than the respective non-paddy Andosol topsoils (45 g kg⁻¹ soil), which, in contrast to the Alisol-derived paddy soil, is not accompanied by a difference in the fraction of AAO-extractable Fe (Winkler et al., 2016). The Alisol and Andosol profiles exhibit contrasting Fe profile development in the topsoils, with paddy management clearly resulting in lateral Fe removal since there is no clear accumulation of Fe in the paddy subsoils relative to the non-paddy subsoils (Fig. 3.1). However, in the Andosol paddy profile, a remarkably large concentration of Fe_{DCB} in the horizon below the plough pan suggests partial leaching of Fe^{2+} through the plough pan (Winkler et al., 2016).

3.4.2 Fe phases identified by ⁵⁷Fe Mössbauer spectroscopy

According to Mössbauer analyses, about 80% of the Fe in the non-paddy Alisol topsoil exists as SRO Fe^{III} (oxy-)hydroxide phases that magnetically order along a continuum below 295 K. As the measurement temperature-related growth of the respective Fe^{III} sextet shows (Fig. 3.2), these 80% comprise about 60% Fe^{III} OxHy SRO-1 (orders between 295 K and 140 K) and SRO-2 (orders between 140 K and 77 K) crystallinity classes, 10% Fe^{III} OxHy SRO-3 (orders between 77 K and 40 K) and SRO-4 (orders between 40 K and 4.2 K) crystallinity classes, and 10% highly disordered, nm-sized Fe^{III} phases (Fe^{III} OxHy SRO-5), which are near their blocking temperature at 4.2 K. Well-crystalline goethite, which forms a sextet at 295 K, was not detected. The remaining Fe is present as follows: 8% of the total Fe in haematite, 9% in phyllosilicates and/or Fe-OM complexes, and <1% in ferrous phases (Fig. 3.2 and 3.4, Table 3.3).

For the non-paddy Andosol topsoil, about 75% of the Fe is contained in the continuum of SRO Fe^{III} (oxy-)hydroxides (<295 K). In contrast to the Alisol, where the majority (~60%) of that Fe is binned in the Fe^{III} OxHy SRO-1 and SRO-2 crystallinity classes, more than 50% of the Andosol Fe^{III} OxHy phases are binned in the Fe^{III} OxHy SRO-3 and SRO-4 crystallinity classes, and 15% of the Fe is binned to the highly disordered, nm-sized Fe^{III} phases (Fe^{III} OxHy SRO-5). The

remaining Fe is present as well-crystalline goethite (17%), as haematite (3%), as Fe^{II} in primary minerals, in phyllosilicates and/or adsorbed to organic or mineral surfaces (4%), and as Fe^{II} that is likely adsorbed to magnetically ordered Fe^{III} phases (3%) (Fig. 3.3 and 3.4, Table 3.3).

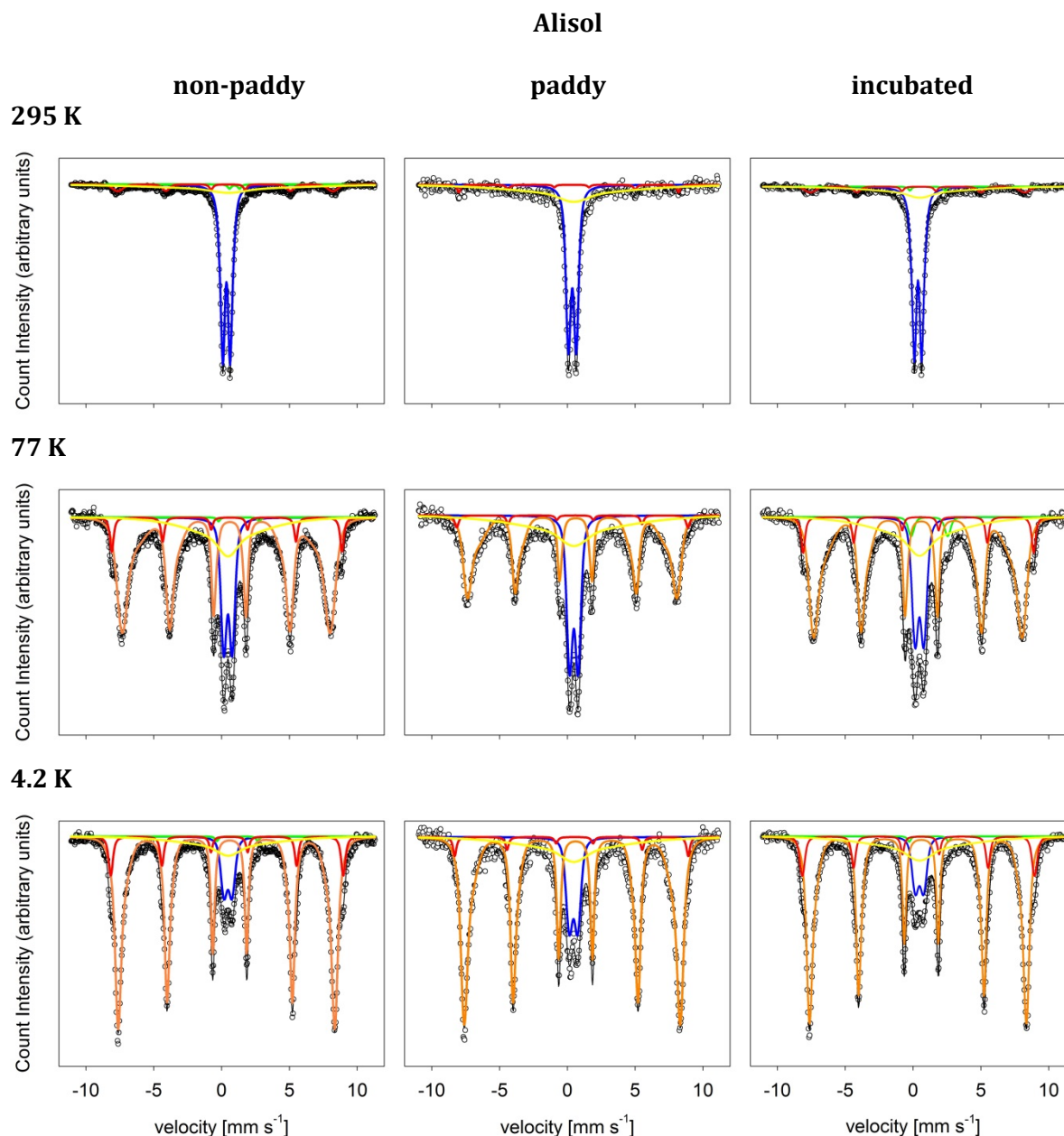


Fig. 3.2 Fitted Mössbauer spectra of Alisol topsoils at 295, 77 and 4.2 K (140 and 40 K spectra can be found in Fig. A-1 of Appendix 2.2). From the incubation experiment spectra of samples with straw addition are presented. The black solid line is the total calculated fit through the discrete data points (circles). The resolved spectral components and assignments are: (1) Q-Fe^{III}, deep central doublet (blue) = Fe^{III} in silicates and in organic complexes (+ paramagnetic Fe^{III} (oxy-)hydroxides), (2) Q-Fe^{II}, wider and smaller doublet (green) = Fe^{II} in primary minerals, clays or sorbed, (3) HFD-OxHy-A, dominant sextet (orange) = magnetically ordered Fe^{III} (oxy-) hydroxides, (4) HFD-Hae, wider and smaller sextet (red) = haematite, (5) HFD-OxHy-B, collapsed sextet (yellow) = Fe^{III} (oxy-)hydroxides near their blocking temperature.

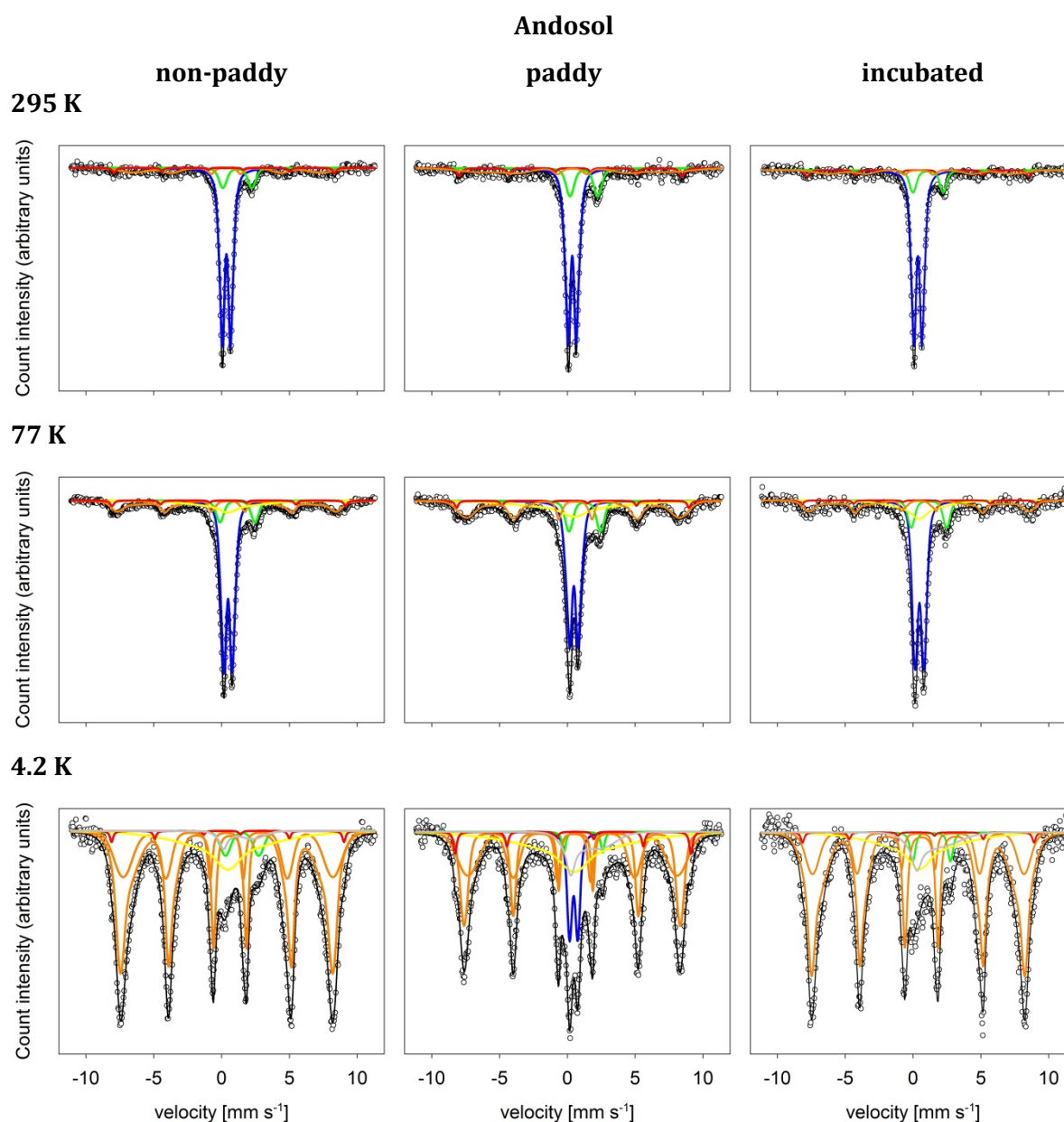


Fig. 3.3 Fitted Mössbauer spectra of Andosol topsoils at 295, 77 and 4.2 K (140, 40 and 13 K spectra can be found in Fig. A-2 of Appendix 2.2). From the incubation experiment spectra of samples with straw addition are presented. The black solid line is the total calculated fit through the discrete data points (circles). The resolved spectral components and assignments are: (1) Q-Fe^{III}, deep central doublet (blue) = Fe^{III} in silicates and in organic complexes (+ paramagnetic Fe^{III} (oxy-)hydroxides), (2) Q-Fe^{II}, wider and smaller doublet (green) = Fe^{II} in primary minerals, clays or sorbed, (3) HFD-OxHy-A, dominant sextet (orange) = magnetically ordered Fe^{III} (oxy-)hydroxides (sharp = (nano-)goethite; smooth = ferrihydrite), (4) HFD-Hae, wider and smaller sextet (red) = haematite, (5) HFD-OxHy-B, collapsed sextet (yellow) = Fe^{III} (oxy-)hydroxides near their blocking temperature, (6) HFD-Fe^{II}, asymmetric collapsed octet (grey) = Fe^{II} adsorbed to magnetically ordered Fe^{III} (oxy-)hydroxides.

Table 3.3 Abundance of Fe in different Fe phases as calculated from respective Mössbauer spectra. Standard deviations in brackets are fitting errors as calculated by Recoil™ software.

Fe [g kg ⁻¹]	Alisol			Andosol		
	non-paddy ¹⁾	paddy ²⁾	incubated ³⁾	non-paddy ⁴⁾	paddy ⁵⁾	incubated ⁶⁾
organic/silicate Fe ^{III}	7 (±1)	10 (±1)	7 (±1)	0 (±0)	7 (±1)	0 (±0)
Fe ^{II} in clays or sorbed	<1 (±<1)	1 (±1)	1 (±<1)	4 (±3)	1 (±1)	3 (±2)
Fe ^{II} on ordered Fe ^{III}	0 (±0)	0 (±0)	0 (±0)	2 (±4)	6 (±2)	7 (±4)
haematite	7 (±1)	2 (±1)	6 (±<1)	3 (±1)	3 (±1)	3 (±1)
goethite	0 (±0)	0 (±0)	0 (±0)	17 (±2)	14 (±2)	13 (±3)
Fe ^{III} OxHy SRO-1	45 (±2)	40 (±2)	47 (±1)	0 (±2)	6 (±2)	6 (±10)
Fe ^{III} OxHy SRO-2	9 (±3)	0 (±3)	3 (±2)	6 (±2)	2 (±2)	2 (±11)
Fe ^{III} OxHy SRO-3	3 (±2)	6 (±3)	5 (±2)	14 (±6)	13 (±3)	18 (±6)
Fe ^{III} OxHy SRO-4	6 (±2)	10 (±3)	2 (±3)	38 (±9)	7 (±5)	32 (±13)
Fe ^{III} OxHy SRO-5	10 (±1)	12 (±2)	14 (±1)	14 (±3)	15 (±3)	13 (±5)

1) Fe_{total} = 87.6 g kg⁻¹

4) Fe_{total} = 95.3 g kg⁻¹

2) Fe_{total} = 79.3 g kg⁻¹

5) Fe_{total} = 73.2 g kg⁻¹

3) Fe_{total} = 86.7 g kg⁻¹

6) Fe_{total} = 93.3 g kg⁻¹

3.4.3 Fe (oxy-)hydroxide changes in soils under paddy management

For the Alisol, the ⁵⁷Fe Mössbauer measurements agree broadly with the chemical extractions of Winkler et al. (2016), which include lower concentrations of crystalline Fe and higher concentrations of SRO Fe in the paddy topsoils than in the respective non-paddy topsoils (Fig. 3.1). While the amount of Fe binned to more crystalline portions of the Mössbauer SRO-Fe continuum (Fe^{III} OxHy SRO-1 and SRO-2) and haematite is smaller following redox fluctuations accompanying paddy cultivation (54 vs. 40 g kg⁻¹ and 7 vs. 2 g kg⁻¹, respectively), the amount of Fe binned to low crystallinity classes (Fe^{III} OxHy SRO-3 to SRO-5) was larger in the paddy than in the non-paddy topsoils (28 vs. 19 g kg⁻¹) (Table 3.3 and Fig. 3.4). Hence, the overall loss of Fe in the Alisol topsoil following paddy cultivation is accompanied by a decrease in Fe oxide crystallinity.

In the Andosol topsoils, however, the ⁵⁷Fe Mössbauer measurements did not broadly agree with the chemical extractions of Winkler et al. (2016), which showed lower concentrations of both crystalline and SRO Fe phases in the paddy than in the respective non-paddy topsoils (Fig. 3.1). Instead, the Mössbauer data propose paddy cultivation results in a loss of primarily SRO-Fe and no loss, or even a slight gain of more crystalline Fe phases. The Mössbauer measurements suggest >30 g kg⁻¹ less Fe^{III} OxHy SRO-4 class phases in the paddy than in the non-paddy topsoils (Table 3.3 and Fig. 3.4). The abundance of the other crystallinity classes remained equal within error, except the most crystalline class (Fe^{III} OxHy SRO-1), which was 6 g kg⁻¹ larger in the paddy than in the respective non-paddy Andosol topsoil. In addition, Fe^{III} in Fe-OM complexes/silicates and Fe^{II} exhibiting partial magnetic ordering (suggesting adsorption to Fe oxides) were about 7 g kg⁻¹ and 4 g kg⁻¹ larger in paddy than in non-paddy topsoils (Table 3.3 and Fig. 3.4). Thus, the

overall loss of Fe in the Andosol topsoil under paddy management reflected a strong depletion of highly disordered and substituted Fe oxides (Fe^{III} OxHy SRO-4), while the mass of the most crystalline components remained unchanged (goethite and haematite) or increased slightly (Fe^{III} OxHy SRO-1). This, in contrast to the Alisol, suggests an overall increase in crystallinity after exposure to redox fluctuation associated with paddy cultivation.

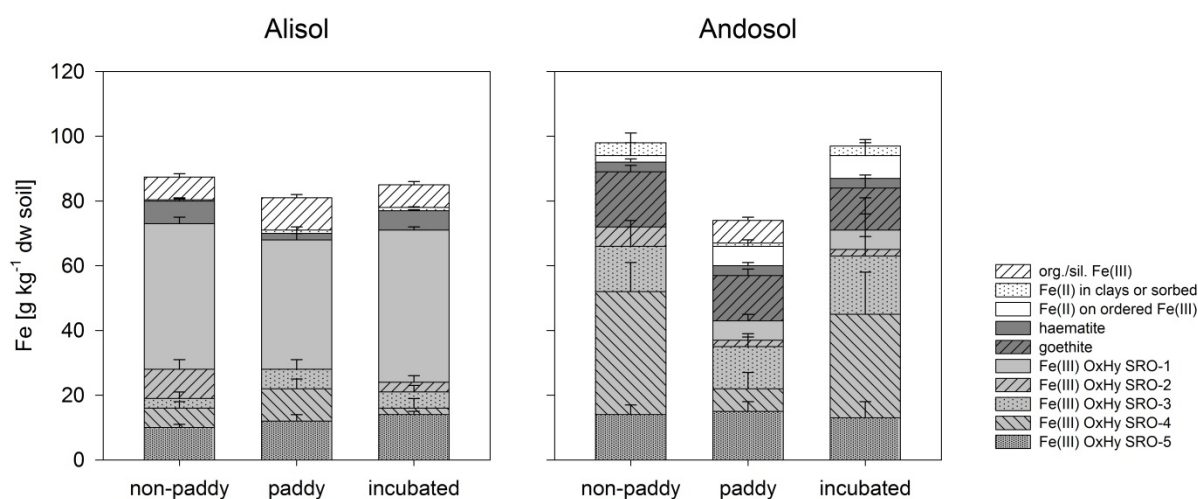


Fig. 3.4 Iron phase composition of Alisols and Andosols under different land use and of laboratory incubated non-paddy soils as calculated from Mössbauer spectra. SRO pools decrease in crystallinity from SRO-1 to SRO-5. Errors are standard deviations of fitting procedure as calculated by Recoil™ software. A more detailed description of the different Fe phases can be found in Table 3.2.

3.4.4 Soil solution composition during incubation of non-paddy topsoils

The experimentally imposed redox alternation caused the expected elevated Fe²⁺ and pH during anoxic conditions and depressed Fe²⁺ and pH during oxic conditions (Fig. 3.5). Oscillation of pH with larger values during anoxic phases is due to the consumption and release of H⁺ that accompanies the reduction and oxidation of Fe, respectively (Kirk, 2004). The redox effect of OM input and its decomposition is also evident. Samples receiving rice straw reached lower redox potentials, larger pH values, and larger aqueous Fe²⁺ concentrations under anoxic conditions than control samples that did not receive straw (Fig. 3.5). Aqueous Fe²⁺ production rates were larger in the Andosol than in the Alisol. Summing up the Fe²⁺ dissolved and withdrawn through sampling throughout the one-year incubation with 8 redox-cycles, the Alisol and Andosol lost 1.0 and 2.1% of their total Fe, respectively. That ratio of losses between the two soils (i.e., ~1:2 for Alisol:Andosol) is similar to the ratio observed in the field paddy soils (15 and 35%).

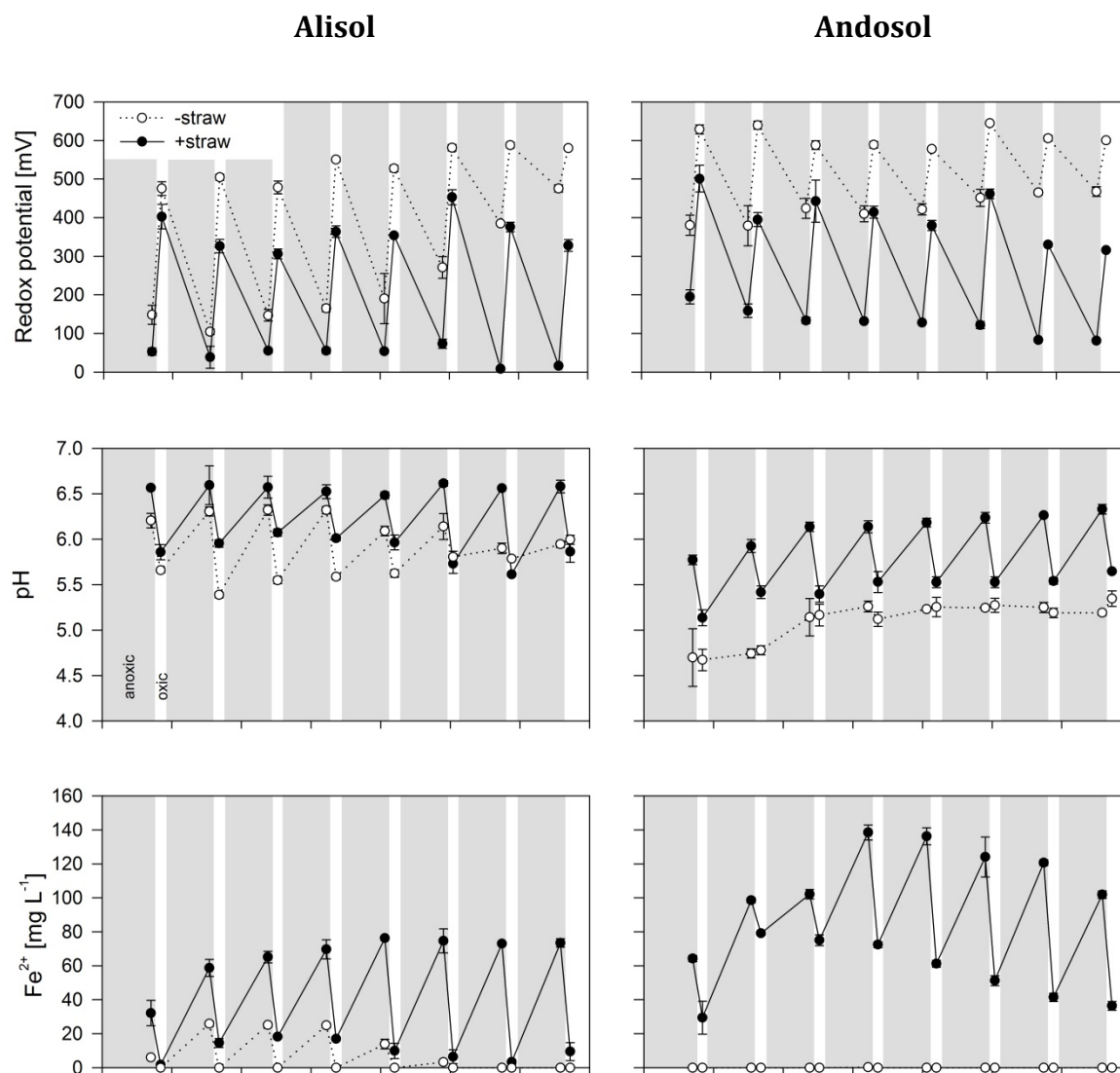


Fig. 3.5 Changes in redox potential, pH and dissolved Fe^{2+} concentrations with time in soil solutions (filtered with $0.45 \mu\text{m}$) of Alisol and Andosol non-paddy topsoils incubated with (+straw) and without straw (-straw) addition. Data points are means with error bars representing standard deviations ($n=3$).

3.4.5 Fe (oxy-)hydroxide changes in laboratory-incubated soils

At the end of the one-year incubation, soils were DCB- and AAO-extracted (data not shown) and underwent Mössbauer analyses. In both cases changes were small compared to the total amount of Fe oxides in the soils and were therefore in the range of calculated standard deviations. In the Mössbauer spectra, the laboratory-incubated Alisol (with straw addition) exhibited a slight decrease in the mass of Fe^{III} OxHy SRO-2 crystallinity class phases, while the mass of Fe phases in the lowest crystallinity class (Fe^{III} OxHy SRO-5) increased slightly (Table 3.3 and Fig. 3.4). This is similar to differences observed for paddy soils relative to non-paddy soils in the field. In the laboratory-incubated Andosol (with straw addition) the main decrease in Fe phases occurred in the Fe^{III} OxHy SRO-4 crystallinity class, which is also similar to what was observed in the field

paddy soils, but at a much lower magnitude (Table 3.3 and Fig. 3.4). In addition, as observed in the field, part of the highly disordered Fe phases appeared to recrystallize to the more ordered Fe^{III} OxHy SRO-1 crystallinity class and the magnetically ordered ferrous phases (suggestive of Fe^{II} adsorbed to Fe oxides) also appeared to increase following laboratory incubations. The formation of Fe^{III} containing organic and/or silicate phases seen in the field paddy soils, is not observed following laboratory incubation of the Andosol (Table 3.3 and Fig. 3.4). But we note that all of these changes were within the range of the calculated fitting errors (Table 3.3).

3.5 Discussion

3.5.1 Contrasting shifts in Fe crystallinity during redox fluctuations

When comparing soils that have been under repeated submergence and drainage for several decades (paddy) to neighboring soils under upland conditions (non-paddy), we found that long-term redox fluctuations associated with rice paddy cultivation resulted in lower amounts of pedogenic Fe in surface soils (Table 3.3 and Fig. 3.4) accompanied by differences in Fe mineral crystallinity. In response to redox fluctuations associated with rice paddy cultivation, the Alisol surface soil, rich in rather crystalline Fe oxides (haematite and Fe^{III} OxHy SRO-1 crystallinity class phases), exhibited lower Fe oxide crystallinity; while the Andosol surface soil, rich in SRO Fe phases (Fe^{III} OxHy SRO-3 to SRO-5 crystallinity class phases), exhibited higher Fe mineral crystallinity than the respective non-paddy topsoils. This suggests that the original Fe phase composition of the studied soils may have influenced the trajectory of its evolution under fluctuating redox conditions. In addition, also other factors such as SOM and soil hydrology, which regulate Fe²⁺ production and removal, likely play a role. Below we discuss the influence of the different factors on the two tested end-member soil types.

3.5.1.1 Decreasing Fe oxide crystallinity in the Alisol

We find that long-term redox fluctuations associated with paddy cultivation have resulted in a lower Fe oxide crystallinity in the Alisol since the paddy cultivated soils have smaller amounts of crystalline and larger amounts of SRO Fe oxides compared to the respective non-paddy Alisol. We suggest that the decrease in crystalline Fe oxides can be attributed in part to their high abundance relative to low crystallinity SRO Fe phases. Generally, Fe reduction rates are higher for SRO Fe oxides than for crystalline Fe oxides (Postma, 1993; Roden and Zachara, 1996; Roden, 2003; Bonneville et al., 2009). However, in soils with substantially more crystalline than SRO Fe

oxides, considerable reductive dissolution of crystalline Fe oxides can occur (Munch et al., 1978; Lovley et al., 2004).

Concomitantly, the increase in SRO Fe oxides might be attributed to soil hydrology. The Alisol-derived paddy soil's texture is finer and the bulk density of the plough pan is higher than it is in the Andosol-derived paddy soil (Table 3.1). This may have restricted leaching in the Alisol and may have favored the re-precipitation of previously dissolved Fe^{2+} , presumably as SRO Fe oxides. Hence, SRO Fe oxides are likely to become enriched in soils with initially large concentrations of crystalline Fe oxides and with restricted leaching when subjected to redox fluctuations. Likewise, Ginn et al. (2017) have proposed and numerically modeled this mechanism of partial dissolution of crystalline phases coupled to re-precipitation of SRO phases to explain how redox fluctuations can increase Fe reduction rates in carbon-rich systems with no leaching. In a field study with considerable leaching, Thompson et al. (2011) also found a preservation of SRO Fe oxides under redox fluctuating conditions. However, the initial fraction of SRO Fe oxides, as suggested by the lowest rainfall site with redox potentials hardly reaching Fe reducing conditions, was quite high ($\text{Fe}_{\text{AAO}}/\text{Fe}_{\text{DCB}} = 0.48$). Mössbauer measurements associated with this study (Thompson et al., 2011) showed that especially the least crystalline Fe phases (collapsed sextet at 4.2 K) were preserved at the highest rainfall site. That fraction might be Fe oxides strongly co-precipitated with OM (SOC contents are >10%), which would likely restrict the re-dissolution of these Fe oxides (Eusterhues et al., 2008). It is thus evident that additional factors besides initial Fe oxide crystallinity and leaching rate (e.g., OC input and storage) influence Fe oxide evolution under redox fluctuating conditions.

3.5.1.2 Increasing Fe oxide crystallinity in the Andosol

In contrast to the non-paddy Alisol, low crystallinity SRO Fe oxides dominate the Fe mineral composition of the non-paddy Andosol. Hence, in these soils, sufficient amounts of readily reducible Fe are likely available as alternative electron acceptors for reductive dissolution during anaerobic soil organic matter decomposition. The preferential dissolution of SRO Fe oxides and subsequent leaching, likely explains the relative enrichment of the remaining crystalline Fe oxides in the rice paddy-cultivated soils relative to the non-paddy soils. A substantial re-precipitation of SRO Fe oxides upon re-oxidation of the soil might be impeded by enhanced leaching or lateral transport due to the coarser texture and lower bulk density compared to the respective Alisol under paddy management (Table 3.1). This is supported by the distinctly larger loss of total Fe from the Andosol compared to the Alisol topsoil (Fig. 3.4) despite both being under paddy management for a similar period of time.

In contrast to our results, the field study of Thompson et al. (2011), which also examined SRO Fe-rich soils under fluctuating redox conditions and with intense leaching, showed crystallinity decrease due to the accumulation of SRO Fe–OM co-precipitates. These soils are under natural vegetation and hence rich in OC (>10%). In our case, agricultural soils were studied with farmers stating that rice straw was burned before spreading it on the field. Consequently, input of OC and further accumulation of Fe–OM co-precipitates in paddy soils was restricted.

An increase in Fe oxide crystallinity could also result from Fe²⁺-facilitated re-crystallization (Kukkadapu et al., 2003; Cornell and Schwertmann, 2003; Pedersen et al., 2005; Hansel et al., 2005; Yang et al., 2010; Tomaszewski et al., 2016) as we note a slight increase in the most ordered crystallinity class (Fe^{III} OxHy SRO-1), as well as an increase in Fe²⁺ adsorbed to Fe^{III} oxides in the Andosol under paddy management (Table 3.3, Fig. 3.3 and 3.4). The transformation is evidently rapid since the laboratory-incubated Andosol exhibits similar shifts in Mössbauer site populations (Table 3.3, Fig. 3.4). Several other redox fluctuation incubation experiments have also shown rapid re-crystallization of less crystalline to more crystalline Fe phases (Mejia et al., 2016; Tomaszewski et al., 2016). In all cases, pure ferrihydrite and hence SRO Fe oxides were used as starting material. Thompson et al. (2006) incubated natural soils rich in SRO Fe oxides, which also showed increasing crystallinity under redox fluctuation in closed systems. A field study of Vogelsang et al. (2016a) showed the transformation of ferrihydrite buried in rice paddy fields to goethite, lepidocrocite, and haematite within one year. So, where SRO Fe oxides dominate, Fe²⁺ emerging from their reductive dissolution likely adsorbs to SRO Fe oxides, which may lead to their re-crystallization as observed in the Andosol under paddy management.

3.5.2 Chemical extraction vs. ⁵⁷Fe Mössbauer spectroscopy

Aside from the Fe^{II} and Fe^{III} in primary minerals and phyllosilicates, all other Fe phases identified by Mössbauer spectroscopy are in theory soluble in dithionite solutions, and thus, should be included as “Fe in pedogenic forms” in a chemical extraction framework. Mössbauer spectroscopy suggests the total pedogenic Fe is at least 90% in the non-paddy Alisol and 95% in the non-paddy Andosol (Table 3.3). Since the DCB extraction solubilized only ~60% (Alisol) and ~50% (Andosol) of the total Fe, the DCB extraction clearly underestimates the fraction of pedogenic Fe in the tested soils. The AAO extraction, used to quantify the SRO Fe oxides in soils, especially ferrihydrite, solubilized 5% and 18% of total Fe for the non-paddy Alisol and Andosol, respectively. That barely accounts for the least crystalline Fe^{III} (oxy-)hydroxide phases (Fe^{III} OxHy SRO-5) in the Alisol (11%) and Andosol (15%) as identified by Mössbauer spectroscopy. Discrepancies between chemical extractions and Mössbauer spectroscopy have been identified previously (e.g., Wada and Wada, 1976; Thompson et al., 2011; Filimonova et al., 2016;

Vogelsang et al., 2016b). The underestimation of total pedogenic and SRO Fe oxides by chemical extractions is probably caused by the partial protection of the respective Fe oxides against dissolution due to their interaction with other mineral phases.

3.5.3 Associations of Fe and OM in the Andosol

Iron can be associated with OM in non-oxidic Fe–OM complexes or as Fe oxides co-precipitated with OM (Schwertmann et al., 2005; Thompson et al., 2011; Karlsson and Persson, 2012). The former is paramagnetic and in the Mössbauer spectrum appears as Fe^{III} doublet even at 4.2 K, while the latter is (fully) ordered and appears as SRO Fe^{III} (oxy-)hydroxide sextet or collapsed sextet at 4.2 K (Schwertmann et al., 2005; Thompson et al., 2011). The co-precipitation of Fe oxides with OM leads to structural disorder and lowers the Mössbauer ordering temperature proportionally as the C/Fe ratio increases (Mikutta et al., 2008; Eusterhues et al., 2008; Chen and Thompson, 2018).

Andosols typically have large OM contents (Table 3.1) due to the high abundance of SRO mineral phases (e.g., ferrihydrite, allophane). The non-paddy Andosol Mössbauer spectra do not contain any Fe^{III} doublets at 4.2 K, which would be consistent with direct Fe–OM complexes, but rather are dominated by highly disordered Fe (oxy-)hydroxide phases (Fe^{III} OxHy SRO-3 crystallinity class and below; Table 3.3 and Fig. 3.4), suggesting the presence of Fe oxide–OM co-precipitates rather than of Fe–OM complexes. This is supported by Filimonova et al. (2016), who published Mössbauer spectra of Andosols indicating the absence of Fe–OM complexes and the presence of Fe oxide–OM co-precipitates. It might be explained by the fact that the formation of Fe (oxy-) hydroxide phases is thermodynamically favored over the formation of Fe–OM complexes at the given pH range (pH > 4; Yuan et al., 1998).

A Fe^{III} doublet at 4.2 K is, however, observed in the Mössbauer spectra of the field Andosol under paddy cultivation. We suspect this does not represent Fe–OM complexes since these should also have formed during the year-long incubation with straw addition. The laboratory-incubated Andosol, though, did not show the respective Fe^{III} doublet at 4.2 K. Hence, a rather long-term process, e.g., Fe substitution during phyllosilicate formation, seems to play a role as will be further discussed below (section 3.5.4).

3.5.4 Fe-substituted halloysite formation probable in the Andosol-derived paddy soil

We only observed a low-temperature ferric doublet in the Andosol-derived paddy soil; none is present in the respective non-paddy soil nor in the laboratory-incubated non-paddy Andosol (Fig. 3.3). A Fe^{III} doublet at 4.2 K can represent Fe in Fe–OM complexes and/or in phyllosilicates.

We suspect this low-temperature ferric doublet forms under long-term paddy management and reflects a slow process, such as Fe substitution during the formation of phyllosilicates. As shown by Winkler et al. (2016), the Andosol under paddy management lost allophane and imogolite-type phases, which were likely partially transformed into halloysite. Substitution of Al by Fe in the octahedral sheet of the halloysite (Joussein et al., 2005) might be promoted during paddy cultivation due to the accumulation of dissolved Fe^{2+} in the anoxic soil solution, which subsequently becomes oxidized during the periodic draining of the soil. This would be consistent with the Fe^{III} doublet at 4.2 K in the oxic Andosol paddy. The suggested substitution of Al by Fe in halloysite leads to a charge difference under anoxic conditions when the structural Fe^{III} is reduced to Fe^{II} . Consequently, the halloysite gains negative surface charge, which increases its cation exchange capacity (Favre et al., 2002). In addition, the halloysite taking up Fe serves as Fe sink, since weathering of clay minerals is much slower than the cycling of Fe oxides. However, the suggested increase in Fe substituted phyllosilicates in the Andosol derived paddy soil might also result from input with irrigation water.

3.6 Conclusions

In a field study of two different soils, long-term fluctuating redox conditions were found to have contrasting effects on the crystallinity of Fe oxides possibly influenced by the initial soil's mineral composition as well as the leaching rate. Compared to the soils cultivated with upland crops, long-term paddy cultivation with redox fluctuation resulted in lower crystallinity in the Alisol initially rich in crystalline Fe oxides and in higher crystallinity in the Andosol initially rich in SRO Fe oxides. Although these trends were most evident in the field soils, short-term incubations involving redox fluctuations over a year, indicate similar trends. Considering similar OM input and decomposition rate, as well as similar redox frequency and duration, we suggest the starting Fe oxide crystallinity and water leaching rate are important factors influencing the trajectory of Fe oxide transformation. In the soil with initially large amounts of crystalline Fe oxides (Alisol), their reductive dissolution might be dominating. In combination with impeded leaching, re-precipitation as SRO Fe oxides is likely, resulting in an overall decrease in Fe oxide crystallinity. Whereas in the soil initially rich in SRO Fe oxides and with stronger leaching (Andosol), preferential reductive dissolution and removal of SRO Fe oxides may lead to the preservation of crystalline Fe oxides. In combination with Fe^{2+} -facilitated re-crystallization of SRO Fe oxides this may lead to the subsequent increase in Fe oxide crystallinity. These findings suggest that the trajectory of Fe mineral transformation in soils and sediments exposed to fluctuating redox conditions may, besides other environmental factors, depend on the initial Fe mineral composition as well as on the water leaching rate. However, for general conclusions on

factors controlling Fe mineral evolution under redox fluctuation, further studies covering additional soil types under a variety of environmental conditions are necessary.

3.7 Acknowledgements

The study was funded by Deutsche Forschungsgemeinschaft – DFG within the research unit FOR995 Biogeochemistry of Paddy Soil Evolution (grants FI 803/8-1, JA 523/16-1, KA 1737/10-1) and the National Science Foundation (EAR-1331841, EAR-1053470, EAR-1451508 and DEB-1457761). We gratefully acknowledge the support of Susanne Horka, Madina Burkitbayeva, Alexandra Boritzki and Christine Krenkewitz during the laboratory work and Jared Wilmoth for assisting with the Mössbauer spectroscopy measurements. We also thank the three anonymous reviewers for their valuable comments that greatly improved the manuscript.

4 Tracing organic carbon and microbial community structure in mineralogically different soils exposed to redox fluctuations

P. Winkler, K. Kaiser, R. Jahn, R. Mikutta, S. Fiedler, C. Cerli, A. Kölbl, S. Schulz, M. Jankowska, M. Schloter, C. Müller-Niggemann, L. Schwark, S. K. Woche, S. Kümmel, S. R. Utami, K. Kalbitz

Author contributions:

P.W. wrote the manuscript; S.R.U. coordinated soil sampling; P.W., K. Kaiser, C.M.-N. and L.S. conducted soil sampling; P.W. and K. Kaiser conducted the incubation experiment P.W., K. Kaiser, R.M., C.C., A.K., S.S., M.J., C.M.-N., S.K.W. and S.K. measured samples and analyzed data; P.W., K. Kaiser, K. Kalbitz, S. F. and R. J. designed the study; all authors commented on the manuscript

Published in Biogeochemistry (2019) 143: 31-54.

4.1 Abstract

Submerged rice cultivation is characterized by redox fluctuations and results in the formation of paddy soils, often accompanied by soil organic carbon (SOC) accumulation. The impact of redox fluctuations and the underlying soil type on the fate of organic carbon (OC) in paddy soils are unknown. Hence, we mimicked paddy soil development in the laboratory by exposing two soil types with contrasting mineral assemblages (Alisol and Andosol) to eight anoxic–oxic cycles over one year. Soils regularly received ^{13}C -labeled rice straw. As control we used a second set of samples without straw addition as well as samples under static oxic conditions with and without straw. Headspaces were analyzed for CO_2 and CH_4 as well as their $\delta^{13}\text{C}$ signatures, whereas soil solutions were analyzed for redox potential, pH, dissolved Fe^{2+} , and dissolved organic carbon (DOC and DO^{13}C). At the end of the experiment, when eight redox cycles were completed, mineral-associated organic matter (MOM) was isolated by density fractionation and characterized for $\delta^{13}\text{C}$, non-cellulosic carbohydrates, and lignin-derived phenols. Moreover, changes in the soil's microbial community structure were measured.

For both soil types, headspace data confirmed less respiration in straw-amended soils with redox fluctuation than in those under static oxic conditions. The $\delta^{13}\text{C}$ data revealed that, irrespective of soil type, straw carbon allocation into MOM was larger in soils with redox fluctuation than in those with static oxic conditions. A net increase in MOM after the one-year incubation, however, was only observed in the respective Andosol, probably due to abundant reactive minerals capable of OC uptake. In the Alisol, straw OC most likely exchanged initial MOM. A potential for lignin accumulation in the MOM of soils incubated with straw and redox fluctuation was observed for both soil types. Lignin and carbohydrates suggest a plant origin of MOM formed under redox fluctuation. The initially similar bacterial community composition of the Alisol and Andosol changed differently under redox fluctuation. The stronger change in the Alisol indicates less protective microbial habitats. In summary, the overall turnover of straw OC in soils under redox fluctuation seems to be independent of soil type, while net accumulation of SOC as well as the evolution of the bacterial community structure may in part depend on soil type, suggesting an impact of the soil's mineral composition.

4.2 Introduction

Redox fluctuation — the periodic alternation of oxic and anoxic conditions — occurs in soils with frequently changing water tables. Paddy soils repeatedly submerged during crop growth and drained for harvest undergo such redox fluctuation. Anoxic conditions evolve when the consumption of O_2 that accompanies organic matter (OM) decomposition is faster than the

diffusive re-plenishment of O₂ from the atmosphere (Reddy and Patrick 1983). The resulting depletion in O₂ as an electron acceptor mainly occurs in submerged soils. Microbes able to use alternative electron acceptors such as nitrate, manganese, iron, and sulfate take advantage and become dominant. The redox potential decreases accordingly. When alternative electron acceptors are used up as well, methanogenic microbes are stimulated, which decompose OC to CO₂ and CH₄ (Kirk 2004). Drainage of submerged soils leads to the reintroduction of O₂ and a rise in redox potential. The ability of the soil's microbial community to adapt to respective redox fluctuation determines its activity and hence the turnover of OC (Pett-Ridge and Firestone 2005; DeAngelis et al. 2010). Nevertheless, the impact of soil type on the microbial community exposed to redox fluctuation has not yet been elucidated (Gupta and Germida 2015). Furthermore, due to its greenhouse gas potential, the emission of CH₄ from paddy soils is of interest (Cao et al. 1996; Yan et al. 2003). The availability of alternative electron acceptors may vary in different soil types and methanogens may thus be more or less active.

Submerged paddy soils with prolonged anoxic periods are generally proposed to store more OC than upland soils due to its less efficient decomposition under anoxic conditions (Pan et al. 2003; Sahrawat 2004; Zhang and He 2004; Cheng et al. 2009; Wissing et al. 2011; Kalbitz et al. 2013; Yan et al. 2013). Especially lignin is known to decompose slowly under anoxic conditions (Hackett et al. 1977; Zeikus et al. 1982), and thus, often accumulates in paddy soils (Olk et al. 1996; Bierke et al. 2008). However, recent data indicate that submerged paddy cultivation does not always lead to enhanced OC sequestration and lignin accumulation. We found larger OC concentrations and stocks in only two out of four paddy soils when comparing them to the respective non-paddy soils in the same region in Indonesia (Winkler et al. 2016). The same non-paddy and paddy soil pairs were analyzed by Urbanski et al. (2017) who found no difference in lignin concentrations, not even in those pairs that showed larger SOC concentrations in paddy than in non-paddy soils. Furthermore, Huang et al. (1998) observed faster decomposition of straw submerged in paddy soils compared to upland soils, which was confirmed in a recent study by Hanke et al. (2013), who found larger OC decomposition during anoxic than oxic phases of incubated paddy soils.

Besides redox dependent decomposition rate, there seem to be additional factors controlling the fate of SOC in paddy soils. Organic matter input influenced by land use intensity and residue management is such a factor (Neue et al. 1997; Kögel-Knabner et al. 2010; Wissing et al. 2011). A long-term field study of Bhattacharyya et al. (2013) showed that two decades of rice straw incorporation into paddy soils resulted in increasing SOC concentrations while paddy soils with straw removal showed constant SOC. Also, studies in the red soil area of south-east China suggest that larger biomass production and consequently larger residue inputs into submerged paddy soils stimulate OC accumulation. This has been explained by increased pH and phosphate availability as a result of reductive dissolution of Fe (oxyhydr-)oxides (in the following

summarized as 'Fe oxides') as well as by reduced leaching of nutrients due to the dense plough pan in paddy soils (Zhang and He 2004; Yan et al. 2013).

A further crucial — yet understudied — factor determining the fate of OC under paddy management is the parent soil type (Kögel-Knabner et al. 2010; Huang et al. 2015). Soils exposed to paddy management can strongly differ in mineral composition, initial pH, and microbial biomass. Variable mineralogical composition and possible mineral transformations under redox fluctuation may impact the soil's OC storage capacity. Redox-sensitive minerals like Fe oxides have large OC storage capacities under oxic conditions but might be lost from paddy topsoils due to their reductive dissolution and leaching during anoxic conditions. Organic carbon associated with Fe oxides can become mobilized and might be lost as well (Said-Pullicino et al. 2016). At the same time, the remaining Fe oxides may transform towards larger or lower crystallinity (Winkler et al. 2018). Iron oxides of low crystallinity are known to have large OC storage potential (Herndon et al. 2017). Changes in Fe oxide crystallinity upon redox fluctuation may thus have an impact on the OC storage capacity of paddy soils (Cheng et al. 2009; Coby et al. 2011; Yan et al. 2013). Furthermore, Neue and Scharpenseel (1987) showed that only for soils with an initial pH > 6, straw mineralization was larger under aerobic than under anaerobic conditions, while in soils with initial pH < 5 there was no difference in mineralization between the different redox states. Hence, in initially acidic soils the pH increase during anoxic phases might stimulate microbial activity (Sahrawat 1998), and thus, likewise cause similar SOC levels as under non-paddy conditions.

Taking the above considerations together, microbial community composition, redox-dependent decomposition rate, OC input, and the soil type under paddy management seem to be important factors controlling OC turnover and SOC formation in paddy soils. The contribution of each factor, however, has not yet been well studied. We therefore performed a one-year incubation experiment with two contrasting soil types (Alisol and Andosol) under redox fluctuation or static oxic conditions and with identical straw input for both redox treatments. In order to determine the fate of OC, the incubation experiment was performed using ¹³C-labeled rice straw. Respiration (CO₂ and CH₄) and soil solution chemistry (including DOC and Fe²⁺) were monitored during the incubation and soils were fractionated by density at the end of the experiment to determine the role of minerals for SOC formation. Since carbohydrates and lignin represent the major constituents of plant residues, their contents in mineral-associated organic matter (MOM) were determined after chemolytic depolymerization. The evolution of the soil's microbial community was analyzed after DNA and cell membrane lipid extractions.

Based on this experiment, we are thus addressing the following research questions:

1. Do decomposition rates of OC differ between different redox regimes and soil types?
2. Do fluctuating redox conditions with regular straw addition cause measurable incorporation of OC into mineral-organic associations?
3. Do certain biomarkers (lignin-derived phenols and non-cellulosic carbohydrates) preferentially contribute to the formation of MOM and are contributing biomarkers plant-derived or microbial derived?
4. Do soil type and redox regime have an impact on the soil microbiome composition and methanogenic communities?

4.3 Materials & Methods

4.3.1 Soil selection and sampling

Soil samples of the Alisol and Andosol were collected from Java (Indonesia), where they represent typical soil types under paddy management. Both sampling sites have a tropical monsoon climate and an andesitic parent material. The Alisol site is located near Jasinga (West Java, 6.54°S, 106.52°E, 250 m a.s.l.). Parent material is Tertiary andesitic tuff. The Alisol is already at an advanced stage of weathering, and thus, has a mineral assemblage comprising kaolinite, high-activity clays, and more crystalline Fe oxides. The Andosol site is near Sukabumi (West Java, 6.88°S, 106.94°E, 900 m a.s.l.), on the terraced slope of Mount Gede. Parent material is a Quaternary lahar, mainly composed of andesitic pyroclasts. The Andosol is a relatively young soil and therefore is comprised of SRO metastable phases such as allophane, imogolite, and ferrihydrite (Winkler et al. 2016).

Both sites were adjacent to paddy fields but have been managed with upland crops including cassava, cabbage and bananas (non-paddy management). Non-paddy soils were used for the incubation experiment to simulate the conversion of a non-paddy soil to a paddy soil. At each site, a main profile was excavated to > 1 m, described according to FAO (2006), classified according to IUSS Working Group (2006), and sampled by horizon. For each horizon, a bulk sample was created by mixing soil from different spots within the profile. Bulk samples were air-dried and sieved to < 2 mm. A detailed profile description is given by Winkler et al. (2016). For the incubation experiment, the second topsoil horizon (Alisol = 7-14 cm, Andosol = 7-16 cm) was used. The initial OC concentration of the respective Alisol was 18.5 g kg⁻¹, pH (CaCl₂) was 5.4 and pedogenic Fe concentration (Fe_{DCB}) was 54.2 g kg⁻¹, with Fe present in SRO phases (Fe_{AAO}) accounting for 7% of total pedogenic Fe (Winkler et al. 2016). The initial Andosol had an OC concentration of 33.2 g kg⁻¹, pH (CaCl₂) was 4.6 and Fe_{DCB} was 44.5 g kg⁻¹, with Fe in SRO phases

accounting for 39% of total pedogenic Fe (Winkler et al. 2016). The characteristics of the initial Alisol and Andosol used for the incubation experiment are summarized in Fig. 4.1.

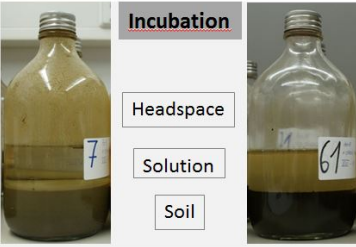
	Alisol	Initial soils	Andosol
OC [g kg ⁻¹]	18.5		33.2
pH _{CaCl2}	5.4		4.6
Fe _{total} [g kg ⁻¹]	87.6		95.3
Fe _{DCB} [g kg ⁻¹]	54.2		44.5
Fe _{AAO} [g kg ⁻¹]	4.1		17.1
Fe _{AAO} /Fe _{DCB}	0.07		0.39
Treatments	8 redox cycles 1 cycle = 5 weeks anoxic + 1 week oxic		static oxic conditions
with straw addition at the beginning of each cycle δ ¹³ C of straw = 230‰	a-o (+)		o (+)
without straw addition	a-o (-)		o (-)
	Headspace	Solution	Soil
Sampling	a-o: every 1-2 weeks o: every week	a-o: after anoxic & oxic phases o: no solution for sampling	at the end of the incubation
Analyses	CO ₂ & CH ₄ δ ¹³ C of CO ₂	Eh, pH, Fe ²⁺ , DOC δ ¹³ C of DOC	density fractionation + δ ¹³ C MOM: biomarkers lipids & microbial taxonomy

Fig. 4.1 Overview of Materials & Methods with data of initial soils from Winkler et al. (2016), with Fe_{DCB} = dithionite-citrate-bicarbonate extractable Fe and Fe_{AAO} = acid-ammonium-oxalate extractable Fe. The different treatments are fluctuation of anoxic and oxic conditions (a-o), static oxic conditions (o), with (+) and without (-) straw addition. The density fraction MOM = mineral-associated organic matter, while biomarkers comprise lignin-derived phenols and non-cellulosic carbohydrates.

4.3.2 Specific surface area and surface element composition of initial soils

In addition to the initial soil characteristics determined by Winkler et al. (2016), we measured soil surface characteristics relevant to SOC stabilization, including specific surface area (SSA), the elemental composition of particle surfaces, and the composition of surface-attached OM. The SSA of OM-free and outgassed initial bulk soils was determined by adsorption of N₂ using the multi-point BET approach (Autosorb iQ surface area analyzer; Quantachrome Instruments, Boynton Beach, FL, USA). Details can be found in Appendix 3.1.

The elemental composition of the soil particle's outmost surface layer was characterized by X-ray photoelectron spectroscopy (XPS, maximum analysis depth about 10 nm). Survey spectra as well as C 1s detail scans were recorded with a Kratos Axis Ultra DLD instrument (Kratos Analytical Ltd., Manchester, UK). Surface elemental composition in terms of atomic-% was evaluated by quantifying the survey scans with the software Vision 2 (Kratos Analytical, Manchester, UK). The Si, Al, Fe, and C content within the particle surface layer was compared to total Si, Al, and Fe contents measured by wavelength-dispersive X-ray fluorescence (XRF)

spectroscopy (SRS 3000 with Rh tube; Siemens AG, Karlsruhe, Germany) and to total organic carbon (TOC) concentrations measured by dry combustion at 950 °C using a Vario MAX elemental analyzer (Elementar Analysensysteme GmbH, Hanau, Germany). Carbon speciation of the XPS C 1s detail scans was performed using the software package Unifit 2016 (Unifit Scientific Software GmbH, Leipzig, Germany), following Poggenburg et al. (2018). Further details can be found in Appendix 3.2.

4.3.3 Laboratory incubation experiment

The incubation of the Alisol and Andosol non-paddy topsoils was performed in triplicates using 1.2-L glass flasks closed by a gas-tight septum at 25 °C in the dark. Two hundred gram aliquots of air-dried soils were pre-incubated with a 5 mM CaCl₂ solution at 50% maximum water holding capacity for two weeks to re-constitute microbial activity. Overall, four treatments were prepared for both soil types:

- (1) redox fluctuation without rice straw = a-o (-),
- (2) redox fluctuation + ¹³C-labeled rice straw = a-o (+),
- (3) static oxic conditions without rice straw = o (-), and
- (4) static oxic conditions + ¹³C-labeled rice straw = o (+).

Soils were prepared for redox fluctuation by submerging them in 500 ml of degassed 5 mM CaCl₂ solution. To initiate the anoxic phase, samples were flushed with N₂. After five weeks, the supernatant soil solution was exchanged by a fresh solution and the one week oxic phase was induced by flushing the soil slurry and headspace with pure O₂ for one minute before closing the flask. The next anoxic phase was initiated by adding straw and flushing with N₂ again. The procedure was repeated until eight redox cycles were completed. Each cycle included a five week anoxic period and a one week oxic period. Anoxic and oxic phases are shorter than in the field but the ratio of 5:1 (anoxic:oxic) roughly represents field conditions. In contrast to submerged samples under redox fluctuation, the set of samples under static oxic conditions was incubated at 50% maximum water holding capacity and with an O₂-filled headspace.

Treatments with rice straw application received ¹³C-labeled rice straw (450 g OC kg⁻¹ straw, δ¹³C = 230‰) at a rate of 0.3 g of straw OC per 1 g of SOC across eight addition time points. Samples of both redox treatments received straw every six weeks, which corresponds to the beginning of each anoxic phase in the treatment with redox fluctuation. The straw had a particle size of < 10 mm and was mixed with the soil by shaking the incubation flasks. To ensure similar conditions for all samples, also flasks without straw addition were homogenized every six weeks.

Within one redox cycle, the headspace of incubation flasks was sampled after the first, third, fifth (end of anoxic phase) and sixth week (end of oxic phase) in order to measure CO₂, CH₄ and δ¹³C of CO₂. Flasks with submerged soil were shortly shaken end-over-end about 24 hours before each headspace sampling. The headspace of flasks incubated under static oxic conditions was sampled weekly without prior shaking. Gas samples were taken into pre-evacuated gas vials and the pressure within incubation flasks and sample vials before and after sampling was recorded. As headspace sampling reduced pressure in the flasks, N₂ (anoxic phase) or O₂ (oxic phase) were added to re-establish atmospheric pressure.

Incubation flasks of samples under redox fluctuation were opened after each anoxic and each oxic phase in order to directly measure pH and Eh (referenced to the standard H₂ electrode) in the supernatant, immediately after opening the flasks under laboratory atmosphere (24 h after homogenization and sedimentation). Soil solution samples of 300 ml (supernatant) were retrieved from submerged samples under redox fluctuation and replaced by fresh CaCl₂ solution. To gain comparable soil solution data, soils exposed to redox fluctuation were submerged with the same soil-to-solution ratio for the oxic phases as for anoxic phases. The establishment of oxic conditions, despite being submerged, was ensured by using pure O₂. The collected soil solutions were filtered (< 0.45 μm, polyethersulfone membranes) either in a glove box with argon atmosphere (anoxic samples) or in the laboratory atmosphere (oxic samples). The low water content of samples under static oxic conditions did not allow for solution sampling.

Soil sampling was performed under oxic conditions at the end of the experiment. One part of soil samples was directly frozen at -20 °C for microbial analyses; the remaining part was freeze-dried and stored at room temperature until analyses. The different treatments, kind of samples and their analyses are summarized in Fig. 4.1.

4.3.4 Headspace analyses

As a measure of microbial activity, concentrations of CO₂ and CH₄ in gas samples were measured with a ThermoQuest Trace GC 2000 gas chromatograph with flame ionization detector (FID) (Thermo Scientific, Milan, Italy). The amount of CO₂ and CH₄ in the headspace of the incubation flasks was calculated by the general gas law. For the submerged soils, the CO₂ and CH₄ dissolved in the soil solution were also calculated using the respective Bunsen absorption coefficients and pH of the soil solution. The total amount of CO₂ and CH₄ in the flask at the time of sampling was calculated by adding the amount of CO₂/CH₄ in the headspace and the amount of CO₂/CH₄ dissolved in the soil solution. In order to obtain comparable results for both soil types, we divided the produced CO₂/CH₄ by the amount of OC in the incubation flasks including the native OC of the initial soil plus the OC added with straw at the beginning of each cycle minus the OC

mineralized since the beginning of the incubation. The amounts of CO₂/CH₄ (in mg g⁻¹ OC) produced in between two sampling time points were summed up for the entire incubation period of 48 weeks.

The δ¹³C of CO₂ in the headspace samples was analyzed by a Trace Gas chromatograph (Elementar UK, Manchester, UK) equipped with a Gilson GX-271 autosampler (Gilson Inc., Middleton, United States) and coupled with an Isoprime 100 isotope ratio mass spectrometer (IRMS) (Elementar UK, Manchester, UK). Isotope ratios were expressed as delta notation in parts per thousand (‰) relative to the international standard Vienna Pee Dee belemnite (V-PDB). The proportion of CO₂-C derived from straw was calculated according to Balesdent et al. (1990). For cost reasons, the δ¹³C of CH₄ could not be measured directly. The fraction of CH₄ from straw was instead estimated via the total OC budget, as outlined in section 4.3.7. Details on headspace measurements and gas data analyses are given in Appendix 3.3.

4.3.5 Soil solution analyses

Solutions of submerged soil samples were analyzed for dissolved Fe²⁺ by the ferrozine method (modified after Stookey 1970) in a glove box (anoxic solutions) or under laboratory atmosphere (oxic solutions). The remaining solutions were frozen for DOC measurements; concentrations of DOC were determined as difference between total and inorganic carbon by a TOC-VCPH/CPN (Shimadzu Corp., Kyoto, Japan).

The δ¹³C value of DOC was analyzed directly in solution using a high-temperature combustion system (Federherr et al. 2014; Kirkels et al. 2014). For this, an isoTOC cube (Elementar group, Langenselbold, Germany) TOC analyzer was coupled with a continuous flow IRMS (Isoprime 100, Elementar UK, Manchester, UK). The proportion of DOC derived from straw was calculated according to Balesdent et al. (1990). For the final budget, only the DOC from straw that had been removed with each sampling was considered since the remaining DOC in the flask could be mineralized or transferred into mineral-organic associations during the subsequent cycles. Additional details on soil solution measurements and data analyses are given in Appendix 3.4.

4.3.6 Density fractionation of soil OM

Soil OM was separated into three density fractions (free particulate OM = FPOM, occluded particulate OM = OPOM, mineral-associated OM = MOM) using a Na₆(H₂W₁₂O₄₀) solution with a density of 1.6 g cm⁻³ (Christensen 1992). Based on preliminary tests performed according to Cerli et al. (2012), we applied sonication energy of 50 J ml⁻¹ to the Andosol and 200 J ml⁻¹ to the Alisol samples in order to quantitatively recover the OPOM fraction. The yield of all fractions

was determined and their OC concentrations were measured using a Vario MAX elemental analyzer (Elementar Analysensysteme GmbH, Hanau, Germany); the $\delta^{13}\text{C}$ of each fraction was measured by an EA (Eurovector Hekatech, Wegberg, Germany) coupled via Conflo III interface to a Delta V Advantage IRMS (Thermo Scientific, Bremen, Germany), and the proportion of FPOM, OPOM, and MOM derived from straw was calculated according to Balesdent et al. (1990). Additional details on density fractionation and data analyses are given in Appendix 3.5.

4.3.7 Calculation of OC budget

For CO_2 , DOC, FPOM, OPOM, and MOM, the amount of carbon from straw was calculated based on their ^{13}C values, summed up for each incubation flask, and compared to the C added with straw. The amount of CH_4 from straw could not be measured. However, the static oxic samples showed no CH_4 formation and the calculated recovery of straw carbon for the Alisol and Andosol was 99 and 94%, respectively. Based on these high recoveries, we considered the difference in the OC budget (added straw OC minus straw OC in all fractions) as the amount of straw-derived $\text{CH}_4\text{-C}$ released during submergence. Exact values for the total as well as the straw OC budget are given in Table A-4.1 in Appendix 4.

4.3.8 Lignin-derived phenols

The mineral-associated OM was analyzed for lignin-derived constituents by digesting lignin through alkaline CuO oxidation according to Hedges and Ertel (1982) and analyses of resulting monomers by GCMS-QP 2010 (Shimadzu Corp., Kyoto, Japan). As indicator for the lignin content of a soil, the VSC was determined by adding the vanillyl (V), syringyl (S) and cinnamyl (C) units, with V = vanillin + acetovanillone + vanillic acid, S = syringaldehyde + acetosyringone + syringic acid and C = p-coumaric acid + ferulic acid. Also, the acid-to-aldehyde ratio of vanillyl, $(\text{Ac}/\text{Al})_v$, and syringyl units, $(\text{Ac}/\text{Al})_s$, was calculated as indicator for the oxidation state of lignin compounds with larger ratios representing stronger microbial oxidation (Ziegler et al. 1986). Analyses were done in triplicate. Additional details are given in Appendix 3.6.

4.3.9 Non-cellulosic carbohydrates

Non-cellulosic carbohydrates in the mineral-associated OM were analyzed after hydrolysis with 4 M trifluoroacetic acid according to Eder et al. (2010). Gas chromatographic separation and detection with FID was carried out on a GC Agilent 6890 (Agilent Technologies, Waldbronn,

Germany). Analyses were done in triplicate. The sum of carbohydrate-C (rhamnose + fucose + arabinose + xylose + mannose + galactose + glucose) and the ratio of (galactose + mannose) and (arabinose + xylose) = GM/AX were calculated. Prevalence of plant sugars was considered at GM/AX <0.5, and of microbial sugars at GM/AX >2 (Oades 1984). The $\delta^{13}\text{C}$ of individual carbohydrates was determined by GC-IRMS featuring a CTC CombiPAL autosampler (CTC Analytics AG, Zwingen, Switzerland), a 7890A GC device (Agilent Technologies), and a GC IsoLink interface connected via a ConFlo IV open split system to a MAT 253 IRMS (Thermo Scientific, Bremen, Germany). The proportion of straw-derived OC in individual carbohydrates was calculated according to Balesdent et al. (1990). Additional details are given in Appendix 3.7.

4.3.10 Microbial DNA extraction and sequencing data analysis

The composition of the microbial community of the initial field soils as well as of the final soils incubated with straw was analyzed from the DNA pool based on the 16S rRNA gene. DNA was extracted from 500 mg frozen soil by using the NucleoSpin®Soil Kit (Macherey-Nagel, Düren, Germany). The quality of the DNA was checked with a Nanodrop 1000 spectrophotometer (PeqLab, Erlangen, Germany). The quantity of the DNA was determined with the Quant-iT PicoGreen dsDNA Assay Kit (Life Technologies, Carlsbad, CA, USA). Next generation amplicon sequencing was performed using the MiSeq technology and basically followed the “16S Metagenomic Sequencing Library Preparation” protocol (Illumina Inc., San Diego, CA, USA) and the guidelines published by Schöler et al. (2017). After each PCR the concentration of the PCR product was measured with the Quant-iT PicoGreen dsDNA Assay Kit and the size of the amplicon was checked on a Bioanalyzer 2100 instrument (Agilent Technologies, USA) using a DNA 7500 chip (Agilent Technologies, Santa Clara, CA, USA). Finally, libraries were diluted to 4 nM and sequenced with the MiSeq Reagent kit v3 (600 cycles) (Illumina Inc.) for paired-end sequencing. Sequences have been submitted to the NCBI Sequence Read Archive with SRP148981 as accession number.

Sequencing data were analyzed with the QIIME software package version 1.9.1 (Caporaso et al. 2010) as described by Estendorfer et al. (2017). The sequencing dataset was rarefied to 19,508 reads per sample, to ensure comparability of the samples. The rarefaction curve (Fig. A-4.3 in Appendix 4) demonstrates that still a sufficient coverage was reached for all of the samples. Additional analyses were done with the R environment version 3.1.2 (Team 2008). To display the distance of the samples (β -diversity), a principal coordinate analysis plot (PCoA) was created using ggplot2 (Wickham 2009). Additional details are given in Appendix 3.8.1 and 3.8.2.

4.3.11 Microbial cell membrane lipids

Microbial cell membrane core lipids are relatively stable in soils and hence provide a long-term integrated picture of microbial activity. Core lipids of isoprenoid glycerol dialkyl glycerol tetraethers (iGDGTs) were obtained by automated solvent extraction using an ASE 200 (Dionex, Sunnyvale, CA, USA) at a temperature of 75 °C and a pressure of 5.0×10^6 Pa. All samples were analyzed by atmospheric pressure chemical ionization–mass spectrometry (HPLC–APCI–MS), following the analytical protocol described by Hopmans et al. (2000) and Schouten et al. (2007). HPLC–MS was performed using a Quattro LC triple quadrupole mass spectrometer (Micromass UK, Wilmslow, UK) equipped with an atmospheric pressure chemical ionization interface operated in positive ion mode. Further details are given in Appendix 3.8.3. The ratio of GDGT-0 versus Crenarchaeol was used as indicator for the presence of methanogenic archaea, with a ratio >2 indicating the dominance of methanogenic lineages within the archaea (Ayari et al. 2013).

4.3.12 Statistics

All treatments of the laboratory incubation experiment were prepared in triplicates. Respective data are given as means and errors are presented as standard deviations. For comparison of means of initial soils and their treatments, we applied a one-way repeated measures ANOVA. If statistically significant differences ($p < 0.05$) were found, an all pairwise multiple comparison procedure with familywise error rate control (Holm-Sidak method, $\alpha = 0.05$) followed, in order to isolate groups that differed from the others. Respiration data were tested by comparing the final cumulative values. For comparison of redox potential, pH and dissolved Fe^{2+} in samples with and without straw addition, the means of respective data of all anoxic and all oxic time points were determined separately. Then means of samples with and without straw addition were compared by paired t-tests with $\alpha = 0.05$. The same test was used to compare data pairs showing the fate of straw under redox fluctuation and static oxic conditions. The significance of differences in the abundance of bacterial families was tested with pairwise t-tests adjusted with Bonferroni correction for multiple testing with $\alpha = 0.05$. Correlation was analyzed by linear regression. Statistical analyses were performed using Sigma-Plot version 11.0 (SPSS Inc.).

4.4 Results

4.4.1 Surface characteristics of initial soils

The SSA of the initial Alisol's and Andosol's mineral matrix after removal of surface OM was 62 and 124 m² g⁻¹, respectively (Table 4.1). The elemental composition of the initial particle surfaces comprised oxygen (O) as the main component, carbon (C) and nitrogen (N) in organic components, and Si, Al, Fe, titanium (Ti), calcium (Ca), and sodium (Na) in minerals. The two initial soils showed some marked differences. The Alisol surface layer had a significantly lower C and N content and higher Fe and Si content than the Andosol surface layer ($p < 0.001$; data not shown). The ratios of surface Si, Al, and Fe to bulk sample Si, Al, and Fe were <1 for both soil types, indicating a depletion of these elements within the particle surface layer, while ratios of surface OC to bulk sample OC were >1 , indicating surface accumulation of OC. A more pronounced depletion of Si, Al, and Fe as well as larger accumulation of OC at the Andosol's than at the Alisol's surfaces indicate a larger OC coverage of mineral particles in the original Andosol (Table 4.1). In addition, we noted distinct differences between the soil types with respect to abundant C species present at mineral surfaces. While reduced C species (C—C, C=C) dominated particle surfaces of the Alisol, more oxidized C species (C-O bonds) as contained in carbohydrates prevailed in case of the Andosol (Fig. A-4.1 in Appendix 4).

Table 4.1 Ratio of surface element composition as determined by X-ray photoelectron spectroscopy (XPS) and total element concentration as determined by X-ray fluorescence (XRF) spectroscopy (Si, Al, Fe) and elemental analyzer (C). Concentrations of OC refer to the mineral associated OC since respective data were determined after the removal of particulate OC via density fractionation. A ratio <1 indicates surface depletion and a ratio >1 surface accumulation of the respective element. Specific surface area (SSA) is given for soils after OM removal.

surface element concentration / total element concentration both in [weight %]	Si	Al	Fe	C	SSA [m ² g ⁻¹]	C loading [mg m ⁻²]
Alisol	0.8	0.9	0.6	3.2	62	0.30
Andosol	0.6	0.7	0.4	4.9	124	0.27

4.4.2 Soil respiration

The total production of CO₂-C and CH₄-C per g OC was higher in Alisol (> 200 mg g⁻¹) than in Andosol samples (< 200 mg g⁻¹) ($p = 0.001$) and was generally larger in samples with straw addition (> 150 mg g⁻¹) than without straw addition (< 50 mg g⁻¹) ($p < 0.001$) (Fig. 4.2). In samples of both soil types incubated with regular addition of straw, mineralization was

significantly larger under permanently oxalic than under alternating redox conditions ($p = 0.003$). In samples without straw addition, respiration was larger under fluctuating redox conditions in the Alisol ($p < 0.001$), while it was larger under static oxalic conditions in the Andosol ($p < 0.001$) (Fig. 4.2). Incubation under alternating redox conditions resulted in the production of CH_4 only in the soils with straw addition, with CH_4 production starting distinctly later and being significantly lower in the Andosol than in the Alisol ($p < 0.003$) (Fig. A-4.2 in Appendix 4).

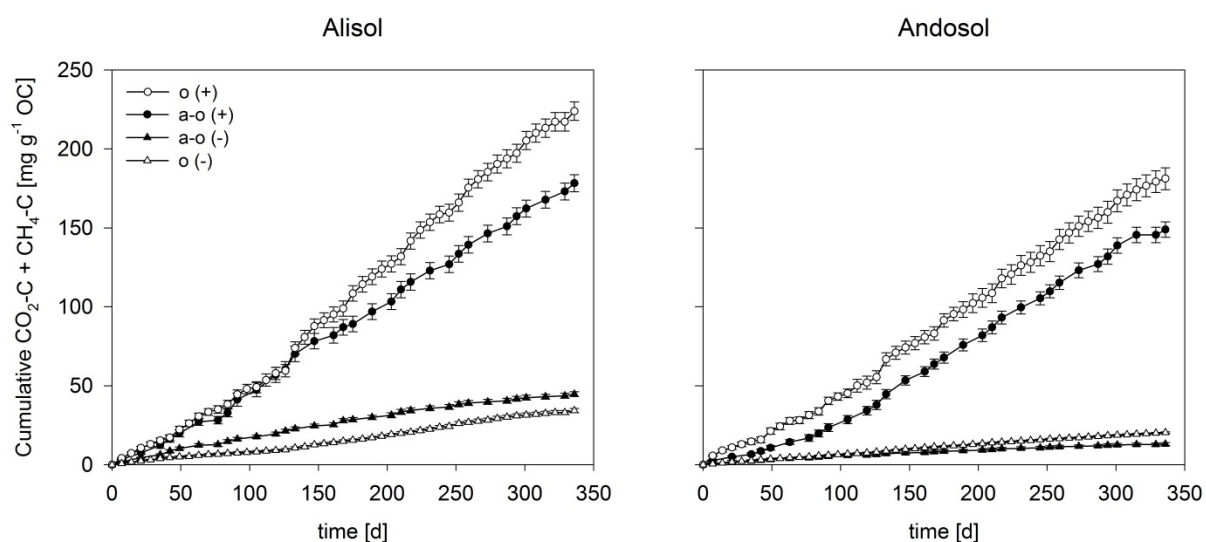


Fig. 4.2 Cumulative sum of $\text{CO}_2\text{-C}$ and $\text{CH}_4\text{-C}$ respired from the Alisol (left) and Andosol (right) incubated with alternating redox (a-o) and permanently oxalic (o) conditions as well as with (+) and without (-) straw addition. Respiration refers to total OC, which takes into account OC of initial soils, added straw OC, and OC mineralized in between sampling dates. Error bars represent standard deviations with $n = 9$ (1st cycle), $n = 6$ (2nd & 3rd cycle), and $n = 3$ (4th-8th cycle).

4.4.3 Soil solution chemistry during incubation

The imposed redox alternation caused the expected increase in Fe^{2+} concentrations and pH during anoxic conditions (Fig. 4.3a-d). Samples receiving rice straw reached lower redox potentials (< 200 mV), higher pH values (> 6), and higher dissolved Fe^{2+} concentrations under anoxic conditions than control samples not receiving straw (Fig. 4.3a-d). Tests showed that these differences were statistically significant ($p < 0.008$), except the difference between the pH values in the oxalic Alisol samples. Dissolved Fe^{2+} was significantly higher in the Andosol (up to 140 mg L^{-1}) than in the Alisol (up to 70 mg L^{-1}) ($p < 0.002$). Despite the addition of straw, DOC concentrations were low ($\approx 5 \text{ mg L}^{-1}$) and fluctuation in DOC concentrations coincided with redox fluctuation only in the Andosol when straw had been applied (Fig. 4.3e-f).

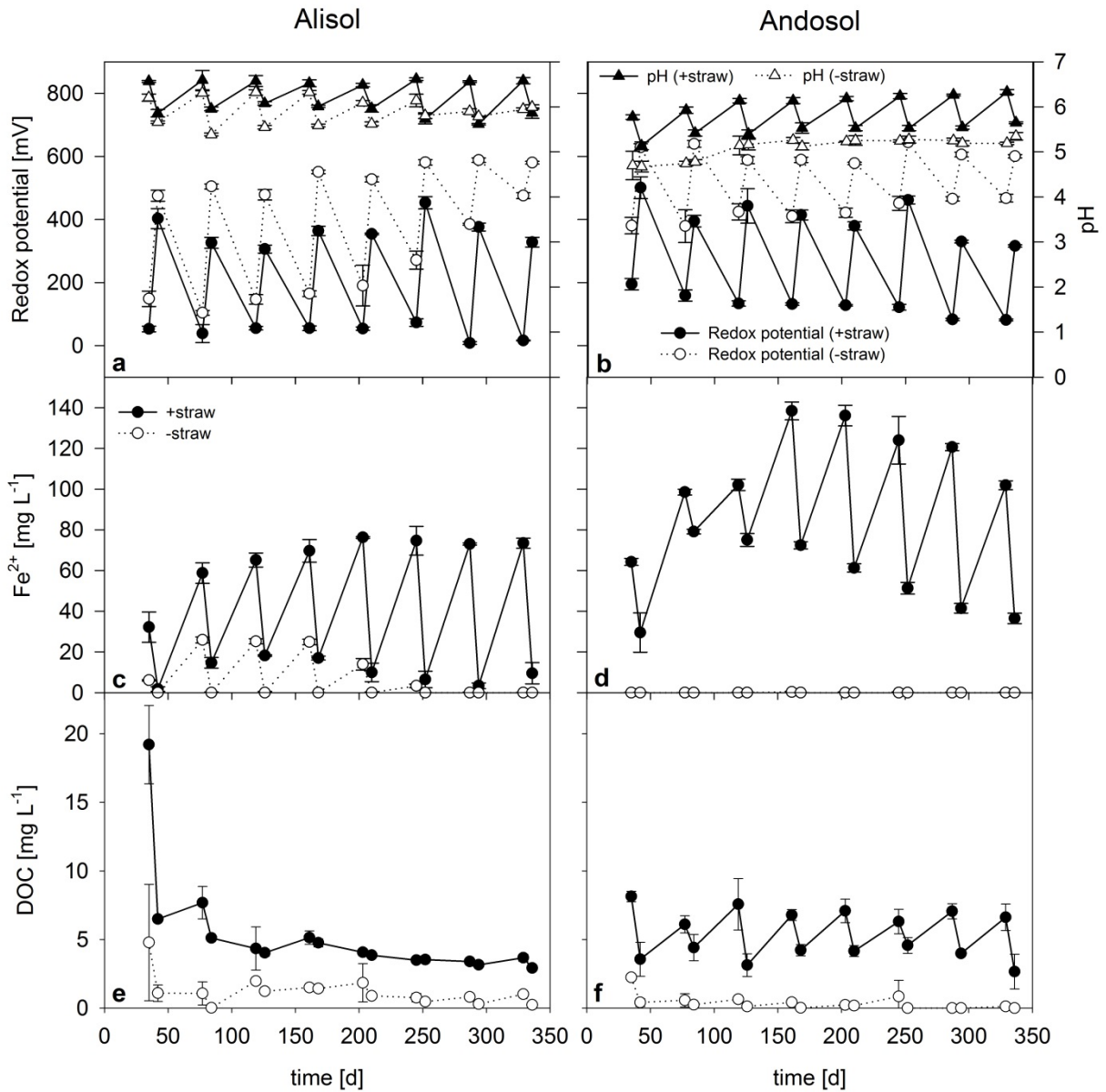


Fig. 4.3 Evolution of redox potential (a and b), pH (a and b), dissolved Fe²⁺ (c and d), and DOC (e and f) concentrations in soil solutions of the Alisol (left) and Andosol (right) incubated with redox fluctuation and straw addition (+straw) or without straw addition (-straw). Data points are means with error bars representing standard deviations (n = 3). Partly re-drawn from Winkler et al. (2018).

4.4.4 Organic matter fractions

Most OM in initial soils was associated with minerals, with significantly larger amounts in the Andosol (34 g OC kg⁻¹ soil) than in the Alisol (18 g kg⁻¹) ($p < 0.001$) (Fig. 4.4). For the Alisol with straw addition, only the incubation under static oxic conditions caused a significant ($p < 0.001$) alteration of OM fractions as reflected by an increase in FPOM (from 0.6 to 1.3 g kg⁻¹) as well as MOM (from 18 to 20 g kg⁻¹). Andosol samples incubated with straw showed a significant ($p < 0.001$) increase in OM, which was mainly due to increasing MOM (from 34 to 38 g kg⁻¹) when incubated under alternating redox conditions, and FPOM (from 1 to 5 g kg⁻¹) when incubated

under permanently oxidic conditions. Control soils incubated without straw addition lost MOM irrespective of redox conditions; however, the decrease relative to the initial soil was only significant ($p < 0.003$) in the Alisol (Fig. 4.4).

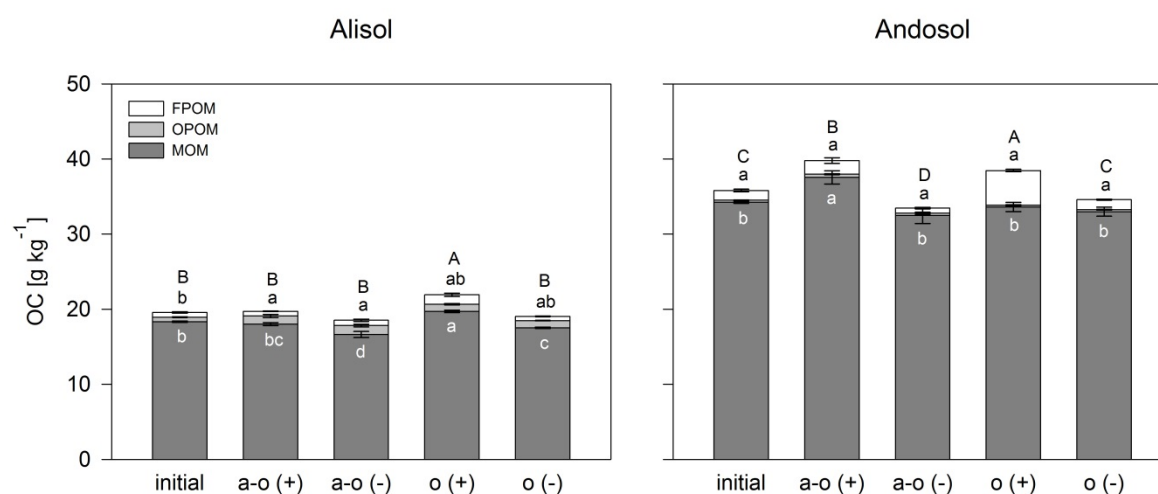


Fig. 4.4 Amount of OC in different density fractions in g per kg of soil (FPOM = free particulate organic matter, OPOM = occluded particulate organic matter, MOM = mineral associated organic matter) before (initial) and after the incubation experiment. Error bars represent standard deviations with $n = 3$. Different black upper case letters, black lower case letters and white letters indicate significant differences ($p < 0.05$) between treatments for FPOM, OPOM, and MOM, respectively.

4.4.5 Fate of straw OC

Most of the added rice straw was mineralized in the Alisol (a-o = $68 \pm 2\%$, o = $65 \pm 1\%$) and Andosol (a-o = $60 \pm 3\%$, o = $56 \pm <1\%$), with the proportion of straw OC mineralized being slightly larger under alternating redox (a-o) than under permanently oxidic (o) conditions (Fig. 4.5). That difference between redox treatments, however, was statistically not significant. Under permanently oxidic conditions, straw OC was solely mineralized to CO_2 , while under fluctuating redox conditions CO_2 and CH_4 were produced. The fraction of straw-derived CH_4 — not measured directly but calculated as described in section 4.3.7 — was probably overestimated as indicated by the total OC budget of the incubation experiment (total $\text{CH}_4 < \text{straw-derived CH}_4$; Table A-4.1 in Appendix 4).

The transfer of straw OC into MOM was smaller under static oxidic conditions (Alisol: $22 \pm 2\%$, Andosol: $10 \pm <1\%$) than under fluctuating redox conditions (Alisol: $28 \pm 2\%$, Andosol: $30 \pm 5\%$). That difference, however, was only significant ($p = 0.016$) for the Andosol samples. Accordingly, the fraction of straw OC remaining as FPOM was significantly ($p < 0.012$) larger under static oxidic conditions (Alisol: $12 \pm 2\%$, Andosol: $28 \pm 2\%$) than under fluctuating redox conditions (Alisol: $1 \pm <1\%$, Andosol: $8 \pm 2\%$).

Comparing the two soil types indicated that under alternating redox conditions similar fractions of the added straw were mineralized to CO₂ in the Alisol (27 ± 2%) and Andosol (26 ± 1%). The mineralization of straw to CH₄, however, was significantly larger in Alisol (41 ± 2%) than in Andosol samples (34 ± 2%) (p = 0.01), which resulted in significantly lower fractions of straw OC remaining as FPOM in the Alisol (1 ± <1%) than in the Andosol (8 ± 2%) (p = 0.004). The fraction of straw OC in DOC and OPOM was generally small (0-3%).

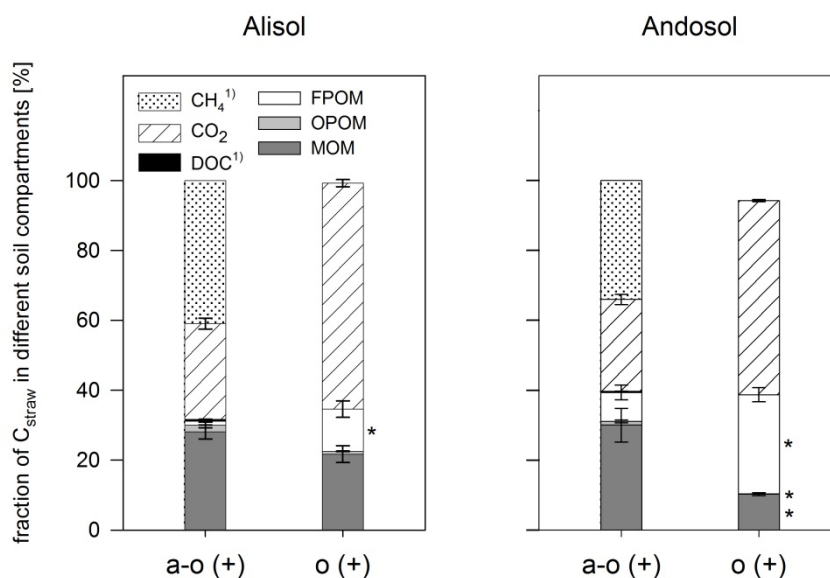


Fig. 4.5 Fate of straw OC as calculated by $\delta^{13}\text{C}$ of CO₂ in headspace samples, of DOC in soil solutions¹⁾ and of different density fractions (FPOM = free particulate organic matter, OPOM = occluded particulate organic matter, MOM = mineral-associated organic matter) in soils. Error bars represent standard deviations with n = 3. Paired t-tests were performed to compare samples incubated under redox fluctuation (a-o) and static oxic conditions (o). Straw-derived C fractions showing statistically significant differences (p < 0.05) between redox treatments of one soil type are indicated by an asterisk.

¹⁾ For calculation of the contribution of DOC and CH₄, please refer to the Materials & Methods section 4.3.5 and 4.3.7.

4.4.6 Lignin-derived phenols in mineral-associated OM

Concentrations of lignin-derived phenols (VSC) in MOM were small in the initial Alisol (6 g kg⁻¹ OC) and Andosol (9 g kg⁻¹ OC). For the Alisol, incubation with straw resulted in significantly larger concentrations of VSC than in the initial soil (p < 0.001), with VSC being slightly but significantly larger under redox fluctuation (15 mg kg⁻¹ OC) than under permanently oxic conditions (13 mg kg⁻¹ OC) (p = 0.013). For the Andosol, similar trends were observed; however, no significant levels were reached (Fig. 4.6).

The (Ac/Al)_v and (Ac/Al)_s ratios were in the range of 0.6 for the initial Alisol and samples incubated without straw addition; in the treatments with straw addition (Ac/Al)_v and (Ac/Al)_s changed with redox conditions. Under fluctuating redox conditions, (Ac/Al)_v was significantly

smaller (0.4) than in the initial Alisol ($p = 0.002$) whereas under static oxic conditions $(Ac/Al)_s$ was significantly larger (0.8) ($p < 0.001$). Acid-to-Aldehyde ratios of the Andosol samples were generally higher (up to 1.1) than those of the Alisol samples ($p < 0.001$) but remained unchanged when comparing the different treatments to the initial Andosol. When treatments with and without straw were compared, straw application partly resulted in significantly ($p = 0.001$) smaller $(Ac/Al)_v$ values (Fig. 4.6).

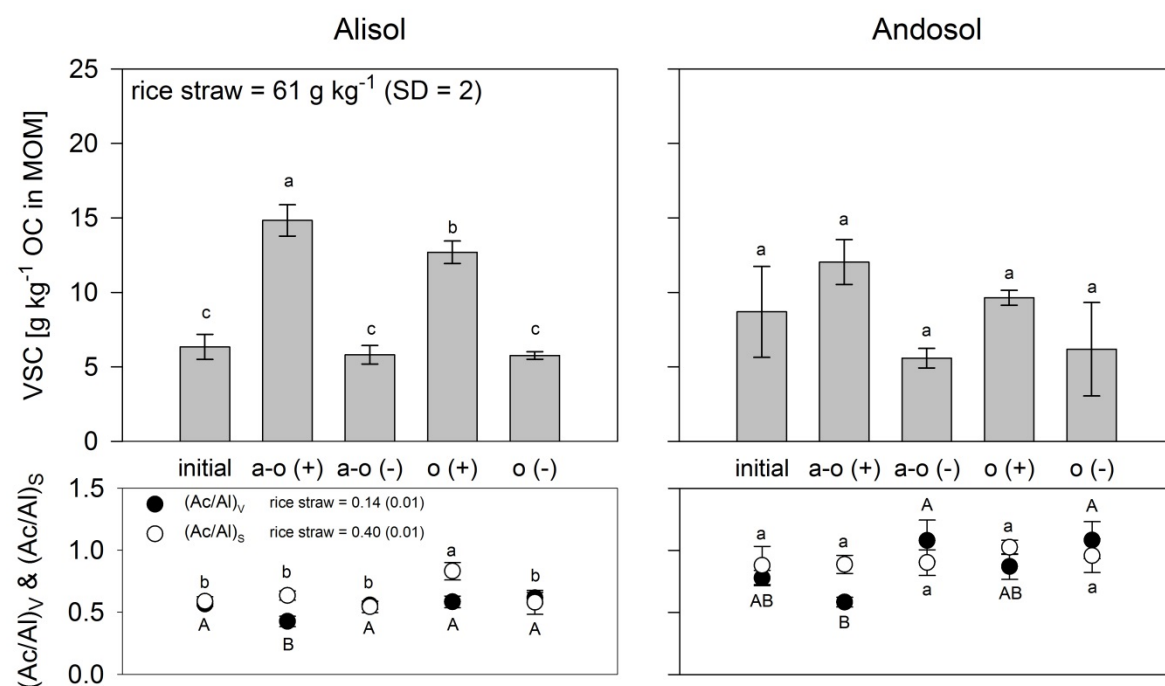


Fig. 4.6 Lignin-derived mineral-associated OM (VSC; sum of Vanillyl (V), Syringyl (S) and Cinnamyl (C) units resulting from CuO oxidation). Acid-to-Aldehyde ratio of Vanillyl $((Ac/Al)_v)$ and Syringyl $((Ac/Al)_s)$ units as indicator for oxidation state of lignin compounds. Error bars represent standard deviations with $n = 3$. Different letters indicate significant differences ($p < 0.05$) between treatments (lower case letters = VSC and $(Ac/Al)_s$, upper case letters = $(Ac/Al)_v$).

4.4.7 Non-cellulosic carbohydrates in mineral-associated OM

The initial Alisol contained significantly larger proportions of non-cellulosic carbohydrates in MOM (200 g kg⁻¹ OC) than the initial Andosol (150 g kg⁻¹ OC) ($p = 0.04$) but a lower GM/AX ratio (1.5 vs. 2.0) ($p = 0.001$) (Fig. 4.7). The fraction of carbohydrates in MOM significantly decreased in the Alisol samples incubated with straw addition ($p < 0.003$). The ratio of GM/AX significantly decreased in the Alisol incubated with straw and redox fluctuation ($p < 0.001$) and significantly increased in the Alisol incubated without straw and static oxic conditions ($p < 0.001$). In the MOM fraction of the incubated Andosol, proportions of carbohydrates showed no significant

changes compared to the initial Andosol. The ratio of GM/AX significantly decreased in the Andosol incubated with straw and redox fluctuation ($p < 0.001$).

Analyses of $\delta^{13}\text{C}$ of individual non-cellulosic carbohydrates showed that the decrease in GM/AX observed for the Alisol and Andosol incubated with straw and redox alternation was associated with a relatively large fraction of straw OC in Xylose ($6 \pm 1\%$). For all other non-cellulosic carbohydrates the fraction of straw-derived OC was in the range of the respective standard deviation (1-2%). Respective data can be found in Table A-4.2 in Appendix 4.

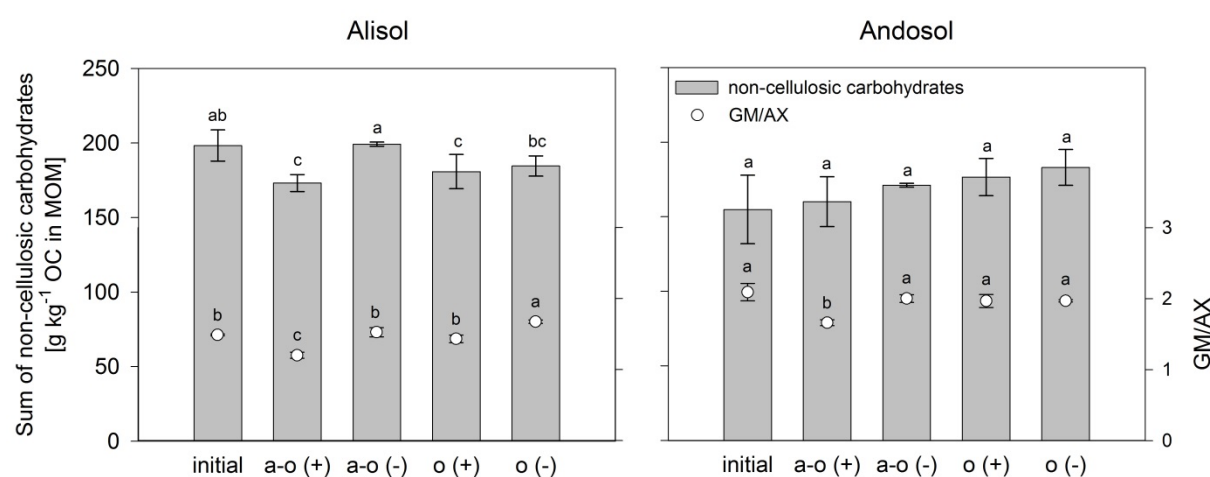


Fig. 4.7 Sum of concentrations of non-cellulosic carbohydrates in mineral-associated OM. GM/AX = (Galactose + Mannose)/(Arabinose + Xylose) with plant sugars showing GM/AX < 0.5 and microbial sugars showing GM/AX > 2. Error bars represent standard deviations with $n = 3$. Different letters indicate significant differences ($p < 0.05$) between treatments.

4.4.8 Microbial community composition

The principal coordinate analysis (PCoA) revealed significant differences between the treatments ($p = 0.001$, 999 permutations; Fig. 4.8) in terms of bacterial community composition. A clear difference between Alisol and Andosol samples along the first principal component when only considering the presence and absence of operational taxonomic units (OTUs) (unweighted PCoA in Fig. 4.8a) was observed. The Alisol incubated with redox fluctuation exhibited a bacterial composition that clearly differed from the Alisol incubated under static oxic conditions along the second principal component. In case of the Andosol, the samples incubated with redox fluctuation and under static oxic conditions showed similar bacterial composition. When the OTU abundance was also considered (weighted PCoA in Fig. 4.8b), the incubated Alisol separated even stronger while the incubated Andosol became more similar. At the same time, the bacterial community composition of the initial Alisol and Andosol were quite similar based

on the weighted PCoA. In total, the unweighted PCoA plots explained 46% and the weighted PCoA plots 57% of the total community variance.

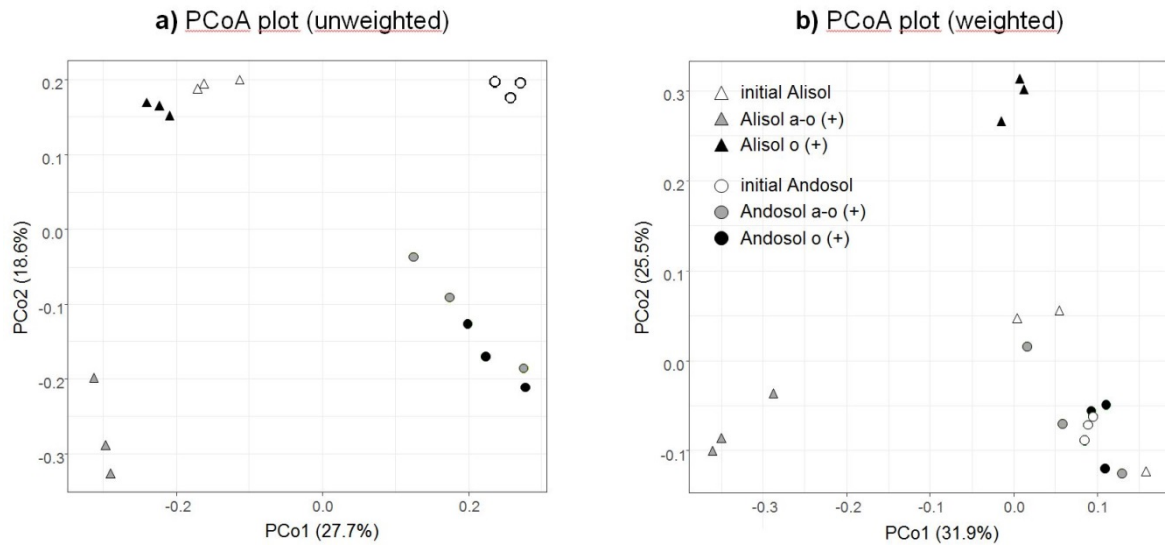


Fig. 4.8 Principal Coordinate Analysis (PCoA) plot based on DNA sequencing and the resulting unweighted (a) and weighted (b) UniFrac distance matrix of initial non-paddy soils and soils incubated with straw addition. PCoA indicates similarity of samples in terms of microbial composition. Unweighted PCoA considers presence or absence of OTUs and weighted PCoA additionally considers abundance of different OTUs.

The phylogenetic affiliation of OTUs revealed that the majority of reads was represented by two phyla in the initial Alisol and by four phyla in the initial Andosol. Those are *Actinobacteria* (29%) and *Proteobacteria* (19%) in the Alisol and *Actinobacteria* (15%), *Proteobacteria* (15%), *Acidobacteria* (28%) and *AD3* (19%) in the Andosol. Figure 4.9 displays the relative abundance of the dominant families (>3%) in the initial Alisol and Andosol and how they were affected by the redox treatment. Overall, more families were detected that — upon incubation — significantly ($p < 0.05$) changed in abundance in Alisol (136) than in Andosol (31) samples, which confirms the results of the PCoA. In Alisol samples, the degree of change in family abundance was similar for both redox treatments; the families with an increase in abundance upon incubation, however, were different for redox fluctuation and static oxic conditions, respectively. The Alisol incubated with redox fluctuation showed an increase in a number of families of the phyla *Proteobacteria* and *Acidobacteria*. Especially the family *Myxococcaceae* increased significantly under redox fluctuation compared to the initial Alisol. In the Alisol under static oxic conditions, especially members of the *Actinobacteria* increased significantly including *Streptomyetaceae*, *Pseudonocardiaceae*, *Nocardioidaceae* and *Micromonosporaceae*. In the Andosol samples, the most significant change was a strong decrease in the initially most abundant families: an unknown *AD3* family, an unknown *Acidobacteria* family as well as *Koribacteraceae*. That decrease occurred in Andosol samples under both redox treatments. The

family *Burkholderiaceae*, in turn, increased independent of redox conditions, while an unknown family of the *Actinobacteria* increased only under redox fluctuation and *Streptococcaceae* increased only under static oxidic conditions.

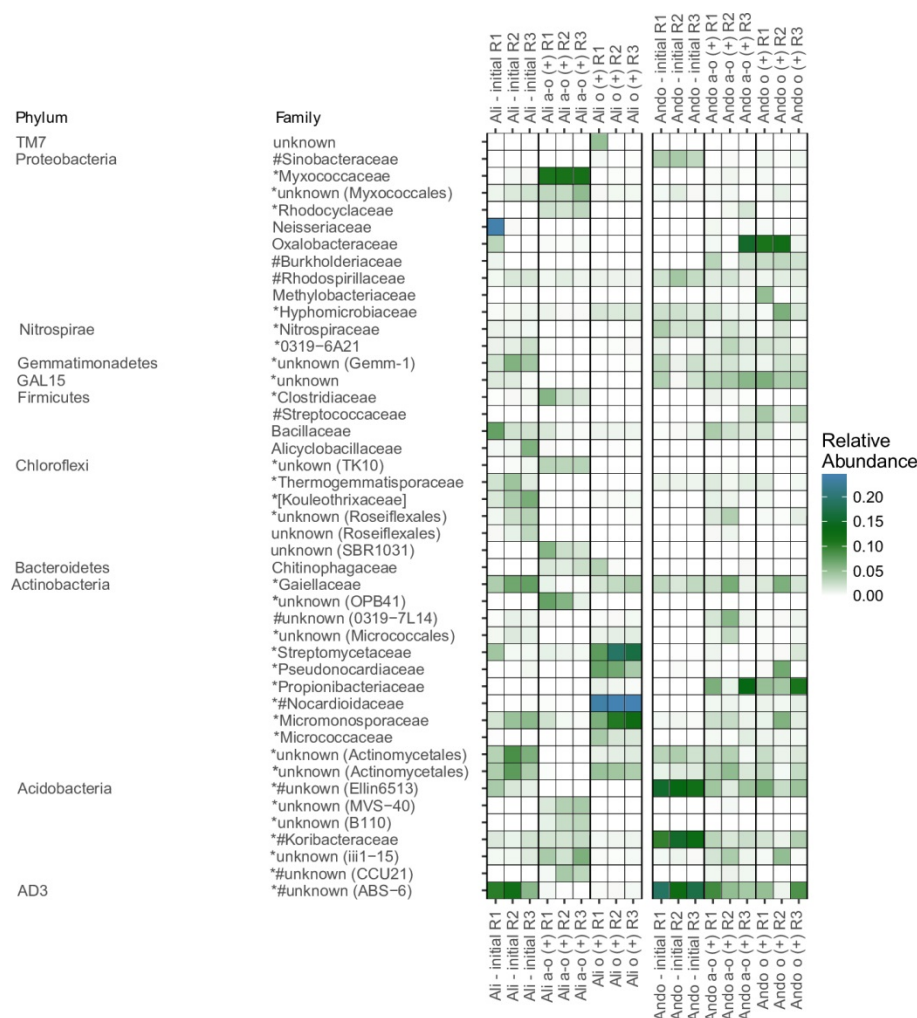


Fig. 4.9 Heatmap of the relative abundance of bacterial families based on 16S rRNA gene sequences. Only families, which account for at least 3% of the total abundance, are displayed. If a phylogenetic affiliation on family level was not possible the next highest assigned level was mentioned in brackets. Each replicate is displayed in a single column. ANOVA was used to calculate significant ($p < 0.05$) difference within one soil. Significant differences of the Andosol are indicated by a hash and for the Alisol by an asterisk.

The ratio of GDGT-0 versus Crenarchaeol lipids in bulk samples, indicating the presence of methanogenic archaea, was significantly ($p < 0.001$) larger in samples incubated with straw addition and redox fluctuation than in the initial soils and all other treatments (Fig. 4.10). In accordance with CH_4 emission data (as reported in section 4.4.2), the ratio was distinctly larger in the Alisol with straw addition and alternating redox conditions than in the respective Andosol (Fig. 4.10).

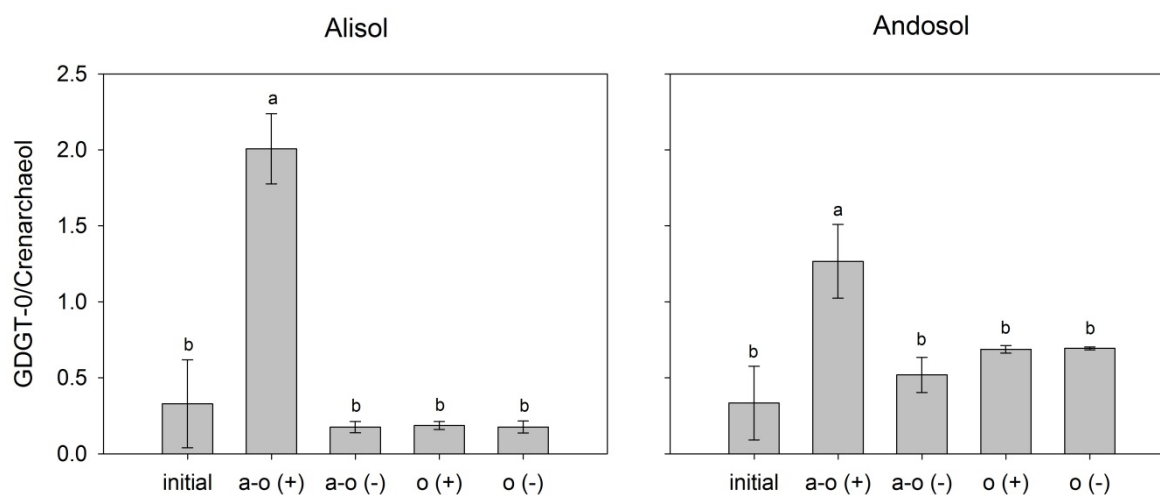


Fig. 4.10 Ratio of GDGT-0 and Crenarchaeol lipids in bulk samples, whereby large ratio indicates presence of methanogenic archaea. Error bars represent standard deviations with $n=3$. Different letters indicate significant differences ($p < 0.05$) between treatments.

4.5 Discussion

4.5.1 Respiration and OC storage in bulk samples under different redox regimes

Respiration data confirmed that in soils under fluctuating redox conditions and with straw addition mineralization is restricted compared to respective soils under static oxidic conditions (Fig. 4.2), which is in line with the consensus of lower decomposition rates in paddy compared to non-paddy soils (Pan et al. 2003; Sahrawat 2004; Zhang and He 2004). The increase of the initial pH from 5.4 (Alisol) and 4.6 (Andosol) to > 6 under anoxic conditions (Fig. 4.3) and a likely related increase in microbial activity could not compensate for the less efficient decomposition under anoxic conditions. However, after one year of incubation with regular straw addition and eight redox cycles, a generally larger OC concentration in soils under redox fluctuation than in those under oxidic conditions could not be observed. Larger bulk OC storage in Alisol samples with straw addition and redox fluctuation compared to those under static oxidic conditions was not found despite distinctly smaller respiration rates. In the Andosol with straw addition, we found slightly but not significantly increased bulk OC levels in the samples incubated with redox oscillation than in those incubated under static oxidic conditions. However, we calculated that the difference in respiration would lead to a maximum difference in SOC of only 0.1%, which is difficult to measure.

Despite restricted mineralization in paddy soils, larger OC storage in topsoils might be impeded by leaching of DOC. Reductive dissolution of Fe oxides as well as the subsequent increase in pH during anoxic conditions of submerged paddy soils are known to enhance the release of DOC (Hagedorn et al. 2000; Hanke et al. 2013; Said-Pullicino et al. 2016). The DOC concentrations measured at the end of each anoxic phase of our experiment were relatively small ($\approx 5 \text{ mg L}^{-1}$;

Fig. 4.3) and the DOC removed throughout the entire experiment accounted for $\leq 0.5\%$ of the initial + added OC, which indicates that DOC released due to anoxic conditions may have been prone to mineralization before the exchange of soil solution. Hence, loss of OC due to removal as DOC did not play a prominent role in the incubated soils.

4.5.2 SOC formation depends on soil type

Similar proportions of straw OC were transferred into MOM in the Alisol and Andosol under redox fluctuation (Fig. 4.5). However, a net increase in MOM, as exhibited by the Andosol, was not found in the Alisol (Fig. 4.4), indicating that straw-derived OC partly exchanged native MOM in the Alisol. The pronounced increase in MOM in the Andosol under redox fluctuation but not in the respective Alisol might be explained by the different mineral composition of these soil types (e.g. Heckman et al. 2018). While the Alisol is dominated by kaolinite, gibbsite, and crystalline Fe oxides, the Andosol additionally contained highly reactive allophane and imogolite-type phases as well as large amounts of SRO Fe oxides (Winkler et al. 2016, 2018). In result, the SSA of the original Andosol was distinctly larger than that of the original Alisol (Table 4.1). Large surface area implies a higher OC sorption capacity (Table 4.1), which might explain the larger concentration and further increase of mineral-associated OC in the Andosol but not in the Alisol under redox fluctuation (Fig. 4.4; Mayer 1994; Saidu et al. 2012; Wissing et al. 2013; Coward et al. 2017).

The more effective OC stabilization in the Andosol than in the Alisol is also confirmed by the lack of dissolved Fe^{2+} in the Andosol incubated with redox fluctuation but without straw addition (Fig. 4.3d). Even though the initial Andosol contained distinctly more native OC than the initial Alisol (Fig. 4.4), its incubation without an additional OC source did not result in reductive Fe oxide dissolution. Consequently, the OC in the initial Andosol was poorly available to microbes so that Fe^{3+} was not required as an alternative electron acceptor in samples with restricted O_2 replenishment. The stability of OC in the initial Andosol is also underlined by the large abundance of oligotrophic bacteria (Fig. 4.9), which are adapted to poorly available OC sources. In addition, the bacterial community structure hardly changed despite incubation under different redox regimes indicating protective habitats and limited adaptation to changing redox conditions. This is in line with the smaller respiration rate in the Andosol than in the Alisol. Hence, stabilization of OC might not only be the result of mineral-OC associations but also of limited mobility of bacteria residing in microhabitats and of exoenzyme immobilization through adsorption to the highly reactive mineral surfaces of the Andosol (Lützwow et al. 2006; Yan et al. 2010; Lammirato et al. 2010).

4.5.3 Role of Fe oxides for SOC stabilization

The SRO Fe oxides abundant in the Andosol are usually more easily reducible than the crystalline ones dominating the Alisol, as confirmed by the distinctly larger dissolved Fe^{2+} concentrations in the soil solution of submerged Andosol samples incubated with straw (Fig. 4.3c-d). In fact, a positive correlation of Fe^{2+} concentrations with DOC was observed in solutions from the Andosol (Fig. A-4.4 in Appendix 4). This suggests the release of adsorbed or co-precipitated OC during reductive dissolution of Fe oxides in the Andosol incubated with straw and redox fluctuation. In result, OC associated with SRO Fe oxides may have been prone to mineralization during anoxic phases (Dubinsky et al. 2010), meaning that these Fe phases may not facilitate long-term OC storage in Andosol samples under redox fluctuation. The re-occurrence of oxic phases, though, may lead to the co-precipitation and stabilization of remaining Fe oxides and DOM. That effect, however, depends on the soil's leaching rate (Winkler et al. 2018). In our case, 16% of the SRO Fe (Fe_{AAO}) in the Andosol was dissolved throughout the incubation with straw and redox fluctuation. Only about 10% of this dissolved Fe^{2+} re-precipitated after removal of the majority of the Fe^{2+} during solution sampling. Hence, other mineral phases with large SSA but not being redox reactive, such as Al hydroxides, allophane and imogolite-type phases, might be responsible for the increase in MOM in the Andosol incubated with straw and redox fluctuation.

The observed incomplete reduction of SRO Fe oxides in the Andosol is in line with recent findings that organic coatings can effectively impair the reductive dissolution of Fe oxides (Poggenburg et al. 2018). The dominating Fe^{III} -reducing microbial taxa in sediments and comparable environments, that was also detected in our samples, is *Geobacter*. It requires direct contact to the Fe oxide, which can be blocked by adsorbed OC or indirectly by OC-induced aggregation of Fe oxide particles (Lovley et al. 2004; Coby et al. 2011; Eusterhues et al. 2014; Poggenburg et al. 2018). In that case, the association of Fe and OC would protect the Fe from reductive dissolution and the OC from microbial decomposition (Herndon et al. 2017). Hence, the overall role of SRO Fe oxides for OC storage in soils under redox fluctuation remains unclear and warrants further research addressing the effects of long-term redox fluctuation on the coupling of Fe oxides and OC cycling.

4.5.4 Impact of soil water on SOC formation

Despite differences in respiration (Fig. 4.2), there were no significant differences in OC concentrations between straw-receiving Andosol samples under different redox regimes. Compared to the initial Andosol, however, OC concentrations of the incubated Andosol with straw addition increased significantly in both redox treatments (Fig. 4.4). Interestingly, this

increase was mainly associated with OC allocation to the MOM fraction in the Andosol with redox fluctuation but to the FPOM fraction in the Andosol under static oxic conditions. This finding is confirmed by the fate of straw OC, which indicated a larger transfer of the added straw OC to MOM in samples under redox fluctuation, while a larger proportion remained as FPOM under static oxic conditions (Fig. 4.5). The fate of straw in the incubated Alisol showed the same trend but less pronounced. That finding of significant proportions of straw remaining as FPOM under static oxic conditions but being converted to MOM under redox fluctuation might be explained by the different water content of the soils under different redox regime. Submergence of samples under fluctuating redox conditions probably caused larger dissolution of straw compared to samples at static oxic conditions with a water content equivalent to 50% maximum water holding capacity (Kalbitz et al. 2000). At the same time, the larger water content of soils under redox fluctuation increases the mobility of DOC, which may have supported the transport of DOC to so far juvenile mineral surfaces (Guggenberger and Kaiser 2003; Ouyang and Li 2013). Under static oxic conditions, dissolution of straw as well as mobility of substrates and accessibility of mineral surfaces may have been limited due to relatively low water contents. That, in turn, may have caused the lower decomposition of straw, and hence, the larger fraction of straw remaining as FPOM. Nevertheless, it has to be considered that the overall respiration was larger under static oxic than under fluctuating redox conditions, indicating stronger mineralization of native OC including DOC. In contrast, submergence of soils and resulting redox fluctuation favored the formation of MOM by enhanced dissolution, diffusion, and direct adsorption of straw OC, especially in the Andosol with abundant reactive surfaces.

4.5.5 Lignin-derived phenols in mineral-associated OM

Alisol and Andosol samples incubated with straw under fluctuating redox conditions showed largest concentrations of lignin-derived phenols in the MOM fraction (Fig. 4.6), indicating preferential accumulation of lignin in paddy soils with rice straw incorporation. This is in line with the findings of Olk et al. (1996) and Bierke et al. (2008). The decrease of the oxidation state of the mineral-associated lignin compounds in samples with straw addition and redox fluctuation (Fig. 4.6) supports the idea that OM added to mineral surfaces during incubation with submergence is less processed by the soil microbiome than the OM added to minerals under static oxic conditions as discussed in section 4.5.4. Most remarkably, also samples with straw addition and static oxic conditions exhibited increased concentrations of lignin-derived phenols in MOM (Fig. 4.6). This indicates that the increase in lignin-derived phenols compared to the initial soil is strongly controlled by the input of straw and less by redox conditions. In addition, the relatively low concentrations of lignin-derived phenols in the MOM fractions

compared to concentrations of the added straw shows that lignin from straw is to a large extent decomposed also in soils with long anoxic periods, which is in accordance with findings of Wissing et al. (2013) and Urbanski et al. (2017). The regular occurrence of oxic periods seems to enable the de-polymerization of lignin, allowing for further decomposition of lignin-derived compounds under anoxic conditions (Colberg and Young 1982; Benner et al. 1984). The increase in lignin-derived phenol concentrations in samples with straw addition and the stronger increase in those under fluctuating redox conditions were only statistically significant ($p < 0.013$) for the Alisol. The less pronounced effects in the Andosol might be explained by a less efficient extraction of lignin-derived phenols bound to mineral phases (Hernes et al. 2013).

4.5.6 Non-cellulosic carbohydrates in mineral-associated OM

Concentrations of non-cellulosic carbohydrates in the MOM fraction of the Alisol mainly decreased during incubation, especially in samples with straw addition, while there were no significant changes in carbohydrate concentrations of the Andosol (Fig. 4.7). Hence, preferential accumulation of carbohydrates during incubation was not observed, which is in line with a study of Urbanski et al. (2017) who found preferential degradation of carbohydrates in paddy soils. The enhanced microbial activity in the Alisol with straw addition seems to have promoted the decomposition of mineral-associated carbohydrates, while they may have been better stabilized in the respective Andosol. However, both soil types under redox fluctuation and with straw addition showed a significant ($p < 0.001$) decline of the GM/AX ratio (Fig. 4.7). This observation is accompanied by a remarkable proportion of straw OC in xylose, a largely plant-derived carbohydrate. Hence, carbohydrates associated with minerals in the initial soil were partly exchanged for carbohydrates from the added straw and those newly added carbohydrates were less microbially processed than the original carbohydrates. This supports our idea of enhanced abiotic straw dissolution and direct adsorption of a significant proportion of the resulting DOC to mineral surfaces in submerged soils with long periods of anoxic conditions as discussed in section 4.5.4.

4.5.7 Soil type has an impact on bacterial community composition

Our data revealed distinct responses of the soil bacteria to redox conditions depending on the initial soil type. In Alisol samples, incubation strongly altered the bacterial community with distinct differences between redox fluctuation and static oxic conditions, while in Andosol samples only minor changes occurred and the bacterial community structure was similar under both redox treatments. As many microbes colonize particle surfaces, biopores and aggregates

(Gupta and Germida 2015), this observation might be linked to differences in SSA, pore architecture and aggregate stability of both soil types. Submergence of soils, as conducted in our treatment with redox fluctuation, results in the destruction of aggregates and consequently in the disturbance of microbial habitats (Kirk 2004; Totsche et al. 2018). Part of the Andosol habitats, however, may have been maintained since the Andosol contains allophane, which forms extremely stable micro-aggregates (Matus et al. 2014; Huang et al. 2016). Hence, the majority of the bacterial community of the Andosol may have been sustained by stable protective microhabitats, while bacteria in the Alisol samples were more exposed, hence more sensitive, to redox fluctuation, leading to adaptation of the bacterial community structure and consequently larger respiration rates (Zhang et al. 2007; Gupta and Germida 2015; Totsche et al. 2018). The restricted changes in bacterial community composition in the Andosol incubated with redox fluctuation might also be an effect of pH, which dropped to < 6 during oxic phases. Since soil bacteria prefer neutral soil pH values, as they occurred in the respective Alisol samples, changes in the bacterial community of the Andosol might have been restricted to rather acidophilic groups.

The bacterial family *Myxococcaceae*, that increased in the Alisol incubated with redox fluctuation, is known to feed on methanotrophs (Murase and Frenzel 2007). This indicates that the CH_4 produced during anoxic phases may have been oxidized by methanotrophs during oxic phases and the methanotrophs may have supported the growth of *Myxococcaceae* in Alisol samples. Methane production also occurred in Andosol samples with redox fluctuation. *Myxococcaceae*, however, were not detected. This supports the hypothesis of better protection of microbes (e.g. from predators) in the Andosol due to stable microhabitats.

The strong decrease in *Acidobacteria* in Andosol samples independent of redox conditions is probably an effect of straw addition since members of *Acidobacteria* are slowly growing oligotrophs that were found to negatively correlate with OC availability (Fierer et al. 2007). With the addition of straw, a readily available source of OC was added so that oligotrophic *Acidobacteria* may have been outcompeted by eutrophic bacteria. That *Acidobacteria* were highly abundant in the initial Andosol is in line with the large amount of mineral-associated OC of restricted availability.

4.5.8 Activity of methanogens depends on soil type

A field study of Mueller-Niggemann et al. (2016) indicated the enhanced presence of methanogenic archaea in soils under paddy management compared to adjacently located non-paddy soils. Our results from the laboratory experiment confirm the increase of methanogenic archaea in soils incubated under conditions as in paddy fields (straw addition and redox

fluctuation). This shows that the archaeal community can quickly adapt as soon as anoxic periods become abundant. This effect was more pronounced in the Alisol than in the Andosol (Fig. 4.10) and confirmed by respective differences in CH₄ production (Fig. A-4.2 in Appendix 4). The larger concentration of SRO Fe oxides in the Andosol, which can serve as alternative electron acceptors under reducing conditions and which are more easily reducible than the crystalline Fe oxides (Postma 1993; Roden 2003; Bonneville et al. 2009), probably causes a postponed shift of the system into the methanogenic phase (Teh et al. 2008), as indicated by the later occurrence and the smaller total CH₄ production in the Andosol than in the Alisol samples (Fig. A-4.2 in Appendix 4). The distinctly lower redox potentials during anoxic phases of the Alisol than the Andosol also underline that the Alisol is more prone to reach the methanogenesis stage, while the redox potential of the Andosol seems to be buffered by the larger amount of easily reducible SRO Fe oxides. This finding confirms the study of Achnich et al. (1995), who showed that the addition of SRO Fe oxides to paddy soils depleted in alternative electron acceptors alleviates methanogenesis more effectively than the addition of more crystalline Fe oxides.

4.6 Summary & Conclusions

The long-term laboratory incubation experiment revealed a clear impact of the redox regime and soil type on the soil microbiome, straw decomposition, and SOC formation. Referring to our initial research questions we can state the following:

1. The controlled laboratory incubation of an Alisol and Andosol under static oxic vs. fluctuating redox conditions and with regular straw incorporation revealed inhibited respiration in samples exposed to redox fluctuation. Hence, restricted decomposition of OC in submerged soils with long anoxic periods is confirmed and indicates a potential for OC storage in soils under long-term paddy management.
2. Despite distinctly smaller respiration, no significant increase in OC in both soils under redox fluctuation relative to those under static oxic conditions was found after one year of incubation with regular straw addition.
3. A major proportion of the added straw was mineralized in both soils, with a similar extent of straw mineralization under both redox regimes. Total mineralization, however, was larger under static oxic than redox fluctuating conditions, indicating more mineralization of native SOC in static oxic soils. In general, straw mineralization was larger in the Alisol than in the Andosol. In both soil types, a larger proportion of the

added straw was converted to the MOM fraction under fluctuating redox conditions than under static oxic conditions, reflecting better stabilization of OM in submerged soils.

4. For both soil types and redox regimes, the regular addition of straw during incubation resulted in an increased fraction of lignin-derived phenols in MOM. The increase was even slightly larger under redox fluctuation, suggesting a potential for preferential accumulation of lignin in paddy soils. Accumulation of non-cellulosic carbohydrates was not observed. Both biomarkers indicate the direct transfer of plant-derived compounds to the MOM fraction and/or exchange of microbial-derived by plant-derived compounds at the mineral surfaces in samples under redox fluctuation.
5. The bacterial community structure that developed under redox fluctuation strongly varied for the two soil types. It changed less in the Andosol indicating more protective microbial habitats. For methanogens a stronger response to fluctuating redox conditions was observed in the Alisol than in the Andosol.

Besides redox regime and soil type, an impact of the water content on SOM formation was indicated by the larger conversion of straw OC into MOM in submerged soils despite lower respiration. Submergence seems to promote straw dissolution as well as DOC mobility, allowing for plant-derived biomolecules to access mineral surfaces without previous microbial processing. Although that effect was observed for both soil types, an absolute increase in MOM was only observed in the Andosol under redox fluctuation, probably due to the abundance of reactive minerals (SRO Fe oxides, Al hydroxides, allophane and imogolite-type phases). The role of the redox-sensitive Fe oxides for OC stabilization, however, remains unclear since OC adsorbed to or co-precipitated with Fe oxides is at least partly re-mobilized during reductive dissolution of Fe oxides.

Overall, the importance of the soil type for SOC stabilization and microbial community development under redox fluctuation was revealed, thereby highlighting that paddy management induced biogeochemical processes do not have the same effects in different soils under paddy cultivation.

4.7 Acknowledgements

The study was funded by the DFG within the research unit FOR995 Biogeochemistry of Paddy Soil Evolution initiated by Ingrid Kögel-Knabner. We gratefully acknowledge the support of Jorin Schoorl, Susanne Horika, Alexandra Boritzki, Christine Krenkewitz, Gudrun von Koch, Simal Dhimal, Heike Maennicke, Marianne Benesch, Bruno Glaser, Gisle Vestergaard, Gabi Albert, and Madina Burkitbayeva during laboratory work and data analyses.

5 Synthesis

5.1 Discussion

5.1.1 Do several decades of paddy management have an effect on minerals and OC stocks of Vertisol, Alisol, and Andosol?

Long-range-ordered (LRO) clay minerals (smectite, secondary chlorite and kaolinite) exhibited no clear change under long-term paddy management, while the transformation of short-range-ordered (SRO) allophane and imogolite-type phases seemed to be enhanced. The amount of allophane and imogolite-type phases was distinctly smaller in the Andosol-derived paddy soil compared to the respective non-paddy soil, while the amount of halloysite seemed to be larger (Chapter 2). This is in line with the proposed transformation of allophane to halloysite (Violante and Wilson, 1983; Steefel and Van Cappellen, 1990). The Andosol contained an Al-rich allophane with a Si/Al ratio of 1:2, while halloysite usually has a Si/Al ratio of 1:1 (Joussein et al., 2005). This means the transformation of allophane to halloysite requires resilication. Resilication is possible in Si-rich soil solutions, which may occur in soils with stagnant water and rich in soluble phytoliths (Aomine and Wada, 1962; Malucelli et al., 1999; Dubroeuq et al., 2002). Flooded paddy soils are characterised by a dense plough pan enabling a stagnant water regime for several months per year. In addition, rice plants form phytoliths that are recycled in paddy topsoils (Seyfferth et al., 2013). Hence, a Si-rich soil solution may have been present and the transformation of allophane and imogolite-type phases to halloysite is likely in Andosol-derived paddy soils. These halloysites might be characterised by Al^{3+} to Fe^{2+} substitution (Joussein et al., 2005) as indicated by a Fe-silicate phase identified by Mössbauer spectroscopy in the Andosol-derived paddy soil but not in the respective non-paddy soil (Chapter 3). The incorporation of Fe into the halloysite octahedra is likely during anoxic conditions characterized by large concentrations of dissolved Fe^{2+} .

Due to its sensitivity to redox changes the iron oxide composition of most studied paddy soils was strongly altered compared to their non-paddy counterparts. Total Fe oxide contents were significantly lower in paddy than non-paddy topsoils, indicating reductive dissolution of Fe oxides and partial removal of the resulting dissolved Fe^{2+} with drainage water. The Vertisol was least sensitive to paddy management due to small initial amounts of Fe oxides and strong self-mulching, which re-homogenizes the soil material (Chapter 2).

Two out of four non-paddy and paddy soil pairs exhibited larger soil organic carbon (SOC) stocks in the paddy than the respective non-paddy soil, which we consider as paddy-management induced SOC accumulation. Organic carbon (OC) stocks of the Vertisol-derived paddy soil and its non-paddy counterpart were similar. Also the non-paddy Vertisol might undergo longer periods of anoxic conditions due to its heavy texture and its position in a

floodplain likely resulting in reduced decomposition rates similar to those in the respective paddy soil. Consequently, a difference in SOC between the Vertisol-derived paddy soil and its non-paddy counterpart was not found. Also, the clayey Alisol-derived paddy soil showed no change in OC stocks when compared to the respective non-paddy soil. Its texture was less heavy than that of the Vertisol and it was situated on a terraced slope so that the non-paddy clayey Alisol should be more effectively drained than the non-paddy Vertisol. Hence, the clayey Alisol and the respective paddy soil exhibited the typical difference in water and redox regime likely resulting in a smaller OM decomposition rate in the paddy than the non-paddy clayey Alisol. The lack of SOC accumulation in the paddy soil might thus be attributed to differences in OM input. The smaller decomposition rate in the paddy soil might be compensated by a smaller OM input resulting in similar SOC stocks in the non-paddy clayey Alisol and the respective paddy soil. Moreover, the clayey Alisol's OC storage potential — represented by Fe oxides and clay minerals — changed least compared to the other soil types under paddy management. The Fe oxide content was largest of all paddy soils and the total amount of SRO Fe oxides — being more effective in OC stabilization than crystalline Fe oxides — even increased in the clayey Alisol under paddy management. That there was still no difference in SOC stocks between the non-paddy and the paddy soil underlines the hypothesis of smaller OM inputs to the clayey Alisol under paddy management than to the respective non-paddy soil.

Other than the Vertisol and the clayey Alisol, the Andosol and the sandy Alisol showed larger SOC stocks in the paddy than the respective non-paddy soil. Hence, in this case, the effect of smaller decomposition rates under paddy management seems to be confirmed. The Andosol was rich in reactive minerals (SRO Fe oxides, allophane and imogolite-type phases) — which are of utmost importance for the stabilization of OC (Torn et al., 1997; Wagai and Mayer, 2007; Kögel-Knabner et al., 2008) — and stored additional OC despite the partial loss of these minerals under paddy management. Also, the sandy Alisol-derived paddy soil gained OC even though it was the soil with the smallest clay content and the strongest paddy management-induced loss of Fe oxides. Although the OC storage capacity is reduced under paddy management, it is still large enough to support OC accumulation.

Consequently, paddy management does not necessarily result in SOC accumulation and OC storage capacity does not seem to be the limiting factor for OC stabilization. It is rather suggested that — besides limited drainage also of non-paddy soils as in case of the Vertisol — SOC formation is controlled by OM input, which may differ between the non-paddy and paddy sites. In case of the sandy Alisol, which accumulated OC under paddy management, the amounts of OC in the respective non-paddy soil were very small indicating limited OM input. In contrast, the clayey Alisol, which did not accumulate OC under paddy management, had large OC stocks indicating large OM input, and hence, distinct SOC formation also under non-paddy conditions.

5.1.2 Do several decades of redox fluctuation in Alisol- and Andosol-derived paddy soils result in increasing or decreasing Fe oxide crystallinity?

The overall crystallinity of the Fe oxides remaining after several decades of reductive dissolution and mobilization of Fe was larger or lower, likely depending on the initial ratio of SRO to crystalline Fe oxides as well as on the leaching rate (Chapter 2 and 3). Generally, SRO Fe oxides are preferentially reduced relative to crystalline Fe oxides (Postma, 1993; Roden, 2003; Zhao et al., 2017). Hence, in soils with an initially large fraction of SRO Fe oxides (Andosol) most of the dissolved Fe^{2+} leached from the soil during drainage originated from SRO Fe oxides leading to the relative enrichment of the remaining crystalline Fe oxides (Fig. 5.1). Crystalline Fe oxides may have further accumulated due to Fe^{2+} -facilitated re-crystallization of SRO Fe oxides (Pedersen et al., 2005; Hansel et al., 2005; Tomaszewski et al., 2016). Soils initially rich in easily reducible SRO Fe oxides exhibit large concentrations of dissolved Fe^{2+} , which can adsorb to the remaining SRO Fe oxides. The adsorbed Fe^{2+} ions transfer electrons to the SRO Fe oxides, causing their partial dissolution and subsequent re-arrangement to more crystalline phases. If the initial Fe oxide composition of a soil under paddy management was in turn dominated by crystalline Fe oxides (clayey and sandy Alisol) considerable amounts of crystalline Fe oxides could be reductively dissolved in the topsoil despite lower solubility. In that case also crystalline Fe oxides contribute considerably to the dissolved Fe^{2+} removed during drainage (Fig. 5.1). At the same time, rapid oxidation of topsoils during drainage usually results in the re-precipitation of the remaining dissolved Fe^{2+} as SRO Fe oxides. The effect of oxidative re-precipitation probably depends on the paddy soil's texture and respective permeability. In the clayey Alisol and Vertisol, restricted permeability may have diminished the leaching of dissolved Fe^{2+} so that considerable amounts remained in the topsoil. These could precipitate during oxidation as indicated by the absolute increase in SRO Fe oxides (Chapter 2 and 3). The sandy Alisol also lost considerable amounts of crystalline Fe oxides, however, without a change in the amount of SRO Fe oxides (Chapter 2). This is probably due to its sandy texture allowing most of the dissolved Fe^{2+} to be leached from the soil.

Overall, for SRO Fe oxide-rich soils under paddy management our observations suggest increasing Fe oxide crystallinity and for paddy soils initially rich in crystalline Fe oxides we found decreasing Fe oxide crystallinity. The effect of dissolved Fe^{2+} mainly deriving from either SRO or LRO Fe oxides and being subjected to either leaching or re-precipitation as SRO Fe oxides is further influenced by the soil's leaching rate as determined by parent material related permeability .

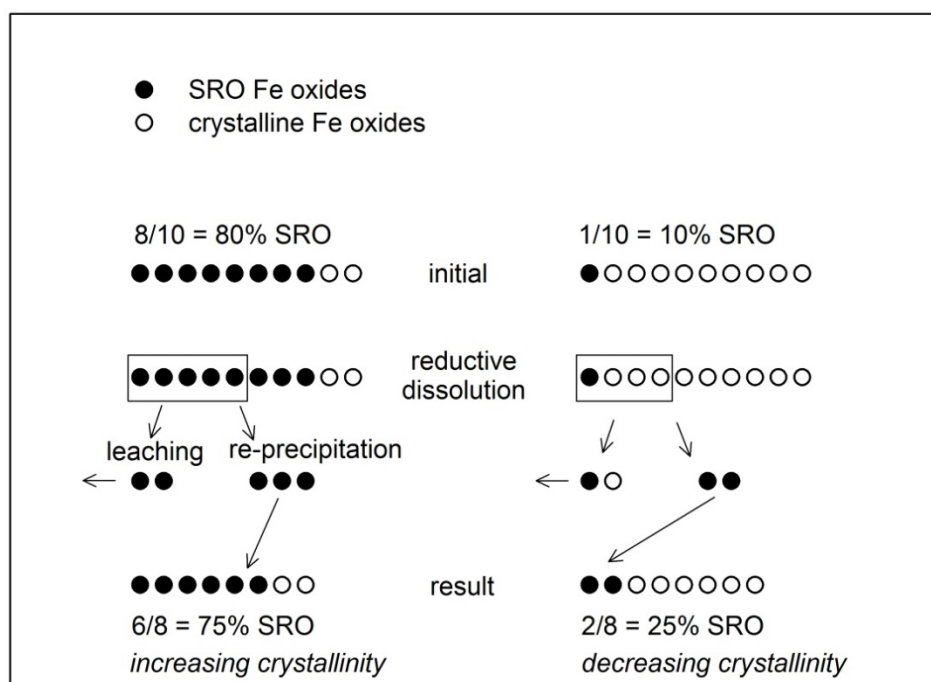


Fig. 5.1 Example of how the initial portion of short-range-ordered (SRO) Fe oxides may influence Fe oxide crystallinity changes in paddy soils with redox fluctuation. During one redox cycle, part of the initial Fe oxides is reductively dissolved, part of the resulting dissolved Fe^{2+} is leached followed by rapid oxidative re-precipitation of the remaining dissolved Fe^{2+} as SRO Fe oxides. Same leaching rate was considered.

5.1.3 What is the effect of Alisol and Andosol incubation with eight redox cycles on OM turnover and microbial communities? Do we find similar effects in the field paddy soils?

The controlled laboratory incubation of the clayey Alisol and the Andosol under static oxic vs. fluctuating redox conditions and with regular straw incorporation revealed inhibited respiration in samples exposed to redox fluctuation (Chapter 4). Hence, the consensus of lower OM decomposition rates in paddy compared to non-paddy soils due to long anoxic periods (Pan et al., 2003; Sahrawat, 2004; Zhang and He, 2004) is confirmed and indicates a potential for OC storage in soils under long-term paddy management. Methane emissions were detected for soils incubated with straw addition and redox fluctuation. Emissions were smaller for incubated Andosols than Alisols highlighting the buffering effect of easily reducible SRO Fe oxides abundantly available as alternative electron acceptors in the Andosol (Chapter 4).

When comparing the incubated soils to the initial soils, a distinct increase in SOC in both Andosols incubated with straw addition was revealed. That increase was attributed to the free particulate OM fraction in the Andosol under static oxic conditions and to the mineral-associated

OM fraction in the Andosol with redox fluctuation (Chapter 4). Although the incubated Alisol did not show a clear change in total SOC, the fate of ^{13}C -marked straw revealed that like in the Andosol also in the Alisol more straw was converted to the mineral-associated OM fraction under fluctuating redox than under static oxic conditions (Chapter 4), reflecting better stabilization of OM in soils with fluctuating redox conditions.

At the same time, biomarker analyses (lignin and polysaccharides) revealed that, irrespective of soil type, the mineral-associated OM in soils that had been incubated with redox fluctuation and straw addition was less microbially processed than the initial mineral-associated OM (Chapter 4). The soils incubated with redox alternation were submerged, which may have facilitated the release of organic compounds from the added straw as well as their direct transport to mineral surfaces (Kalbitz et al., 2000; Guggenberger and Kaiser, 2003; Ouyang and Li, 2013; Das et al., 2019). Thus, plant-derived compounds may have been stabilized through association with minerals before they could be processed by microbes. A similar incubation experiment was performed by Ye et al. (2019). However, their soils under redox fluctuation were kept at a constant water content of 60% of the soil's water holding capacity. As in our case, respiration was smaller than in the static oxic control but particulate OM — and not the mineral-associated OM — increased. This underlines that long reducing phases only in combination with large water contents promote OC stabilization.

That an absolute increase in the mineral-associated OM was observed in the Andosol but not in the clayey Alisol incubated with redox fluctuation and straw addition highlights the importance of the mineral composition for SOC storage (e.g. Heckman et al. 2018). While the Alisol was dominated by kaolinite, gibbsite, and crystalline Fe oxides, the Andosol additionally contained highly reactive allophane and imogolite-type phases as well as large amounts of SRO Fe oxides (Chapter 2 and 3), which are of utmost importance for the stabilization of OC (Torn et al., 1997; Wagai and Mayer, 2007; Kögel-Knabner et al., 2008). Soil OC data from field paddy soils stressed the impact of OM input on SOC accumulation (Chapter 2). However, if sufficient and comparable OM input is ensured — as in the incubation experiment — the role of the mineral composition is pointed out (Chapter 4).

Chapter 4 on OM turnover in soils incubated with redox fluctuation were not directly compared to field data from actual paddy soils due to incomplete knowledge about the quantity of OM input. At this point, however, we compare SOM quality of the artificial paddy soils resulting from the experiment and the actual paddy soils from the field to see if the results of the incubation experiment can be verified. At least for the Andosol, SOM quality data from field paddy soils (Table 5.1) — accessed by XPS and biomarker analyses — point into the same direction as those of the incubation experiment. The percentage of reduced C species (C-C, C=C) on mineral surfaces was larger in paddy than non-paddy soils, while the percentage of oxidized C species (C-O) was smaller (Table 5.1). Similar to the Andosol incubated with redox fluctuation and

straw, mineral-associated lignin-derived compounds were less oxidized in the paddy than the non-paddy Andosol, as indicated by the lower $(Ac/Al)_v$ and $(Ac/Al)_s$ ratios. The smaller $(Galactose + Mannose)/(Arabinose + Xylose)$ ratio of mineral-associated carbohydrates in paddy than non-paddy Andosol suggests that the fraction of microbial sugars is smaller in paddy than respective non-paddy soils, which confirms the results of the Andosol incubated under paddy conditions. Measurable exchange of microbial-derived OM by plant-derived OM on mineral surfaces found for the Alisol incubated with redox fluctuation and straw was not found for the Alisol-derived paddy soil in the field. This might be attributed to insufficient input of OM to field paddy soils as already hypothesized in section 5.1.1.

Taking these results together, the input of fresh OM into submerged soils with redox alternation seems to promote the stabilization of plant-derived organic compounds through their direct association with minerals, alleviating their microbial processing. An absolute increase in mineral-associated, and thus, stabilized OC is achieved if sufficient reactive mineral surfaces are available like in the Andosol.

Table 5.1 C species at mineral surfaces of field soils according to fitted C 1s spectra of X-ray photoelectron spectroscopy (XPS) as well as Acid-to-Aldehyde ratio of Vanillyl $((Ac/Al)_v)$ and Syringyl $((Ac/Al)_s)$ units as indicator for oxidation state of lignin compounds and $GM/AX = (Galactose + Mannose)/(Arabinose + Xylose)$ with plant sugars showing $GM/AX < 0.5$ and microbial sugars showing $GM/AX > 2$. Numbers in brackets represent standard deviations with $n = 3$.

[%]	clayey Alisol		Andosol	
	non-paddy	paddy	non-paddy	paddy
C-C, C=C	55 (3)	63 (3)	27 (1)	53 (20)
C-O	28 (5)	24 (4)	58 (1)	36 (20)
C=O	12 (1)	8 (3)	8 (<1)	8 (2)
COO	5 (4)	6 (2)	6 (1)	3 (1)
$(Ac/Al)_v$	0.57 (0.02)	0.56 (0.04)	0.78 (0.06)	0.69 (0.08)
$(Ac/Al)_s$	0.59 (0.04)	0.56 (0.17)	0.88 (0.15)	0.80 (0.02)
GM/AX	1.49 (0.01)	1.49 (0.02)	2.09 (0.12)	1.38 (0.02)

The initial microbial community structure of the clayey Alisol and Andosol was relatively similar. Upon incubation, the microbial community of the Alisol distinctly changed upon redox alternation, while that of the Andosol exhibited only minor changes, probably due to the addition of a readily available OC source (Chapter 4). These differences are likely the result of the contrasting mineral composition of the initial soils used for incubation. While the mineral assemblage of the Alisol was dominated by kaolinite and crystalline Fe oxides, the mineral assemblage of the Andosol was dominated by allophane and imogolite-type phases as well as

SRO Fe oxides (Chapter 2 and 3). These SRO minerals in the Andosol probably result in a microporous structure providing protective microhabitats for microorganisms (Kögel-Knabner et al., 2008; Matus et al., 2014; Totsche et al., 2018). Hence, microbes in the Andosol under redox fluctuation were able to withstand unfavourable conditions and the overall microbial community was less forced to adapt to redox fluctuation (Ranjard et al., 1997). In contrast, the microbial community in the Alisol seemed more sensitive to changing redox conditions, and thus, may have adapted more rapidly. This is underlined by the larger respiration rate and smaller OM stabilization in the Alisol than Andosol under redox fluctuation. Besides stabilizing OM, the SRO allophane and ferrihydrite of the Andosol are also known to adsorb enzymes. Once sorbed the mobility of enzymes and substrates is restricted so that their interaction and thus substrate degradation is likely limited, which may also have contributed to the SOC increase in the Andosol (Kobayashi and Aomine, 1967; Allison, 2006). Hence, stabilization of OC might not only be the result of stable mineral-OC associations but also of limited mobility of bacteria residing in microhabitats and of exoenzymes adsorbed to the highly reactive mineral surfaces of the Andosol.

5.1.4 Do Fe oxide dynamics in paddy soils promote OC stabilization?

The biogeochemical cycles of Fe and OC are strongly interacting (Zhao et al., 2017). In tropical soils with limited O₂ availability, Fe oxides are usually the most important alternative electron acceptors during OM decomposition (Kirk, 2004). The respective reduction of Fe increases its mobility. Reductive dissolution and subsequent mobilization of Fe in paddy soils was indicated by the distinctly smaller Fe oxide concentrations in paddy topsoils compared to neighbouring Andosol and Alisol topsoils (Chapter 2). Hence, Fe oxides in paddy soils were used as alternative electron acceptors, and thus, supported anoxic OM decomposition. This is confirmed by the incubation experiment, which showed elevated concentrations of dissolved Fe²⁺ and distinct CO₂ production during anoxic phases (Chapter 4).

Besides facilitating anoxic OM decomposition, Fe oxides also contribute to the stabilization of OM. Especially SRO Fe oxides with their large surface area and positive surface charge provide vast sorption capacity for OM, which is usually characterized by negative surface charge. Sorption often occurs via ligand exchange, resulting in stable innersphere complexes (Kaiser and Guggenberger, 2000; Kleber et al., 2005). This is confirmed by the correlation ($r = 0.70$) of SRO Fe oxides and SOC of the studied non-paddy and paddy topsoils as shown in Fig. 5.2.

Considering the stabilizing effect of Fe oxides, their removal from paddy topsoils may have a negative impact on SOC storage. In the field study, however, topsoils with the strongest loss in Fe oxides (40 and 70% in Andosol and sandy Alisol, respectively) exhibited a distinct increase in

SOC, while soils with a less pronounced (<20% in clayey Alisol) or no Fe oxide loss (Vertisol) showed no change in SOC stocks (Fig. 5.2 and Chapter 2). These findings were confirmed by the incubation experiment, resulting in stronger reductive dissolution of Fe oxides and increased SOC in the Andosol, compared to less pronounced Fe oxide dissolution and unchanged SOC contents in the clayey Alisol (Chapter 4). Hence, the overall removal of Fe oxides from paddy topsoils did not result in subsequent losses of SOC.

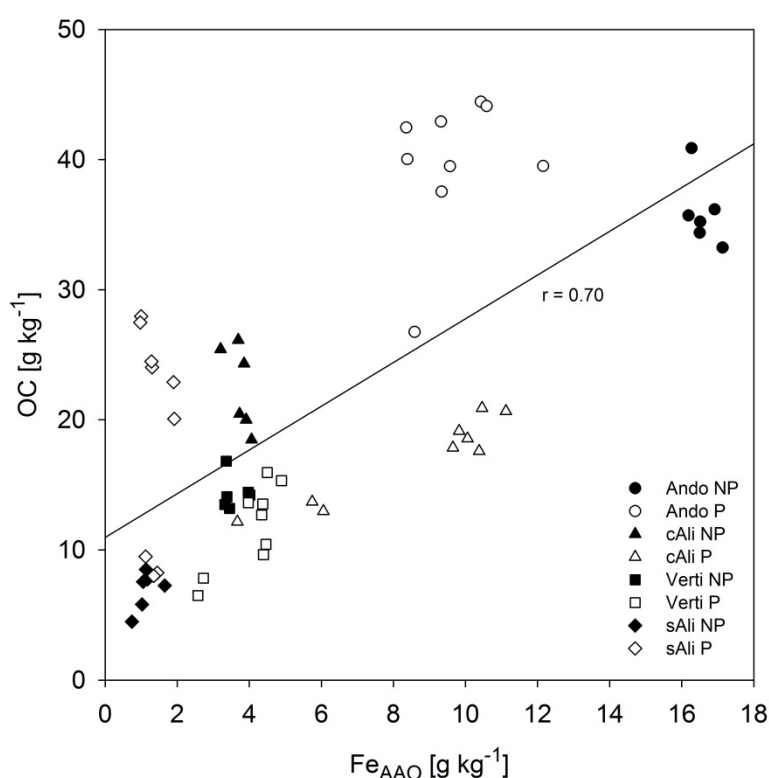


Fig. 5.2 Concentration of organic carbon (OC) plotted against acid ammonium oxalate-extractable Fe (= Fe_{AAO} representing SRO Fe oxides) of non-paddy (NP) and paddy (P) topsoils with Ando = Andosol, cAli = clayey Alisol, Verti = Vertisol and sAli = sandy Alisol. The correlation coefficient r results from Pearson Product Moment Correlation analysis performed with Sigma-Plot version 11.0 (SPSS Inc.).

Considering a maximum specific surface area of the Fe oxides of 400 m² g⁻¹ (Cornell and Schwertmann, 2003) and a maximum sorption of 2 mg OC m⁻² (Kaiser and Guggenberger, 2007; Kögel-Knabner et al., 2008), the OC adsorption potential of dithionite-citrate-bicarbonate (DCB) extractable Fe oxides was 17-22 g OC kg⁻¹ soil for the Andosol-derived and 6-9 g OC kg⁻¹ soil for the sandy Alisol-derived paddy topsoils. The actual SOC concentration of respective topsoils (40-44 and 20-28 g kg⁻¹, respectively), however, greatly exceeded these potentials.

One explanation might be an underestimation of potential surface loading by adsorption experiments (Kögel-Knabner et al., 2008). Steric effects during SOC adsorption on Fe oxide surfaces in soils under natural conditions may lead to larger surface loadings than those achieved during adsorption experiments in the laboratory. Moreover, the extraction of Fe oxides

with DCB was found to underestimate the true amount of pedogenic Fe oxides in soils (Chapter 3). Consequently, the actual adsorption potential of Fe oxides in paddy soils might be larger than calculated above. The non-paddy Andosol exhibiting increasing SOC when incubated under paddy conditions contained smaller amounts of Fe oxides than the incubated Alisol. The proportion of SRO Fe oxides — having larger surface area, and thus, being more effective in OC stabilization than crystalline Fe oxides (Kleber et al., 2005) — however, was distinctly larger in the Andosol than the Alisol. Moreover, the pH was generally lower in the incubated Andosol than in the Alisol, enhancing the positive surface charge of Fe oxides responsible for adsorption and stabilization of OC (Gu et al., 1994; Chapter 4).

Another explanation for the observed SOC contents exceeding the estimated SOC adsorption potential of remaining Fe oxides might be the formation of OC-rich coprecipitates. These might form when dissolved Fe^{2+} resulting from reductive Fe oxide dissolution and DOC released during anoxic OM decomposition mutually precipitate during re-oxidation (Lalonde et al., 2012; Chen et al., 2014). Upon recurring anoxic conditions, these coprecipitates stabilize OC more effectively than adsorption of OC to Fe oxides (Han et al., 2019). Coprecipitation of Fe with OC results in Fe oxides with low crystallinity as represented by the Mössbauer crystallinity classes \leq SRO-3. At least for the Andosol under paddy management, where Mössbauer data are available for the topsoil, the amount of Fe oxides assigned to these crystallinity classes actually decreased compared to the respective non-paddy soil (Chapter 3), indicating no increase in Fe-OC coprecipitates under paddy management. However, an increase in the Mössbauer doublet at 4.2K — representing Fe^{III} in phyllosilicates and Fe-OM complexes — was observed in the Andosol under paddy management (Chapter 3), which was attributed to Fe substitution in halloysite forming during paddy management. However, one might also speculate that the Mössbauer doublet at 4.2K represents ternary complexes of clay minerals, Fe oxides and OM, which have been described by Wagai and Mayer (2007). These might be the result of cation bridging. Dissolved Fe^{3+} is suggested to serve as cation bridge between clay mineral surfaces and OM both usually having negative charge (Oades, 1988). The studied paddy soils, however, exhibited $\text{pH} > 4$, which is not low enough for considerable acid-induced Fe oxide dissolution and respective release of dissolved Fe^{3+} . Reductive dissolution of Fe oxides in paddy soils, however, results in considerable release of dissolved Fe^{2+} . Organic matter stabilization under anoxic conditions by cation bridging with Fe^{2+} instead of Fe^{3+} could thus be assumed (Ahmed et al., 2002). Re-oxidation of the adsorbed Fe^{2+} may then result in ternary complexes of clay minerals, Fe oxides and OM.

Due to the uncertainties described above, the net effect of Fe oxides serving as alternative electron acceptors for anaerobic OM decomposition, the resulting reductive dissolution of the Fe oxides and subsequent destabilization of associated OM and the oxidative re-precipitation of the dissolved Fe^{2+} as SRO Fe oxides offering large reactive surface area or as Fe-OM-coprecipitates

— both contributing to the stabilization of OM — remains partly unresolved (Fig. 5.3; Han et al., 2016; Zhao et al., 2017).

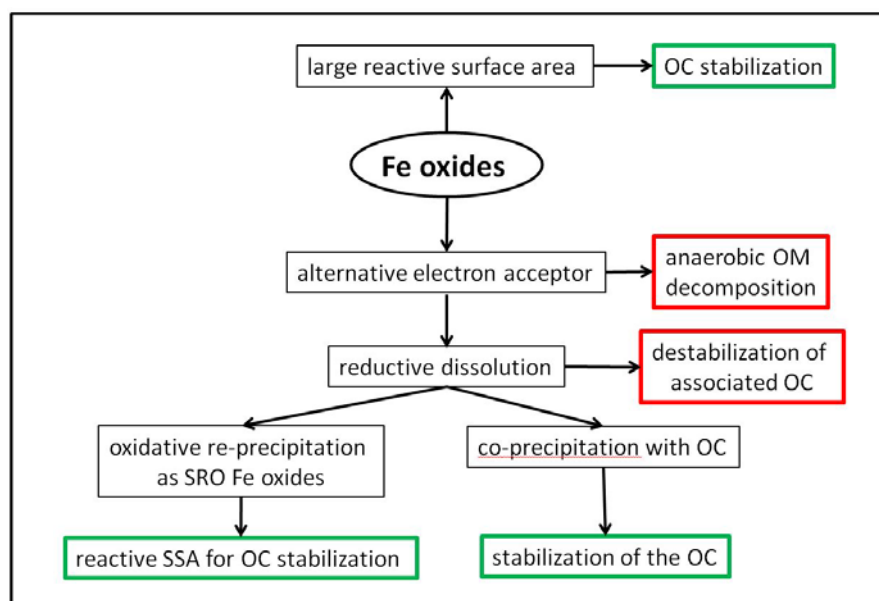


Fig. 5.3 Stabilizing and destabilizing effects of (short-range-ordered = SRO) Fe oxides on organic carbon (OC) in soils with redox fluctuation.

Finally, minerals other than Fe oxides and not redox-sensitive may have been responsible for the stabilization of SOC in some of the studied paddy soils (Kögel-Knabner et al., 2008). In the Andosol-derived paddy soil, allophane and imogolite-type phases as well as SRO Al hydroxides might play a role (Torn et al., 1997; Dahlgren et al., 2004; Matus et al., 2014). In the sandy Alisol, gibbsite and secondary chlorite might contribute to SOC stabilization (Parfitt et al., 1977; Singh et al., 2018; Chapter 2). The clayey Alisol-derived paddy soil exhibiting no changes in SOC was dominated by kaolinite, which has limited OC stabilizing effects (Han et al., 2016; Singh et al., 2018). This is supported by the incubation experiment with redox alternation and regular OM input, resulting in an increase in mineral-associated OM in the Andosol but not the clayey Alisol (Chapter 4). The mineral assemblage of the Vertisol-derived paddy soil was dominated by smectite allowing for SOC stabilization (Saidy et al., 2012). The amount of Fe oxides being more effective in OC stabilization than clay minerals (Mikutta and Kaiser, 2011), however, was small. That probably is the major reason for the overall OC stocks of the Vertisol being least of all studied soils. The Vertisol site was also characterized by rice straw burning, which may have restricted the input, and hence, the accumulation of OM in respective paddy soils (Chapter 2).

5.1.5 Do paddy management-induced processes described above depend on the initial soil type?

Changes in minerals were largest for the Andosol and smallest for the Vertisol under paddy management. Hence, rates of mineral transformations increase with increasing content of SRO minerals and pedogenic Fe oxides and are slow with phyllosilicates dominating the clay mineral assemblage. Changes in the mineral composition of paddy soils depend on the initial soil type.

Quantitative changes in SOC seem to depend on the mineral assemblage of the soil type under paddy management given that there is a sufficient input of OM. Especially the Andosol gained SOC when used for paddy cultivation likely due to the stabilizing effect of the allophane and imogolite-type phases as well as Al hydroxides. The role of Fe oxides in the soil types under paddy management is unclear since SOC stocks increased in the sandy Alisol-derived paddy soil despite distinct losses of Fe oxides but showed no change in the clayey Alisol-derived paddy soil despite increasing stocks of SRO Fe oxides (Chapter 2). Qualitative changes in mineral-associated OM, however, seem to be independent of soil type. The composition of mineral-associated OM as determined by XPS differed in the non-paddy Alisol and Andosol but became more similar in the respective field paddy soils. For both soil types incubated under paddy conditions, polysaccharide and lignin indicators suggested that abiotic effects of submergence seem to facilitate the direct association of plant-derived OM with mineral surfaces (Chapter 4).

Also, the microbial community structure seems to depend on the initial soil type under paddy management. The incubation of Alisol and Andosol with an initially similar microbial community structure resulted in the development of differing microbial communities upon exposure to redox fluctuation. We related this observation to the variation in mineral assemblage, likely providing protective microhabitats in the Andosol but not the Alisol. Hence, the microbial community of the Alisol was more sensitive to redox fluctuation, and thus, adapted more effectively (Chapter 4).

5.2 Summary & Conclusions

Overall, paddy management-induced biogeochemical processes do not have identical effects in different soil types. The mineral assemblage of the soil type under paddy management seems to be the driving factor for the intensity and direction of mineral transformations, for stabilization of OM, and for the adaptability and subsequent activity of the microbial community. Short-range-ordered minerals are more prone to transformation, have a larger OC stabilization potential and provide protective microhabitats reducing the necessity of the microbial community to adapt to redox fluctuation. Consequently, soils under paddy management and rich in SRO minerals are more prone to mineral transformation and SOC accumulation. Another important factor

specifically determining the effect of paddy management on Fe oxide translocation and crystallinity changes is the soil texture related leaching rate. Strong leaching of anoxic Fe²⁺-rich soil solution results in Fe losses from paddy topsoils. Short-range-ordered Fe oxides are preferentially reduced and leached. With the SRO Fe oxides the respective paddy soil loses OC storage potential. But it also depletes in alternative electron acceptors so that the methanogenic phase is reached more rapidly fuelling CH₄ emissions and climate change. Also, long periods of large water contents responsible for redox fluctuation seem to have an effect on OC stabilization. Soluble compounds of returned rice straw are more easily released into the soil solution and are more mobile at large water contents. Simultaneous anoxic conditions slow down the decomposition of these plant-derived compounds so that they can be stabilized by reactive minerals. For that reason, the Andosol rich in SRO minerals accumulated SOC under paddy management and the OM added to mineral surfaces was more plant-derived than the mineral-associated OM in soils with smaller water contents and predominantly oxic conditions. Short-range-ordered minerals may further decrease OM decomposition rates by adsorbing microorganisms, their exoenzymes and substrates thus restricting their interaction. Differences in SOC stocks of paddy and neighboring non-paddy soils further depend on differences in OM input and hence on the landuse type of the non-paddy soils. If the input at the non-paddy site is distinctly larger than at the paddy site, SOC contents might be smaller in the paddy soil despite less efficient decomposition.

The studied Andosol was most sensitive to paddy management due to its SRO mineral assemblage being subject to transformation and translocation. At the same time, the SRO minerals facilitated stabilization of additional OC. On the one hand, the enhanced transformation and translocation may lead to accelerated weathering of the SRO minerals, thereby reducing the OC stabilization potential characteristic for Andosol. On the other hand, enhanced mineral weathering in combination with rice straw application may facilitate the formation of stable OM-metal complexes. In order to understand if Andosol under paddy management contribute to long-term OC stabilization it would be necessary to study in more detail the association of OC with the different types of SRO minerals and if respective associations are stable under conditions of paddy management. It is, e.g., still not fully known if the association of OC with Fe oxides prevents the Fe oxides from reductive dissolution, and hence, the associated OC from mineralization.

The studied Vertisol was least sensitive to paddy management. It was situated in a floodplain with alluvial deposits. Its texture was characterized by large clay contents and the mineral assemblage was dominated by smectite. Wet smectites swell so that even under non-paddy conditions strong rain events – typical for the given tropical monsoon climate – lead to long-lasting water saturation of the soil. In combination with the annual dry season, redox fluctuation similar to those in paddy soils likely also occurs in non-paddy soils. Seemingly, the specific

hydrology of Vertisol is best utilized under rice paddy cultivation. The effect of redox alternation is minimal due to the Vertisol's small content of redox-sensitive Fe oxides and is compensated by deep self-mulching. Stabilization and hence sequestration of OC could probably be enhanced if rice straw was not burned but returned to the soil. The overall OC content of the Vertisol was surprisingly small, especially when considering its large clay content. This may question the oftentimes suggested importance of smectites in OC stabilization.

Further research on the effect of redox alternation in soils is of importance since with climate change an increase in intensity and frequency of draught and strong rain events as well as of temperature, and thus, microbial activity is likely and may lead to pronounced redox alternation also in many non-paddy soils.

Summary

Wetland rice cultivation in paddy fields is characterized by soil submergence during plant growth and drainage during harvest. The respective paddy soils undergo redox fluctuations resulting in clay mineral transformations and changes in amounts and crystallinity of redox-sensitive Fe oxides. The influence of the initial soil type on the extent of these changes has not yet been well studied. Also, the effects of the mineral transformations on organic carbon (OC) storage are poorly understood.

These research questions were addressed by studying paddy soils from Indonesia and China that have been exposed to redox fluctuations for several decades and that derived from three different soil types (Vertisols, Andosols, clayey/sandy Alisols). Adjacent non-paddy soils predominantly under oxic conditions were sampled as references. Soil samples from non-paddy and paddy profiles were analyzed for texture, mineral composition (XRD for clay minerals and chemical extraction of Fe oxides and allophane-imogolite phases), bulk density, pH, cation exchange capacity (CEC), base saturation and soil organic carbon (SOC). To gain insights into Fe phases and mineral-associated organic matter (MOM), topsoil samples of the clayey Alisol and Andosol and respective paddy soils were analyzed by Mössbauer and X-ray photoelectron spectroscopy (XPS). Clayey Alisol and Andosol non-paddy topsoils were further used for a one-year incubation experiment with eight redox cycles, mimicking paddy soil development. Incubated soils received rice straw labelled with ^{13}C at the beginning of each redox cycle. As control we used a second set of samples without straw addition as well as samples under static oxic conditions with and without straw. Emissions of CO_2 and CH_4 as well as the geochemistry of the soil solution were monitored. At the end of the experiment, mineral-associated OM was isolated by density fractionation and analyzed for $\delta^{13}\text{C}$ and biomarkers (lignin and polysaccharides). Moreover, incubation-induced changes in the soil's microbial community structure were measured via sequence analyses of the 16S rRNA gene.

Only the sandy Alisol-derived paddy soil showed textural changes, compared to the non-paddy soil, most likely caused by clay migration. The Vertisol and both Alisols revealed no measurable changes in phyllosilicates upon paddy management, while the Andosol rich in short-range-ordered (SRO) minerals showed loss of allophane and imogolite-type phases and increase in halloysite. All soils but the Vertisol lost Fe oxides from the topsoil, with the remaining Fe oxides exhibiting lower crystallinity in both Alisols and higher crystallinity in the Andosol. Reductive dissolution of Fe oxides during anoxic phases and partial leaching of the dissolved Fe^{2+} were responsible for the Fe losses, while the crystallinity of the remaining Fe oxides is i.a. influenced by precipitation of re-oxidized Fe as SRO Fe oxides. The extent to which reductively dissolved Fe is leached or re-oxidized likely depends on soil permeability. We further suggest that the Fe mineral composition of the initial soil (dominance of crystalline or SRO Fe oxides) has an impact

on the Fe oxide evolution under alternating redox-conditions, since SRO Fe oxides are more easily reducible and hence more prone to dissolution and leaching than crystalline Fe oxides. Accumulation of Fe oxides in paddy subsoils was not found, likely due to rather lateral transport of dissolved Fe. Overall, redox-mediated mineral transformations were found in soils with large contents of SRO minerals and pedogenic Fe oxides. Phyllosilicate-dominated soils showed little to no changes in mineral assemblage upon paddy management.

Despite losses in potential OC storage capacity (i.e., Fe oxides, allophanes), paddy soils derived from Andosols and sandy Alisols had larger OC concentrations in the topsoil, whereby the other soils showed no change in OC under paddy management. Therefore, paddy management does not necessarily enhance carbon sequestration. Differences in OM input between non-paddy and paddy soils in the field may determine whether OC is accumulated under paddy management or not. Moreover, a direct influence of Fe oxide redistribution on OC stabilization was not observed. XPS analyses revealed that the initially different composition of the mineral-associated OM in the clayey Alisol and Andosol was more similar in the respective field paddy soils. Effects of paddy management on CEC were little and mainly due to OC accumulation and removal of Fe oxide coatings from clay minerals.

In the laboratory incubation experiment, Eh, pH and dissolved Fe^{2+} responded as anticipated, with elevated Fe^{2+} concentrations during the anoxic periods as well as low Eh and high pH. For both soil types (clayey Alisol and Andosol), headspace data confirmed less respiration in straw-amended soils with redox fluctuation than in those under static oxic conditions. The $\delta^{13}\text{C}$ data revealed that, irrespective of soil type, straw carbon allocation into MOM was larger in soils with redox fluctuation than in those with static oxic conditions. A net increase in MOM after the one-year incubation, however, was only observed in the respective Andosol, likely due to abundant reactive minerals capable of OC uptake. Biomarkers revealed that OM bound to minerals during incubation with redox fluctuation was less microbially processed than the initial OM, irrespective the soil type. In addition to long anoxic periods with less efficient OM decomposition, large water contents enhancing diffusion of plant-derived dissolved OM seems to play a role here. The initially similar bacterial community composition of the clayey Alisol and Andosol changed differently under redox fluctuation. In summary, the overall turnover of straw OC in soils under redox fluctuation seems to be independent of soil type, while net accumulation of SOC as well as the evolution of the bacterial community structure may in part depend on soil type, suggesting an impact of the soil's mineral composition.

Overall, biogeochemical changes induced by paddy management were partly influenced by the original soil and the parent material. The main characteristics of the initial soil type were preserved and not overridden by several decades of paddy management.

Zusammenfassung

Nassreisanbau ist durch Wasserüberstau des Bodens während der Wachstumsphase sowie durch Drainage zur Ernte der Reispflanzen gekennzeichnet. Reisböden unterliegen daher alternierenden Redoxbedingungen, die zur Transformation von Tonmineralen sowie zu Veränderungen der Menge und Kristallinität von Eisen (Fe)-Oxiden führen. Der Einfluss des Ausgangsbodentyps auf das Ausmaß dieser Veränderungen ist noch nicht vollständig aufgeklärt. Es ist zudem nicht bekannt, wie sich die Mineralveränderungen der Böden unter Reisanbau, insbesondere die Umverteilung der Eisenoxide, auf die Speicherung organischer Substanz auswirken.

Wir haben daher Reisböden (Paddy) in Indonesien und China untersucht, die seit mehreren Dekaden Redoxfluktuation ausgesetzt waren und aus drei verschiedenen Bodentypen (Vertisol, Andosol, toniger/sandiger Alisol) hervorgegangen sind. Benachbarte Böden mit überwiegend oxidischen Bedingungen (Non-Paddy) wurden als Referenz beprobt. Bodenproben von Profilen der Non-Paddy- und Paddy-Standorte wurden hinsichtlich Textur, Mineralzusammensetzung (XRD für Tonminerale und chemische Extraktion von Fe-Oxiden und Allophan-Imogolit-Phasen), Lagerungsdichte, pH, Kationenaustauschkapazität (KAK), Basensättigung und organischem Kohlenstoff (OC) analysiert. Für Detailuntersuchungen zu den Fe-Phasen und der mineralgebundenen organischen Substanz (OS) wurden Oberbodenproben des tonigen Alisols und des Andosols sowie der entsprechenden Reisböden für Mössbauer- bzw. Röntgenphotoelektronen-Spektroskopie (XPS) ausgewählt. Die Non-Paddy-Oberböden des tonigen Alisols und des Andosols wurden zudem für ein einjähriges Inkubationsexperiment mit acht Redoxzyklen zur Simulation der Reisbodenentwicklung verwendet. Den inkubierten Böden wurde zu Beginn jedes Redoxzyklus ^{13}C -markiertes Stroh hinzugegeben. Als Kontrolle wurde ein zweiter Satz Proben ohne Strohzugabe sowie eine permanent oxische Variante mit und ohne Strohzugabe verwendet. Während der Inkubation wurden die CO_2 - und CH_4 -Emissionen sowie die Zusammensetzung der Bodenlösungen bestimmt. Am Ende des Experiments wurde die mineralassoziierte OS durch Dichtefraktionierung isoliert und auf $\delta^{13}\text{C}$ und Biomarker (Lignin und Polysaccharide) analysiert. Darüber hinaus wurden bei der Inkubation hervorgerufene Veränderungen der mikrobiellen Gemeinschaft durch Sequenzanalyse des 16S-rRNA-Gens untersucht.

Nur der aus dem sandigen Alisol hervorgegangene Reisboden zeigte gegenüber dem entsprechenden Non-Paddy-Boden Texturveränderungen. Diese wurden wahrscheinlich durch Tonverlagerung hervorgerufen. Der Vertisol sowie beide Alisole zeigten keine messbaren Veränderungen der Tonminerale durch Reisanbau. Der Andosol hingegen, welcher reich an schwach-kristallinen Mineralen war, zeigte Anzeichen für eine Abnahme an Allophanen und eine Zunahme an Halloysit. Mit Ausnahme des Vertisol wiesen alle Böden unter Reisanbau einen

Verlust an Fe-Oxiden im Oberboden auf, wobei die Kristallinität der verbleibenden Fe-Oxide in den Alisolen abnahm und im Andosol zunahm. Reduktive Auflösung von Fe-Oxiden unter anoxischen Bedingungen und partielle Auswaschung des gelösten Eisens sind verantwortlich für die Fe-Verluste, während die Kristallinität der verbleibenden Fe-Oxide unter anderem von der Ausfällung re-oxidierten Eisens in Form schwach-kristalliner Fe-Oxide abhängt. Das Ausmaß, in dem reduktiv gelöstes Fe ausgewaschen oder re-oxidiert wird, hängt wahrscheinlich von der Permeabilität des Bodens ab. Des Weiteren vermuten wir, dass die Fe-Mineral-Zusammensetzung des Ausgangsbodens (Dominanz kristalliner oder schwach-kristalliner Fe-Oxide) einen Einfluss auf die Fe-Oxid-Entwicklung unter alternierenden Redoxbedingungen hat, da schwach-kristalline Fe-Oxide leichter reduzierbar und damit anfälliger gegenüber Auflösung und Auswaschung sind als kristalline Fe-Oxide. Eine Akkumulation von Fe im Unterboden von Reisböden wurde nicht gefunden, wahrscheinlich infolge lateraler Abfuhr gelösten Eisens. Mineraltransformationen wurden in Böden mit großen Mengen an schwach-kristallinen Mineralen und pedogenen Fe-Oxiden gefunden, waren jedoch nicht messbar in tonmineral-dominierten Böden.

Trotz des Verlusts an potentieller Speicherkapazität (Fe-Oxide, Allophane) zeigten die Reisböden, die sich auf sandigem Alisol und Andosol entwickelten, erhöhte Gehalte an OC im Oberboden, während die anderen Böden unter Reisanbau keine Veränderung zeigten. Demnach führt Reisanbau nicht zwangsläufig zu erhöhter Kohlenstoff (C)-Speicherung. Unterschiede im Eintrag OS zwischen Non-Paddy- und Paddy-Böden könnten mitbestimmen, ob es unter Reisanbau zu C-Akkumulation kommt oder nicht. Zudem wurde kein direkter Einfluss der Fe-Oxid-Umverteilung auf die C-Speicherung beobachtet. XPS-Analysen zeigten, dass die anfänglich unterschiedliche Zusammensetzung der mineral-assoziierten OS im tonigen Alisol und im Andosol infolge Reisanbaus einander ähnlicher wurde. Der Einfluss des Reisanbaus auf die KAK war gering und konnte hauptsächlich auf OC-Akkumulation sowie die Entfernung von Fe-Oxid-Belägen von Tonmineralen zurückgeführt werden.

Im Inkubationsexperiment verhielten sich Redoxpotential, pH-Wert und die Konzentration an gelöstem Fe^{2+} wie erwartet: anoxische Phasen waren gekennzeichnet durch erhöhte Fe^{2+} -Konzentrationen bei geringem Redoxpotential und erhöhtem pH-Wert. Für beide Bodentypen (toniger Alisol und Andosol) bestätigen die Gasdaten geringere Respiration in Böden mit Strohzugabe und wechselnden Redoxbedingungen als in solchen mit permanent oxischen Bedingungen. Die $\delta^{13}C$ -Daten verdeutlichten, dass unabhängig vom Bodentyp der Übergang von Stroh-C in die mineral-assoziierte Fraktion in Böden mit Redoxfluktuation größer war als in denen mit permanent oxischen Bedingungen. Eine Netto-Zunahme mineral-assoziiertes OS nach einjähriger Inkubation wurde jedoch nur im entsprechenden Andosol gefunden, wahrscheinlich aufgrund des hohen Gehalts an reaktiven Mineralen, die zur OC-Speicherung beitragen. Biomarker-Analysen zeigten, dass unabhängig vom Bodentyp OS, die während der Inkubation an

Minerale gebunden wurde, weniger mikrobiell umgesetzt war als die ursprüngliche OS. Neben gehemmtem Abbau während der langen anoxischen Phasen, scheinen hohe Wassergehalte, die die Diffusion pflanzenbürtiger gelöster OS fördern, eine Rolle zu spielen. Die anfänglich ähnliche Zusammensetzung der mikrobiellen Gemeinschaft des tonigen Alisols und Andosols divergierte unter Redoxfluktuation. Zusammengefasst scheint der Umsatz von Stroh in Böden unter Redoxfluktuation weitgehend unabhängig vom Bodentyp zu verlaufen, während die Netto-Akkumulation von OC sowie die Entwicklung der mikrobiellen Gemeinschaft teilweise vom Bodentyp abhängen, was auf einen Einfluss der Mineralzusammensetzung des Bodens hindeutet.

Insgesamt konnte gezeigt werden, dass durch Reisanbau induzierte biogeochemische Veränderungen zum Teil vom Ausgangsboden beeinflusst sind. Die Haupteigenschaften der Ausgangsbodentypen blieben erhalten und wurden auch nach jahrzehntelangem Reisanbau nicht überprägt.

References

- Achtnich C., Bak F. and Conrad R. (1995) Competition for electron donors among nitrate reducers, ferric iron reducers, sulfate reducers, and methanogens in anoxic paddy soil. *Biol. Fertil. Soils* **19**, 65–72.
- Ahmad N. (1996) Occurrence and distribution of Vertisols. In *N. Ahmad and A. Mermut (Eds.) Developments in Soil Science. Vertisols and Technologies for their Management*. Elsevier. pp. 1–41.
- Ahmad N. and Jones R. L. (1969) Genesis, chemical properties and mineralogy of Caribbean Grumusols. *Soil Sci.* **107**, 166–174.
- Ahmed N., Varadachari C. and Ghosh K. (2002) Soil clay–humus complexes. II. Bridging cations and DTA studies. *Soil Res.* **40**, 705–713.
- Allison S. D. (2006) Soil minerals and humic acids alter enzyme stability: implications for ecosystem processes. *Biogeochemistry* **81**, 361–373.
- Amelung W., Flach K.-W. and Zech W. (1999) Lignin in particle-size fractions of native grassland soils as influenced by climate. *Soil Sci. Soc. Am. J.* **63**, 1222–1228.
- Anda M., Chittleborough D. J. and Fitzpatrick R. W. (2009) Assessing parent material uniformity of a red and black soil complex in the landscapes. *Catena* **78**, 142–153.
- Aomine S. and Wada K. (1962) Differential weathering of volcanic ash and pumice, resulting in formation of hydrated halloysite. *Am. Mineral.* **47**, 1024–1048.
- Ayari A., Yang H. and Xie S. (2013) Flooding impact on the distribution of microbial tetraether lipids in paddy rice soil in China. *Front. Earth Sci.* **7**, 384–394.
- Baldock J. A. and Skjemstad J. O. (2000) Role of the soil matrix and minerals in protecting natural organic materials against biological attack. *Org. Geochem.* **31**, 697–710.
- Balesdent J., Mariotti A. and Boissgonnier D. (1990) Effect of tillage on soil organic carbon mineralization estimated from ¹³C abundance in maize fields. *J. Soil Sci.* **41**, 587–596.
- Benner R., Maccubbin A. E. and Hodson R. E. (1984) Anaerobic biodegradation of the lignin and polysaccharide components of lignocellulose and synthetic lignin by sediment microflora. *Appl. Environ. Microbiol.* **47**, 998–1004.
- Bertsch B. M. and Bloom B. R. (1996) Aluminium. In *D. L. Sparks, A. L. Page, P. A. Helmke, R. H. Loeppert, P. N. Soltanpour, M. A. Tabatabai, C. T. Johnston, and M. E. Sumner (Eds.) Methods of soil analysis*. Agronomy Monograph No. 5. SSSA, Madison, WI, USA. pp. 517–550.
- Bhattacharyya T., Pal D. K., Ray S. K., Chandran P., Mandal C., Telpande B., Deshmukh A. S. and Tiwary P. (2013) Simulating change in soil organic carbon in two long term fertilizer experiments in India : with the RothC model. *Clim. Change Environ. Sustain.* **1**, 104–117.
- Bierke A., Kaiser K. and Guggenberger G. (2008) Crop residue management effects on organic matter in paddy soils — The lignin component. *Geoderma* **146**, 48–57.
- Blake G. R. and Hartge K. H. (1986) Bulk Density. In *Klute, A. (Ed.) Methods of soil analysis*. Agronomy Monograph No. 9. SSSA, Madison, WI, USA. pp. 363–375.

- Blakemore L. C., Searle P. L. and Daly B. K. (1981) *Methods for chemical analysis of soils.*, New Zealand Soil Bureau Scientific Report 10A.
- Blume H.-P., Brümmer G. W., Horn R., Kandeler E., Kögel-Knabner I., Kretzschmar R., Stahr K. and Wilke B.-M. (2010) *Scheffer/Schachtschabel: Lehrbuch der Bodenkunde*. 16th ed., Springer Spektrum, Berlin Heidelberg.
- Bonneville S., Behrends T. and Van Cappellen P. (2009) Solubility and dissimilatory reduction kinetics of iron(III) oxyhydroxides: A linear free energy relationship. *Geochim. Cosmochim. Acta* **73**, 5273–5282.
- Bräuer T., Grootes P. M., Nadeau M.-J. and Andersen N. (2013) Downward carbon transport in a 2000-year rice paddy soil chronosequence traced by radiocarbon measurements. *Nucl. Instrum. Methods Phys. Res. Sect. B* **294**, 584–587.
- Bridges E. M. (1997) *World soils.*, Cambridge University Press, Cambridge.
- Brinkman R. (1970) Ferrollysis, a hydromorphic soil forming process. *Geoderma* **3**, 199–206.
- Buurman P., Rodeja E. G., Cortizas A. M. and van Doesburg J. D. J. (2004) Stratification of parent material in European volcanic and related soils studied by laser-diffraction grain-sizing and chemical analysis. *Catena* **56**, 127–144.
- Cao M., Gregson K., Marshall S., Dent J. B. and Heal O. W. (1996) Global methane emissions from rice paddies. *Chemosphere* **33**, 879–897.
- Caporaso J. G., Kuczynski J., Stombaugh J., Bittinger K., Bushman F. D., Costello E. K., Fierer N., Peña A. G., Goodrich J. K., Gordon J. I., Huttley G. A., Kelley S. T., Knights D., Koenig J. E., Ley R. E., Lozupone C. A., McDonald D., Muegge B. D., Pirrung M., Reeder J., Sevinsky J. R., Turnbaugh P. J., Walters W. A., Widmann J., Yatsunenko T., Zaneveld J. and Knight R. (2010) QIIME allows analysis of high-throughput community sequencing data. *Nat. Methods* **7**, 335–336.
- Cerli C., Celi L., Kalbitz K., Guggenberger G. and Kaiser K. (2012) Separation of light and heavy organic matter fractions in soil — Testing for proper density cut-off and dispersion level. *Geoderma* **170**, 403–416.
- Chacon N., Silver W. L., Dubinsky E. A. and Cusack D. F. (2006) Iron reduction and soil phosphorus solubilization in humid tropical forest soils: The roles of labile carbon pools and an electron shuttle compound. *Biogeochemistry* **78**, 67–84.
- Chadwick O. A. and Chorover J. (2001) The chemistry of pedogenic thresholds. *Geoderma* **100**, 321–353.
- Charman P. E. V. and Murphy B. W. (2007) *Soils their properties and management*. 3rd ed., Oxford University Press, South Melbourne.
- Chen C., Dynes J. J., Wang J. and Sparks D. L. (2014) Properties of Fe-organic matter associations via coprecipitation versus adsorption. *Environ. Sci. Technol.* **48**, 13751–13759.
- Chen C. and Thompson A. (2018) Ferrous iron oxidation under varying pO₂ levels: The effect of Fe(III)/Al(III) oxide minerals and organic matter. *Environ. Sci. Technol.* **52**, 597–606.
- Chen L.-M., Zhang G.-L. and Effland W. R. (2011) Soil characteristic response times and pedogenic thresholds during the 1000-year evolution of a paddy soil chronosequence. *Soil Sci. Soc. Am. J.* **75**, 1807–1820.

- Cheng Y.-Q., Yang L.-Z., Cao Z.-H., Ci E. and Yin S. (2009) Chronosequential changes of selected pedogenic properties in paddy soils as compared with non-paddy soils. *Geoderma* **151**, 31–41.
- Christensen B. T. (1992) Physical fractionation of soil and organic matter in primary particle size and density separates. *Advances in Soil Science* **20**. Springer, New York, NY. pp. 1–90.
- Coby A. J., Picardal F., Shelobolina E., Xu H. and Roden E. E. (2011) Repeated anaerobic microbial redox cycling of iron. *Appl. Environ. Microbiol.* **77**, 6036–6042.
- Colberg P. J. and Young L. Y. (1982) Biodegradation of lignin-derived molecules under anaerobic conditions. *Can. J. Microbiol.* **28**, 886–889.
- Connell W. E. and Patrick W. H. (1969) Reduction of sulfate to sulfide in waterlogged soil. *Soil Sci. Soc. Am. J.* **33**, 711–715.
- Cornell R. M. and Schwertmann U. (2003) *The Iron Oxides: Structure, Properties, Reactions, Occurrences and Uses.*, John Wiley & Sons, Weinheim, Germany.
- Coumou D. and Rahmstorf S. (2012) A decade of weather extremes. *Nat. Clim. Change* **2**, 491–496.
- Coward E. K., Thompson A. T. and Plante A. F. (2017) Iron-mediated mineralogical control of organic matter accumulation in tropical soils. *Geoderma* **306**, 206–216.
- Dahlgren R. A., Saigusa M. and Ugolini F. C. (2004) The nature, properties and management of volcanic soils. *Adv. Agron.* **82**, 114–183.
- Dahlgren R., Shoji S. and Nanzyo M. (1993) Mineralogical characteristics of volcanic ash soils. *Dev. Soil Sci.* **21**, 101–143.
- Das S., Richards B. K., Hanley K. L., Krounbi L., Walter M. F., Walter M. T., Steenhuis T. S. and Lehmann J. (2019) Lower mineralizability of soil carbon with higher legacy soil moisture. *Soil Biol. Biochem.* **130**, 94–104.
- DeAngelis K. M., Silver W. L., Thompson A. W. and Firestone M. K. (2010) Microbial communities acclimate to recurring changes in soil redox potential status. *Environ. Microbiol.* **12**, 3137–3149.
- DeSantis T. Z., Hugenholtz P., Larsen N., Rojas M., Brodie E. L., Keller K., Huber T., Dalevi D., Hu P. and Andersen G. L. (2006) Greengenes, a chimera-checked 16S rRNA gene database and workbench compatible with ARB. *Appl. Environ. Microbiol.* **72**, 5069–5072.
- Driessen P. M. and Dudal R. (1991) *The major soils of the world - Lecture notes on their geography, formation, properties and use.*, Wageningen University, The Netherlands and Katholieke Universiteit Leuven, Belgium.
- Dubinsky E. A., Silver W. L. and Firestone M. K. (2010) Tropical forest soil microbial communities couple iron and carbon biogeochemistry. *Ecology* **91**, 2604–2612.
- Dubroeuq D., Geissert D., Barois I. and Ledru M.-P. (2002) Biological and mineralogical features of Andisols in the Mexican volcanic highlands. *Catena* **49**, 183–202.
- Dudal R. (1963) Dark clay soils of tropical and subtropical regions. *Soil Sci.* **95**, 264.

- Eaqub M. and Blume H.-P. (1982) Genesis of a so-called ferrolysed soil of Bangladesh. *Z. für Pflanzenernähr. Bodenkd.* **145**, 470–482.
- Eder E., Spielvogel S., Kölbl A., Albert G. and Kögel-Knabner I. (2010) Analysis of hydrolysable neutral sugars in mineral soils: Improvement of alditol acetylation for gas chromatographic separation and measurement. *Org. Geochem.* **41**, 580–585.
- Edgar R. C. (2010) Search and clustering orders of magnitude faster than BLAST. *Bioinformatics* **26**, 2460–2461.
- Estendorfer J., Stempfhuber B., Haury P., Vestergaard G., Rillig M. C., Joshi J., Schröder P. and Schloter M. (2017) The influence of land use intensity on the plant-associated microbiome of *Dactylis glomerata* L. *Front. Plant Sci.* **8**, 930.
- Eusterhues K., Hädrich A., Neidhardt J., Küsel K., Keller T. F., Jandt K. D. and Totsche K. U. (2014) Reduction of ferrihydrite with adsorbed and coprecipitated organic matter: microbial reduction by *Geobacter bremensis* vs. abiotic reduction by Na-dithionite. *Biogeosciences* **11**, 4953–4966.
- Eusterhues K., Wagner F. E., Häusler W., Hanzlik M., Knicker H., Totsche K. U., Kögel-Knabner I. and Schwertmann U. (2008) Characterization of ferrihydrite-soil organic matter coprecipitates by X-ray diffraction and Mössbauer spectroscopy. *Environ. Sci. Technol.* **42**, 7891–7897.
- FAO (2006) *Guidelines for soil description*. 4th ed., FAO, Rome.
- Favre F., Tessier D., Abdelmoula M., Génin J. M., Gates W. P. and Boivin P. (2002) Iron reduction and changes in cation exchange capacity in intermittently waterlogged soil. *Eur. J. Soil Sci.* **53**, 175–183.
- Federherr E., Cerli C., Kirkels F. M. S. A., Kalbitz K., Kupka H. J., Dunsbach R., Lange L. and Schmidt T. C. (2014) A novel high-temperature combustion based system for stable isotope analysis of dissolved organic carbon in aqueous samples. I: development and validation. *Rapid Commun. Mass Spectrom.* **28**, 2559–2573.
- Fierer N., Bradford M. A. and Jackson R. B. (2007) Toward an ecological classification of soil bacteria. *Ecology* **88**, 1354–1364.
- Filimonova S., Kaufhold S., Wagner F. E., Häusler W. and Kögel-Knabner I. (2016) The role of allophane nano-structure and Fe oxide speciation for hosting soil organic matter in an allophanic Andosol. *Geochim. Cosmochim. Acta* **180**, 284–302.
- Finlow-Bates T. and Stumpfl E. F. (1981) The behaviour of so-called immobile elements in hydrothermally altered rocks associated with volcanogenic submarine-exhalative ore deposits. *Miner. Deposita* **16**, 319–328.
- Funakawa S., Watanabe T. and Kosaki T. (2008) Regional trends in the chemical and mineralogical properties of upland soils in humid Asia: With special reference to the WRB classification scheme. *Soil Sci. Plant Nutr.* **54**, 751–760.
- Ginn B., Meile C., Wilmoth J., Tang Y. and Thompson A. (2017) Rapid iron reduction rates are stimulated by high-amplitude redox fluctuations in a tropical forest soil. *Environ. Sci. Technol.* **51**, 3250–3259.

- Grable A. R. and Siemer E. G. (1968) Effects of bulk density, aggregate size, and soil water suction on oxygen diffusion, redox potentials, and elongation of corn roots. *Soil Sci. Soc. Am. J.* **32**, 180–186.
- Greenland D. J. (1997) *The sustainability of rice farming.*, CAB International, Wallingford.
- GRiSP (2013) *Rice Almanac*. 4th ed., International Rice Research Institute, Los Banos, Philippines.
- Gu B., Schmitt J., Chen Z., Liang L. and McCarthy J. F. (1994) Adsorption and desorption of natural organic matter on iron oxide: Mechanisms and models. *Environ. Sci. Technol.* **28**, 38–46.
- Guggenberger G. and Kaiser K. (2003) Dissolved organic matter in soil: challenging the paradigm of sorptive preservation. *Geoderma* **113**, 293–310.
- Gupta V. V. S. R. and Germida J. J. (2015) Soil aggregation: Influence on microbial biomass and implications for biological processes. *Soil Biol. Biochem.* **80**, A3–A9.
- Hackett W. F., Connors W. J., Kirk T. K. and Zeikus J. G. (1977) Microbial decomposition of synthetic ¹⁴C-labeled lignins in nature: lignin biodegradation in a variety of natural materials. *Appl. Environ. Microbiol.* **33**, 43–51.
- Hagedorn F., Kaiser K., Feyen H. and Schleppei P. (2000) Effects of redox conditions and flow processes on the mobility of dissolved organic carbon and nitrogen in a forest soil. *J. Environ. Qual.* **29**, 288–297.
- Han G.-Z., Zhang G.-L., Li D.-C. and Yang J.-L. (2015) Pedogenetic evolution of clay minerals and agricultural implications in three paddy soil chronosequences of south China derived from different parent materials. *J. Soils Sediments* **15**, 423–435.
- Han L., Sun K., Jin J. and Xing B. (2016) Some concepts of soil organic carbon characteristics and mineral interaction from a review of literature. *Soil Biol. Biochem.* **94**, 107–121.
- Han L., Sun K., Keiluweit M., Yang Yu, Yang Yan, Jin J., Sun H., Wu F. and Xing B. (2019) Mobilization of ferrihydrite-associated organic carbon during Fe reduction: Adsorption versus coprecipitation. *Chem. Geol.* **503**, 61–68.
- Hanke A., Cerli C., Muhr J., Borken W. and Kalbitz K. (2013) Redox control on carbon mineralization and dissolved organic matter along a chronosequence of paddy soils. *Eur. J. Soil Sci.* **64**, 476–487.
- Hansel C. M., Benner S. G. and Fendorf S. (2005) Competing Fe(II)-induced mineralization pathways of ferrihydrite. *Environ. Sci. Technol.* **39**, 7147–7153.
- Hassannezhad H., Pashaee A., Khormali F. and Mohammadian M. (2008) Effect of soil moisture regime and rice cultivation on mineralogical characteristics of paddy soils of Mazandaran Province, Northern Iran, Amol. *Int. J. Soil Sci.* **3**, 138–148.
- Heckman K., Lawrence C. R. and Harden J. W. (2018) A sequential selective dissolution method to quantify storage and stability of organic carbon associated with Al and Fe hydroxide phases. *Geoderma* **312**, 24–35.
- Hedges J. I. and Ertel J. R. (1982) Characterization of lignin by gas capillary chromatography of cupric oxide oxidation products. *Anal. Chem.* **54**, 174–178.

- Hendershot W. H., Lalonde H. and Duquette M. (2008) Ion exchange and exchangeable cations. In *M. R. Carter and E. G. Gregorich (Eds.) Soil Sampling and Methods of Analysis*. Canadian Soil Science Society - Taylor & Francis, Boca Raton, FL, USA. pp. 197–206.
- Henneberry Y. K., Kraus T. E. C., Nico P. S. and Horwath W. R. (2012) Structural stability of coprecipitated natural organic matter and ferric iron under reducing conditions. *Org. Geochem.* **48**, 81–89.
- Herndon E., AlBashaireh A., Singer D., Roy Chowdhury T., Gu B. and Graham D. (2017) Influence of iron redox cycling on organo-mineral associations in Arctic tundra soil. *Geochim. Cosmochim. Acta* **207**, 210–231.
- Hernes P. J., Kaiser K., Dyda R. Y. and Cerli C. (2013) Molecular trickery in soil organic matter: Hidden lignin. *Environ. Sci. Technol.* **47**, 9077–9085.
- Heyng A. M., Mayr C., Lücke A., Moschen R., Wissel H., Striewski B. and Bauersachs T. (2015) Middle and late holocene paleotemperatures reconstructed from oxygen isotopes and GDGTs of sediments from Lake Pupuke, New Zealand. *Quat. Int.* **374**, 3–14.
- Hodson M. E. (2002) Experimental evidence for mobility of Zr and other trace elements in soils. *Geochim. Cosmochim. Acta* **66**, 819–828.
- Hopmans E. C., Schouten S., Pancost R. D., Meer M. T. J. van der and Damsté J. S. S. (2000) Analysis of intact tetraether lipids in archaeal cell material and sediments by high performance liquid chromatography/atmospheric pressure chemical ionization mass spectrometry. *Rapid Commun. Mass Spectrom.* **14**, 585–589.
- Huang D., Zhu P., Wang Z. and Yu X. (1998) A study and question on the decomposition rate of organic carbon under upland and submerged soil conditions. *Acta Pedol. Sin.* **35**, 482–492.
- Huang L.-M., Thompson A., Zhang G.-L., Chen L.-M., Han G.-Z. and Gong Z.-T. (2015) The use of chronosequences in studies of paddy soil evolution: A review. *Geoderma* **237–238**, 199–210.
- Huang, Yu-Tuan, Lowe, David J., Churchman, G. Jock, Schipper, Louis A., Cursons, Ray, Zhang, Heng, Chen, Tsan-Yao and Cooper, Alan (2016) DNA adsorption by nanocrystalline allophane spherules and nanoaggregates, and implications for carbon sequestration in Andisols. *Appl. Clay Sci.* **120**, 40–50.
- IUSS Working Group (2006) *World reference base for soil resources: International soil classification system for naming soils and creating legends for soil maps*, FAO, Rome.
- Jahn R. and Asio V. B. (1998) Soils of the tropical forests of Leyte, Philippines I: Weathering, soil characteristics, classification and site qualities. In *A. Schulte, D. Ruhayat (Eds.) Soils of tropical forest ecosystems: Characteristics, ecology and management*, Springer, Berlin, Heidelberg. pp. 29–36.
- Janssen I., Peng X. and Horn R. (2006) Physical soil properties of paddy fields as a function of cultivation history and texture. *Adv. Geoecology* **38**, 446–455.
- Janssen M. and Lennartz B. (2007) Horizontal and vertical water and solute fluxes in paddy rice fields. *Soil Tillage Res.* **94**, 133–141.
- Janssen M. and Lennartz B. (2006) Horizontal and vertical water fluxes in paddy rice fields of subtropical China. *Adv. Geoecology* **38**, 344–354.

- Jongmans A. G., Verburg P., Nieuwenhuysen A. and van Oort F. (1995) Allophane, imogolite, and gibbsite in coatings in a Costa Rican Andisol. *Geoderma* **64**, 327–342.
- Joussein E., Petit S., Churchman J., Theng B., Righi D. and Delvaux B. (2005) Halloysite clay minerals – a review. *Clay Miner.* **40**, 383–426.
- Kaiser K. and Guggenberger G. (2003) Mineral surfaces and soil organic matter. *Eur. J. Soil Sci.* **54**, 219–236.
- Kaiser K. and Guggenberger G. (2007) Sorptive stabilization of organic matter by microporous goethite: sorption into small pores vs. surface complexation. *Eur. J. Soil Sci.* **58**, 45–59.
- Kaiser K. and Guggenberger G. (2000) The role of DOM sorption to mineral surfaces in the preservation of organic matter in soils. *Org. Geochem.* **31**, 711–725.
- Kalbitz K., Kaiser K., Fiedler S., Kölbl A., Amelung W., Bräuer T., Cao Z., Don A., Grootes P., Jahn R., Schwark L., Vogelsang V., Wissing L. and Kögel-Knabner I. (2013) The carbon count of 2000 years of rice cultivation. *Glob. Change Biol.* **19**, 1107–1113.
- Kalbitz K., Solinger S., Park J.-H., Michalzik B. and Matzner E. (2000) Controls on the dynamics of dissolved organic matter in soils: A review. *Soil Sci.* **165**, 277–304.
- Karlsson T. and Persson P. (2012) Complexes with aquatic organic matter suppress hydrolysis and precipitation of Fe(III). *Chem. Geol.* **322–323**, 19–27.
- Kawaguchi K. and Matsuo Y. (1957) Re-investigation on distribution of active and inactive oxides along soil profiles in time series of dry rice fields in polder lands of Kojima basin; Okayama Prefecture, Japan. *J. Soil Sci. Plant Nutr.* **3**, 29–35.
- Kay B. D. (1989) Soil structure and organic carbon - a review. In Lal, R., Kimble, J.M., Follett, R.F., Stewart, B.A. (Ed.) *Soil Processes and the Carbon Cycle*, CRC Press, Boca Raton, FL, pp. 169–197
- Kayler Z. E., Kaiser M., Gessler A., Ellerbrock R. H. and Sommer M. (2011) Application of $\delta^{13}\text{C}$ and $\delta^{15}\text{N}$ isotopic signatures of organic matter fractions sequentially separated from adjacent arable and forest soils to identify carbon stabilization mechanisms. *Biogeosciences* **8**, 2895–2906.
- Keersebilck N. C. and Soeprapto S. (1985) Physical measurements in lowland soils - techniques and standardization. In *Soil Physics and Rice*. International Rice Research Institute, Los Banos, Philippines. pp. 99–111.
- Kirk G. (2004) *The Biogeochemistry of Submerged Soils.*, John Wiley & Sons.
- Kirk G. J. D., Yu T. R. and Choudhury F. A. (1990) Phosphorus chemistry in relation to water regime. In *Phosphorus requirements for sustainable agriculture in Asia and Oceania*. International Rice Research Institute, Manila, Philippines. pp. 211–223.
- Kirkels F. M. S. A., Cerli C., Federherr E., Gao J. and Kalbitz K. (2014) A novel high-temperature combustion based system for stable isotope analysis of dissolved organic carbon in aqueous samples. II: optimization and assessment of analytical performance. *Rapid Commun. Mass Spectrom.* **28**, 2574–2586.
- Kleber M., Eusterhues K., Keiluweit M., Mikutta C., Mikutta R. and Nico P. S. (2015) Mineral-organic associations: Formation, properties, and relevance in soil environments. In D. L. Sparks (Ed.) *Advances in Agronomy*. Academic Press. pp. 1–140.

- Kleber M., Mikutta R., Torn M. S. and Jahn R. (2005) Poorly crystalline mineral phases protect organic matter in acid subsoil horizons. *Eur. J. Soil Sci.* **56**, 717–725.
- Klindworth A., Pruesse E., Schweer T., Peplies J., Quast C., Horn M. and Glöckner F. O. (2013) Evaluation of general 16S ribosomal RNA gene PCR primers for classical and next-generation sequencing-based diversity studies. *Nucleic Acids Res.* **41**, e1.
- Kobayashi Y. and Aomine S. (1967) Mechanism of inhibitory effect of allophane and montmorillonite on some enzymes. *Soil Sci. Plant Nutr.* **13**, 189–194.
- Kögel-Knabner I. (2002) The macromolecular organic composition of plant and microbial residues as inputs to soil organic matter. *Soil Biol. Biochem.* **34**, 139–162.
- Kögel-Knabner I., Amelung W., Cao Z., Fiedler S., Frenzel P., Jahn R., Kalbitz K., Kölbl A. and Schloter M. (2010) Biogeochemistry of paddy soils. *Geoderma* **157**, 1–14.
- Kögel-Knabner I., Guggenberger G., Kleber M., Kandeler E., Kalbitz K., Scheu S., Eusterhues K. and Leinweber P. (2008) Organo-mineral associations in temperate soils: Integrating biology, mineralogy, and organic matter chemistry. *J. Plant Nutr. Soil Sci.* **171**, 61–82.
- Kölbl A., Schad P., Jahn R., Amelung W., Bannert A., Cao Z. H., Fiedler S., Kalbitz K., Lehndorff E., Müller-Niggemann C., Schloter M., Schwark L., Vogelsang V., Wissing L. and Kögel-Knabner I. (2014) Accelerated soil formation due to paddy management on marshlands (Zhejiang Province, China). *Geoderma* **228–229**, 67–89.
- Kukkadapu R. K., Zachara J. M., Fredrickson J. K., Smith S. C., Dohnalkova A. C. and Russell C. K. (2003) Transformation of 2-line ferrihydrite to 6-line ferrihydrite under oxic and anoxic conditions. *Am. Mineral.* **88**, 1903–1914.
- Kyuma K. (2004) *Paddy soil science*. Kyoto University and Trans Pacific Press, Kyoto and Melbourne.
- Kyuma K. and Kawaguchi K. (1966) Major soils of Southeast Asia and the classification of soils under rice cultivation (Paddy soils). *Tonan Ajia Kenkyu Southeast Asian Stud.* **4**, 290–312.
- Lalonde A. E., Rancourt D. G. and Ping J. Y. (1998) Accuracy of ferric/ferrous determinations in micas: A comparison of Mössbauer spectroscopy and the Pratt and Wilson wet-chemical methods. *Hyperfine Interact.* **117**, 175–204.
- Lalonde K., Mucci A., Ouellet A. and Gélinas Y. (2012) Preservation of organic matter in sediments promoted by iron. *Nature* **483**, 198–200.
- Lamirato C., Miltner A., Wick L. Y. and Kästner M. (2010) Hydrolysis of cellobiose by β -glucosidase in the presence of soil minerals – Interactions at solid–liquid interfaces and effects on enzyme activity levels. *Soil Biol. Biochem.* **42**, 2203–2210.
- Lehmann J. and Kleber M. (2015) The contentious nature of soil organic matter. *Nature* **528**, 60–68.
- Levard C., Doelsch E., Basile-Doelsch I., Abidin Z., Miche H., Masion A., Rose J., Borschneck D. and Bottero J.-Y. (2012) Structure and distribution of allophanes, imogolite and proto-imogolite in volcanic soils. *Geoderma* **183–184**, 100–108.
- Li Z., Velde B. and Li D. (2003) Loss of K-bearing clay minerals in flood-irrigated, rice-growing soils in Jiangxi Province, China. *Clay Clay Miner.* **51**, 75–82.

- Lovley D. R., Holmes D. E. and Nevin K. P. (2004) Dissimilatory Fe(III) and Mn(IV) reduction. *Advances in Microbial Physiology* **49**, 219–286.
- Lovley D. R. and Phillips E. J. P. (1988) Novel mode of microbial energy metabolism: Organic carbon oxidation coupled to dissimilatory reduction of iron or manganese. *Appl. Environ. Microbiol.* **54**, 1472–1480.
- Lozupone C. and Knight R. (2005) UniFrac: A new phylogenetic method for comparing microbial communities. *Appl. Environ. Microbiol.* **71**, 8228–8235.
- Lützw M. v, Kögel-Knabner I, Ekschmitt K., Matzner E., Guggenberger G., Marschner B. and Flessa H. (2006) Stabilization of organic matter in temperate soils: Mechanisms and their relevance under different soil conditions – A review. *Eur. J. Soil Sci.* **57**, 426–445.
- Malucelli F., Terribile F. and Colombo C. (1999) Mineralogy, micromorphology and chemical analysis of Andosols on the Island of São Miguel (Azores). *Geoderma* **88**, 73–98.
- Mansfeldt T., Schuth S., Häusler W., Wagner F. E., Kaufhold S. and Overesch M. (2012) Iron oxide mineralogy and stable iron isotope composition in a Gleysol with petroglycic properties. *J. Soils Sediments* **12**, 97–114.
- Maréchal Y. (2007) *The hydrogen bond and the water molecule.*, Elsevier, Amsterdam.
- Marschner B., Brodowski S., Dreves A., Gleixner G., Gude A., Grootes P. M., Hamer U., Heim A., Jandl G., Ji R., Kaiser K., Kalbitz K., Kramer C., Leinweber P., Rethemeyer J., Schäffer A., Schmidt M. W. I., Schwark L. and Wiesenberg G. L. B. (2008) How relevant is recalcitrance for the stabilization of organic matter in soils? *J. Plant Nutr. Soil Sci.* **171**, 91–110.
- Matus F., Rumpel C., Neculman R., Panichini M. and Mora M. L. (2014) Soil carbon storage and stabilisation in andic soils: A review. *Catena* **120**, 102–110.
- Mayer L. M. (1994) Relationships between mineral surfaces and organic carbon concentrations in soils and sediments. *Chem. Geol.* **114**, 347–363.
- McDonald D., Price M. N., Goodrich J., Nawrocki E. P., DeSantis T. Z., Probst A., Andersen G. L., Knight R. and Hugenholtz P. (2012) An improved greengenes taxonomy with explicit ranks for ecological and evolutionary analyses of bacteria and archaea. *ISME J.* **6**, 610–618.
- McGeehan S. L., Fendorf S. E. and Naylor D. V. (1998) Alteration of arsenic sorption in flooded-dried soils. *Soil Sci. Soc. Am. J.* **62**, 828–833.
- McKenzie R. M. (1980) The adsorption of lead and other heavy metals on oxides of manganese and iron. *Soil Res.* **18**, 61–73.
- Mehra O. P. and Jackson M. L. (1960) Iron oxide removal from soils and clays by a dithionite citrate system buffered with sodium bicarbonate. *Clay Clay Miner.* **7**, 317–327.
- Mejia J., Roden E. E. and Ginder-Vogel M. (2016) Influence of oxygen and nitrate on Fe (hydr)oxide mineral transformation and soil microbial communities during redox cycling. *Environ. Sci. Technol.* **50**, 3580–3588.
- Mikutta C., Mikutta R., Bonneville S., Wagner F., Voegelin A., Christl I. and Kretzschmar R. (2008) Synthetic coprecipitates of exopolysaccharides and ferrihydrite. Part I: Characterization. *Geochim. Cosmochim. Acta* **72**, 1111–1127.

- Mikutta R. and Kaiser K. (2011) Organic matter bound to mineral surfaces: Resistance to chemical and biological oxidation. *Soil Biol. Biochem.* **43**, 1738–1741.
- Mikutta R., Lorenz D., Guggenberger G., Haumaier L. and Freund A. (2014) Properties and reactivity of Fe-organic matter associations formed by coprecipitation versus adsorption: Clues from arsenate batch adsorption. *Geochim. Cosmochim. Acta* **144**, 258–276.
- Mikutta R., Mikutta C., Kalbitz K., Scheel T., Kaiser K. and Jahn R. (2007) Biodegradation of forest floor organic matter bound to minerals via different binding mechanisms. *Geochim. Cosmochim. Acta* **71**, 2569–2590.
- Miller A. J., Schuur E. A. G. and Chadwick O. A. (2001) Redox control of phosphorus pools in Hawaiian montane forest soils. *Geoderma* **102**, 219–237.
- Mizota C., Carrasco M. A. and Wada K. (1982) Clay mineralogy and some chemical properties of Ap horizons of Ando soils used for paddy rice in Japan. *Geoderma* **27**, 225–237.
- Moore D. M. and Reynolds R. C. (1997) *X-ray diffraction and the identification and analysis of clay minerals.*, Oxford University Press, New York.
- Moormann F. R. and van Breemen N. (1978) *Rice: Soil, Water, Land.*, Int. Rice Res. Inst.
- Mueller-Niggemann C., Utami S. R., Marxen A., Mangelsdorf K., Bauersachs T. and Schwark L. (2016) Distribution of tetraether lipids in agricultural soils – differentiation between paddy and upland management. *Biogeosciences* **13**, 1647–1666.
- Munch J. C., Hillebrand T. and Ottow J. C. G. (1978) Transformations in the Fe_o/Fe_d ratio of pedogenic iron oxides affected by iron-reducing bacteria. *Can. J. Soil Sci.* **58**, 475–486.
- Murad E. and Cashion J. (2004) Iron Oxides. In *Mössbauer spectroscopy of environmental materials and their industrial utilization*, Kluwer Academic, New York, 159–188.
- Murad E. and Schwertmann U. (1983) The influence of aluminium substitution and crystallinity on the Moessbauer spectra of goethite. *Clay Miner.* **18**, 301–312.
- Murase J. and Frenzel P. (2007) A methane-driven microbial food web in a wetland rice soil. *Environ. Microbiol.* **9**, 3025–3034.
- Ndayiragije S. and Delvaux B. (2003) Coexistence of allophane, gibbsite, kaolinite and hydroxy-Al-interlayered 2:1 clay minerals in a perudic Andosol. *Geoderma* **117**, 203–214.
- Neue H. U., Gaunt J. L., Wang Z. P., Becker-Heidmann P. and Quijano C. (1997) Carbon in tropical wetlands. *Geoderma* **79**, 163–185.
- Neue H. U. and Scharpenseel H. W. (1987) Decomposition pattern of ¹⁴C-labeled rice straw in aerobic and submerged rice soils of the Philippines. *Sci. Total Environ.* **62**, 431–434.
- Oades J. M. (1984) Soil organic matter and structural stability: mechanisms and implications for management. *Plant Soil* **76**, 319–337.
- Oades J. M. (1988) The retention of organic matter in soils. *Biogeochemistry* **5**, 35–70.
- Oades J. M. (1993) The role of biology in the formation, stabilization and degradation of soil structure. In *L. Brussaard and M.J. Kooistra (Eds.), Int. Workshop on Methods of Research*

- on *Soil Structure/Soil Biota Interrelationships. Geoderma*, 56. Elsevier, Amsterdam. pp. 377–400.
- Okazaki M., Wada H. and Takai Y. (1981) Reducing organic substances responsible for removal of Fe(III) and Mn(IV) from subsurface horizon of lowland rice soil. In *Institute Soil Sci., Acad. Sinica (Ed.) Proceedings of Symposium on Paddy Soils*. Springer Verlag, Berlin. pp. 235–250.
- Olk D. C., Cassman K. G., Randall E. W., Kinchesh P., Sanger L. J. and Anderson J. M. (1996) Changes in chemical properties of organic matter with intensified rice cropping in tropical lowland soil. *Eur. J. Soil Sci.* **47**, 293–303.
- Ottow J. C. G. (1981) Mechanisms of bacterial iron-reduction in flooded soils. In *Institute Soil Sci., Acad. Sinica (Ed.) Proceedings of Symposium on Paddy Soils*. Springer Verlag, Berlin. pp. 330–343.
- Ottow J. C. G. (2011) *Mikrobiologie von Böden.*, Springer, Berlin Heidelberg.
- Ouyang Y. and Li X. (2013) Recent research progress on soil microbial responses to drying–rewetting cycles. *Acta Ecol. Sin.* **33**, 1–6.
- Pan G., Li L., Wu L. and Zhang X. (2003) Storage and sequestration potential of topsoil organic carbon in China's paddy soils. *Glob. Change Biol.* **10**, 79–92.
- Pan Y., Koopmans G. F., Bonten L. T. C., Song J., Luo Y., Temminghoff E. J. M. and Comans R. N. J. (2014) Influence of pH on the redox chemistry of metal (hydr)oxides and organic matter in paddy soils. *J. Soils Sediments* **14**, 1713–1726.
- Parfitt R. L., Fraser A. R. and Farmer V. C. (1977) Adsorption on hydrous oxides. III. Fulvic acid and humic acid on goethite, gibbsite and imogolite. *J. Soil Sci.* **28**, 289–296.
- Parfitt R. L., Russell M. and Orbell G. E. (1983) Weathering sequence of soils from volcanic ash involving allophane and halloysite, New Zealand. *Geoderma* **29**, 41–57.
- Parfitt R. L. and Saigusa M. (1985) Allophane and humus-aluminium in Spodosols and Andepts formed from the same volcanic ash beds in New Zealand. *Soil Sci.* **139**, 149.
- Parfitt R. L., Saigusa M. and Cowie J. D. (1984) Allophane and halloysite formation in a volcanic ash bed under different moisture conditions. *Soil Sci.* **138**, 360.
- Parfitt R. L. and Wilson A. D. (1985) Estimation of allophane and halloysite in three sequences of volcanic soils, New Zealand. In *E. F. Caldas and D. H. Yaalon (Eds.) Volcanic Soils*. Catena Supplement. Catena Verlag, Cremlingen, Germany. pp. 1–8.
- Patrick Jr. W. H. (1981) The role of inorganic redox systems in controlling reduction in paddy soils. In *Institute Soil Sci., Acad. Sinica (Ed.) Proceedings of symposium on paddy soils*. Springer Verlag, Berlin. pp. 107–117.
- Patrick W. H. and Jugsujinda A. (1992) Sequential reduction and oxidation of inorganic nitrogen, manganese, and iron in flooded soil. *Soil Sci. Soc. Am. J.* **56**, 1071–1073.
- Pedersen H. D., Postma D., Jakobsen R. and Larsen O. (2005) Fast transformation of iron oxyhydroxides by the catalytic action of aqueous Fe(II). *Geochim. Cosmochim. Acta* **69**, 3967–3977.

- Peters V. and Conrad R. (1996) Sequential reduction processes and initiation of CH₄ production upon flooding of oxic upland soils. *Soil Biol. Biochem.* **28**, 371–382.
- Pett-Ridge J. and Firestone M. K. (2005) Redox fluctuation structures microbial communities in a wet tropical soil. *Appl. Environ. Microbiol.* **71**, 6998–7007.
- Piccolo A. (2001) The supramolecular structure of humic substances. *Soil Sci.* **166**, 810–832.
- Piccolo A., Nardi S. and Concheri G. (1996) Macromolecular changes of humic substances induced by interaction with organic acids. *Eur. J. Soil Sci.* **47**, 319–328.
- Poggenburg C., Mikutta R., Schippers A., Dohrmann R. and Guggenberger G. (2018) Impact of natural organic matter coatings on the microbial reduction of iron oxides. *Geochim. Cosmochim. Acta* **224**, 223–248.
- Ponnamperuma F. N. (1972) The chemistry of submerged soils. *Adv. Agron.* **24**, 29–96.
- Postma D. (1993) The reactivity of iron oxides in sediments: A kinetic approach. *Geochim. Cosmochim. Acta* **57**, 5027–5034.
- Rancourt D. G. (1998) Mössbauer spectroscopy in clay science. *Hyperfine Interact.* **117**, 3–38.
- Rancourt D. G. and Ping J. Y. (1991) Voigt-based methods for arbitrary-shape static hyperfine parameter distributions in Mössbauer spectroscopy. *Nucl. Instrum. Methods Phys. Res. Sect. B Beam Interact. Mater. At.* **58**, 85–97.
- Ranjard L., Richaume A., Jocteur-Monrozier L. and Nazaret S. (1997) Response of soil bacteria to Hg(II) in relation to soil characteristics and cell location. *FEMS Microbiol. Ecol.* **24**, 321–331.
- Ratering S. and Schnell S. (2000) Localization of iron-reducing activity in paddy soil by profile studies. *Biogeochemistry* **48**, 341–365.
- Reddy K. R. and Patrick W. H. (1983) Effects of aeration on reactivity and mobility of soil constituents. In *D.W. Nelson (Ed.) Chemical Mobility and Reactivity in Soil Systems* Madison, WI, USA. pp. 11–33.
- Rideout J. R., He Y., Navas-Molina J. A., Walters W. A., Ursell L. K., Gibbons S. M., Chase J., McDonald D., Gonzalez A., Robbins-Pianka A., Clemente J. C., Gilbert J. A., Huse S. M., Zhou H.-W., Knight R. and Caporaso J. G. (2014) Subsampled open-reference clustering creates consistent, comprehensive OTU definitions and scales to billions of sequences. *PeerJ* **2**, e545.
- Roden E. E. (2003) Fe(III) oxide reactivity toward biological versus chemical reduction. *Environ. Sci. Technol.* **37**, 1319–1324.
- Roden E. E. and Zachara J. M. (1996) Microbial reduction of crystalline iron(III) oxides: Influence of oxide surface area and potential for cell growth. *Environ. Sci. Technol.* **30**, 1618–1628.
- Roth C. B., Jackson M. L. and Syers J. K. (1969) Deferration effect on structural ferrous-ferric iron ratio and CEC of vermiculites and soils. *Clays Clay Miner.* **17**, 253–264.
- Roth P. J., Lehdorff E., Cao Z. h, Zhuang S., Bannert A., Wissing L., Schloter M., Kögel-Knabner I. and Amelung W. (2011) Accumulation of nitrogen and microbial residues during 2000 years of rice paddy and non-paddy soil development in the Yangtze river delta, China. *Glob. Change Biol.* **17**, 3405–3417.

- Sahrawat D. K. L. (2004) Terminal electron acceptors for controlling methane emissions from submerged rice soils. *Commun. Soil Sci. Plant Anal.* **35**, 1401–1413.
- Sahrawat K. L. (2005) Fertility and organic matter in submerged rice soils. *Curr. Sci.* **88**, 735–739.
- Sahrawat K. L. (1998) Flooding soil: a great equalizer of diversity in soil chemical fertility. *Oryza* **35**, 300–305.
- Sahrawat K. L. (2004) Organic matter accumulation in submerged soils. *Adv. Agron.* **81**, 169–201.
- Said-Pullicino D., Miniotti E. F., Sodano M., Bertora C., Lerda C., Chiaradia E. A., Romani M., Maria S. C. de, Sacco D. and Celi L. (2016) Linking dissolved organic carbon cycling to organic carbon fluxes in rice paddies under different water management practices. *Plant Soil* **401**, 273–290.
- Saidy A. R., Smernik R. J., Baldock J. A., Kaiser K., Sanderman J. and Macdonald L. M. (2012) Effects of clay mineralogy and hydrous iron oxides on labile organic carbon stabilisation. *Geoderma* **173–174**, 104–110.
- Schmieder R. and Edwards R. (2011) Fast identification and removal of sequence contamination from genomic and metagenomic datasets. *PLoS ONE* **6**, e17288.
- Schöler A., Jacquiod S., Vestergaard G., Schulz S. and Schloter M. (2017) Analysis of soil microbial communities based on amplicon sequencing of marker genes. *Biol. Fertil. Soils* **53**, 485–489.
- Schouten S., Hugué C., Hopmans E. C., Kienhuis M. V. M. and Sinninghe Damsté J. S. (2007) Analytical methodology for TEX86 paleothermometry by high-performance liquid chromatography/atmospheric pressure chemical ionization-mass spectrometry. *Anal. Chem.* **79**, 2940–2944.
- Schubert M., Lindgreen S. and Orlando L. (2016) AdapterRemoval v2: rapid adapter trimming, identification, and read merging. *BMC Res. Notes* **9**, 88.
- Schulten H.-R. and Leinweber P. (2000) New insights into organic-mineral particles: composition, properties and models of molecular structure. *Biol. Fertil. Soils* **30**, 399–432.
- Schwertmann U. (1964) Differenzierung der Eisenoxide des Bodens durch Extraktion mit Ammoniumoxalat-Lösung. *Z. für Pflanzenernähr. Düng. Bodenkd.* **105**, 194–202.
- Schwertmann U., Friedl J. and Kyek A. (2004) Formation and properties of a continuous crystallinity series of synthetic ferrihydrites (2- to 6-line) and their relation to FeOOH forms. *Clays Clay Miner.* **52**, 221–226.
- Schwertmann U., Wagner F. and Knicker H. (2005) Ferrihydrite–humic associations. *Soil Sci. Soc. Am. J.* **69**, 1009–1015.
- Seyfferth A. L., Kocar B. D., Lee J. A. and Fendorf S. (2013) Seasonal dynamics of dissolved silicon in a rice cropping system after straw incorporation. *Geochim. Cosmochim. Acta* **123**, 120–133.
- Sharma P. K. and De Datta S. K. (1985) Effects of puddling on soil physical properties and processes. In *Soil Physics and Rice*. International Rice Research Institute, Los Banos, Philippines. pp. 217–234.

- Sharma P. K. and De Datta S. K. (1986) Physical properties and processes of puddled rice soils. In *B.A. Stewart (Ed.) Advances in Soil Science*. Springer New York. pp. 139–178.
- Shoji S. and Fujiwara Y. (1984) Active aluminium and iron in the humus horizons of Andosols from northeastern Japan: their forms, properties, and significance in clay weathering. *Soil Sci.* **137**, 216.
- Shoji S., Fujiwara Y., Yamada I. and Saigusa M. (1982) Chemistry and clay mineralogy of Ando soils, brown forest soils, and podzolic soils formed from recent Towada ashes, northeastern Japan. *Soil Sci.* **133**, 69.
- Singh M., Sarkar B., Sarkar S., Churchman J., Bolan N., Mandal S., Menon M., Purakayastha T. J. and Beerling D. J. (2018) Chapter Two - Stabilization of soil organic carbon as influenced by clay mineralogy. In *D. L. Sparks (Ed.) Advances in Agronomy*. Academic Press. pp. 33–84.
- Six J., Elliott E. T. and Paustian K. (2000) Soil macroaggregate turnover and microaggregate formation: a mechanism for C sequestration under no-tillage agriculture. *Soil Biol. Biochem.* **32**, 2099–2103.
- Sørensen L. H. (1972) Stabilization of newly formed amino acid metabolites in soil by clay minerals. *Soil Sci.* **114**, 5–11.
- Steeffel C. I. and Van Cappellen P. (1990) A new kinetic approach to modeling water-rock interaction: The role of nucleation, precursors, and Ostwald ripening. *Geochim. Cosmochim. Acta* **54**, 2657–2677.
- Stewart B. D., Nico P. S. and Fendorf S. (2009) Stability of uranium incorporated into Fe (hydr)oxides under fluctuating redox conditions. *Environ. Sci. Technol.* **43**, 4922–4927.
- Stookey L. L. (1970) Ferrozine---a new spectrophotometric reagent for iron. *Anal. Chem.* **42**, 779–781.
- Takai Y. and Kamura T. (1966) The mechanism of reduction in waterlogged paddy soil. *Folia Microbiol. (Praha)* **11**, 304–313.
- Takeda I. and Fukushima A. (2004) Phosphorus purification in a paddy field watershed using a circular irrigation system and the role of iron compounds. *Water Res.* **38**, 4065–4074.
- Tan K. H. (2008) *Soils in the humid tropics and monsoon region of Indonesia.*, CRC Press, Boca Raton, FL, USA.
- Tan K. H. (1968) The genesis and characteristics of paddy soils in Indonesia. *Soil Sci. Plant Nutr.* **14**, 117–121.
- Tange O. (2011) GNU Parallel: The command-line power tool. *USENIX Mag.* **36**, 42–47.
- Team R. C. (2008) A language and environment for statistical computing. In *R foundation for statistical computing* <https://www.R-project.org>.
- Teh Y. A., Dubinsky E. A., Silver W. L. and Carlson C. M. (2008) Suppression of methanogenesis by dissimilatory Fe(III)-reducing bacteria in tropical rain forest soils: Implications for ecosystem methane flux. *Glob. Change Biol.*, 413–422.
- Thompson A., Chadwick O. A., Rancourt D. G. and Chorover J. (2006) Iron-oxide crystallinity increases during soil redox oscillations. *Geochim. Cosmochim. Acta* **70**, 1710–1727.

- Thompson A., Rancourt D. G., Chadwick O. A. and Chorover J. (2011) Iron solid-phase differentiation along a redox gradient in basaltic soils. *Geochim. Cosmochim. Acta* **75**, 119–133.
- Tian-ren Y. (1985) *Physical chemistry of paddy soils.*, Science Press, Beijing, and Springer Verlag, Berlin, Heidelberg, New York, Tokyo.
- Tomaszewski E. J., Cronk S. S., Gorski C. A. and Ginder-Vogel M. (2016) The role of dissolved Fe(II) concentration in the mineralogical evolution of Fe (hydr)oxides during redox cycling. *Chem. Geol.* **438**, 163–170.
- Torn M. S., Trumbore S. E., Chadwick O. A., Vitousek P. M. and Hendricks D. M. (1997) Mineral control of soil organic carbon storage and turnover. *Nature* **389**, 170–173.
- Totsche K. U., Amelung W., Gerzabek M. H., Guggenberger G., Klumpp E., Knief C., Lehndorff E., Mikutta R., Peth S., Prechtel A., Ray N. and Kögel-Knabner I. (2018) Microaggregates in soils. *J. Plant Nutr. Soil Sci.* **181**, 104–136.
- Urbanski L., Kölbl A., Lehndorff E., Houtermans M., Schad P., Zhang G.-L., Utami S. R. and Kögel-Knabner I. (2017) Paddy management on different soil types does not promote lignin accumulation. *J. Plant Nutr. Soil Sci.* **180**, 366–380.
- Van Breemen N. (1988) Long-term chemical, mineralogical, and morphological effects of iron-redox processes in periodically flooded soils. In *J. W. Stucki, B. A. Goodman, and U. Schwertmann(Eds.) Iron in soils and clay minerals*. NATO ASI series. D. Reidel Publishing Co., Boston, MA, USA. pp. 811–823.
- Van Breemen N. and Buurman P. (2002) *Soil formation*. 2nd ed., Kluwer Academic Publishers, Dordrecht, Boston, London.
- Van Ranst E. and De Coninck F. (2002) Evaluation of ferrollysis in soil formation. *Eur. J. Soil Sci.* **53**, 513–520.
- Violante P. and Wilson M. J. (1983) Mineralogy of some Italian Andosols with special reference to the origin of the clay fraction. *Geoderma* **29**, 157–174.
- Vitousek P. M., Chadwick O. A., Crews T. E., Fownes J. H., Hendricks D. M. and Herbert D. (1997) Soil and ecosystem development across the Hawaiian islands. *GSA Today* **7**, 1–8.
- Vogelsang V., Fiedler S., Jahn R. and Kaiser K. (2016a) In-situ transformation of iron-bearing minerals in marshland-derived paddy subsoil. *Eur. J. Soil Sci.* **67**, 676–685.
- Vogelsang V., Kaiser K., Wagner F. E., Jahn R. and Fiedler S. (2016b) Transformation of clay-sized minerals in soils exposed to prolonged regular alternation of redox conditions. *Geoderma* **278**, 40–48.
- Wada K. and Wada S.-I. (1976) Clay mineralogy of the B horizons of two hydrandepts, a Torrox and a Humitropept in Hawaii. *Geoderma* **16**, 139–157.
- Wagai R. and Mayer L. M. (2007) Sorptive stabilization of organic matter in soils by hydrous iron oxides. *Geochim. Cosmochim. Acta* **71**, 25–35.
- Wakatsuki T., Ishikawa I., Araki S. and Kyuma K. (1984) Changes in clay mineralogy in a chronosequence of polder paddy soils from Kojima basin, Japan. *Soil Sci. Plant Nutr.* **30**, 25–38.

- Wang H. D., White G. N., Dixon J. B. and Turner F. T. (1993) Ferrihydrite, lepidocrocite, and goethite in coatings from east Texas vertic soils. *Soil Sci. Soc. Am. J.* **57**, 1381–1386.
- Wang Q., Garrity G. M., Tiedje J. M. and Cole J. R. (2007) Naïve Bayesian Classifier for rapid assignment of rRNA sequences into the new bacterial taxonomy. *Appl. Environ. Microbiol.* **73**, 5261–5267.
- Weber K. A., Urrutia M. M., Churchill P. F., Kukkadapu R. K. and Roden E. E. (2006) Anaerobic redox cycling of iron by freshwater sediment microorganisms. *Environ. Microbiol.* **8**, 100–113.
- Wickham H. (2009) Elegant graphics for data analysis. In *ggplot2. Use R Use R*. Springer, New York.
- Willett I. R. and Higgins M. L. (1978) Phosphate sorption by reduced and reoxidized rice soils. *Aust. J. Soil Res.* **16**, 319–326.
- Winkler P., Kaiser K., Kölbl A., Kühn T., Schad P., Urbanski L., Fiedler S., Lehndorff E., Kalbitz K., Utami S. R., Cao Z., Zhang G., Jahn R. and Kögel-Knabner I. (2016) Response of Vertisols, Andosols, and Alisols to paddy management. *Geoderma* **261**, 23–35.
- Winkler P., Kaiser K., Thompson A., Kalbitz K., Fiedler S. and Jahn R. (2018) Contrasting evolution of iron phase composition in soils exposed to redox fluctuations. *Geochim. Cosmochim. Acta* **235**, 89–102.
- Wissing L., Kölbl A., Häusler W., Schad P., Cao Z.-H. and Kögel-Knabner I. (2013) Management-induced organic carbon accumulation in paddy soils: The role of organo-mineral associations. *Soil Tillage Res.* **126**, 60–71.
- Wissing L., Kölbl A., Vogelsang V., Fu J.-R., Cao Z.-H. and Kögel-Knabner I. (2011) Organic carbon accumulation in a 2000-year chronosequence of paddy soil evolution. *Catena* **87**, 376–385.
- Yan J., Pan G., Li L., Quan G., Ding C. and Luo A. (2010) Adsorption, immobilization, and activity of β -glucosidase on different soil colloids. *J. Colloid Interface Sci.* **348**, 565–570.
- Yan X., Ohara T. and Akimoto H. (2003) Development of region-specific emission factors and estimation of methane emission from rice fields in the East, Southeast and South Asian countries. *Glob. Change Biol.* **9**, 237–254.
- Yan X., Zhou H., Zhu Q. H., Wang X. F., Zhang Y. Z., Yu X. C. and Peng X. (2013) Carbon sequestration efficiency in paddy soil and upland soil under long-term fertilization in southern China. *Soil Tillage Res.* **130**, 42–51.
- Yang L., Steefel C. I., Marcus M. A. and Bargar J. R. (2010) Kinetics of Fe(II)-catalyzed transformation of 6-line ferrihydrite under anaerobic flow conditions. *Environ. Sci. Technol.* **44**, 5469–5475.
- Ye C., Hall S. J. and Hu S. (2019) Controls on mineral-associated organic matter formation in a degraded Oxisol. *Geoderma* **338**, 383–392.
- Ye R., Doane T. A. and Horwath W. R. (2016) Comparison of isotope methods for partitioning methane production and soil C priming effects during anaerobic decomposition of rice residue in soil. *Soil Biol. Biochem.* **95**, 51–59.
- Yu T. R. (1985) *Physical chemistry of paddy soils*. Springer Verlag, Beijing-New York.

- Yuan G., Soma M., Seyama H., Theng B. K. G., Lavkulich L. M. and Takamatsu T. (1998) Assessing the surface composition of soil particles from some Podzolic soils by X-ray photoelectron spectroscopy. *Geoderma* **86**, 169–181.
- Yuan Q., Pump J. and Conrad R. (2012) Partitioning of CH₄ and CO₂ production originating from rice straw, soil and root organic carbon in rice microcosms. *PLOS ONE* **7**, e49073.
- Zeikus J. G., Wellstein A. L. and Kirk T. K. (1982) Molecular basis for the biodegradative recalcitrance of lignin in anaerobic environments. *FEMS Microbiol. Lett.* **15**, 193–197.
- Zhang G.-L. and Gong Z.-T. (2003) Pedogenic evolution of paddy soils in different soil landscapes. *Geoderma* **115**, 15–29.
- Zhang M. and He Z. (2004) Long-term changes in organic carbon and nutrients of an Ultisol under rice cropping in southeast China. *Geoderma* **118**, 167–179.
- Zhang P., Zheng J., Pan G., Zhang X., Li L. and Rolf T. (2007) Changes in microbial community structure and function within particle size fractions of a paddy soil under different long-term fertilization treatments from the Tai Lake region, China. *Colloids Surf. B Biointerfaces* **58**, 264–270.
- Zhao Q., Adhikari D., Huang R., Patel A., Wang X., Tang Y., Obrist D., Roden E. E. and Yang Y. (2017) Coupled dynamics of iron and iron-bound organic carbon in forest soils during anaerobic reduction. *Chem. Geol.* **464**, 118–126.
- Ziegler F., Kögel I. and Zech W. (1986) Alteration of gymnosperm and angiosperm lignin during decomposition in forest humus layers. *Z. für Pflanzenernähr. Bodenkd.* **149**, 323–331.

List of Abbreviations

(Ac/Al) _v	acid-to-aldehyde ratio of vanillyl units
(Ac/Al) _s	acid-to-aldehyde ratio of syringyl units
Al _{AAO}	acidic ammonium-oxalate-extractable aluminum
ANOVA	analysis of variance
a-o (+)	oscillation of anoxic and oxic conditions with straw addition
a-o (-)	oscillation of anoxic and oxic conditions without straw addition
a.s.l.	above sea level
BD	bulk density
BS	base saturation
CEC	cation exchange capacity
CEC _{pot}	potential cation exchange capacity
DOC	dissolved organic carbon
DOM	dissolved organic matter
Eh	redox potential
Fe ^{III}	ferric iron
Fe ^{II}	ferrous iron
Fe ²⁺	aqueous ferrous iron
Fe _{AAO}	acidic ammonium-oxalate-extractable iron
Fe _c	crystalline iron oxides
Fe _{DCB}	dithionite–citrate–bicarbonate-extractable iron
Fe _{total}	total iron concentrations
FID	flame ionization detector
FPOM	free particulate organic matter
GC	gas chromatograph
GM/AX	(galactose + mannose)/(arabinose + xylose)
HPLC	high pressure liquid chromatography
IC	inorganic carbon concentrations
ICP-OES	inductively coupled plasma – optical emission spectrometry
iGDGTs	isoprenoid glycerol dialkyl glycerol tetraethers
IRMS	isotope ratio mass spectrometer
MOM	mineral-associated organic matter
MS	mass spectrometry
NP	non-paddy

List of Abbreviations

o (+)	static oxic conditions with straw addition
o (-)	static oxic conditions without straw addition
OC	organic carbon
OM	organic matter
OPOM	occluded particulate organic matter
OTUs	operational taxonomic units
OxHy	(oxy-)hydroxide
P	paddy
PCoA	principal coordinate analysis
Si _{AAO}	acidic ammonium-oxalate-extractable silicon
SOC	soil organic carbon
SRO	short-range-ordered
SSA	specific surface area
TC	total carbon concentrations
TOC	total organic carbon
V-PDB	international standard Vienna Pee Dee belemnite
VSC	lignin-derived phenols
XPS	X-ray photoelectron spectroscopy
XRD	X-ray diffraction
XRF	X-ray fluorescence spectroscopy

Danksagung

Ich danke **Klaus Kaiser**, der mich all die Jahre unterstützt und gefördert hat. Danke Klaus, dass du mir während des Inkubationsexperiments im Labor (auch an Weihnachten und Neujahr) geholfen hast. Auch wenn es lange gedauert hat, bis die einzelnen Manuskripte fertig waren, hast du sie immer schnell gelesen und wichtige Tipps zur Verbesserung gehabt. Außerdem hast du es möglich gemacht hast, dass ich auch nach Ablauf des Doktorandenvertrages in Lohn und Brot stehe. Und danke, dass ich nie ein schlechtes Gewissen haben musste, wenn ich um drei Feierabend gemacht habe, um für meine Kinder da zu sein.

Ich möchte mich auch bei **Karsten Kalbitz** für seine stets ehrlichen und kompetenten Kommentare bedanken. Wenn ich manchmal den Wald vor lauter Bäumen nicht mehr gesehen habe, hast du mich wieder auf die richtige Spur gebracht.

Ein Dank geht an **Reinhold Jahn** und **Sabine Fiedler** für ihre Geduld und Unterstützung. Danke Herr Jahn, dass sie mir damals die Möglichkeit gegeben haben, in ihrer Arbeitsgruppe anzufangen. Danke Sabine, dass du dich dafür eingesetzt hast, dass ich kurzfristig doch noch mit nach Indonesien reisen konnte. Den Forschungsantrag, der meiner Arbeit zugrunde lag, habt ihr gemeinsam mit Klaus und Karsten so gut durchdacht, dass eine erfolgreiche Umsetzung des Projektes möglich war. Danke auch für die schnellen und hilfreichen Korrekturen von Manuskripten und Tagungsbeiträgen.

Ganz herzlich danken möchte ich auch **Angelika Kölbl**. Angelika, du hast mich damals auf die Doktorandenstelle in Halle aufmerksam gemacht und mir somit zu meinem Sechser im Lotto — Doktorandenstelle mit spannendem Thema am Arbeitsort meines damaligen Freundes und heutigen Mannes — verholfen. Du hast nicht nur das Paddy-Projekt super koordiniert, sondern warst auch immer bei Fragen sowie zum Korrekturlesen schnell und präzise für mich da. Danke für die schöne Zeit in Freising während der Probenaufbereitung.

Danken möchte ich zudem **Ingrid Kögel-Knabner** für die Initiierung des Projektes sowie **Sri R. Utami** und **Zihong Cao** für die Organisation der Probenahmen in Indonesien und China. Der Deutschen Forschungsgemeinschaft (DFG) danke ich für die Finanzierung des Projektes.

Danke an **Peter Schad**, **Miriam Houtermans**, **Urs Dieterich** und **Susanne Drechsler** für die teils gemeinsamen Probenahmen in Indonesien und China.

Vielen Dank an **Alexandra Boritzki**, **Christine Krenkewitz**, **Gudrun von Koch**, **Heike Maennicke**, **Chiara Cerli**, **Susanne Horka** und **Gabriele Kummer** für ihre Unterstützung im

Labor sowie für die angenehme Arbeitsatmosphäre. Ich habe mich in allen Laboren stets sehr wohl gefühlt und immer ein offenes Ohr gefunden.

Danke an **Aaron Thompson** für seine Geduld bei der Mössbauer-Auswertung und Interpretation sowie an **Robert Mikutta** für das Interesse an meiner Arbeit, für die XPS-Analysen und für die wertvollen Tipps zu Manuskripten und Tagungsbeiträgen.

Ein großer Dank geht auch an meine Projektpartner und Co-Autoren **Livia Urbanski, Eva Lehndorff, Stefanie Schulz, Michael Schloter, Cornelia Müller-Niggemann, Lorenz Schwark, Susanne Woche** und **Steffen Kümmel** für ihre Unterstützung bei Analysen sowie für das Korrekturlesen der gemeinsamen Manuskripte.

Für die überaus angenehme und humorvolle Arbeitsatmosphäre danke ich meinen Kollegen **Daniela Busch, Thomas Kühn, Thimo** und **Anika Klotzbücher, Ronny Surey, Aleksey Prays** und **Nico Köbernich**. Außerdem möchte ich mich bei **Nadia Prays** für die gemeinsamen Abende und Nächte in der Bibliothek bedanken sowie bei **Marlen Heinz** für das Korrekturlesen der Endfassung dieser Arbeit.

Schließlich danke ich meinem Mann für die faire Aufteilung der Elternzeiten und für seine Begleitung und Kinderbetreuung bei Tagungen. Danke André für die Sonntagnachmittage, die du mit dem Großen im Zoo verbracht hast, wenn ich mal wieder ein Manuskript überarbeiten musste. Vielen Dank an meine **Schwiegereltern** für die Unterstützung mit den Kindern. Ich danke euch sowie **Franzi** und **Bille** für das ausdauernde Interesse an meiner Arbeit. **Mama, Papa, Jule** und **Oma**, ich danke euch, dass ihr immer an mich geglaubt und mich unterstützt habt. Ohne euch hätte ich es nie soweit geschafft!

Appendix

Appendix 1: Fe extraction techniques

Appendix 1.1: Extraction of total pedogenic Fe with dithionite–citrate–bicarbonate solution (Fe_{DCB})

The following method to extract total pedogenic Fe from soils is based on the outline of Mehra and Jackson (1960).

Extractants:

- solid $\text{Na}_2\text{S}_2\text{O}_4$ (Na-dithionite)
- 0.3 M $\text{Na}_3\text{C}_6\text{H}_5\text{O}_7$ (Na-citrate) solution
- 1M NaHCO_3 solution
- 0.05 M MgSO_4 solution

Procedure:

- 2.000 g of air dried soil were weighed into a 100 ml polycarbonate centrifugal tube
- 40 ml of Na-citrate and 10 ml of NaHCO_3 solution were added to the tube
- tube was placed into a water bath at 75-80°C
- when suspension had warmed, 1 g of Na-dithionite was added to react with the soil for 15 minutes while regularly stirred
- suspension was centrifuged for 10 minutes with 2000 rpm
- supernatant was poured over a filter and filtrate was collected in a 100 ml flask
- the procedure was repeated with remaining soil pellet in the centrifugal tube
- remaining pellet was suspended in 20 ml MgSO_4 solution
- suspension was centrifuged for 10 minutes with 2000 rpm
- supernatant was poured over the same filter
- filter was rinsed with distilled water
- flask was filled to 100 ml with distilled water
- Fe content of extracts in flask were measured with ICP-OES

Appendix 1.2: Extraction of pedogenic short-range-ordered Fe with acidic ammonium oxalate at pH 3 (Fe_{AAO})

The following method to extract short-range-ordered pedogenic Fe from soils is based on the outline of Schwertmann (1964).

Extractants:

- solution A: 0.2 M (NH₄)₂C₂O₄*H₂O (NH₄ oxalate)
- solution B: 0.2 M H₂C₂O₄*2H₂O (oxalic acid)
- working solution: 4 parts of solution A and 3 parts of solution B were mixed, pH was checked and solution A or B were added until pH 3.0 was reached

Procedure

- 1.000 g of air dried soil were weighed into a 250 ml centrifugal tube
- 100 ml of working solution were added to the tube
- suspension was shaken in the dark for 2h
- suspension was centrifuged for 5 minutes with 2000 rpm
- supernatant was poured over a filter and filtrate was collected in a 100 ml flask
- Fe content of extracts in flask were measured with ICP-OES

Appendix 2: Supplemental Mössbauer information

Appendix 2.1: Identification of different ⁵⁷Fe Mössbauer components

In Mössbauer spectroscopy, each spectral component corresponds either to one defined Fe-bearing solid phase or to a group of unresolved Fe-bearing solid phases. The most abundant Fe-bearing minerals in soils exhibit spectral components that take the form of a doublet or sextet, depending on their magnetic properties at the given measurement temperature. Fe^{III} oxides and (oxy-)hydroxides (e.g., haematite, goethite, ferrihydrite) order magnetically, and thereby transform from a doublet into a sextet in the Mössbauer spectrum at a characteristic measurement temperature, based on their relative crystallinity.

Well-crystallized haematite and goethite can easily be identified as they form sextets at 295 K that can be distinguished by their width (Murad and Cashion, 2004; Thompson et al., 2011).

Differentiation of nano-goethite and ferrihydrite, which both form similar-width sextets at temperatures <77 K, can be made on the basis of quadrupole splitting (QS) of the sextets, with nano-goethite exhibiting QS values between ~ -0.9 and -0.16 mm s⁻¹ and ferrihydrite exhibiting near zero QS values (-0.3 mm s⁻¹ <QS> 0.3 mm s⁻¹) (Thompson et al., 2011). However, in many natural systems nano-goethite and ferrihydrite are strongly substituted with foreign ions and

co-precipitated with organic matter, yielding a continuum of quadrupole splitting parameters within those respective ranges. Extracting precise proportions of nano-goethite and ferrihydrite thus becomes difficult unless they co-exist in similar abundance. Distinguishing these phases is also likely of little environmental value given that they likely both behave similarly in terms of sorption/desorption or dissolution reaction kinetics. In this work, we refrain from differentiating nano-goethite and ferrihydrite (except when two distinct sites improve the spectral fit), but instead use a subdivision of the respective Fe^{III} (oxy-)hydroxide phases (nano-goethite + ferrihydrite = Fe^{III} OxHy) based on ordering temperature, and hence, crystallinity (Fe^{III} OxHy SRO-1 to SRO-5). Fe oxides of lower crystallinity require lower measurement temperatures to magnetically order (and hence form a sextet) than Fe oxides of higher crystallinity. The ordering temperature of both nano-goethite and ferrihydrite phases is decreased by small particle size, which can be caused by co-precipitation with OM (Mikutta et al., 2008; Eusterhues et al., 2008) as well as by substitution of Fe by Si and Al (Murad and Schwertmann, 1983; Schwertmann et al., 2004; Thompson et al., 2011). The area of the nano-goethite + ferrihydrite sextet increases as the measurement temperature decreases since Fe^{III} oxyhydroxide phases of lower crystallinity – still represented by a doublet at a higher measurement temperature – are added to the respective sextet at the lower measurement temperature. The proportions of SRO Fe^{III} (oxy-)hydroxide phases binning to a certain crystallinity class were calculated by subtracting the area of the respective Fe^{III} (oxy-)hydroxide sextet measured at a higher temperature from the area of the Fe^{III} (oxy-)hydroxide sextet measured at a lower temperature, (e.g., Fe^{III} OxHy SRO-1 = (SRO Fe^{III} OxHy sextet at 140 K) - (SRO Fe^{III} OxHy sextet at 295 K)).

Iron that has not yet ordered at a specific measurement temperature appears as either a collapsed sextet or as part of the Fe^{III} doublet in the Mössbauer spectrum. A collapsed sextet is indicative of Fe^{III} phases near their blocking temperature (i.e., the temperature at which the spectral area of the Fe population is intermediate between a sextet and a doublet). At the lowest measurement temperature (4.2 K in our case), there are sometimes highly disordered phases that remain as a collapsed sextet; these portions of the population represent the least ordered Fe^{III} (oxy-)hydroxide phases, sometimes termed “nano-Fe” (Murad and Cashion, 2004; Thompson et al., 2011).

In addition to paramagnetic Fe^{III} oxides, the Fe^{III} doublet can also contain Fe^{III} in phyllosilicates and/or in Fe^{III}-OM complexes, which remain paramagnetic at all temperatures and therefore never order magnetically because the Fe atoms are too distant from one another to exhibit magnetic coupling (Schwertmann et al., 2005; Thompson et al., 2011). Hence, when all Fe^{III} oxides have ordered into a (collapsed) sextet at 4.2 K, the remaining Fe^{III} doublet represents Fe^{III} in phyllosilicates and/or in Fe-OM complexes.

Ferrous phases form a doublet that is shifted to a higher velocity range than the Fe^{III} doublet. This ferrous doublet represents Fe^{II} in primary minerals, in phyllosilicates and/or adsorbed to organic or mineral surfaces (Thompson et al., 2011). At low temperatures (4.2 K in our case), some ferrous populations can order into a collapsed octet characterized by strong asymmetry, which likely represents Fe^{II} sorbed onto a magnetically ordered Fe^{III} phase.

Appendix 2.2: Additional Mössbauer data

Fig. A-1 and A-2 show additional Mössbauer spectra of the Alisol and Andosol samples. Table A-1 lists the fitting parameters as well as calculated Mössbauer parameters.

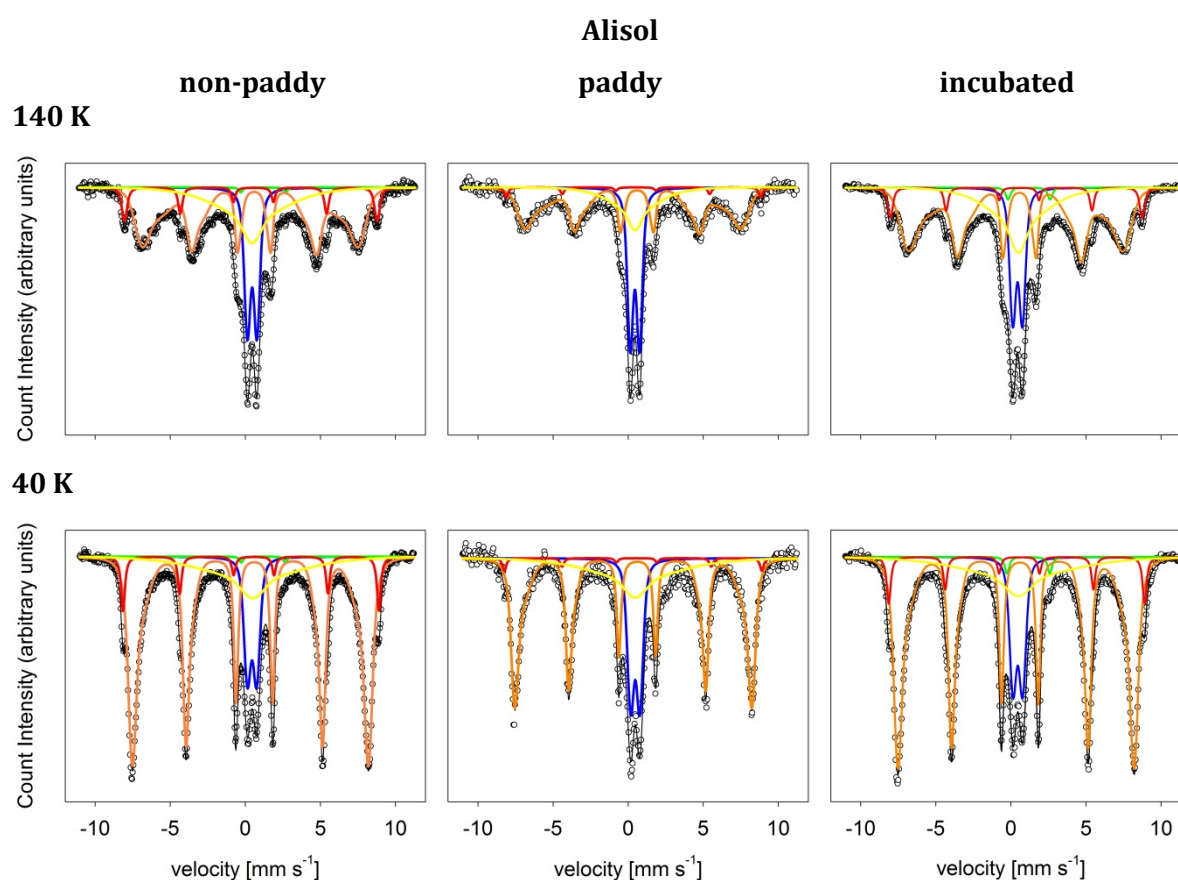


Fig. A-1: Fitted Mössbauer spectra of Alisol topsoils at 140 and 40 K. From the incubation experiment spectra of samples with straw addition are presented. The black solid line is the total calculated fit through the discrete data points (circles). The resolved spectral components and assignments are: (1) Q-Fe^{III}, deep central doublet (blue) = Fe^{III} in silicates and in organic complexes + paramagnetic Fe^{III} (oxy-)hydroxides, (2) Q-Fe^{II}, wider and smaller doublet (green) = Fe^{II} in primary minerals, clays or sorbed, (3) HFD-OxHy-A, dominant sextet (orange) = magnetically ordered Fe^{III} (oxy-)hydroxides, (4) HFD-Hae, wider and smaller sextet (red) = haematite, (5) HFD-OxHy-B, collapsed sextet (yellow) = Fe^{III} (oxy-)hydroxides near their blocking temperature.

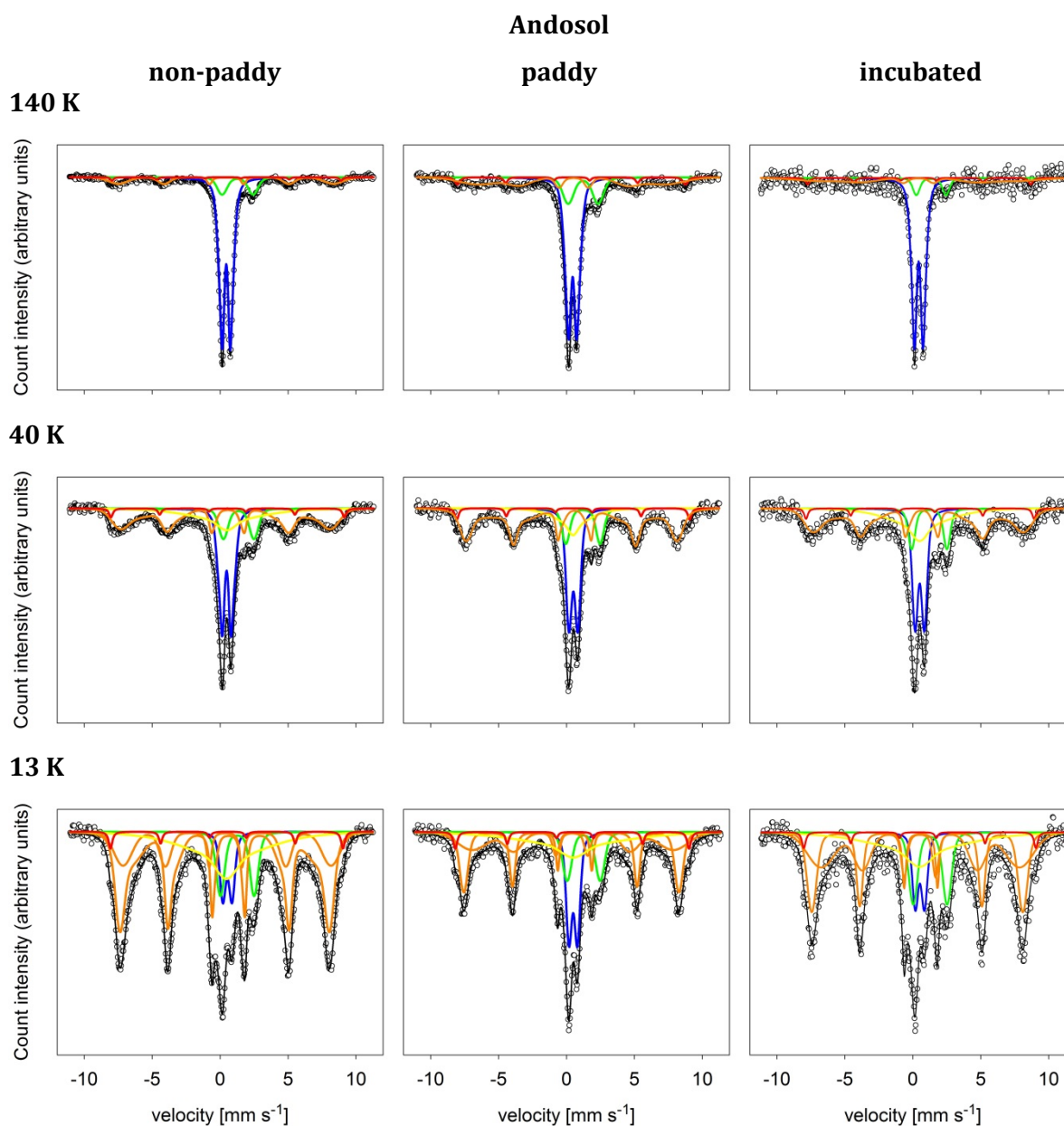


Fig. A-2: Fitted Mössbauer spectra of Andosol topsoils at 140, 40 and 13 K. The black solid line is the total calculated fit through the discrete data points (circles). The resolved spectral components and assignments are: (1) Q-Fe^{III}, deep central doublet (blue) = Fe^{III} in silicates and in organic complexes + paramagnetic Fe^{III} (oxy-)hydroxides, (2) Q-Fe^{II}, wider and smaller doublet (green) = Fe^{II} in clays or sorbed, (3) HFD-OxHy-A, dominant sextet (orange) = magnetically ordered Fe^{III} (oxy-)hydroxides, (4) HFD-Hae, wider and smaller sextet (red) = haematite, (5) HFD-OxHy-B, collapsed sextet (yellow) = Fe^{III} (oxy-)hydroxides near their blocking temperature.

Table A-1: Fitting parameters and calculated Mössbauer parameters

Sample	Phase	Spectral area		δ_0 mm/s	ϵ_0 mm/s	P %	Δ or H mm/s or T	σ mm/s or T	Red- χ^2	$\langle CS \rangle$ mm/s	$\langle \epsilon \rangle$ mm/s	$\langle QS \rangle$ or $\langle H \rangle$ mm/s or T	s.d. mm/s or T
		MC*mm/s	%										
Alisol non-paddy 295K (2Q, 2H) (BG = 1.255 MC/ch)	Q-Fe ^{III}	0.128	64	0.364	n/a	71	0.507	0.120	0.71	0.364	n/a	0.601	0.225
						29	0.830	0.250					
	Q-Fe ^{II}	0.003	1	0.960	n/a	100	0.740	0.080		0.955	n/a	0.739	0.077
	HFD-Hae	0.020	10	0.378	-0.108	100	49.2	1.970		0.378	-0.108	49.2	1.966
	HFD-OxHy-B	0.050	25	0.52*	0*	100	0*	44.6		0.520	0	35.6	26.9
Alisol non-paddy 140K (2Q, 3H) (BG = 1.372 MC/ch)	Q-Fe ^{III}	0.055	18	0.458	n/a	100	0.637	0.273	0.89	0.458	n/a	0.639	0.269
	Q-Fe ^{II}	0.001	<1	1.200	n/a	100	3.000	0.000			1.200	n/a	3.000
	HFD-Hae	0.023	8	0.456	-0.088	100	52.2	0.630		0.456	-0.088	52.2	0.631
	HFD-OxHy-A	0.151	51	0.461	-0.124	43	44.9	2.520		0.461	-0.124	41.2	5.852
						57	38.4	6.100					
	HFD-OxHy-B	0.067	23	0.46*	0*	100	0*	19.3		0.460	0	15.4	11.7
Alisol non-paddy 77K (2Q, 3H) (BG = 1.479 MC/ch)	Q-Fe ^{III}	0.048	16	0.474	n/a	100	0.627	0.286	1.13	0.474	n/a	0.630	0.279
	Q-Fe ^{II}	0.001	<1	1.280	n/a	100	3.000	0.000			1.278	n/a	3.000
	HFD-Hae	0.018	6	0.485	-0.091	100	52.6	0.280		0.485	-0.091	52.6	0.279
	HFD-OxHy-A	0.185	61	0.477	-0.133	58	47.6	1.880		0.477	-0.133	45.8	4.400
						42	43.2	5.570					
	HFD-OxHy-B	0.050	17	0.48*	0*	100	0*	22.4		0.480	0	17.9	13.5
Alisol non-paddy 40K (2Q, 3H) (BG = 2.720 MC/ch)	Q-Fe ^{III}	0.085	12	0.449	n/a	100	0.620	0.326	1.98	0.449	n/a	0.627	0.312
	Q-Fe ^{II}	0.003	<1	1.200	n/a	100	2.940	0.000			1.200	n/a	2.937
	HFD-Hae	0.050	7	0.474	-0.097	100	52.8	0.180		0.474	-0.096	52.8	0.184
	HFD-OxHy-A	0.447	64	0.470	-0.129	58	48.8	1.182		0.470	-0.129	47.7	2.941
						42	46.1	3.770					
	HFD-OxHy-B	0.113	16	0.5*	0*	100	0*	26.4		0.500	0	21.0	15.9
Alisol non-paddy 4.2K (2Q, 3H) (BG = 1.267 MC/ch)	Q-Fe ^{III}	0.024	9	0.474	n/a	100	0.592	0.334	1.08	0.474	n/a	0.602	0.315
	Q-Fe ^{II}	0.001	<1	1.160	n/a	100	3.010	0			1.159	n/a	3.014
	HFD-Hae	0.025	71	0.488	-0.084	100	53.2	0.490		0.488	-0.084	53.2	0.490
	HFD-OxHy-A	0.202	9	0.483	-0.119	53	49.5	0.790		0.483	-0.119	49.0	2.231
						47	48.3	3.030					
	HFD-OxHy-B	0.032	11	0.500	0*	100	0*	27.0		0.500	0	21.5	16.3
Alisol incubated 295K (2Q, 2H)	Q-Fe ^{III}	0.148	66	0.363	n/a	73	0.509	0.114	0.94	0.360	n/a	0.602	0.226
						27	0.860	0.260					
	Q-Fe ^{II}	0.003	1	1.064	n/a	100	2.600	0		1.060	n/a	2.599	<0.001
	HFD-Hae	0.021	9	0.379	-0.053	100	49.0	2.000		0.379	-0.053	49.0	2.000

Appendix

(BG = 1.451 MC/ch)	HFD-OxHy-B	0.051	23	0.5*	0*	100	0*	28.2	0.500	0	22.5	17.0	
Alisol incubated 140K (2Q, 3H) (BG = 6.864 MC/ch)	Q-Fe ^{III}	0.260	17	0.445	n/a	100	0.641	0.286	1.99	0.445	n/a	0.644	0.280
	Q-Fe ^I	0.019	1	1.210	n/a	100	2.796	0.143		1.210	n/a	2.796	0.143
	HFD-Hae	0.102	7	0.452	-0.093	100	52.0	0.588		0.452	-0.093	52.0	0.588
	HFD-OxHy-A	0.847	54	0.449	-0.120	48	44.6	2.830		0.449	-0.120	40.8	6.356
						52	37.3	6.710					
	HFD-OxHy-B	0.336	21	0.5*	0*	100	0*	15.8	0.500	0	12.6	9.518	
Alisol incubated 77K (2Q, 3H) (BG = 1.661 MC/ch)	Q-Fe ^{III}	0.058	15	0.473	n/a	100	0.644	0.331	1.21	0.472	n/a	0.650	0.318
	Q-Fe ^I	0.009	2	1.203	n/a	100	2.696	0.290		1.203	n/a	2.696	0.294
	HFD-Hae	0.024	6	0.468	-0.076	100	52.7	0.360		0.468	-0.076	52.7	0.358
	HFD-OxHy-A	0.216	58	0.482	-0.124	54	47.8	1.590		0.482	-0.124	46.0	3.725
						46	43.9	4.340					
	HFD-OxHy-B	0.067	18	0.48*	0*	100	0*	25.1	0.480	0	20.1	15.2	
Alisol incubated 40K (2Q, 3H) (BG = 3.444 MC/ch)	Q-Fe ^{III}	0.112	13	0.460	n/a	100	0.639	0.330	2.05	0.460	n/a	0.646	0.317
	Q-Fe ^I	0.010	1	1.167	n/a	100	2.851	0.110		1.167	n/a	2.851	0.113
	HFD-Hae	0.053	6	0.472	-0.089	100	52.8	0.250		0.472	-0.089	52.8	0.254
	HFD-OxHy-A	0.536	63	0.470	-0.127	57	48.8	1.137		0.470	-0.127	47.7	2.856
						43	46.3	3.680					
	HFD-OxHy-B	0.139	16	0.5*	0*	100	0*	29.1	0.500	0	23.2	17.5	
Alisol incubated 4.2K (2Q, 3H) (BG = 1.315 MC/ch)	Q-Fe ^{III}	0.026	8	0.471	n/a	100	0.611	0.348	1.10	0.471	n/a	0.622	0.328
	Q-Fe ^I	0.002	1	1.159	n/a	100	2.890	0		1.159	n/a	2.887	0.011
	HFD-Hae	0.032	10	0.482	-0.088	100	53.1	0.73		0.482	-0.088	53.1	0.726
	HFD-OxHy-A	0.202	65	0.483	-0.123	60	49.7	0.76		0.483	-0.123	49.0	1.789
						40	48.0	2.36					
	HFD-OxHy-B	0.049	16	0.48*	0*	100	0*	29.7	0.480	0	23.7	17.9	
Alisol paddy 295K (1Q, 2H) (BG = 1.121 MC/ch)	Q-Fe ^{III}	0.044	57	0.365	n/a	100	0.582	0.211	0.70	0.365	n/a	0.583	0.210
	HFD-Hae	0.003	4	0.209	-0.105	100	50.3	0		0.209	-0.105	50.3	0.004
	HFD-OxHy-B	0.029	38	0.470	0*	100	0*	36.1	0.474	0	28.8	21.7	
Alisol paddy 140K (2Q, 3H) (BG = 7.327 MC/ch)	Q-Fe ^{III}	0.100	27	0.449	n/a	100	0.620	0.242	0.59	0.449	n/a	0.621	0.240
	Q-Fe ^I	0.005	1	1.279	n/a	100	3.000	0.090		1.279	n/a	3.000	0.085
	HFD-Hae	0.010	3	0.439	-0.083	100	52.6	0.000		0.439	-0.083	52.6	0.003
	HFD-OxHy-A	0.185	51	0.458	-0.126	40	44.9	2.420		0.458	-0.126	41.2	5.976
						60	38.8	6.400					
	HFD-OxHy-B	0.065	18	0.46*	0*	100	0*	13.0	0.460	0	10.4	7.844	

Alisol paddy 77K (2Q, 3H) (BG = 0.885 MC/ch)	Q-Fe ^{III}	0.036	23	0.479	n/a	100	0.626	0.291	0.81	0.479	n/a	0.629	0.284
	Q-Fe ^{II}	0.002	1	1.128	n/a	100	2.760	0		1.128	n/a	2.763	0.006
	HFD-Hae	0.004	3	0.470	-0.100	100	52.9	0.400		0.470	-0.100	52.9	0.400
	HFD-OxHy-A	0.076	49	0.490	-0.130	51	48.0	1.370		0.490	-0.130	46.1	3.591
						49	44.1	4.100					
	HFD-OxHy-B	0.036	24	0.49*	0*	100	0*	33.1		0.490	0	26.4	20.0
Alisol paddy 40K (2Q, 3H) (BG = 5.624 MC/ch)	Q-Fe ^{III}	0.062	20	0.473	n/a	100	0.615	0.315	0.77	0.473	n/a	0.621	0.303
	Q-Fe ^{II}	0.006	2	1.199	n/a	100	2.840	0.200		1.199	n/a	2.838	0.199
	HFD-Hae	0.007	2	0.451	-0.119	100	53.2	0.000		0.450	-0.119	53.2	0.001
	HFD-OxHy-A	0.182	57	0.475	-0.130	59	49.0	1.020		0.475	-0.129	47.8	2.657
						41	46.1	3.300					
	HFD-OxHy-B	0.061	19	0.480	0*	100	0*	24.2		0.482	0	19.3	14.6
Alisol paddy 4.2K (1Q, 3H) (BG = 0.843 MC/ch)	Q-Fe ^{III}	0.017	13	0.452	n/a	100	0.621	0.352	0.88	0.452	n/a	0.632	0.332
	HFD-Hae	0.004	3	0.420	-0.116	100	53.4	0.100		0.420	-0.116	53.4	0.141
	HFD-OxHy-A	0.091	69	0.482	-0.123	55	49.5	0.950		0.482	-0.123	48.5	2.506
						45	47.4	3.260					
	HFD-OxHy-B	0.020	15	0.48*	0*	100	0*	30.7		0.480	0	24.5	18.5
Andosol non-paddy 295K (2Q, 2H) (BG = 1.864 MC/ch)	Q-Fe ^{III}	0.090	68	0.360	n/a	66	0.546	0.120	0.63	0.360	n/a	0.671	0.240
						34	0.910	0.230					
	Q-Fe ^{II}	0.015	12	1.165	n/a	100	2.137	0.450		1.165	n/a	2.137	0.450
	HFD-Hae	0.005	3	0.263	-0.061	100	50.4	0.100		0.263	-0.061	50.4	0.117
	HFD-OxHy-A	0.023	17	0.380	0.050	100	43.0	6.100		0.376	0.047	43.0	6.105
Andosol non-paddy 140K (2Q, 2H) (BG = 2.344 MC/ch)	Q-Fe ^{III}	0.169	69	0.452	n/a	61	0.552	0.137	0.78	0.452	n/a	0.702	0.283
							0.940	0.290					
	Q-Fe ^{II}	0.030	12	1.287	n/a	39	2.282	0.601		1.287	n/a	2.282	0.601
	HFD-Hae	0.005	2	0.337	0.136	100	52.3	0		0.337	0.136	52.3	0.007
	HFD-OxHy-A	0.040	17	0.45*	-0.024	100	49.2	3.970		0.450	-0.024	49.2	3.966
Andosol non-paddy 77K (2Q, 3H) (BG = 2.341 MC/ch)	Q-Fe ^{III}	0.153	52	0.480	n/a	82	0.580	0.196	0.91	0.480	n/a	0.678	0.281
						18	1.110	0.173					
	Q-Fe ^{II}	0.027	9	1.170	n/a	100	2.577	0.428		1.170	n/a	2.577	0.428
	HFD-Hae	0.008	3	0.515	0.026	100	53.4	0.330		0.515	0.026	53.4	0.331
	HFD-OxHy-A	0.068	23	0.433	-0.048	43	50.2	2.170		0.433	-0.048	45.9	7.117
					57	42.8	7.800						
	HFD-OxHy-B	0.037	13	0.44*	0*	100	0*	20*		0.440	0	16.0	12.1
Andosol	Q-Fe ^{III}	0.087	30	0.477	n/a	71	0.616	0.177	0.91	0.477	n/a	0.790	0.335

Appendix

non-paddy 40K	Q-Fe ^{II}	0.031	11	1.366	n/a	29	1.210	0.240					
(2Q, 3H)	HFD-Hae	0.009	3	0.542	0.015	100	2.249	0.542	1.366	n/a	2.249	0.542	
(BG = 2.231 MC/ch)	HFD-OxHy-A	0.109	38	0.486	-0.088	57	48.2	3.550	0.486	-0.088	44.2	6.869	
	HFD-OxHy-B	0.052	18	0.49*	0*	43	39.0	6.600					
						100	0*	22.0	0.490	0	17.4	13.2	
Andosol non-paddy 13K	Q-Fe ^{III}	0.028	7	0.535	n/a	100	0.678	0.304	0.95	0.535	n/a	0.681	0.298
(2Q, 4H)	Q-Fe ^{II}	0.035	9	1.264	n/a	100	2.478	0.486		1.264	n/a	2.478	0.486
(BG = 2.116 MC/ch)	HFD-Hae	0.010	2	0.530	-0.042	100	53.1	0.290		0.530	-0.042	53.1	0.290
	HFD-OxHy-A1	0.177	45	0.477	-0.140	54	47.9	1.710		0.477	-0.140	45.5	4.646
						46	42.6	5.400					
	HFD-OxHy-A2	0.072	18	0.455	0.053	100	47.5	3.760		0.455	0.053	47.5	3.760
	HFD-OxHy-B	0.075	19	0.47*	0*	100	0*	25.9		0.470	0	20.6	15.6
Andosol non-paddy 4.2K	Q-Fe ^{III} + Q-Fe ^{II}	0.009	4	1.520	n/a	100	2.450	0.650	0.89	1.516	n/a	2.454	0.647
(1Q, 5H)	HFD-Hae	0.003	1	0.248	0.211	100	53.1	0		0.248	0.211	53.1	0.018
(BG = 1.596 MC/ch)	HFD-OxHy-A1	0.128	54	0.498	-0.121	44	48.6	1.400		0.498	-0.121	47.0	4.075
						56	45.8	4.940					
	HFD-OxHy-A2	0.054	23	0.423	0.054	100	48.0	3.830		0.423	0.054	48.0	3.830
	HFD-OxHy-B	0.036	15	0.470	0*	100	0*	27.0		0.470	0	21.8	16.5
	HFD-Fe ^{II}	0.006	3	1.200	1.050	100	0*	5.000		1.200	1.054	4.000	3.015
Andosol incubated 295K	Q-Fe ^{III}	0.095	69	0.363	n/a	54	0.515	0.090	0.49	0.363	n/a	0.654	0.229
(2Q, 2H)						46	0.820	0.240					
(BG = 3.567 MC/ch)	Q-Fe ^{II}	0.017	12	1.111	n/a	100	2.240	0.380		1.111	n/a	2.244	0.383
	HFD-Hae	0.007	5	0.405	-0.048	100	50.7	0.630		0.405	-0.048	50.6	5.891
	HFD-OxHy-A	0.019	14	0.490	0.070	100	42.0	5.900		0.494	0.073	42.0	0.631
Andosol incubated 140K	Q-Fe ^{III}	0.049	67	0.435	n/a	75*	0.610	0.170	0.56	0.435	n/a	0.710	0.274
(2Q, 2H)						25	1.000	0.280					
(BG = 3.855 MC/ch)	Q-Fe ^{II}	0.007*	9	1.350	n/a	100	2.190	0.380*		1.351	n/a	2.192	0.380
	HFD-Hae	0.003	4	0.450	0.020	100	50.9	0.359*		0.449	0.021	50.9	0.359
	HFD-OxHy-A	0.015	20	0.370	-0.040	100	43.9	11.0*		0.368	-0.041	43.9	11.0
Andosol incubated 77K	Q-Fe ^{III}	0.078	51	0.473	n/a	100	0.668	0.272	0.76	0.473	n/a	0.669	0.269
(2Q, 3H)	Q-Fe ^{II}	0.016	10	1.165	n/a	100	2.609	0.372		1.165	n/a	2.609	0.372
(BG = 2.862 MC/ch)	HFD-Hae	0.003	2	0.550	-0.090	100	53.8	0.200		0.555	-0.090	53.8	0.172
	HFD-OxHy-A	0.034	22	0.434	-0.001	51	50.5	2.200		0.434	-0.001	45.2	7.985
						49	39.6	8.000					
	HFD-OxHy-B	0.022	15	0.440*	0*	100	0*	15.0		0.440	0	11.6	8.795

Appendix

Andosol incubated 40K (2Q, 3H) (BG = 2.369 MC/ch)	Q-Fe ^{III}	0.036	25	0.507	n/a	100	0.685	0.286	0.55	0.507	n/a	0.687	0.283
	Q-Fe ^{II}	0.014	10	1.214	n/a	100	2.594	0.364		1.214	n/a	2.594	0.364
	HFD-Hae	0.005	3	0.411	0.122	100	52.1	0.3*		0.411	0.122	52.1	0.300
	HFD-OxHy-A	0.059	41	0.534	-0.117	52	48.3	3.500		0.534	-0.117	43.2	8.233
	HFD-OxHy-B	0.029	20	0.5*	0*	100	0*	18.0		0.500	0	14.4	10.9
Andosol incubated 13K (2Q, 4H) (BG = 2.720 MC/ch)	Q-Fe ^{III}	0.014	9	0.519	n/a	100	0.676	0.301	0.57	0.519	n/a	0.678	0.296
	Q-Fe ^{II}	0.019	12	1.279	n/a	100	2.490	0.520		1.279	n/a	2.492	0.520
	HFD-Hae	0.004	3	0.447	0.072	100	53.0	0.3*		0.447	0.072	53.0	0.300
	HFD-OxHy-A1	0.045	28	0.460	-0.131	100	48.2	1.760		0.460	-0.131	48.2	1.765
	HFD-OxHy-A2	0.051	32	0.537	0.016	100	45.3	5.900		0.537	0.016	45.3	5.915
HFD-OxHy-B	0.029	18	0.5*	0*	100	0*	29.0		0.500	0	23.4	17.6	
Andosol incubated 4.2K (1Q, 5H) (BG = 2.641 MC/ch)	Q-Fe ^{III} + Q-Fe ^{II}	0.004	3	1.362	n/a	100	2.780	0.230	0.60	1.362	n/a	2.781	0.233
	HFD-Hae	0.002	1	0.310	0.075	100	52.9	0		0.309	0.075	52.9	0.001
	HFD-OxHy-A1	0.096	58	0.500	-0.122	29	48.8	0.930		0.500	-0.122	47.6	3.981
	HFD-OxHy-A2	0.028	17	0.386	-0.003	100	48.4	2.700		0.386	-0.003	48.4	2.712
	HFD-OxHy-B	0.023	14	0.480	0*	100	0*	24.3		0.480	0	19.4	14.6
HFD-Fe ^{II}	0.012	7	1.200	0.930	100	0*	8.3		1.200	0.930	6.600	4.991	
Andosol paddy 295K (2Q, 2H) (BG = 1.822 MC/ch)	Q-Fe ^{III}	0.066	61	0.360	n/a	55	0.535	0.099	0.58	0.360	n/a	0.693	0.284
	Q-Fe ^{II}	0.016	15	1.217	n/a	100	2.042	0.320		1.217	n/a	2.042	0.462
	HFD-Hae	0.006	6	0.331	-0.078	100	51.0	0.720		0.331	-0.078	51.0	0.717
	HFD-OxHy-A	0.021	19	0.450	0.090	100	43*	9.500		0.454	0.086	43.0	9.495
Andosol paddy 140K (2Q, 2H) (BG = 5.056 MC/ch)	Q-Fe ^{III}	0.172	54	0.453	n/a	52	0.531	0.180	0.82	0.453	n/a	0.715	0.340
	Q-Fe ^{II}	0.049	15	1.226	n/a	100	0.910	0.360					
	HFD-Hae	0.014	4	0.372	-0.007	100	2.206	0.683		1.226	n/a	2.206	0.682
	HFD-OxHy-A	0.085	27	0.451	-0.071	100	52.0	0.7*		0.372	-0.007	52.0	0.700
Andosol paddy 77K (2Q, 3H) (BG = 2.241 MC/ch)	HFD-OxHy-A	0.085	27	0.451	-0.071	100	42.4	8.480		0.451	-0.071	42.4	8.485
	Q-Fe ^{III}	0.087	39	0.476	n/a	38	0.544	0.122	0.60	0.476	n/a	0.730	0.341
	Q-Fe ^{II}	0.024	11	1.279	n/a	100	0.840	0.390					
	HFD-Hae	0.006	3	0.271	0.133	100	2.320	0.440		1.279	n/a	2.317	0.440
	HFD-OxHy-A	0.065	29	0.505	-0.088	84	53.1	0.100		0.271	0.133	53.1	0.136
HFD-OxHy-B	0.041	18	0.5*	0*	100	48.7	3.710		0.505	-0.088	46.9	5.595	
						16	37.3	3.600					
						100	0*	27*		0.500	0	21.5	16.3

Appendix

Andosol paddy 40K (2Q, 3H) (BG = 3.711 MC/ch)	Q-Fe ^{III}	0.073	27	0.503	n/a	100	0.657	0.296	0.77	0.503	n/a	0.660	0.290
	Q-Fe ^I	0.028	11	1.210	n/a	100	2.515	0.448		1.210	n/a	2.515	0.448
	HFD-Hae	0.010	4	0.509	-0.017	100	53.2	0.3*		0.509	-0.017	53.2	0.300
	HFD-OxHy-A	0.125	47	0.487	-0.109	48	48.2	2.230		0.487	-0.109	43.3	8.899
	HFD-OxHy-B	0.031	12	0.48*	0*	100	0*	10.2		0.480	0	8.5	6.448
Andosol paddy 13K (2Q, 4H) (BG = 2.065 MC/ch)	Q-Fe ^{III}	0.037	17	0.490	n/a	100	0.621	0.286	0.76	0.490	n/a	0.624	0.279
	Q-Fe ^I	0.025	11	1.261	n/a	100	2.430	0.550		1.261	n/a	2.430	0.550
	HFD-Hae	0.009	4	0.519	-0.104	100	53.4	0.350		0.519	-0.104	53.4	0.345
	HFD-OxHy-A1	0.057	26	0.483	-0.127	100	49.1	1.500		0.483	-0.127	49.1	1.499
	HFD-OxHy-A2	0.053	24	0.425	0.041	100	45.9	6.400		0.425	0.041	45.9	6.397
HFD-OxHy-B	0.043	19	0.5*	0*	100	0*	32.0		0.500	0	25.1	19.0	
Andosol paddy 4.2K (2Q, 5H) (BG = 1.846 MC/ch)	Q-Fe ^{III}	0.020	10	0.465	n/a	100	0.606	0.218	0.67	0.465	n/a	0.607	0.217
	Q-Fe ^I	0.003	2	1.175	n/a	100	2.860	0.080		1.175	n/a	2.863	0.084
	HFD-Hae	0.007	3	0.497	-0.077	100	53.9	0		0.497	-0.077	53.9	0.001
	HFD-OxHy-A1	0.055	27	0.487	-0.132	100	49.4	1.440		0.487	-0.132	49.4	1.440
	HFD-OxHy-A2	0.060	29	0.433	-0.053	100	47.9	4.490		0.433	-0.053	47.9	4.488
HFD-OxHy-B	0.043	21	0.5*	0*	100	0*	31.8		0.500	0	25.4	19.2	
HFD-Fe ^{II}	0.017	8	1.290	1.050	100	0*	7.043		1.294	1.048	5.620	4.246	

Notes

All fits performed using the Voigt-based fitting method of (Rancourt and Ping, 1991) with the Recoil™ software.

All fitting and calculated parameters are as defined in by Rancourt and Ping (1991).

All delta-1 couplings between CS and z (or DELTA) were taken to be zero.

All line-1 to line-2 area ratios in all (distributed) elemental doublets were taken to be 1.

All line-2/line-3 and line-1/line-3 area ratios in all (distributed and symmetric) elemental sextets were taken to be 2 and 3, respectively.

All epsilon-1 couplings between epsilon and z (in a HFD) are taken to be 0.

BG = background level, in mega-counts per channel (MC/ch).

phase = assigned spectral component, as described in the text.

Δ = the center (or position) of a Gaussian component in the quadrupole splitting distribution (QSD) of a given doublet spectral component.

H = the center (or position) of a Gaussian component in the hyperfine field distribution (HFD) of a given 'sextet' spectral component.

σ = the Gaussian standard deviation width of a given Gaussian component of a given QSD or HFD.

P (in %) is the weight factor for a given Gaussian component in a given QSD or HFD.

<A> signifies the average of the absolute value of A.

Appendix

$\langle H \rangle$ is the average magnitude of the hyperfine field (expressed as an excited state Zeeman splitting, in mm/s) in a given HFD of a given sextet spectral component.

$\langle QS \rangle$ is the average magnitude of the quadrupole splitting in a given QSD of a given doublet spectral component.

$\langle \epsilon \rangle$ is the average magnitude of the slave distribution of quadrupole shifts (epsilons) associated to a given HFD of a given sextet spectral component.

s.d. is the standard deviation width of a given distribution (QSD, HFD, or slave distributions)

Red- χ^2 is the reduced chi-squared value for the fit: chi-squared divided by the number of degrees of freedom. It has an ideal value of 1 for a correct model.

All center shifts (CSs, δ_0 , $\langle CS \rangle$) are given with respect to the CS of metallic Fe at 295K.

Appendix 3: Detailed methods description

Appendix 3.1: Specific surface area (SSA)

Before estimation of SSA, the initial bulk soils were treated twice with NaOCl (pH 8) at room temperature for 18 hours to oxidize the organic matter (OM) (Kaiser and Guggenberger 2003). The air dried, OM free soils were outgassed at 20 °C for 48 hours (Kaiser and Guggenberger 2003) and then analyzed by adsorption of N₂ (77 K) by using the multi-point BET approach (Autosorb iQ surface area analyzer; Quantachrome Instruments, Boynton Beach, FL, USA).

Appendix 3.2: Elemental composition and C speciation of particle surfaces

The elemental composition of the soil particle's outmost surface layer was characterized by X-ray photoelectron spectroscopy (XPS, maximum analysis depth about 10 nm). After removal of the particulate OM (according to method described in section ESM 1.5 of the Online Resource 1), samples of the initial Alisol und Andosol were fixed on a sample bar with carbon conductive tape (Agar Scientific Electron Technology UK Ltd., Stansted, UK). Survey spectra as well as C 1s detail scans were recorded with a Kratos Axis Ultra DLD instrument (Kratos Analytical Ltd., Manchester, UK), using monochromated AlK α radiation (1486.6 eV), operated at 20 mA and 12 kV. Pass energy was 160 eV for the survey and 20 eV for the C 1s detail scans. Surface elemental composition in terms of atomic-% was evaluated by quantifying the survey scans with the software Vision 2 (Kratos Analytical, Manchester, UK), using a linear baseline and the implemented relative sensitivity factors. Carbon speciation of the C 1s detail scans was performed using the software package Unifit 2016 (Unifit Scientific Software GmbH, Leipzig, Germany), following Poggenburg et al. (2018).

Appendix 3.3: Headspace analyses and calculation of proportion of straw-derived CO₂ and CH₄

Concentrations of CO₂ and CH₄ in gas samples were measured with a ThermoQuest Trace GC 2000 gas chromatograph (Thermo Scientific, Milan, Italy) equipped with a Restek HSQ 80-100 column (OD 1/8", ID 2.0 mm, length 2 m) coupled with a Restek HSN 80-100 column (OD 1/8", ID 2.0 mm, length 1 m) and flame ionization detector (FID). The amount of CO₂ [mol] in the headspace of the incubation bottles was calculated by the general gas law assuming ideal gases:

$$\text{CO}_2 \text{ in headspace [mol]} = \frac{(P_{\text{bottle before}} + 1000) \times \left(V_{\text{headspace}} \left(\frac{\text{CO}_2}{1.000.000} \right) \right)}{R \times T_{\text{sampling}}} \quad (1)$$

where $P_{\text{bottle before}}$ = pressure in the incubation bottle before sampling [hPa], $V_{\text{headspace}}$ = headspace volume of the incubation bottle [L], CO_2 = concentration of CO₂ as measured in the sample vial

[ppm], R = ideal gas constant (= 83.1446 L hPa mol⁻¹ K⁻¹), T_{sampling} = actual temperature during sampling (= 298.15 K). Pressures in the incubation bottles were measured as over- and underpressures relative to the atmospheric pressure. For calculations, we considered a mean atmospheric pressure of 1000 hPa, which was added to the pressure of the bottle. The calculation of CH₄ in the headspace was performed accordingly.

For the submerged soils with redox fluctuation, the CO₂ dissolved in the soil solution was also calculated:

$$\text{CO}_2 \text{ dissolved [mol]} = \alpha \times \text{CO}_2 \text{ headspace} \times \frac{V_{\text{liquid}}}{V_{\text{headspace}}} \times (1 + 10^{(-\text{pKa}+\text{pH})}) \quad (2)$$

where α = Bunsen absorption coefficient (= 0.75 at 298.15 K), $\text{CO}_2 \text{ headspace}$ = CO₂ in the headspace of the incubation bottle [mol], V_{liquid} = solution volume [L], $V_{\text{headspace}}$ = headspace volume [L], pKa = dissociation constant (= 6.38 for the dissociation of CO₂ in water). The calculation of CH₄ dissolved in the soil solution was performed accordingly, however, with $\alpha = 0.03$ and without the last term of formula (2), since CH₄ hardly dissociates in water. The total amount of CO₂ and CH₄ in the bottle at the time of sampling was calculated by adding the amount of CO₂/CH₄ in the headspace and the amount of CO₂/CH₄ dissolved in the soil solution. The headspace was fully exchanged by pure N₂/O₂ only at the end of each anoxic and each oxic phase, meaning that the amount of CO₂/CH₄ measured within an anoxic phase (after the third and fifth week) is a mixture of the CO₂/CH₄ that remained in the flask after the previous sampling and the CO₂ that was produced since the previous sampling. To account for that, we also calculated the amount of CO₂ [mol] in the headspace of the incubation flask after sampling (same CO₂/CH₄ concentration as before but different pressure) and subtracted that from the amount of CO₂/CH₄ at the time of next sampling. In order to obtain comparable results for both soil types, we divided the produced CO₂/CH₄ by the amount of OC in the incubation flasks including the native OC of the initial soil plus the OC added with straw at the beginning of each cycle minus the OC mineralized since the beginning of the incubation. The amounts of CO₂/CH₄ (in mg g⁻¹ OC) produced in between two sampling time points were summed up for the entire incubation period of 48 weeks.

The $\delta^{13}\text{C}$ of CO₂ in the headspace samples was analyzed by a Trace Gas chromatograph (Elementar UK, Manchester, UK) equipped with a Gilson GX-271 autosampler (Gilson Inc., Middleton, United States) and coupled with an Isoprime 100 isotope ratio mass spectrometer (IRMS) (Elementar UK, Manchester, UK). Isotope ratios were expressed as delta notation in parts per thousand (‰) relative to the international standard Vienna Pee Dee belemnite (V-PDB). According to Balesdent et al. (1990) the $\delta^{13}\text{C}$ of CO₂ in the headspace samples was composed of:

$$\delta^{13}\text{C} - \text{CO}_2_{\text{sample}} = f \times \delta^{13}\text{C} - \text{CO}_2_{\text{from straw}} + (f - 1) \times \delta^{13}\text{C} - \text{CO}_2_{\text{from SOC}} \quad (3)$$

Formula (3) was re-arranged in order to calculate the fraction of CO₂-C coming from straw:

$$f = \frac{\delta^{13}\text{C} - \text{CO}_2_{\text{sample}} - \delta^{13}\text{C} - \text{CO}_2_{\text{from SOC}}}{\delta^{13}\text{C} - \text{CO}_2_{\text{from straw}} - \delta^{13}\text{C} - \text{CO}_2_{\text{from SOC}}} \quad (4)$$

The $\delta^{13}\text{C} - \text{CO}_2_{\text{from SOC}}$ is given by $\delta^{13}\text{C} - \text{CO}_2$ of samples incubated without straw addition and considers the fractionation that occurs when soil OC is mineralized to CO₂. The $\delta^{13}\text{C} - \text{CO}_2_{\text{from straw}}$ was not measured; however, ¹³C enrichment of labeled straw was high, so that the $\delta^{13}\text{C}$ of the labeled straw could be used. The disregarded fractionation (which is relatively small for CO₂) leads to acceptable errors (Yuan et al. 2012; Ye et al. 2016). The proportion of CO₂-C from straw determined for each sampling point was multiplied by the total amount of CO₂-C in the flask (headspace + dissolved) of the respective sampling point. The total amount of CO₂-C produced by mineralization of straw is given by the sum of all CO₂-C from straw produced since last sampling.

For cost reasons the $\delta^{13}\text{C}$ of CH₄ could not be measured directly. The proportion of CH₄ from straw was instead estimated via the total OC budget as outlined in section 2.7.

Appendix 3.4: Measurement of DO¹³C and calculation of proportion of straw-derived DOC

The $\delta^{13}\text{C}$ value of DOC was analyzed directly in solution using a high-temperature combustion system (Federherr et al. 2014; Kirkels et al. 2014). For this, an isoTOC cube (Elementar group, Langenselbold, Germany) total organic carbon (TOC) analyzer was coupled with a continuous flow IRMS (Isoprime 100, Elementar UK, Manchester, UK). All samples were manually acidified to pH \approx 2 by HCl (37%) in order to remove dissolved inorganic C and/or prevent (re)dissolution of atmospheric CO₂. Samples were injected four times and only the last three injections were used for data analyses. Injection volume ranged between 0.2 and 1 ml, depending on the OC content. Both at the beginning and at the end of each sequence, a set of international standards (Caffeine IAEA-600, Sucrose IAEA-CH6) dissolved in the blank water at an OC concentration similar to the one expected for the samples were run as samples, allowing for two-point normalization. To be able to use a two-point normalization for labeled samples also, artificial standards were prepared by thoroughly mixing non-labeled and 99%-labeled glucose in proportions to obtain the desired label. The mixtures were then normalized vs. international standard as solid using an Elemental Analyzer (vario isoTOC cube, Elementar group, Hanau, Germany) coupled to IRMS (IsoPrime100, Elementar UK, Manchester, UK) and then used to prepare the standard solutions as described above. The artificial solid mixtures were checked several times during the entire period of analyses to ensure the consistency of the obtained values. Blank samples of the same water used for the preparation of the normalizing standards

were analyzed before, after, and between samples. All calculations for corrections and normalization were done according to those described in Kirkels et al. (2014).

The $\delta^{13}\text{C}$ -DOC measured in the solution samples is composed of (Balesdent et al. 1990):

$$\delta^{13}\text{C} - \text{DOC}_{\text{sample}} = f \times \delta^{13}\text{C} - \text{DOC}_{\text{from straw}} + (f - 1) \times \delta^{13}\text{C} - \text{DOC}_{\text{from SOC}} \quad (5)$$

Formula (5) was re-arranged in order to calculate the fraction of DOC coming from straw:

$$f = \frac{\delta^{13}\text{C} - \text{DOC}_{\text{sample}} - \delta^{13}\text{C} - \text{DOC}_{\text{from SOC}}}{\delta^{13}\text{C} - \text{DOC}_{\text{from straw}} - \delta^{13}\text{C} - \text{DOC}_{\text{from SOC}}} \quad (6)$$

The $\delta^{13}\text{C}$ -DOC_{from SOC} is given by $\delta^{13}\text{C}$ -DOC of samples incubated without straw. Respective data, however, was incomplete, so we decided to use the $\delta^{13}\text{C}$ of the initial soils, which was similar to the $\delta^{13}\text{C}$ -DOC_(-straw) that we could measure. The $\delta^{13}\text{C}$ -DOC_{from straw} could not be measured; as for CO₂ from straw, we used the $\delta^{13}\text{C}$ of the straw directly. In that case, fractionation is not considered, but errors should be relatively low due to the ¹³C enrichment in the straw.

Appendix 3.5: Density fractionation of soil OM and calculation of proportion of straw-derived OC

Soil OM was separated into three density fractions (free particulate OM = FPOM, occluded particulate OM = OPOM, mineral-associated OM = MOM) based on the method described by Christensen (1992). For the separation of FPOM, 25 g of air dried soil were mixed with 125 ml of a Na₆(H₂W₁₂O₄₀) solution (density of 1.6 g cm⁻³). The FPOM fraction was floating on the surface of the solution and was separated by centrifuging (15 min at 6300 x g) the suspension, filtrating the supernatant, and then washing (to an electric conductivity of the washing water of <50 μS cm⁻¹) and drying (40 °C) the filtrate, which represents the FPOM. The procedure was repeated before proceeding with the other fractions. In order to separate the OPOM fraction, the remaining soil was again suspended in 125 ml Na₆(H₂W₁₂O₄₀) solution. Sonication was used to break up soil aggregates, and hence, to release the previously occluded particulate OM, which then floated on the solution's surface. The sonication energy required to break up aggregates depends on the studied soil and was determined in advance for both soil types by successively applying increasing energy to one sample, gaining the resulting OPOM separately for the different energy levels and measuring their OC content (Cerli et al. 2012). The application of insufficient energy levels results in the release of OPOM with some mineral particles attached, while the application of excessive ultrasonic energy leads to the dispersion of mineral particles, which end up as part of the OPOM. Hence, the OC concentration of the OPOM gained at increasing energy levels should first increase followed by a decrease. The OPOM with the highest OC content is the purest and the respective ultrasonic energy is the desired energy level. According to that test we applied 50 J ml⁻¹ to the Andosol and 200 J ml⁻¹ to the Alisol samples.

The suspension was again centrifuged, the supernatant filtered, and then washed and dried. The procedure was repeated without additional sonication. After these steps, the remaining soil only contained mineral-associated OM; it was also washed and freeze-dried. The yield of all fractions and their OC concentrations (Vario MAX elemental analyzer; Elementar Analysensysteme GmbH, Hanau, Germany) were determined in order to calculate the amount of OC [g] in the different fractions per kg of soil.

The $\delta^{13}\text{C}$ of the different OM fractions was determined by EA (Eurovector Hekatech, Wegberg, Germany) coupled via Conflo III interface to a Delta V Advantage IRMS (Thermo Fischer, Bremen, Germany). On the basis of descriptions of Balesdent et al. (1990), the fraction of soil OC coming from straw was calculated by:

$$f_{\text{FPOM}} = \frac{\delta^{13}\text{C}_{\text{FPOM sample}} - \delta^{13}\text{C}_{\text{FPOM NP}}}{\delta^{13}\text{C}_{\text{straw}} - \delta^{13}\text{C}_{\text{FPOM NP}}} \quad (7)$$

$$f_{\text{OPOM}} = \frac{\delta^{13}\text{C}_{\text{OPOM sample}} - \delta^{13}\text{C}_{\text{OPOM NP}}}{\delta^{13}\text{C}_{\text{OPOM from straw}} - \delta^{13}\text{C}_{\text{OPOM NP}}} \quad (8)$$

$$f_{\text{MOM}} = \frac{\delta^{13}\text{C}_{\text{MOM sample}} - \delta^{13}\text{C}_{\text{MOM NP}}}{\delta^{13}\text{C}_{\text{MOM from straw}} - \delta^{13}\text{C}_{\text{MOM NP}}} \quad (9)$$

The conversion of straw to OPOM and MOM probably includes some fractionations, which were not considered here. As for CO_2 and DOC from straw, we directly used the $\delta^{13}\text{C}_{\text{straw}}$.

Appendix 3.6: Lignin-derived phenols

The mineral-associated OM was analyzed for lignin-derived constituents by digesting lignin through alkaline CuO oxidation according to Hedges and Ertel (1982). Samples of 400 mg (Alisol) or 200 mg (Andosol) were mixed with 100 mg $(\text{NH}_4)_2\text{Fe}(\text{SO}_4)_2 \cdot 6 \text{H}_2\text{O}$, 500 mg CuO, 50 mg glucose and 15 ml 2M NaOH (Amelung et al. 1999) and oxidized for 2 h at 170 °C in a pressure digester (Groteklaes, Jülich, Germany). Phenols released were solid phase extracted from the extracts using C_{18} columns (Bakerbond spe™, Mallinckrodt Baker Corp., Phillipsburg, NJ, USA) after acidification to $\text{pH} \approx 2$. Lignin phenols were eluted from the columns by applying $10 \times 500 \mu\text{l}$ ethyl acetate. The ethyl acetate was removed by rotary evaporation. Residues were dissolved in 200 μl BSTFA (bis-(trimethylsilyl)-trifluoroacetamide) as derivatization reagents (1:2 ratio, 2 h reaction time at room temperature). Derivatized phenols were analyzed with a GCMS-QP 2010 (Shimadzu Corp., Kyoto, Japan). Ethyl vanillin was added as internal standard prior to the CuO oxidation, and phenyl acetic acid before derivatization. Identification and quantification was carried out with an external standard mixture, containing known amounts of phenols. Analyses were carried out in triplicate.

Appendix 3.7: Non-cellulosic carbohydrates

Non-cellulosic carbohydrates of the mineral-associated OM were analyzed after hydrolyses of the respective carbohydrates with 4 M trifluoroacetic acid according to Eder et al. (2010). After hydrolysis, EDTA was added to keep iron in a non-reactive form in solution and to avoid possible co-precipitation of dissolved organic matter. The next steps were the reduction of the released sugar monomers to the corresponding alcohols with NaBH₄ and their derivatization with acetic anhydride. Gas chromatographic separation and detection with FID was carried out on a GC Agilent 6890 (Agilent Technologies, Waldbronn, Germany).

The $\delta^{13}\text{C}$ of individual carbohydrates was determined by GC-IRMS featuring a CTC CombiPAL autosampler (CTC Analytics AG, Zwingen, Switzerland), a 7890A GC device (Agilent Technologies), and a GC IsoLink interface connected via a ConFlo IV open split system to a MAT 253 IRMS (Thermo Scientific, Bremen, Germany). Samples of 1-5 μl were injected with a split ratio of 1:5. Chromatographic separation was done on a Zebron ZB-5HT INFERNO column (30 m, 0.25 mm, 0.25 μm ; Phenomenex Inc., USA) at a constant helium carrier gas flow of 2.0 ml min⁻¹ with the following temperature program: 40 °C for 5 min, 20 °C min⁻¹ to 160 °C, 1 °C min⁻¹ to 170 °C for 20 min, 2 °C min⁻¹ to 250 °C for 5 min. The injector temperature was set to 300 °C. Each sample was measured in at least three technical replicates. The fraction of neutral sugars from straw was determined by:

$$f = \frac{\delta^{13}\text{C}_{\text{neutral sugar sample}} - \delta^{13}\text{C}_{\text{neutral sugar NP}}}{\delta^{13}\text{C}_{\text{straw}} - \delta^{13}\text{C}_{\text{neutral sugar NP}}}$$

Appendix 3.8: Microbial analyses

Appendix 3.8.1: DNA extraction and sequencing library preparation

DNA was extracted from 500 mg frozen soil by using the NucleoSpin®Soil Kit (Macherey-Nagel, Düren, Germany). For cell lysis buffer SL1 was used. As control an extraction blank without soil was processed. The quality of the DNA was checked with the Nanodrop 1000 spectrophotometer (PeqLab, Erlangen, Germany) at the wavelength 230 nm, 260 nm and 280 nm. The quantity of the DNA was determined with the Quant-iT PicoGreen dsDNA Assay Kit (Life Technologies, Carlsbad, CA, USA). The DNA extract was stored at -20 °C until further use.

Next generation amplicon sequencing was performed using the MiSeq technology and basically followed the “16S Metagenomic Sequencing Library Preparation” protocol (Illumina Inc., San Diego, CA, USA) and the guidelines published by Schöler et al. (2017). Briefly, the first PCR was performed using the primers 27F and 357R (Klindworth et al. 2013) with Illumina specific overhangs. The PCR reaction was performed in triplicates. The PCR Master Mix contained 5 ng DNA or the same volume of water for PCR negative controls, 5 pmol (0.5 μl) per primer, 2 μl 3%

BSA, 12.5 µl NEB Next High Fidelity Master Mix (New England Biolabs Inc., Ipswich, MA, USA) and was filled up to 25 µl with DEPC treated water. The PCR cycling program was as follows: hotstart (5 min, 98 °C) followed by 30 cycles of denaturation (10 sec, 98 °C), primer annealing (30 sec, 60 °C) and elongation (30 sec, 72 °C) and a final elongation of 5 min, 72 °C. The triplicate PCR products were pooled and purified by using the PCR Clean-up Gel Extraction Kit (Macherey-Nagel) with a 1:4 diluted NTI buffer. The indexing PCR was performed with 10 ng of purified PCR products, 2.5 µl of each indexing primer (Nextera® XT Index Kit v2 Set B) and 12.5 µl NEB Next High Fidelity Master Mix. The PCR program started with a hotstart (30 sec, 98 °C), followed by 8 cycles of denaturation (10 sec, 98 °C), primer annealing (30 sec, 55 °C) and elongation (30 sec, 72 °C) and a final elongation of 5 min, 72 °C. After the indexing PCR samples were purified again. After each PCR the concentration of the PCR product was measured with the Quant-iT PicoGreen dsDNA Assay Kit and the size of the amplicon was checked on a Bioanalyzer 2100 instrument (Agilent Technologies, Santa Clara, CA, USA) using a DNA 7500 chip (Agilent Technologies, USA). Finally, libraries were diluted to 4 nM and sequenced with the MiSeq Reagent kit v3 (600 cycles) (Illumina Inc.) for paired-end sequencing. Moreover, 1% PhiX was added to the sequencing run. Sequences have been submitted to the NCBI Sequence Read Archive with SRP148981 as accession number.

Appendix 3.8.2: Sequencing data analysis and statistics

Sequencing data were analyzed with QIIME (Quantitative Insights into Microbial Ecology) software package version 1.9.1 (Caporaso et al. 2010) and as described by Estendorfer et al. (2017). Scripts were run in parallel by using GNU parallel (Tange 2011). First, FASTQ files were trimmed and merged (Phred score = 15, minimum read length = 50) by using AdapterRemoval (Schubert et al. 2016). Second, DeconSeq (Schmieder and Edwards 2011) was used to remove PhiX contaminations and archaeal reads (no reads were found). For quality filtering (Phred score =19), length filtering (300-400 bp) and the removal of chimeric sequences, the usearch61 algorithm was used (Edgar 2010) and run against the Greengenes Database (version 13_8) (DeSantis et al. 2006; McDonald et al. 2012) at 99% sequence identity. A summary of the sequencing run and sequence processing with QIIME is given in Table ESM-2.3 of the Online Resource 2. Biopieces (<http://www.biopieces.org>) was used to plot the read length and set length filtering options. To call operational taxonomic units (OTU) on 97% sequence similarity, the subsampled open-reference clustering was used (Rideout et al. 2014) with the RDP classifier 2.2 (Wang et al. 2007) retrained with the Greengenes database. The obtained output was filtered with an abundance cut-off of 0.005%. Finally, QIIME was used to analyze the assigned sequences. Therefore, all samples were rarefied to a sequence depth of 19,508 reads, according to the sample with the lowest number of reads.

Additional analyses were done with the R environment version 3.1.2 (Team 2008). To display the distance of the samples, a principal coordinate analysis plot (PCoA) was created using ggplot2 (Wickham 2009). The basis for these plots was either a weighted (considering presence and abundance of OTUs) or unweighted (considering presence or absence of OTUs) UniFrac distance matrix (Lozupone and Knight 2005). The significant difference between the plotted groups was calculated by analysis of similarities (ANOSIM) with 999 permutations. For PCoA plots, the filtered biome file was used.

Appendix 3.8.3: Microbial cell membrane lipids

Core lipids of isoprenoid glycerol dialkyl glycerol tetraethers (iGDGTs) were obtained by automated solvent extraction using an ASE 200 (Dionex, Sunnyvale, CA, USA) at a temperature of 75 °C and a pressure of 5.0×10^6 Pa. Each sample was extracted for 20 min using a solvent mixture of dichloromethane (DCM) / MeOH (93:7, v/v). The total lipid extracts were separated over an aluminium oxide column into apolar and polar fractions using n-hexane / DCM (9:1, v/v) and DCM / MeOH (1:1, v/v) as respective eluents. The polar fractions were dried under a gentle stream of N₂, re-dissolved in n-hexane = 2-propanol (99:1, v/v) and filtered through 0.45 µm polytetrafluoroethylene (PTFE) filters prior to analysis. All samples were analyzed by atmospheric pressure chemical ionization–mass spectrometry (HPLC–APCI–MS) following the analytical protocol described by Hopmans et al. (2000) and Schouten et al. (2007). Briefly, iGDGTs were eluted using an Alliance 2690 HPLC (Waters Ltd., Elstree, UK) equipped with a Prevail Cyano column (2.1 x 150 mm, 3 µm; Grace, Columbia, ML, USA). HPLC/MS was performed using a Quattro LC triple quadrupole mass spectrometer (Micromass UK, Wilmslow, UK) equipped with an atmospheric pressure chemical ionization (APCI) interface operated in positive ion mode. The MS was operated as outlined in Heyng et al. (2015), with iGDGTs being detected in the selected ion recording (SIR) mode of their protonated molecules [M+H]⁺.

Appendix 4: Additional Tables & Figures

Table A-4.1 Total organic carbon (OC) budget of the incubation experiment showing soil OC amounts of initial soils, amount of added straw OC, mineralized OC, retrieved DOC and final SOC amounts. The budget with identical units for all C fractions [mg flask⁻¹] allowed for the calculation of OC recovery [%]. Data are means with standard deviations (n = 3) in brackets.

Initial [mg flask ⁻¹]	Alisol				Andosol			
	a-o (+)	a-o (-)	o (+)	o (-)	a-o (+)	a-o (-)	o (+)	o (-)
FPOM	118	(17)			208	(27)		
OPOM	111	(7)			46	(7)		
MOM	3414	(17)			5552	(24)		
added straw OC [mg flask ⁻¹]	1141		1141		1746		1746	
during incubation [mg flask ⁻¹]								
CO ₂ -C total	479	(13)	166	(6)	908	(24)	128	(5)
CO ₂ -C from straw	313	(18)			738	(11)		
CH ₄ -C total	255	(17)	1	(0)	0	(0)	0	(0)
CH ₄ -C from straw*	467	(17)			0	(0)		
DOC total	25	(1)	6	(1)				
DOC from straw	6	(0)			26	(1)	2	(0)
after incubation [mg flask ⁻¹]								
FPOM total	116	(6)	130	(29)	233	(41)	104	(8)
FPOM from straw	13	(4)			138	(27)		
OPOM total	200	(42)	223	(34)	178	(18)	177	(5)
OPOM from straw	22	(9)			9	(1)		
MOM total	3356	(34)	3097	(74)	3669	(30)	3264	(18)
MOM from straw	321	(23)			248	(28)		
Recovery total [%]	93		99		104		101	
Recovery straw* [%]	100				99			

* CH₄ from straw was calculated by subtracting sum of straw-derived CO₂, DOC and SOC from total amount of added straw OC resulting in a theoretical straw OC recovery of 100%.

Table A-4.2 Proportion of straw OC in individual non-cellulosic carbohydrates [%] based on respective $\delta^{13}\text{C}$ measurements. Data are means with standard deviations (n = 3) in brackets.

OC from straw [%]	Alisol		Andosol	
	a-o(+)	o(+)	a-o(+)	o(+)
Galactose	1.6 (1.5)	2.5 (1.4)	2.1 (1.0)	1.1 (1.1)
Mannose	1.9 (2.7)	1.5 (1.0)	0.5 (0.7)	1.4 (0.7)
Arabinose	1.7 (0.5)	2.1 (0.8)	1.9 (0.5)	0.7 (1.3)
Xylose	6.4 (0.6)	5.6 (1.2)	6.3 (0.6)	1.9 (1.3)

Table A-4.3 Summary of the sequencing run and sequence processing with QIIME.

Sample	after sequencing	after Adapter removal	after filtering	after assignment	after Chloroplast removal
Ando initial R1	135569	130419	125405	100679	100669
Ando initial R2	143299	138347	128328	93979	93968
Ando initial R3	108645	104089	98397	75077	75072
Ando a-o (+) R1	165105	134660	121506	110480	109167
Ando a-o (+) R2	165580	143836	135719	88921	72352
Ando a-o (+) R3	141032	111913	104989	93013	69519
Ando o (+) R1	160507	133643	121980	103901	103463
Ando o (+) R2	75244	63655	59639	46317	44303
Ando o (+) R3	80102	69948	66822	57314	19508
Ali initial R1	132287	125692	115652	82951	82896
Ali initial R2	173548	163901	152789	108875	108815
Ali initial R3	174433	162669	150482	99934	99856
Ali a-o (+) R1	187776	176985	164743	124328	124306
Ali a-o (+) R2	133388	126427	116522	88268	88266
Ali a-o (+) R3	117843	111255	102652	79437	79417
Ali o (+) R1	166055	156246	146012	116921	116888
Ali o (+) R2	142651	135266	127610	99060	99031
Ali o (+) R3	128120	120640	112858	85453	85440

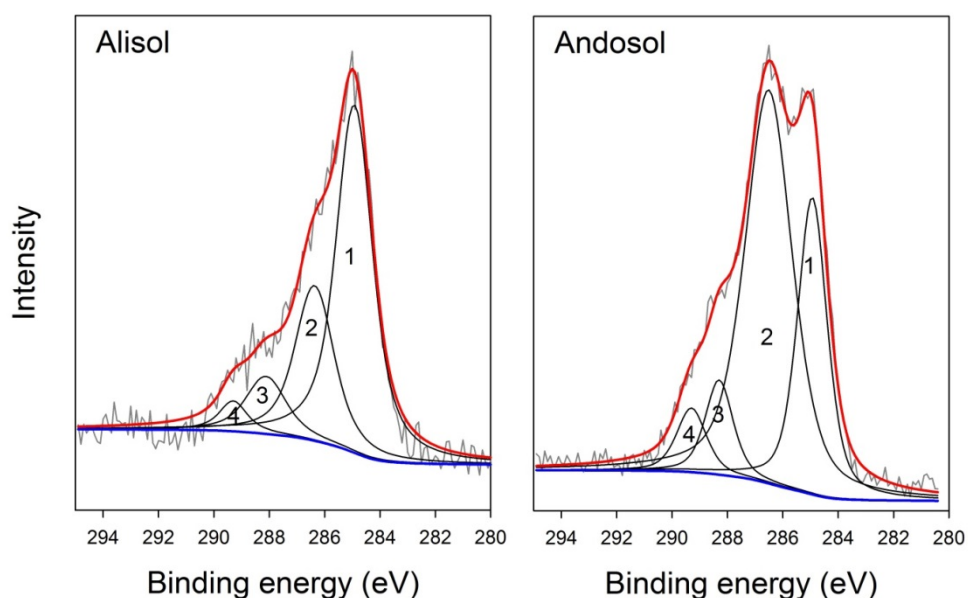


Fig. A-4.1 Exemplary C 1s spectra of mineral-organic associations isolated from each soil, with peaks fitted with subcomponents (in black) reflecting different carbon oxidation states: 1) C—C, C=C; 2) C-O, C-N; 3) C=O, O-C-O, O=C-N; 4) O-C=O, O=C-N. The red curve represents the sum curve while the blue one denotes the fitted background curve.

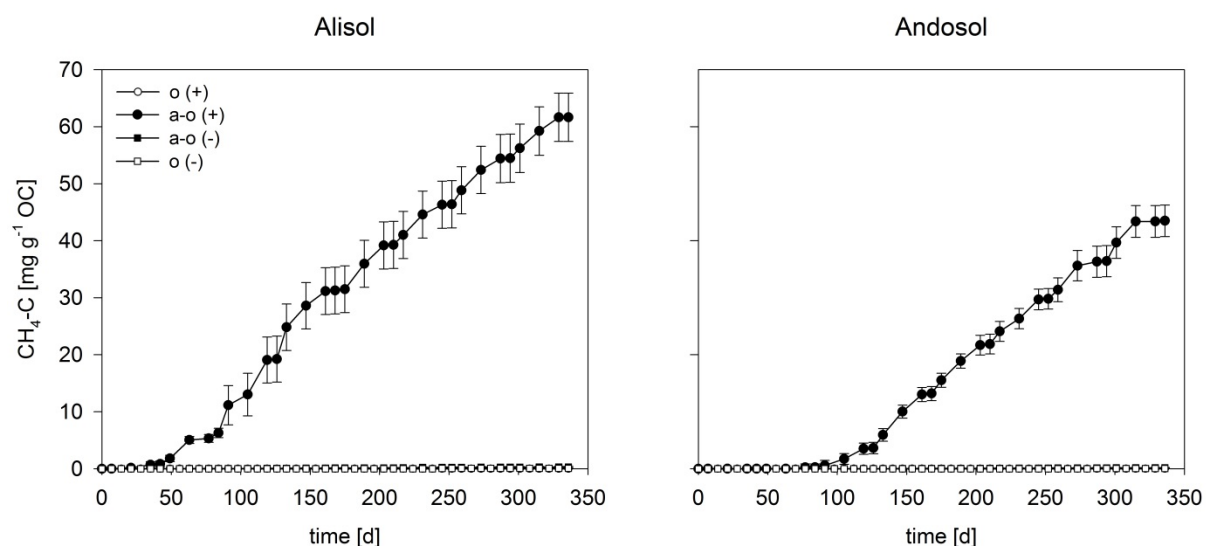


Fig. A-4.2 Cumulative CH₄-C emitted from the Alisol (left) and Andosol (right) incubated with alternating redox (a-o) and permanently oxalic (o) conditions as well as with (+) and without (-) straw addition. Cumulative CH₄-C refers to total OC, which takes into account OC of initial soils, added straw OC, and OC mineralized in between sampling dates. Error bars represent standard deviations with n=9 (1st cycle), n=6 (2nd & 3rd cycle), and n=3 (4th-8th cycle).

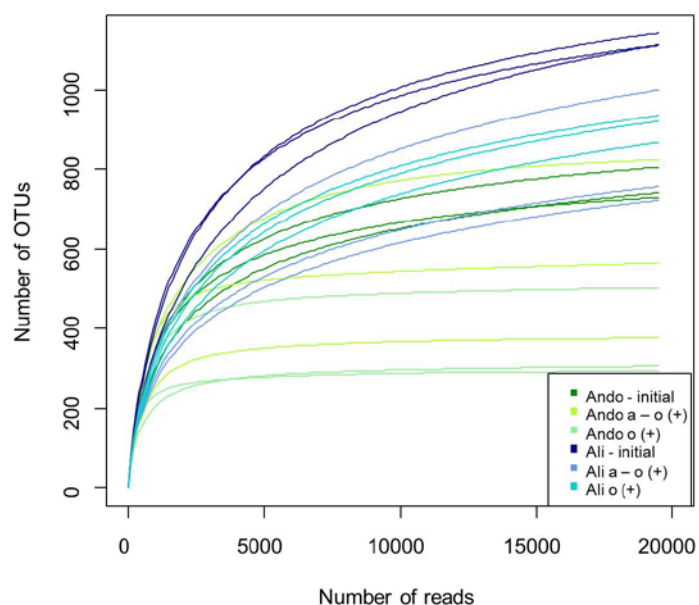


Fig. A-4.3 Rarefaction curve of 16S rRNA sequences of all samples rarefied to a sequence level of 19,508 reads per sample. Plotted is the number of reads against the number of operational taxonomic units (OTUs) on 97% similarity level per sample. Displayed are initial field soils and soils incubated with straw application (+) under redox fluctuation (a-o) or static oxalic conditions (o) (n=3).

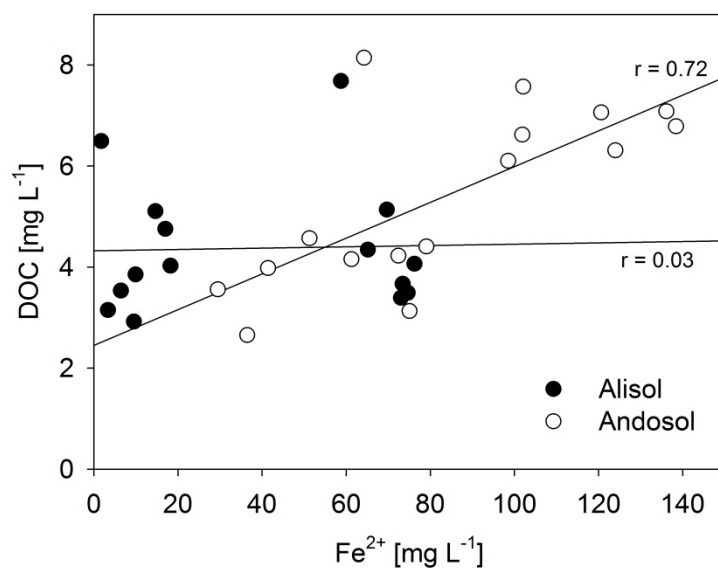


Fig. A-4.4 Concentrations of dissolved organic carbon (DOC) plotted over Fe²⁺ concentrations of Alisol and Andosol samples incubated with straw addition and redox fluctuation. The correlation coefficient r results from Pearson Product Moment Correlation analysis performed with Sigma-Plot version 11.0 (SPSS Inc.).

Publikationsliste (List of publications)

Winkler, P., Kaiser, K., Kölbl, A., Kühn, T., Schad, P., Urbanski, L., Fiedler, S., Lehndorff, E., Kalbitz, K., Utami, S.R., Cao, Z., Zhang, G., Jahn, R., Kögel-Knabner, I. (2016) Response of Vertisols, Andosols, and Alisols to paddy management. *Geoderma* 261, 23-35.

Lehndorff, E., Houtermans, M., **Winkler, P.**, Kaiser, K., Kölbl, A., Romani, M., Said-Pullicino, D., Utami, S.R., Zhang, G.L., Cao, Z.H., Mikutta, R., Guggenberger, G., Amelung, W. (2016) Black carbon and black nitrogen storage under long-term paddy and non-paddy management in major reference soil groups. *Geoderma* 284, 214-225.

Winkler, P., Kaiser, K., Thompson, A., Kalbitz, K., Fiedler, S., Jahn, R. (2018) Contrasting evolution of Fe phase composition in soils exposed to redox fluctuations. *Geochimica et Cosmochimica Acta* 235, 89-102.

Winkler, P., Kaiser, K., Jahn, R., Mikutta, R., Fiedler, S., Cerli, C., Kölbl, A., Schulz, S., Jankowska, M., Schloter, M., Müller-Niggemann, C., Schwark, L., Woche, S.K., Kümmel, S., Utami, S.R., Kalbitz, K. (2019) Tracing organic carbon and microbial community structure in mineralogically different soils exposed to redox fluctuations. *Biogeochemistry* 143, 31-54.

Tagungsbeiträge

Winkler, P., Kaiser, K., Jahn, R., Fiedler, S., Kölbl, A., Mikutta, R., Woche, S.K., Kalbitz, K. (2019) Changes in minerals and organic-mineral associations in soils under redox fluctuation. Tagung der European Geosciences Union (EGU), Wien, Österreich. (Vortrag)

Winkler, P., Kaiser, K., Thompson, A., Kalbitz, K., Fiedler, S., Jahn, R. (2017) Changes in Fe mineral composition in Alisols and Andosols exposed to alternating redox conditions. Tagung der Deutschen Bodenkundlichen Gesellschaft (DBG), Göttingen. (Poster)

Winkler, P., Kaiser, K., Cerli, C., Fiedler, S., Jahn, R., Kalbitz, K. (2016) Fate of organic carbon in paddy soils with contrasting mineralogy. Workshop SOMmic – Microbial Contribution and Impact on Soil Organic Matter, Structure and Genesis, Leipzig. (Poster)

Winkler, P., Cerli, C., Fiedler, S., Utami, S.R., Woche, S., Jahn, R., Kalbitz, K., Kaiser, K. (2016) Fate of organic carbon in paddy soils – results of Alisol and Andosol incubation with ¹³C marker. Tagung der European Geosciences Union (EGU), Wien, Österreich. (Vortrag)

Winkler, P., Cerli, C., Fiedler, S., Jahn, R., Kalbitz, K., Kaiser, K. (2015) Organic matter controls re-distribution of Fe oxides in soils subjected to submersion. Tagung der Deutschen Bodenkundlichen Gesellschaft (DBG), München. (Vortrag)

Geier, P., Cerli, C., Fiedler, S., Jahn, R., Kalbitz, K., Kaiser, K. (2014) Organic matter controls re-

distribution of Fe oxides in soils subjected to submersion. Workshop: Biogeochemistry of submerged agro-ecosystems: properties, processes, cycles and functions, Freising. (Vortrag)

Geier, P., Kaiser, K., Kölbl, A., Urbanski, L., Schad, P., Fiedler, S., Utami, S.R., Cao, Z.H., Jahn, R., Kögel-Knabner, I. (2014) Alisol, Andosols and Vertisols from Indonesia and China and their differential change due to paddy management. Workshop: Biogeochemistry of submerged agro-ecosystems: properties, processes, cycles and functions, Freising. (Poster)

Geier, P., Cerli, C., Fiedler, S., Jahn, R., Kalbitz, K., Kaiser, K. (2014) Organic matter controls redistribution of Fe oxides in soils subjected to submersion. BIOGEOMON: 8th International Symposium on Ecosystem Behavior, Bayreuth. (Vortrag)

Geier, P., Kaiser, K., Kalbitz, K., Jahn, R., Fiedler, S. (2013) Divergent redistribution and transformation of Fe oxides upon paddy cultivation of different soils. Tagung der Deutschen Bodenkundlichen Gesellschaft (DBG), Rostock. (Vortrag)

Lebenslauf (Curriculum Vitae)

Persönliche Daten

Name: Pauline Winkler (geb. Geier)
Adresse: August-Bebel-Str. 29, 06108 Halle (Saale)
E-Mail: pauline.winkler@landw.uni-halle.de
Geburtsdatum & -ort: 23.11.1984, Finsterwalde

Ausbildung & Beruf

- seit 03/2017 Wissenschaftliche Mitarbeiterin an der Martin-Luther-Universität Halle-Wittenberg:
- Thema: "The leak in the phosphorus cycle – exploring the mechanisms and controls of phosphorus leaching in soils of acquiring and recycling forest ecosystems"
 - Teilprojekt des DFG-Schwerpunktprogramms „Forest Strategies for limited Phosphorus Resources“
 - 8-monatige Unterbrechung durch Mutterschutz- & Elternzeit
- 2012 - 2016 Wissenschaftliche Mitarbeiterin (Doktorandin) an der Martin-Luther-Universität Halle-Wittenberg:
- Thema: "Changes in minerals and organic-mineral associations during paddy soil development"
 - Teilprojekt des DFG-Verbundprojektes „Biogeochemistry of paddy soil evolution“
 - 8-monatige Unterbrechung durch Mutterschutz- & Elternzeit
- 2005 - 2011 Studium der Geoökologie an der TU Bergakademie Freiberg:
- Vertiefungen: Bodenkunde, Umweltanalytik, Hydrogeologie
 - Studienarbeit: "Landuse and Soil Fertility in Northeastern Brazil"; Note: 1,3
 - Diplomarbeit: "Impact of Organic Soil Conditioners on the Soil Structure of No-Till Fields"; Note: 1,2
 - Abschlussnote: 1,2
 - Georgius-Agricola-Medaille für hervorragende Leistungen während des Studiums
- 1997 – 2004 Sängerstadt Gymnasium Finsterwalde (Brandenburg):
Abitur, Abschlussnote: 1,1

Praktische & internationale Erfahrungen

- | | |
|-------------------|---|
| 03/2012 | 3-wöchige Bodenprobenahme in Indonesien im Rahmen der Dissertation |
| 08/2010 | Teilnahme an 3-wöchiger bodengeografischer und agrar-ökologischer Exkursion durch Russland |
| 06/2009 – 11/2009 | 6-monatiges Praktikum am “Institute for Research of Development” in Hanoi, Vietnam; Thema: “Indicators for the sustainable agricultural development of small-scale farms under a PES contract “ |
| 07/2008 – 08/2008 | Teilnahme an 6-wöchiger geochemischer Kartierung in Brasilien; Grundlage für Studienarbeit |
| 08/2007 | 4-wöchiges Praktikum am Forschungsinstitut für Bergbaufolgelandschaften in Finsterwalde |

Halle (Saale), den

Unterschrift

Eidesstattliche Erklärung / *Declaration under Oath*

Ich erkläre an Eides statt, dass ich die Arbeit selbstständig und ohne fremde Hilfe verfasst, keine anderen als die von mir angegebenen Quellen und Hilfsmittel benutzt und die den benutzten Werken wörtlich oder inhaltlich entnommenen Stellen als solche kenntlich gemacht habe.

I declare under penalty of perjury that this thesis is my own work entirely and has been written without any help from other people. I used only the sources mentioned and included all the citations correctly both in word or content.

Datum / Date

Unterschrift der Antragstellerin / *Signature of the applicant*

Erklärung über bestehende Vorstrafen und anhängige Ermittlungsverfahren
/Declaration concerning Criminal Record and Pending Investigations

Hiermit erkläre ich, dass ich weder vorbestraft bin noch dass gegen mich Ermittlungsverfahren anhängig sind.

I hereby declare that I have no criminal record and that no preliminary investigations are pending against me.

Datum / Date

Unterschrift der Antragstellerin / *Signature of the applicant*